Lappeenranta
University of Technology

Polina Belova

QUASICLASSICAL APPROACH TO THE VORTEX STATE IN IRON-BASED SUPERCONDUCTORS

Thesis for the degree of Doctor of Science (Technology) to be presented with due permission for public examination and criticism in the Auditorium 1382 at Lappeenranta University of Technology, Lappeenranta, Finland on the 21st of November, 2012, at noon.

Acta Universitatis
Lappeenrantaensis 490

Supervisors Professor Erkki Lähderanta and
D. Sc. Konstantin Traito
Department of Mathematics and Physics
Lappeenranta University of Technology
Finland

Reviewers Professor Alexander Granovsky
Department of Magnetism
Faculty of Physics
Moscow State University
Russia

Professor Sergey Savel'ev
Department of Physics
Loughborough University
United Kindom

Opponent Professor Alexander Tagantsev
Materials Science and Engineering
Swiss Federal Institute of Technology
Switzerland

ISBN 978-952-265-314-7
ISBN 978-952-265-315-4 (PDF)
ISSN 1456-4491

Lappeenrannan teknillinen yliopisto
Digipaino 2012

Abstract

Polina Belova
QUASICLASSICAL APPROACH TO THE VORTEX STATE IN IRON-BASED SUPERCONDUCTORS
Lappeenranta, 2012
132 p.
Acta Universitatis Lappeenrantaensis 490
Diss. Lappeenranta University of Technology
ISBN 978-952-265-314-7, ISBN 978-952-265-315-4 (PDF), ISSN 1456-4491

The quasiclassical approach was applied to the investigation of the vortex properties in the iron-based superconductors. The special attention was paid to manifestation of the nonlocal effects of the vortex core structure. The main results are as follows:
(i) The effects of the pairing symmetries ($s^{\pm}$ and s_{++}) on the cutoff parameter of field distribution, ξ_h, in stoichiometric (like LiFeAs) and nonstoichiometric (like doped $BaFe_2As_2$) iron pnictides have been investigated using Eilenberger quasiclassical equations. Magnetic field, temperature and impurity scattering dependences of ξ_h have been calculated. Two opposite behavior have been discovered. The ξ_h/ξ_{c2} ratio is less in $s^{\pm}$ symmetry when intraband impurity scattering (Γ_0) is much larger than one and much larger than interband impurity scattering (Γ_π), i.e. in nonstoichiometric iron pnictides. Opposite, the value ξ_h/ξ_{c2} is higher in $s^{\pm}$ case and the field dependent curve is shifted upward from the "clean" case ($\Gamma_0 = \Gamma_\pi = 0$) for stoichiometric iron pnictides ($\Gamma_0 = \Gamma_\pi \ll 1$).
(ii) Eilenberger approach to the cutoff parameter, ξ_h, of the field distribution in the mixed state of high κ-superconductors is developed. It is found that normalized value of ξ_h/ξ_{c2} decreases both with temperature (due to Kramer-Pesch effect) and with impurity scattering rate Γ. The theory explains μSR experiments in some low-field superconductors and different ξ_h values from the Ginzburg-Landau theory predictions in isotropic s-wave superconductors. A comparison with another characteristic length ξ_1, describing the gradient of the order parameter in the vortex center, is done. They have very different Γ-dependences: monotonous suppression of $\xi_h(B)$ values and crossing behavior of the $\xi_1(B)$ curves at various Γ. This is explained by the nonlocal effects in the Eilenberger theory.
(iii) The generalized London equation in the mixed state of high-κ s-wave pairing superconductors with impurities is considered as a projection of the quasiclassical nonlocal nonlinear Eilenberger theory. Both nonlocal effects originated from extended states between the vortices and bound Andreev states in the vortex are taken into account. Comparison with different analytical nonlocal linear approaches (the Kogan-Gurevich, Amin-Franz-Affleck, Kogan-Zhelezina models) including only extended states is done. The influence of the impurities on the ratio of the cutoff parameter ξ_h and the Ginzburg-Landau coherence length ξ_{c2} is considered. Quasiparticle scattering by impurities and lowering of the temperature reduces the value of ξ_h to the values much less than ξ_{c2}. This is different from the prediction of the local Ginzburg-Landau theory where ξ_h is scaled by ξ_{c2}. It is found that impurities influence by different way on the cutoff parameter ξ_h and the order parameter coherence length ξ_1. The ξ_h decreases monotonously with the impurity scattering time in contrast to the nonmonotonous behavior of ξ_1.

Keywords: cutoff parameter, quasiclassic, mixed state, Eilenberger, Kramer-Pesch

UDC 538.945:537.312.6:621.38

Happy 80th Anniversary, Grandma (25.11.2012)!
Бабушка, поздравляю тебя с юбилеем!

Acknowledgements

This work was carried out at the Department of Mathematics and Physics in Lappeenranta University of Technology between the years 2009 and 2012. My deepest gratitude is to one of my Supervisors, Professor Erkki Lähderanta, for the support and guidance throughout my dissertation. I am truly indebted and thankful to Konstantin Traito. I am sure this dissertation would have not been possible without his help.

I would like to express my heart-felt gratitude to my family who always support me.

I am grateful to my ex-Supervisor, Alexandr Lashkul, for endless jokes and all sweets he gave me during these years. I would like to thank my co-autors and colleagues, Mikhail Safonchik, for helpful disscussions and also Ivan Zakharchuk and his Maria for pleasant time spending in our office. Special thanks to V. A. Gurtov for guidance during my studies at Petrozavodsk State University.

I would like to take this opportunity to thank my colleagues all over the world (Nino, Andreas, Sergey U., Juha, Andrey, Ville, Teemu, Arkadiy), fellow students, co-workers and the personnel of the Department of Mathematics and Physics in Lappeenranta University of Technology and Petrozavodsk State University for pleasant atmosphere.

I express my gratitude both to Professor Alexander Granovsky and Professor Sergey Savel'ev for reviewing the thesis and for valuable comments. I would also like to thank Professor Alexander Tagantsev for taking the time to be my opponent.

My never-ending words of gratitude go to my closest people and my friends who have always been a major source of inspiration, supporting to me and I deeply appreciate their belief in me: Sergey, Natasha, Olga Zh., Liuda and Sasha Sm., Lena R., Oleg G, Masha, Pasha.

Many friends have helped me stay cheerful and in a good mood through these years, my friends from Petrozavodsk: Ksenia S., Sasha G., Kolya, Alexey T., Anna K., Ivan G., Yulia Sh.; my Saint-Petersburg and Moscow ones: Armen and Yulia, Katya and Sasha V., Roman and Maria K., Sergey and Julia Podpls, Senya, Lesha; guys, which I met in LUT: Dima, Viktoria, Natalia S., Andrey, Alex M., Daria and Iliya, Misha S., Mitya T., Alex Sok., Julia and Katteden, and others, I definitely should stop somewhere. I greatly value their friendship.

Finally, I appreciate the financial support from Finnish Cultural Foundation (Suomen Kulttuurirahasto) and the Research Foundation of LUT (LTY:n Tukisäätiö).

Lappeenranta, 2012

Polina Belova

Preface

The analysis of the field distribution experimental results in mixed state of type-II superconductors is usually done [Sonier (2004, 2007)] in the framework of the Hao-Clem theory (analytical solution of the Ginzburg-Landau theory, AGL [Hao et al. (1991); Yaouanc et al. (1997)]). Strictly speaking, Ginzburg-Landau theory is valid only near T_c but it is often used in whole temperature range taking the cutoff parameter ξ_v and penetration depth λ as fitting parameters. Recently an effective London model with the effective cutoff parameter $\xi_h(B)$ as a fitting parameter was obtained for clean [Laiho et al. (2007)] and dirty [Laiho et al. (2008)] superconductors, using self-consistent solution of quasiclassical nonlinear Eilenberger equations. To emphasize the differences between calculated cutoff parameter and variational parameter of the AGL we changed the notations $\xi_v \rightarrow \xi_h$. In this approach the coherence length obtained from the Ginzburg-Landau model is extended over the whole field and temperature range. In this case the effects of bound states in the vortex cores leading to Kramer-Pesch effect [Kramer and Pesch (1974)], their delocalization between the vortices [Ichioka et al. (1999a)] and non-local electrodynamic [Kogan et al. (1996a)] are self-consistently included. In this model the magnetic field distribution is given by [Laiho et al. (2008)]

$$h_{EHC}(\mathbf{r}) = \frac{\Phi_0}{S} \sum_{\mathbf{G}} \frac{F(G) e^{i\mathbf{G}\mathbf{r}}}{1 + \lambda^2 G^2}, \tag{1}$$

where $F(\mathbf{G}) = uK_1(u)$, $K_1(u)$ is the modified Bessel function, $u = \xi_h G$, $\mathbf{G}$ is a reciprocal lattice vector and S is the area of the vortex lattice unit cell. Because the magnetic field distribution is similar to the Hao-Clem model we will call this approach as Eilenberger-Hao-Clem model. Here, λ is not a fitting parameter but is calculated from the microscopical theory of the Meissner state and cutoff parameter ξ_h is calculated from Eilenberger theory of the mixed state.

The subjects of the original publications are (i) the field distribution in the mixed state of iron-based superconductors was investigated using Eilenberger quasiclassical equations taking into account possible pairing symmetries ($s^{\pm}$ and s_{++}). The $s^{\pm}$ pairing symmetry is mediated by ferromagnetic spin fluctuation while s_{++} is created by moderate electron-phonon interaction due to Fe-ion oscillation and critical orbital fluctuation. The cutoff parameter ξ_h was calculated numerically using the Riccati parametrization of the Eilenberger equations. The results are presented in **Papers 1-3.** The physical properties of iron-based superconductors are described in Introduction and Chapter II. The model for $s^{\pm}$ and s_{++} are presented in comment in **Papers 1** and **2**, respectively. Comments to **Paper 3** is devoted to experimental μSR results in iron pnictides. Transformation of the Eilenberger Equations to a Riccati equation is described in the Chapter III. (ii) The comparison between nonlinear nonlocal Eilenberger approach and local Ginzburg-Landau and Usadel models, and linear nonlocal Kogan-Gurevich, Kogan-Zhelezina theories is done in **Papers 4-6**. The analytical Ginzburg-Landau model is considered in the comments to **Paper 4**. The Kramer-Pesch effect which is absent in the local theories is described in the comments to **Paper 5**. Usadel model and its comparison with μSR experiments is presented in the comments to **Paper 6**. The importance of the nonlocal effects in the calculation of cutoff parameter ξ_h is discussed in detail in **Papers 4-6**.

The obtained results can be used for interpretation of muon spin resonance and small angular neutron scattering measurements data.

List of publications

This thesis consists of an introduction (Chapter I), a review and discussion of the subject (Chapters II-III), and comments (Chapter IV) on six original publications:

1 **P. Belova, M. Safonchik, K. B. Traito and E. Lähderanta**, Quasiclassical Eilenberger approach to the vortex state in pnictide superconductors, *Journal of Physics: Conference Series*, **303**, 012113, 2011.

2 **P. Belova, M. Safonchik, K. B. Traito and E. Lähderanta**, Cutoff parameter of the field distribution in the mixed state of iron pnictides with $s^{\pm}$ and s_{++} pairing symmetries, *Physical Review B*, **83**, 104518, 2011.

3 **P. Belova, I. Zakharchuk, K. B. Traito and E. Lähderanta**, Effects of the order parameter symmetry on the vortex core structure in the iron pnictides, *Journal of Physics: Conference Series*, in press.

4 **P. Belova, K. B. Traito and E. Lähderanta**, Eilenberger and Ginzburg-Landau models of the vortex core in high κ-superconductors, *Journal of applied physics*, **110**, 033911, 2011.

5 **P. Belova, I. Zakharchuk, M. Safonchik, K. B. Traito and E. Lähderanta** Generalized London theory of the mixed state of high-κ superconductors as a projection of the quasiclassical Eilenberger approach, *Physica C: Superconductivity and its Applications*, **476**, 1, 2012.

6 **P. Belova, M. Safonchik, K. B. Traito and E. Lähderanta**, Coherence length of magnetic field in the mixed state of type-II superconductors, *Journal of Physics: Conference Series*, **303**, 012114, 2011.

Throughout the original papers I took part in formulation of the scientific problems as well as numerical solving of the Eilenberger equations, discussion of the results and writing the articles.

Abstract

Acknowledgments

Preface

List of publications

Part I: Overview of the thesis **11**

1 Introduction **13**

2 Superconductivity in iron pnictides **16**

3 Transformation of the Eilenberger Equations to a Riccati equation **22**
Quasiclassical approach 23
Eilenberger equations along a characteristic line 25
Riccati parametrization of Eilenberger propagator 27

4 Comments on the original publications **33**
Paper 1. Quasiclassical Eilenberger approach to the vortex state in pnictide superconductors 33
Paper 2. Cutoff parameter of the field distribution in the mixed state of iron pnictides with $s^{\pm}$ and s_{++} pairing symmetries 38
Paper 3. Effects of the order parameter symmetry on the vortex core structure in the iron pnictides 45
Paper 4. Eilenberger and Ginzburg-Landau models of the vortex core in high κ-superconductors 51
Paper 5. Generalized London theory of the mixed state of high-κ superconductors as a projection of the quasiclassical Eilenberger approach 57
Paper 6. Coherence length of magnetic field in the mixed state of type-II superconductors 63

5 Conclusions **70**

Bibliography **71**

Part II: Publications **79**

PART I: OVERVIEW OF THE THESIS

CHAPTER I

Introduction

The discovery of superconductivity, in 2008, with $T_c = 26$ K in florine-doped LaFeAsO (1111-type) [Kamihara et al. (2008)] has focused a worldwide interest to the new class of the materials. Such supprising T_c was unexpected for Fe metal, which is ferromagnet. The crystal structure contains FeAs layers with Fe atoms in a square planar lattice arrangement, and these layers alternate with LaO layers along the c-axis. It was found, that applying pressure increases the T_c even further to 43 K [Takahashi et al. (2008)] and then as high as 55 K by replacement of La by other rare earth elements [Chen et al. (2008b)]. A lot of efforts by the condensed-matter community have been devoted during few years after the discovery to understand normal state properties of Fe-based materials, the pairing mechanism, the symmetry and the structure of the pairing gap.

The family of Fe-based pnictides (binary compounds of the elements from the 5th group: N, P, As, Sb, Bi) is already quite large and keeps growing. It includes various Fe-based superconductors (FeSCs) such as 1111 systems RFeAsO (R = rare earth element) with T_c up to 55 K [Kamihara et al. (2008); Chen et al. (2008a,b)], 122 systems $X\mathrm{Fe_2As_2}$ (X = alkaline earth metals) with T_c up to 38 K [Rotter et al. (2011); Ni et al. (2010)], 111 systems like LiFeAs with T_c up to 18 K [Borisenko et al. (2010)], and also 11 Fe-chalcogenides (Fe-based compounds with elements from the 6th group: S, Se, Te) such as $\mathrm{FeTe_{1-x}Se_x}$ [Chen et al. (2009)] and $A\mathrm{Fe_sSe_2}$ (A = K,Rb,Cs) [Guo et al. (2010); Qian et al. (2011)].

Parent compounds of FeSCs are metals, in distinction to cuprate superconductors for which parent compounds are Mott insulators. Still, in similarity with the cuprates, in most cases these parent compounds are antiferromagnetically ordered [Inosov et al. (2010a)]. Because electrons which carry magnetic moments still travel relatively freely from site to site, the magnetic order is often termed as a spin-density-wave (SDW), by analogy with e.g., antiferromagnetic Cr, rather than 'Heisenberg antiferromagnetism' - the latter term is reserved for systems in which electrons are 'nailed down' to particular lattice sites by very strong Coulomb repulsion.

Superconductivity (SC) in FeSCs emerges upon either hole or electron doping (see Fig. 1.1), but can also be induced by pressure or by isovalent replacement of one pnictide element by another, e.g., As by P [Nakai et al. (2010a)]. In some systems, like LiFeAs [Borisenko et al. (2010)] and LaFePO [Kamihara et al. (2006)], SC emerges already at zero doping, instead of a magnetic order. The magnetism, the electronic structure (see Fig. 1.2), the normal state properties of FeSCs, and the interplay between FeSCs and cuprate superconductors have been reviewed in several recent publications [Mazin (2010); Chubukov (2009); Kuroki et al. (2009)].

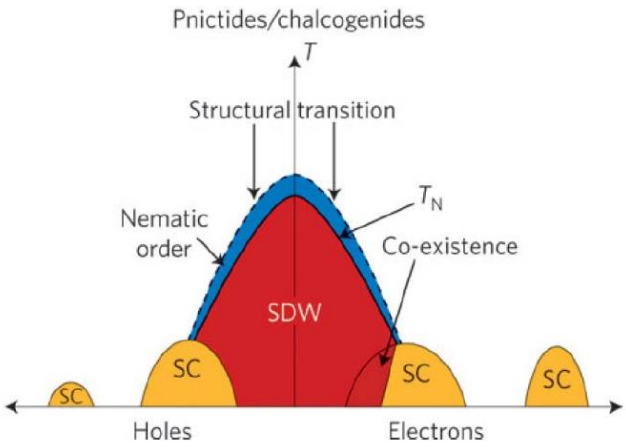

Figure 1.1: Schematic phase diagram of Fe-based pnictides upon hole or electron doping. In the shaded region, superconductivity and antiferromagnetism co-exist. Not all details/phases are shown. Superconductivity can be initiated not only by doping but also by pressure and/or isovalent replacement of one pnictide element by another [Nakai et al. (2010a)]. Nematic order at $T > T_N$ is subject of debates. Superconductors at large doping are KFe_2As_2 for hole doping [Sato et al. (2009); Dong et al. (2010)] and $A_xFe_{2-y}Se_2$ (A = K, Rb, Cs) for electron doping [Guo et al. (2010); Qian et al. (2011)]. Whether superconductivity in pnictides exists at all intermediate dopings is not clear yet. From Ref. [Basov and Chubukov (2011)].

The phenomenon of SC has a long history. SC was discovered by Kamerlingh Onnes a century ago, in 1911. It has been explained in general terms nearly fifty years later, in 1957, by Bardeen, Cooper, and Schrieffer (BCS), who demonstrated that an arbitrary weak attractive interaction between two low-energy fermions is sufficient to pair them into a bound state. At weak coupling, paired fermions immediately form Bose-Einstein condensate and behave as one single macroscopic quantum object and they move coherently under the applied electric field, i.e superconduct. In d-dimensional electronic systems low-energy fermonic states are located, in momentum space, near particular $d-1$ dimensional surfaces, called Fermi surfaces (FS) on which fermionic energy is zero relative to the chemical potential. At weak/moderate coupling, the pairing problem is confined to a near vicinity of a FS. The interaction between fermions is generally non-singular with respect to variations of the distance to the FS and can be approximated by its value right on the FS [Chubukov (2012)].

What causes the attraction between fermions is a more subtle question, and the nature and the origin of the pairing glue have been the subject of great debates in condensed-matter community over the last 50 years. BCS attributed the attraction between fermions to the underlying interaction between electrons and phonons [Bardeen et al. (1957)] (the two electrons effectively interact with each other by emitting and absorbing the same phonon which then serves as a glue which binds electrons into pairs). Electron-phonon mechanism has been successfully applied to explain SC in a large variety of materials, from Hg and Al to recently discovered and extensively studied MgB_2 with the transition temperature T_c = 39 K [Kortus et al. (2001)]. Nonphononic mechanisms of the pairing have also

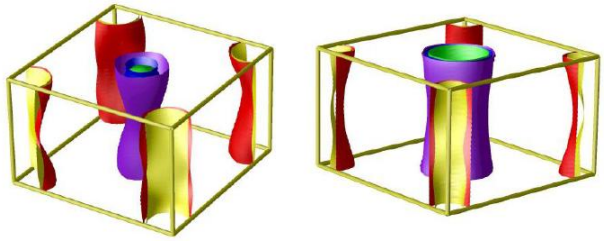

Figure 1.2: The electronic structure of FeSCs. In weakly and moderately electron-doped materials (left panel) the FS consists of quasi-2D warped cylinders centered at (0, 0) and (π, π) in a 2D cross-section. The ones near (0, 0) are hole pockets (filled states are outside cylinders), the ones near (π, π) are electron pockets (filled states are inside cylinders). There also exists a quasi-3D hole pocket near $k_z = \pi$. In hole-doped FeSCs the electronic structure is very similar, but 3D hole pocket becomes quasi-2D warped hole cylinder. From Ref. [Mazin and Schmalian (2009)].

been discussed, most notably in connection with superfluidity in ^{3}He [Anderson and Morel (1961)], but did not become the mainstream before the discovery of SC in LaBaCuO in 1986 [Bednorz and Muller (1986)]. That discovery, and subsequent discoveries of superconductivity at higher T_c in other cuprates signaled the beginning of the new era of 'high-temperature superconductivity' to which FeSCs added a new avenue with quite high traffic over the last four years [Kohn and Luttinger (1965)].

CHAPTER II

Superconductivity in iron pnictides

Superconductivity is quite robust phenomenon. It has been known from early 60's that in isotropic systems the equation for superconducting T_c factorizes if one expands the interaction between the two fermions in partial components corresponding to interactions in the subspaces with a given angular momentum of the two interacting fermions $l = 0$, 1, 2, 3, etc [in spatially isotropic systems $l = 0$ component is called s-wave, $l = 1$ component is called p-wave, $l = 2$ component is called d-wave, and so on]. If just one component with some l is attractive, the system undergoes a SC transition at some temperature $T = T_c$. For phonon-mediate superconductors, s-wave superconductivity is the most likely outcome. In the cuprates, however, the pairing symmetry has been firmly established as d-wave. The vast majority of researches believe that such pairing is not caused by phonons and emerges instead due to screened Coulomb interaction between electrons. The screened Coulomb interaction $U(r)$ is constant and repulsive at short distances but has a complex dependence on r at large distances and may develop an attractive component at some l. One solid reason for the attraction, at least at large l, has been identified by Kohn and Luttinger back in 1965 [Kohn and Luttinger (1965)].

In lattice systems, angular momentum is no longer a good quantum number, and the equation for T_c only factorizes between different irreducible representations of the lattice space group. In tetragonal systems, which include both cuprates and FeSCs , there are four one-dimensional irreducible representations A_{1g}, B_{1g}, B_{2g}, and A_{2g} and one two-dimensional representation E_{2g}. Each representation has infinite set of eigenfunctions. The eigenfunctions from A_{1g} are invariant under symmetry transformations in a tetragonal lattice: $x \to -x$, $y \to -y$, $x \to y$, the eigenfunctions from B_{1g} change sign under $x \to y$, and so on. If a superconducting gap has A_{1g} symmetry, it is often called s-wave because the first eigenfunction from A_{1g} group is just a constant in momentum space (a δ-function in real space). If the gap has B_{1g} or B_{2g} symmetry, it is called d-wave ($d_{x^2-y^2}$ or d_{xy}, respectively), because in momentum space the leading eigenfunctions in B_{1g} and B_{2g} are $\cos k_x - \cos k_y$ and $\sin k_x \sin k_y$, respectively, and these two reduce to $l = 2$ eigenfunctions $cos2\theta$ and $sin2\theta$ in the isotropic limit.

In the cuprates, the superconducting gap has been proved experimentally to have B_{1g} symmetry. This gap symmetry appears quite naturally in the cuprates, in the doping range where they are metals, if one assumes that the glue that binds fermions together is a spin-fluctuation exchange rather than a phonon (see Fig. 2.1). The notion of a spin fluctuation is actually nothing but the convenient way to describe multiple Coulomb interactions between fermions. It is believed, although

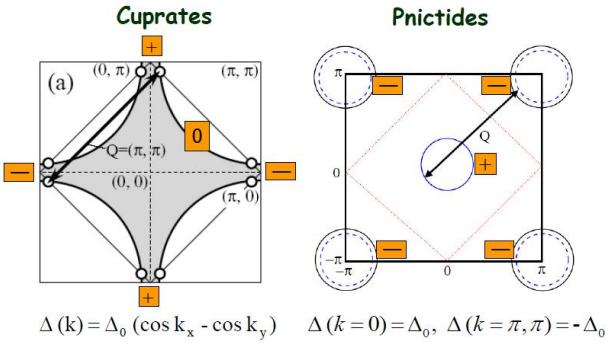

Figure 2.1: A comparison of the pairing state from spin-fluctuation exchange in cuprate SCs and in FeSCs. In the cuprates (left panel) the FS is large, and antiferromagnetic $Q = (\pi, \pi)$ connects points on the same FS. Because spin-mediated interaction is positive (repulsive), the gap must change sign between FS points separated by Q. As the consequences, the gap changes sign twice along the FS. This implies a d-wave gap symmetry. In FeSCs (right panel) scattering by Q moves fermions from one FS to the other. In this situation, the gap must change sign between different FS, but to first approximation remains a constant on a given FS. By symmetry, such a gap is an s-wave gap. It is called $s^{\pm}$ because it changes sign between different FSs. From Ref. [Basov and Chubukov (2011)].

not proved rigorously, that in systems located reasonably close to a magnetic instability, the fully screened Coulomb interaction between fermions can be approximated by an effective interaction in which fermions exchange quanta of their collective fluctuations in the spin channel. That B_{1g} gap is selected is not a surprise because such gap $\Delta(k) \propto \cos k_x - \cos k_y$ changes sign not only under $k_x \to k_y$ but also between $\mathbf{k}$ and $\mathbf{k}' = \mathbf{k} + \mathbf{Q}$ where $\mathbf{Q} = (\pi, \pi)$ is the momenta at which spin fluctuation mediated pairing interaction $U(\mathbf{k}, \mathbf{k}')$ is peaked. This sign change is the crucial element for any electronic mechanism of superconductivity because one needs to extract an attractiv (negative) component from repulsive (positive) screened Coulomb interaction. For B_{1g} gap such a component is $\int d\mathbf{k} d\mathbf{k}' \Delta(k) U(\mathbf{k}, \mathbf{k}') \Delta(k')$, and the integral obviously has a negative value when $U(\mathbf{k}, \mathbf{k}')$ is peaked at (π, π).

In FeSCs, magnetism and superconductivity are also close neighbors on the phase diagram, and it has been proposed [Mazin et al. (2008); Kuroki et al. (2008)] at the very beginning of the Fe era that the pairing mechanism in FeSCs is also a spin-fluctuation exchange. However, the geometry of low energy states in FeSCs and in the cuprates is different, and in most FeSCs the momentum Q connects low-energy fermionic states near the center and the corner of the Brillouin zone (see Fig. 2.1). A simple experimentation with trigonometry then tell us that the SC gap $\Delta(k)$ must be symmetric with respect to $k_x \to k_y$ and $k_x \to -k_x$, but still must change sign under $\mathbf{k} \to \mathbf{k} + \mathbf{Q}$. Such gap belongs to A_{1g} representation, but it only has contributions from a particular subset of A_{1g} states with the form $\cos k_x + \cos k_y$, $\cos(3k_x) + \cos(3k_y)$, etc which all change sign under $\mathbf{k} \to \mathbf{k} + \mathbf{Q}$. Such gap is generally called an extended s-wave gap, or $s^{\pm}$ gap.

Majority of researches do believe that in weakly/moderately doped FeSCs the gap does have $s^{\pm}$

symmetry. However, numerous studies of superconductivity in FeSCs over the last four years demonstrated that the physics of the pairing is more involved than it was originally thought because of multi-orbital/multi-band nature of low-energy fermionic excitations in FeSCs. It turns out that both the symmetry and the structure of the pairing gap result from rather non-trivial interplay between spin-fluctuation exchange, intraband Coulomb repulsion, and momentum structure of the interactions. In particular, an $s^{\pm}$-wave gap can be with or without nodes, depending on the orbital content of low-energy excitations. In addition, the structure of low-energy spin fluctuations evolves with doping, and the same spin-fluctuation mechanism that gives rise to $s^{\pm}$ gap at small/moderate doping in a particular material can give rise to a d-wave gap at strong hole or electron doping.

There is more uncertainly on the theory side. In addition to spin fluctuations, FeSCs possess also charge fluctuations whose strength is the subject of debates. There are proposals [Onari and Kontani (2009); Yin et al. (2010)] that in multi-orbital FeSCs charge fluctuations are strongly enhanced because the system is reasonably close to a transition into a state with an orbital order (e.g., a spontaneous symmetry breaking between the occupation of different orbitals). A counter-argument is that orbital order does not develop on its own but is induced by a magnetic order. If charge fluctuations are relevant, one should consider, in addition to spin-mediated pairing interaction, also the pairing interaction mediated by charge fluctuations. The last interaction can give rise to a conventional, sign-preserving s-wave pairing [Onari and Kontani (2009)]. A 'p-wave' gap scenario (a gap belonging to E_{2g} representation) has also been put forward [Lee and Wen (2008)].

From experimental side, s-wave gap symmetry is consistent with angle-resolved photoemission spectroscopy (ARPES) data on moderately doped KFe_2As_2 and $BaFe_2(As_{1-x}P_x)_2$, which detected only a small variation of the gap along the FSs centered at (0, 0), and with the evolution of the tunneling data in a magnetic field [Hanaguri et al. (2010)]. However, various experimental probes for heavily hole-doped KFe_2As_2[Dong et al. (2010)] indicate the presence of gap nodes, which for the FS geometry in these materials [Sato et al. (2009)] are consistent with a d-wave gap. For the doping range where the gap is very likely an s-wave, the data on some FeSCs were interpreted as evidence for the full gap [Christianson et al. (2008); Malone et al. (2009)], while the data for other FeSCs were interpreted as evidence that the gap has nodes [Fletcher et al. (2009)] or deep minima [Martin et al. (2009)]. In addition, recent nuclear magnetic resonance (NMR) experiments on LiFeAs have been interpreted in favor of a p-wave gap [Brydon et al. (2011)]. All these seemingly very different gap structures (with the exception of a p-wave), actually follow quite naturally from the same underlying physical idea that FeSCs can be treated as moderately interacting itinerant fermionic systems with multiple FS sheets and effective four-fermion intraband and interband interactions in the band basis.

All of the FeAs-based high-T_c superconductors contain square lattice layers of Fe atoms where each Fe atom is at the center of a (usually) distorted As tetrahedron to form an equiatomic FeAs layer (see Fig. 2.2). These FeAs layers are separated by spacer/charge donation layers along the c-axis such as Ba layers in body-centred-tetragonal $BaFe_2As_2$ or LaO layers in primitive tetragonal LaFeAsO. The same structures are sometimes formed when P replaces As, and/or when Co, Ni or other transition metals partially or completely replace the Fe.

Partially replacing isoelectronic P for As in $BaFe_2As_2$ suppresses the long-range structural and antiferromagnetic transitions and induces superconductivity [Jiang et al. (2009)]. Since P is smaller than As, this substitution results in a shrinking of the unit cell, corresponding to what is called 'chemical pressure'. On the other hand, it is known that by substituting isoelectronic Sr for Ba, the unit cell shrinks to the same volume for which $BaFe_2(As_{1-x}Px)_2$ becomes superconducting, but the

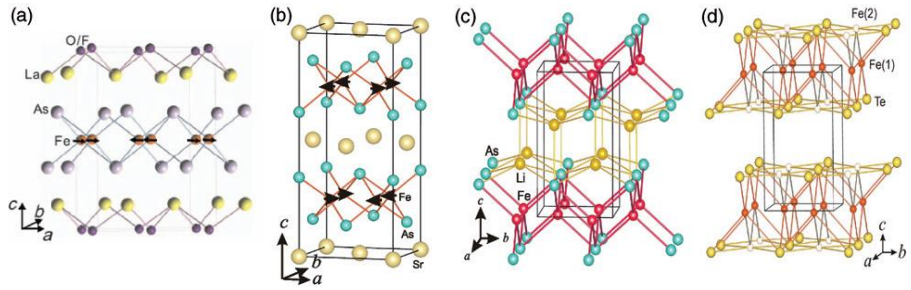

Figure 2.2: Comparison of the crystal structures of (a) $LaFeAsO_{1-x}F_x$, (b) $SrFe_2As_2$, (c) LiFeAs, and (d) $Fe_{1+x}Te$. Each of these structures contains a square lattice of Fe atoms at high temperatures that can distort at low temperatures. Each Fe atom is tetrahedrally coordinated by As (a,b,c) or Te (d). In (b), the outline of the low-temperature orthorhombically distorted unit cell is shown, and ordered magnetic moments on the Fe atoms below the magnetic ordering temperature are shown by arrows. In (d), the Fe(2) atoms are the extra x atoms in $Fe_{1+x}Te$, with $x \sim 1 - 10\%$ [Lynn and Dai (2009)].

Sr substitution does not suppress the crystallographic/antiferromagnetic transition temperature T_0 or induce superconductivity [Wang et al. (2009)]. In fact, Sr substitution monotonically enhances T_0 from 137 K for the pure Ba compound to 205 K for the pure Sr compound. Therefore, the unit cell volume is not the only parameter determining whether the crystallographic and magnetic transitions are suppressed and superconductivity is induced.

Rotter *et al.* [Rotter et al. (2010)] have discovered a significant crystallographic difference between the $(Ba_{1-x}Sr_x)Fe_2As_2$ and $BaFe_2(As_{1-x}P_x)_2$ systems. They find that due to the large size mismatch between P and As, these two atoms are at different heights from the Fe layers, even though they nominally occupy the same crystallographic position. This is the same situation as in the $Fe_{1-y}(Te_{1-x}Se_x)$ system, in which the Se and Te atoms have different heights from the Fe layers [Louca et al. (2010)]. From the crystallographic data and band calculations, Rotter *et al.* infer that the different heights of the P and As layers in the $BaFe_2(As_{1-x}P_x)_2$ system have a dramatic influence on suppressing the magnetic and crystallographic transitions in favor of superconductivity, due to the giant magnetoelastic coupling.

The low temperature structures are distortions of the high temperature structures, rather than a complete rearrangement of the atoms. Remarkably, even though second-order transitions between the two structures are allowed by symmetry since the orthorhombic space groups are, respectively, subgroups of the tetragonal space groups, some of these transitions are reported to be first order such as in $CaFe_2As_2$ [Goldman et al. (2008); Ni et al. (2008)], $SrFe_2As_2$ [Loudon et al. (2010)], and $BaFe_2As_2$ [Huang et al. (2008)]. On the other hand, Wilson *et al.* [Wilson et al. (2009)] found that their magnetic and structural neutron diffraction data on a single crystal of $BaFe_2As_2$ near the SDW transition temperature were consistent with a second-order phase transition.

The relationship between the $a - b$ plane axes in the tetragonal and orthorhombic structures of the 122- and 1111-type compounds is shown in Fig. 2.3. One would expect twinning to occur because the orthorhombic distortion is small. Twins have indeed been observed optically below the

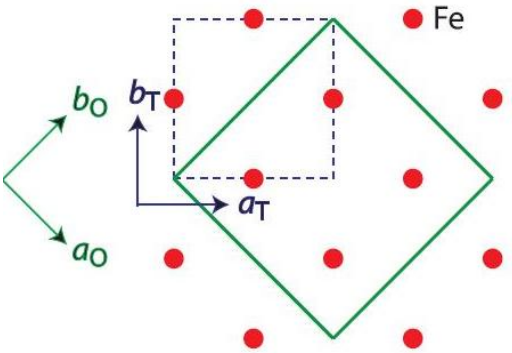

Figure 2.3: Relationships between the basal plane a and b axes of the high temperature tetragonal (T, dashed outline) and the low-temperature orthorhombic (O, solid outline) structures of the 1111-type and 122-type FeAs-based compounds. For clarity, only the Fe atoms in a single layer parallel to the $a-b$ plane of the structures are shown in the figure. The basal-plane lattice parameters are related to each other by $a_T = b_T$, $a_O \approx b_O \approx \sqrt{2}a_T$ (orthorhombic lattice parameters $c_O > a_O > b_O$ for both the 1111-type and 122-type compounds) [Johnston (2010)].

respective tetragonal-orthorhombic transition temperature in $A\text{Fe}_2\text{As}_2$ (A = Ca, Sr, Ba) [Tanatar et al. (2009)] and $\text{Ba}(\text{Fe}_{0.985}\text{Co}_{0.015})_2\text{As}_2$ [Chu et al. (2010)]. The twin boundaries run along the orthorhombic [110] and [1$\bar{1}$0] directions (tetragonal [100] and [010] directions) and form planes that traverse the materials parallel to the c-axis and are separated in the $a-b$ plane by $\approx 10-50$ μm. Transmission electron microscopy of the $A\text{Fe}_2\text{As}_2$ compounds gives similar results except that the twin boundaries are separated by only $0.1-0.4$ μm [Ma et al. (2009)]. In addition, a fine tweed pattern is found in CaFe_2As_2 [Ma et al. (2009)]. It is not clear why optical and electron microscopies give different results for the twin boundary spacing. The reason is possibly associated with the sample preparation needed for the transmission electron microscope measurements that require extremely thin samples.

Within an MX_4 tetrahedron where M is the transition metal atom and X is a pnictogen (Pn = P, As, Sb, Bi) or chalcogen (Ch = S, Se, Te), there is a twofold $X-M-X$ bond angle where the two X atoms are on the same side of the M atom layer along the c axis, and a fourfold $X-M-X$ bond angle where the two X atoms are on opposite sides of the M layer. The twofold and fourfold $X-M-X$ bond angles are given by [Nath et al. (2009)]

$$\theta_2 = \arccos[\frac{-\frac{\alpha^2}{4}+(z-\alpha)^2c^2}{r^2}],\ (\texttt{twofold})$$

$$\theta_4 = \arccos[\frac{-(z-\alpha)^2c^2}{r^2}],\ (\texttt{fourfold}) \tag{2.1}$$

where

$$r^2 = \frac{\alpha^2}{4}+(z-\alpha)^2c^2, \tag{2.2}$$

and $\alpha = 0$, 1/4, 1/2 and 1 for the FeSe-type (11-type), $BaFe_2As_2$-type (122-type), LaFeAsO-type (1111-type) and LiFeAs (111-type) structures, respectively. Here, α and c are the tetragonal lattice parameters, z is the c-axis position parameter of the X atom in a unit cell of the respective structure (e.g. $z \approx 0.25$ in FeSe, $z \approx 0.35$ in $BaFe_2As_2$, $z \approx 0.65$ in LaFeAsO, and $z \approx 0.75$ in LiFeAs), and r is the nearest-neighbor $M - X$ distance within an M-centered MX_4 tetrahedron (all four $M - X$ nearest-neighbor distances are the same in each of the structures). The average bond angle for all six $X - M - X$ bonds is close to the value of 109.47° for an undistorted tetrahedron. Thus if $\theta_2 > 109.47°$ then $\theta_4 < 109.47°$, and vice versa. The M atoms in each structure form a square lattice where the fourfold nearest-neighbor $M - M$ distance in all four structures is $d_{M-M} = a/\sqrt{2}$. The distance (height h) between an M layer and either adjacent X layer is $h = |z - \alpha|c$.

CHAPTER III

Transformation of the Eilenberger Equations to a Riccati equation

The vortex core of traditional high-κ superconductors is well described by the Bardeen-Stephen model [Bardeen and Stephen (1965)] which represents the core by a region of normal electrons. The Bardeen-Stephen model is justified as long as the mean free path, l, is much shorter than the core size, so that the motion of an electron gets randomized before it leaves the core. This condition is not fulfilled in high-T_c superconductors which are generally clean superconductors with $l > \xi_{\|}$. The core of a vortex in a clean superconductor was first studied in the classic papers of Caroli, Matricon, and deGennes [Caroli et al. (1964, 1965)]. These authors calculated the spectrum of quasiparticle states in the core, and showed that electrons and holes form bound states at energies below the bulk energy gap. Further early studies of the excitation spectrum in the core can be found in Refs. [Bardeen et al. (1969)] and [Kramer and Pesch (1974)]. In particular, Bardeen $et\ al.$ [Bardeen et al. (1969)] estimated the bound-state contribution to the circulating current of a vortex and noted that the bound states were most important in weakly type-II superconductors ($\kappa \simeq 1$), i.e., when the current is confined to the core region, $r \lesssim \xi$.

Theoretical work was stimulated by the direct observation of core states in $NbSe_2$ by scanning tunneling spectroscopy (STS) [Hess et al. (1989)]. The report of STS in YBCO [Renner and Ø. Fischer (1995)] provided new information on the excitation spectrum of vortices in the high-T_c cuprates. Consequently, theoretical efforts focused on the tunneling density of states of bound states in isolated vortices and vortex lattices [Klein (1990); Gygi and Schluter (1990)]. These calculations showed that the bound states in the core have a different nature compared with the usual quantum mechanical bound states in a potential well. The core states are coherent superpositions of particle states and hole states, and are formed by repeated Andreev scattering from the pair potential (order parameter) in the core. Andreev scattering is a process of "retroreflection" of excitations: spatial variations of the amplitude or the phase of the order parameter induce branch conversion of electronlike excitations into holelike excitations, and vice versa. Bound states occur at energies at which the phases of multiply reflected electronlike and holelike states interfere constructively. The charge current carried by an incoming electron and an outgoing Andreev reflected hole is identical because the reversal of the velocity in an Andreev reflection process is compensated by the reversal of the charge due to electron-hole conversion. Consequently, Andreev bound states can transport a charge current, unlike bound states in a potential well. Charge conservation requires that the current carried by the bound states inside the core is transported outside the core by bulk supercurrents. This leads to an interplay between supercurrents flowing past the core and the bound states in the core. Hence,

the physics of the "normal core" in clean superconductors is basically the physics of the bound states in contact and intimate exchange with the superconducting environment outside the core.

Consider a stack of "pancake" vortices forming an isolated vortex line whose axis is oriented perpendicular to the layers. A supercurrent in homogeneous superconductors is distributed over all continuum states. These states exhibit Doppler shifts of their energies, $\delta\epsilon = \mathbf{v}_f \cdot \mathbf{p}_s$, in the presence of a phase gradient in the order parameter (or superfluid momentum, $\mathbf{p}_s = (\hbar/2)\nabla\chi - (e/c)\mathbf{A}$). The total current can be obtained by adding the contributions of states with positive shifts from quasiparticles comoving with the flow and the contributions with negative shifts from quasiparticles that are countermoving relative to the flow field. The currents in the core have a very different spectral distribution from bulk supercurrents. The continuum states (scattering states) show smeared out Doppler shifts, and contribute very little to the total current. The dominant contributions to the circulating currents around the vortex center, as well as the currents through the core, come from Andreev bound states. Hence, the physics of vortex cores in clean superconductors ($\xi_\parallel \ll l$) is very different from the physics of the vortex core in a dirty superconductor ($l \ll \xi_\parallel$), which is well described by a continuum of normal electronic states. The bound states react sensitively to the environment outside of the core. This leads to a coupling of the collective degrees of freedom in the London range of the vortex and the bound states in the core, which will produce a rich spectrum of largely unexplored dynamical phenomena.

There are two versions of a quasiclassical formulation of the BCS theory of superconductivity: (a) Andreev's theory [Andreev (1964)] which represents the quasiclassical limit of Bogolyubov's equations [Bogolyubov et al. (1958)], and (b) the quasiclassical theory of Eilenberger [Eilenberger (1968)], Larkin and Ovchinnikov [Larkin and Ovchinnikov (1969)] which represents the quasiclassical limit of Gorkov's Green's function theory. Andreev's theory and the quasiclassical theory are essentially equivalent for clean superconductors, and in this limit the choice of approach is largely a matter of taste. However, the quasiclassical theory has a wider range of application. It is the generalization of Landau's Fermi-liquid theory to the superconducting state, and is capable of describing a broader range of superconducting materials and phenomena, such as dirty superconductors or superconductors with short inelastic lifetimes (strong-coupling superconductors) [Rainer and Sauls (1995)].

Quasiclassical approach

According to the BCS theory of superconductivity the quasiparticle excitations above the Cooper pairing groundstate depend on spin ($\downarrow$ or $\uparrow$) and also on a particle-hole index (+ or -) which indicates the flight direction of a quasiparticle (parallel or antiparallel to the Fermi velocity v_F). Coherent superpositions of such excitations form wave packets that transport energy, momentum, charge and spin inside a superconductor.

In metals and alloys of interest to technical applications of superconductivity the Cooper pairs display an even parity symmetry (spin singlet), and often the influence of paramagnetic effects (Zeeman splitting, Pauli limiting, spinorbit coupling etc.) may be ignored. Then spin and particle-hole indices may be identified. As a result the 4×4-matrix equations of superconductivity may be simplified to 2×2-matrix equations.

It is known that the characteristic length to heal a local (static) perturbation of the Cooper pairing amplitude $\Delta(\mathbf{r}, \mathbf{p}_F)$ in a superconductor (due to the presence of an impurity, a vortex line, an interface etc.) is approximately $\xi = \hbar v_F/\Delta_\infty$, and often the quasiclassical condition $k_F\xi \gg 1$ is

fulfilled, where **r** refers to a point in position space (center of mass of a Cooper pair), and $p_F = \hbar \mathbf{k}_F$ denotes a point on the Fermi surface (FS).

Then, as first shown by Eilenberger [Eilenberger (1968)] and Larkin and Ovchinnikov [Larkin and Ovchinnikov (1969)], the relevant part of the physical information coded in quantum mechanical expectation values (for example the charge density, the current, the pressure functional etc.) may be calculated more efficiently with the help of the quasiclassical propagator

$$\hat{g}(\mathbf{r}; \mathbf{p}_F, i\varepsilon_n) = \begin{pmatrix} g(\mathbf{r}; \mathbf{p}_F, i\varepsilon_n) & f(\mathbf{r}; \mathbf{p}_F, i\varepsilon_n) \\ \bar{f}(\mathbf{r}; \mathbf{p}_F, i\varepsilon_n) & \bar{g}(\mathbf{r}; \mathbf{p}_F, i\varepsilon_n) \end{pmatrix}. \tag{3.1}$$

The quasiclassical propagator is, by definition, just the Green's function of the Gorkov theory of superconductivity in a form where it has been integrated with respect to the kinetic energy of the quasiparticles [Andreev (1964)]. Remarkably, $\hat{g}(\mathbf{r}; \mathbf{p}_F, i\varepsilon_n)$ may be calculated also directly solving a transport type system of ordinary differential equations (the right hand side is a commutator):

$$-i\hbar \mathbf{v}_F \cdot \nabla \hat{g}(\mathbf{r}; \mathbf{p}_F, i\varepsilon_n) = \left[\begin{pmatrix} i\varepsilon_n + \mathbf{v}_F \cdot \frac{e}{c}\mathbf{A}(\mathbf{r}) & -\Delta(\mathbf{r}, \mathbf{p}_F) \\ \Delta^\dagger(\mathbf{r}, \mathbf{p}_F) & -i\varepsilon_n - \mathbf{v}_F \cdot \frac{e}{c}\mathbf{A}(\mathbf{r}) \end{pmatrix}, \quad \hat{g}(\mathbf{r}; \mathbf{p}_F, i\varepsilon_n) \right]. \tag{3.2}$$

The physical solution to this equation must also fulfill a normalization condition:

$$\hat{g}(\mathbf{r}; \mathbf{p}_F, i\varepsilon_n) \cdot \hat{g}(\mathbf{r}; \mathbf{p}_F, i\varepsilon_n) = -\pi^2 \cdot \hat{1}. \tag{3.3}$$

General symmetries of the Gorkov Green's functions imply corresponding symmetries of the quasiclassical propagator:

$$\bar{f}(\mathbf{r}; \mathbf{p}_F, i\varepsilon_n) = -f^*(\mathbf{r}; \mathbf{p}_F, -i\varepsilon_n), \tag{3.4}$$
$$\bar{g}(\mathbf{r}; \mathbf{p}_F, i\varepsilon_n) = g(\mathbf{r}; -\mathbf{p}_F, -i\varepsilon_n), \tag{3.5}$$
$$f(\mathbf{r}; -\mathbf{p}_F, -i\varepsilon_n) = f(\mathbf{r}; \mathbf{p}_F, i\varepsilon_n), \tag{3.6}$$
$$g(\mathbf{r}; \mathbf{p}_F, i\varepsilon_n) = g^*(\mathbf{r}; \mathbf{p}_F, -i\varepsilon_n). \tag{3.7}$$

In equilibrium the quasiclassical propagator displays also a particle-holesymmetry:

$$\bar{g}(\mathbf{r}; \mathbf{p}_F, i\varepsilon_n) = -g(\mathbf{r}; \mathbf{p}_F, i\varepsilon_n). \tag{3.8}$$

This means that the trace of $\hat{g}(\mathbf{r}; \mathbf{p}_F, i\varepsilon_n)$ vanishes. As a traceless 2×2-matrix the square of $\hat{g}$ should be equal to a multiple of unity:

$$\hat{g}^2 = \hat{g}(\mathbf{r}; \mathbf{p}_F, i\varepsilon_n) \cdot \hat{g}(\mathbf{r}; \mathbf{p}_F, i\varepsilon_n) = C \cdot \hat{1}. \tag{3.9}$$

Using the fact, that $\hat{g}^2$ is a solution to the Eilenberger equations (provided $\hat{g}$ is a solution), it follows that $-i\hbar \mathbf{v}_F \cdot \nabla C = 0$, i.e. the scalar C is necessarily a constant along a straight line orientated parallel to the Fermi velocity v_F. But C could still be a function of the form $C = C(\mathbf{r} \wedge \mathbf{v}_F; \mathbf{p}_F, i\varepsilon_n)$. The normalization condition Eq. (3.3) fixes C such that $\hat{g}^2 = -\pi^2 \cdot \hat{1}$ for all straight lines orientated parallel to $\mathbf{v}_F$, and this for all Fermi momenta $\mathbf{p}_F$ on the Fermi surface and also for all Matsubara frequency $i\varepsilon_n$. The particular value $C = -\pi^2$ is chosen in order to achieve consistency with the functional form of the quasiclassical propagator in the bulk.

In thermal equilibrium the pair potential $\Delta(\mathbf{r}, \mathbf{p}_F)$, the electrical current $\mathbf{J}(\mathbf{r})$ associated with a (stationary) flow of quasiparticles, the local density of states $N(\mathbf{r}, E)$, the Gibbs free energy G_S of the superconducting state for weak coupling [Bardeen et al. (1969)], and other observables may be directly calculated using the quasiclassical propagator:

$$\Delta(\mathbf{r}, \mathbf{p}_F) = \int_{FS} d\mathbf{p}'_F N_{FS}(\mathbf{p}'_F) V(\mathbf{p}_F, \mathbf{p}'_F) \cdot K_B T \sum_{|\varepsilon_n|<\omega_c} f(\mathbf{r}; \mathbf{p}'_F, i\varepsilon_n), \tag{3.10}$$

$$\mathbf{J}(\mathbf{r}) = \frac{K_B}{\hbar} T \sum_{\varepsilon_n} \int_{FS} d\mathbf{p}'_F N(\mathbf{p}'_F) \mathbf{v}'_F g(\mathbf{r}; \mathbf{p}'_F, i\varepsilon_n), \tag{3.11}$$

$$N(\mathbf{r}, E) = -\frac{1}{\pi} \int_{FS} d\mathbf{p}'_F N(\mathbf{p}'_F) \mathtt{Im}(\mathbf{r}; \mathbf{p}'_F, i\varepsilon_n \to E + i0^+), \tag{3.12}$$

$$G_s(T) = \int d\mathbf{r} \begin{bmatrix} -2T \cdot \int_{-\infty}^{\infty} dE N(\mathbf{r}, E) \cdot \ln(e^{\frac{E}{2T}} + e^{\frac{-E}{2T}}) \\ + \int_{FS} d\mathbf{p}_F \int_{FS} d\mathbf{p}'_F \Delta^\dagger(\mathbf{r}, \mathbf{p}_F) \circ (V^{-1})_{\mathbf{p}_F, \mathbf{p}'_F} \circ \Delta(\mathbf{r}, \mathbf{p}'_F) \\ + \frac{1}{8\pi} (\nabla \wedge \mathbf{A}(\mathbf{r}) - \mathbf{B}_{ext}(\mathbf{r}))^2 \end{bmatrix}. \tag{3.13}$$

In these expressions the function $N_{FS}(\mathbf{p}_F)$ denotes the (angle resolved) density of states in the normal phase at the Fermi level. This function typically enters as a weight function into Fermi surface integrals (FS denotes the Fermi surface) of the Eilenberger propagator. In the isotropic case $N_{FS}(\mathbf{p}_F)$ simplifies to the usual constant $N(0)$.

The calculation of Fermi surface integrals of the Eilenberger propagator becomes comparatively simple in the bulk, where the pair potential, $\Delta(\mathbf{p}_F)$, is independent on position $\mathbf{r}$, and where the quasiclassical propagator assumes the form:

$$\hat{g}(\mathbf{p}_F, i\varepsilon_n) = \frac{-\pi}{\sqrt{\varepsilon_n^2 + |\Delta(\mathbf{p}_F)|^2}} \begin{pmatrix} i\varepsilon_n & -\Delta(\mathbf{p}_F) \\ \Delta(\mathbf{p}_F)^\dagger & -i\varepsilon_n \end{pmatrix}. \tag{3.14}$$

A considerably more complicated problem is posed when the pair potential depends on position $\mathbf{r}$, for instance near a surface, in the vicinity of an implanted impurity or ion, or around a flux line in a type-II superconductor.

Usually the solution $\hat{g}(\mathbf{r}; \mathbf{p}_F, i\varepsilon_n)$ of the Eilenberger equations must be found numerically. But the task is more difficult than just solving a differential equation. To determine the pair potential $\Delta(\mathbf{r}, \mathbf{p}_F)$ and the magnetic field $\mathbf{B}(\mathbf{r}) = \nabla \times \mathbf{A}(\mathbf{r})$ from the (magnetostatic) Maxwell Equation, $\nabla \times \mathbf{B}(\mathbf{r}) = \frac{4\pi}{c} \mathbf{J}(\mathbf{r})$, one needs to solve a (nonlinear) selfconsistency problem, since $\mathbf{J}(\mathbf{r})$ and $\Delta(\mathbf{r}, \mathbf{p}_F)$ depend themselves on $\hat{g}(\mathbf{r}; \mathbf{p}_F, i\varepsilon_n)$.

Eilenberger equations along a characteristic line

First a layered material assuming normal axis parallel to $\hat{\mathbf{c}}$ was considered, for example, a Fermi velocity $\mathbf{v}_F$ that is orientated predominantly within the ab-plane (Fermi circle). Let the triade $\{\hat{\mathbf{a}}, \hat{\mathbf{b}}, \hat{\mathbf{c}}\}$

span an orthonormal basis in the λ_{ab} frame, while θ denotes the angle the Fermi velocity $\mathbf{v}_F$ makes with the $\hat{\mathbf{a}}$-axis. Clearly, along a straight line

$$\mathbf{r}(x) = x\hat{\mathbf{v}} + y\hat{\mathbf{u}} \equiv \tag{3.15}$$

$$\equiv r_a(x)\hat{\mathbf{a}} + r_b(x)\hat{\mathbf{b}}, \tag{3.16}$$

$$-\infty < x < \infty$$

with $\hat{\mathbf{v}}$ and $\hat{\mathbf{u}}$ denoting unit vectors (orientated parallel and orthogonal to $\mathbf{v}_F$, respectively),

$$\hat{\mathbf{v}} = \cos(\theta)\hat{\mathbf{a}} + \sin(\theta)\hat{\mathbf{b}}, \tag{3.17}$$

$$\hat{\mathbf{u}} = -\sin(\theta)\hat{\mathbf{a}} + \cos(\theta)\hat{\mathbf{b}}, \tag{3.18}$$

the directional derivative $\mathbf{v}_F \cdot \nabla$ in the Eilenberger Equation Eq. (3.2) is equivalent to an ordinary derivative:

$$\hbar\mathbf{v}_F \cdot \nabla\hat{g}(\mathbf{r}; \mathbf{p}_F, i\varepsilon_n) = \hbar\mathbf{v}_F \frac{\partial}{\partial x}\hat{g}[\mathbf{r}(x); \mathbf{p}_F, i\varepsilon_n]. \tag{3.19}$$

The θ-dependent parameter y associated with such a characteristic line $\mathbf{r}(x)$ (see Eq. (3.15)) has the natural meaning of an impact parameter. The straight line $\mathbf{r}(x)$ intersects with a fixed position point

$$\mathbf{r} = r_a(x)\hat{\mathbf{a}} + r_b(x)\hat{\mathbf{b}}, \tag{3.20}$$

where the solution $\hat{g}(\mathbf{r}; \mathbf{p}_F, i\varepsilon_n)$ is sought at the particular parameter value $x = x_P$. Introducing polar coordinates,

$$r_a + ir_b = \sqrt{r_a^2 + ir_b^2} \cdot e^{i\phi}, \tag{3.21}$$

it is evident that

$$r_a(x) + ir_b(x) = (x + iy)e^{i\theta}, \tag{3.22}$$

and

$$x_P + iy = \sqrt{r_a^2 + ir_b^2} \cdot e^{i(\phi-\theta)}. \tag{3.23}$$

The extension to 3-dimensions is straightforward. For instance, for a spherical Fermi surface the unit vectors $\hat{\mathbf{v}}$ and $\hat{\mathbf{u}}$ are parametrised by two angles, the azimutal angle $\theta \in [0, 2\pi)$ and the polar angle $\chi \in [0, \pi)$, respectively:

$$\hat{\mathbf{v}} = \sin(\chi)[\cos(\theta)\hat{\mathbf{a}} + \sin(\theta)\hat{\mathbf{b}}] + \cos(\chi)\hat{\mathbf{c}}, \tag{3.24}$$

$$\hat{\mathbf{u}} = \sin(\chi)[-\sin(\theta)\hat{\mathbf{a}} + \cos(\theta)\hat{\mathbf{b}}] = \frac{\partial}{\partial\theta}\hat{\mathbf{v}}. \tag{3.25}$$

Again, along a straight line, $\mathbf{r}(x) = x\hat{\mathbf{v}} + y\hat{\mathbf{u}} + z\hat{\mathbf{v}} \wedge \hat{\mathbf{u}}$, the directional derivative in the Eilenberger equations becomes just an ordinary derivative. Making the identification $\mathbf{r} \equiv r_a\hat{\mathbf{a}} + r_b\hat{\mathbf{b}} + r_c\hat{\mathbf{c}} = \mathbf{r}(x_P)$ explicit expressions for x_P and both 'impact' parameters y and z in terms of θ, χ and the cartesian coordinates r_a, r_b, r_c of the fixed point $\mathbf{r}$ in position space are easily derived.

Finally, the notation is simplified by dropping the functional dependence of Δ, $\mathbf{A}$ and $\hat{g}$ on arguments that stay constant as x varies from $-\infty$ to ∞:

$$\Delta(x) = \Delta[\mathbf{r}(x), \mathbf{p}_F], \tag{3.26}$$

$$i\tilde{\varepsilon}_n(x) = i\varepsilon_n + \mathbf{v}_F \cdot \frac{e}{c}\mathbf{A}[\mathbf{r}(x)], \tag{3.27}$$

$$\hat{g}(x) = \hat{g}[\mathbf{r}(x); \mathbf{p}_F, i\varepsilon_n]. \tag{3.28}$$

Riccati parametrization of Eilenberger propagator

Any traceless 2×2-matrix may be expanded into the basis

$$\hat{K}_3 = \frac{1}{2}\hat{\tau}_3, \tag{3.29}$$

$$\hat{K}_\pm = -\frac{i}{2} \cdot (\hat{\tau}_1 \pm i\hat{\tau}_2), \tag{3.30}$$

($\hat{\tau}_1$, $\hat{\tau}_2$, and $\hat{\tau}_3$ are standard 2×2-Pauli matrices). It should be noted that

$$[\hat{K}_+, \hat{K}_-] = -2\hat{K}_3, \tag{3.31}$$

$$[\hat{K}_3, \hat{K}_\pm] = \pm\hat{K}_\pm. \tag{3.32}$$

The Eilenberger equations may then be rewritten along a characteristic line $\mathbf{r}(x)$ orientated parallel to the Fermi velocity $\mathbf{v}_F$ in the form:

$$\hbar v_F \frac{\partial}{\partial x}\hat{g}(x) = [-2\tilde{\varepsilon}_n(x)\hat{K}_3 + \Delta(x)\hat{K}_+ - \Delta^\dagger(x)\hat{K}_-, \hat{g}(x)]. \tag{3.33}$$

The following 2×2 system of ordinary differential equations for an auxiliary propagator $\hat{Y}(x)$ (fundamental system) was considered:

$$\hbar v_F \frac{\partial}{\partial x}\hat{Y}(x) = (-2\tilde{\varepsilon}_n(x)\hat{K}_3 + \Delta(x)\hat{K}_+ - \Delta^\dagger(x)\hat{K}_-)\hat{Y}(x), \tag{3.34}$$

$$\hat{Y}(0) = \hat{Y}_0. \tag{3.35}$$

The initial values for $\hat{Y}(x)$ at $x = 0$ may be prescribed in terms of a (yet unknown) constant 2×2 matrix $\hat{Y}_0$ of rank 2. The physical propagator $\hat{g}$ can be reconstructed, the one that solves the Eilenberger equations and respects the normalization condition, $\hat{g}(x) \cdot \hat{g}(x) = -\pi^2 \cdot \hat{1}$, from the fundamental system $\hat{Y}(x)$:

$$\hat{g} = -\pi i \cdot \hat{Y}(x) \cdot 2\hat{K}_3 \cdot \hat{Y}^{-1}(x). \tag{3.36}$$

By putting x at the end of the calculations to the particular value x_P, the physical propagator (i.e. the input into the self consistency equations) is recovered:

$$\hat{g}(x_P) = \hat{g}[\mathbf{r}(x_P); \mathbf{p}_F, i\varepsilon_n] \equiv \hat{g}[\mathbf{r}; \mathbf{p}_F, i\varepsilon_n]. \tag{3.37}$$

The commutator in the Eilenberger equations implies the existence of several invariants along the characteristic line $\mathbf{r}(x)$. For example, if the normalization condition Eq. (3.3) is fulfilled at a particular fixed point $\mathbf{r}(x_0)$, it will be fulfilled everywhere along the line $\mathbf{r}(x)$. Likewise, the determinant $\det\hat{g}(x)$ and the trace $\mathrm{tr}\hat{g}(x)$ remain constant for $-\infty < x < \infty$.

Next the 2×2-matrix $\hat{Y}(x)$ was parameterize in the form

$$\hat{Y} = \exp(a_+\hat{K}_+)\exp(a_3\hat{K}_3)\exp(a_-\hat{K}_-), \tag{3.38}$$

in terms of three unknown functions $a_3(x)$, $a_+(x)$ and $a_-(x)$ (Euler type 'angles' in particle-hole space). The physical propagator, Eq. (3.36), assumes then the form

$$\hat{g}(x) = -\pi i \cdot \begin{bmatrix} [1 - 2a_-(x)a_+(x)\text{exp}(-a_3(x))] \cdot 2\hat{K}_3 \\ +a_+(x) \cdot [a_-(x)a_+(x)\text{exp}(-a_3(x)) - 1] \cdot 2\hat{K}_+ \\ +a_-(x) \cdot \text{exp}(-a_3(x)) \cdot 2\hat{K}_- \end{bmatrix}. \tag{3.39}$$

One finds from the differential equation for $\hat{Y}(x)$ a set of three coupled differential equations for $a_3(x)$, $a_+(x)$ and $a_-(x)$:

$$\dot{a}_3 - 2a_+ \exp(-a_3)\dot{a}_- = -\frac{2\tilde{\varepsilon}_n}{\hbar v_F}, \tag{3.40}$$

$$\exp(-a_3)\dot{a}_- = -\frac{\Delta^\dagger}{\hbar v_F}, \tag{3.41}$$

$$\dot{a}_+ - a_+\dot{a}_3 + a_+^2 \exp(-a_3)\dot{a}_- = \frac{\Delta}{\hbar v_F}. \tag{3.42}$$

Here $\dot{a}(x) \equiv \frac{\partial}{\partial x}a(x)$. It is readily seen that the three equations decouple, and that a_- and a_3 may be expressed in terms of a_+ only:

$$a_3(x) = -\frac{2}{\hbar v_F}[\tilde{\varepsilon}_n x + \int_0^x ds\Delta^\dagger(s)a_+(s)] + a_3^{(0)}, \tag{3.43}$$

$$a_-(x) = -\frac{1}{\hbar v_F} \cdot \int_0^x ds\Delta^\dagger(s)\exp[a_3(s)] + a_-^{(0)}.$$

The differential equation that remains to be solved for $a_+(x)$ is a Riccati equation:

$$\hbar v_F \frac{\partial}{\partial x}a_+(x) + [2\tilde{\varepsilon}_n + \Delta^\dagger(x)a_+(x)]a_+(x) - \Delta(x) = 0. \tag{3.44}$$

However, the accurate numerical calculation of the nested integral for $a_-(x)$ is time consuming (even on a fast computer). To overcome this difficulty one trick can be used. Let $\hat{g}_A(x)$ and $\hat{g}_B(x)$ be two different solutions of the Eilenberger equations. Then not only the linear combination $c_A\hat{g}_A(x) + c_B\hat{g}_B(x)$ is a solution, but also the products $\hat{g}_B(x) \cdot \hat{g}_A(x)$ and $\hat{g}_A(x) \cdot \hat{g}_B(x)$ are solutions as well. For example, the linear combination $\hat{g}_B(x) \cdot \hat{g}_A(x) - \hat{g}_A(x) \cdot \hat{g}_B(x)$ solves the Eilenberger equations and fulfills the necessary condition $\text{tr}\hat{g}(x) = 0$.

Two particular zero trace solutions to the Eilenberger equations are:

$$\hat{g}_A(x) = \hat{Y}_A(x) \cdot \hat{K}_- \cdot [\hat{Y}_A(x)]^{-1}, \tag{3.45}$$

$$\hat{g}_B(x) = \hat{Y}_B(x) \cdot \hat{K}_+ \cdot [\hat{Y}_B(x)]^{-1}, \tag{3.46}$$

with

$$\hat{Y}_A = \exp(a_+\hat{K}_+)\exp(a_3\hat{K}_3)\exp(a_-\hat{K}_-), \tag{3.47}$$

$$\hat{Y}_B = \exp(b_-\hat{K}_-)\exp(b_3\hat{K}_3)\exp(b_+\hat{K}_+), \tag{3.48}$$

denoting two equivalent fundamental systems $\hat{Y}_A(x)$ and $\hat{Y}_B(x)$. The different order of factors in the defining expressions for $\hat{Y}_A$ and $\hat{Y}_B$ serves the purpose to avoid the difficult terms $a_-(x)$ and

$b_+(x)$ in the expressions for $\hat{g}_A$ and $\hat{g}_A$. The evaluation of nested integrals, see Eq. (3.43), is then not necessary.

The set of equations fulfilled by $b_3(x)$ and $b_\pm(x)$ is only slightly different from the one for $a_3(x)$, $a_+(x)$ and $a_-(x)$:

$$\dot{b}_3 + 2b_- \exp(b_3)\dot{b}_+ = -\frac{2\tilde{\varepsilon}_n}{\hbar v_F}, \tag{3.49}$$

$$\exp(b_3)\dot{b}_+ = \frac{\Delta}{\hbar v_F}, \tag{3.50}$$

$$\dot{b}_- + b_-\dot{b}_3 + b_-^2 \exp(b_3)\dot{b}_+ = -\frac{\Delta^\dagger}{\hbar v_F}. \tag{3.51}$$

Here $\dot{b}(x) \equiv \frac{\partial}{\partial x} b(x)$. It is readily seen that the three equations decouple, and that $b_+(x)$ and $b_3(x)$ may be expressed in terms of $b_-(x)$ only :

$$b_3(x) = -\frac{2}{\hbar v_F}[\tilde{\varepsilon}_n x + \int_0^x ds\Delta(s)b_-(s)] + b_3^{(0)}, \tag{3.52}$$

$$b_+(x) = \frac{1}{\hbar v_F} \cdot \int_0^x ds\Delta(s)\exp[-b_3(s)] + b_+^{(0)}. \tag{3.53}$$

The differential equation to be solved for $b_-(x)$ is also a Riccati equation:

$$\hbar v_F \frac{\partial}{\partial x} b_-(x) - [2\tilde{\varepsilon}_n + \Delta(x)b_-(x)]b_-(x) + \Delta^\dagger(x) = 0. \tag{3.54}$$

Any solution of this differential equation is related to the Riccati equation Eq. (3.44) via a reciprocity relation: If $a_+(x)$ solves Eq. (3.44), then

$$b_-(x) = -\frac{1}{a_+(x)}, \tag{3.55}$$

solves Eq. (3.54).

From the defining equations, Eq. (3.45) and Eq. (3.46), the following explicit expressions were found:

$$\hat{g}_A = \exp(-a_3)(\hat{K}_- - 2a_+\hat{K}_3 + a_+^2\hat{K}_+), \tag{3.56}$$

$$\hat{g}_B = \exp(b_3)(\hat{K}_+ + 2b_-\hat{K}_3 + b_-^2\hat{K}_-). \tag{3.57}$$

Note that the square of $\hat{g}_A$ and $\hat{g}_B$ vanishes identically,

$$\hat{g}_A \cdot \hat{g}_A = \hat{0} = \hat{g}_B \cdot \hat{g}_B, \tag{3.58}$$

because $\hat{K}_\pm^2 \equiv 0$. For $x \to \pm\infty$ the propagators $\hat{g}_A$ and $\hat{g}_B$ 'explode', i.e.

$$\hat{g}_{A,B} \sim \exp(\pm\frac{2x}{\hbar v_F}\sqrt{\tilde{\varepsilon}_n + |\Delta|^2}). \tag{3.59}$$

On the other hand, the commutator $[\hat{g}_A(x), \hat{g}_B(x)]$ remains bounded in the limit $x \to \pm\infty$. The observation that a bounded solution to the Eilenberger equations may be constructed using the commutator of two unbounded solutions $\hat{g}_A(x)$ and $\hat{g}_B(x)$ is the well known 'explosion' trick [Thuneberg et al. (1982)].

The general (particle-hole symmetric) solution to the Eilenberger equations (3.2) may be given in the form

$$\hat{g}(x) = c_A \hat{g}_A(x) + c_B \hat{g}_B(x) + [\hat{g}_A(x), \hat{g}_B(x)]. \tag{3.60}$$

Here, c_A and c_B represent initial values, $b_3(0)$ and $a_3(0)$, to the functions $b_3(x)$ and $a_3(x)$, respectively. Of course, in an unbounded region exploding solutions must be forbidden. Then the physical propagator $\hat{g}$ must be written, on either side of the turning point $x = 0$, as a superposition of a decaying solution and a bounded solution:

$$\hat{g}(x) = \begin{cases} c_B \hat{g}_B(x) + [\hat{g}_A(x), \hat{g}_B(x)] & \text{if } x > 0 \\ c_A \hat{g}_A(x) + [\hat{g}_A(x), \hat{g}_B(x)] & \text{if } x < 0 \end{cases}. \tag{3.61}$$

The square of $\hat{g}(x)$ is in this case independent on the constants c_A and c_B:

$$\hat{g}(x) \cdot \hat{g}(x) = [\hat{g}_A(x), \hat{g}_B(x)] \cdot [\hat{g}_A(x), \hat{g}_B(x)] = -\pi^2 \cdot \hat{1}. \tag{3.62}$$

It is not difficult to show, that $c_A = 0 = c_B$, provided the propagators $\hat{g}_A(x)$ and $\hat{g}_B(x)$ are continuous at $x = 0$.

In fact, if the contrary was assumed: $c_A \cdot c_B \neq 0$. Then the continuity of $\hat{g}(x)$ at $x = 0$ leads to

$$c_B \hat{g}_B(0^+) + [\hat{g}_A(0^+), \hat{g}_B(0^+)] = \hat{g}(0) = c_A \hat{g}_A(0^-) + [\hat{g}_A(0^-), \hat{g}_B(0^-)]. \tag{3.63}$$

Both solutions, $\hat{g}_A(x)$ and $\hat{g}_B(x)$, are continuous at $x = 0$. Then it follows from Eq. (3.63): $c_B \hat{g}_B(0) = c_A \hat{g}_A(0)$. This implies, in turn, a vanishing commutator, $[\hat{g}_A(0), \hat{g}_B(0)] = 0$, since $\hat{g}_B(0)$ and $\hat{g}_A(0)$ become proportional. Also, the physical solution $\hat{g}(0)$ at $x = 0$ must fulfill the normalization condition, i.e. $\hat{g}(0) \cdot \hat{g}(0) = -\pi^2 \cdot \hat{1}$. But $\hat{g}_B(0) \cdot \hat{g}_B(0) = \hat{0} = \hat{g}_A(0) \cdot \hat{g}_A(0)$ according to Eqs. (3.58). This is a contradiction! Hence $c_A = 0 = c_B$.

The conclusion is that in an infinitely extended system the physical propagator $\hat{g}_B(x)$ is completely determined by the commutator of the 'exploding' solutions:

$$\hat{g}(x) = [\hat{g}_A(x), \hat{g}_B(x)] = \exp(b_3 - a_3) \cdot \begin{bmatrix} 1 - (a_+ b_-)^2 & 2ia_+(1 + a_+ b_-) \\ -2ib_-(1 + a_+ b_-) & -1 + (a_+ b_-)^2 \end{bmatrix}. \tag{3.64}$$

Then the normalization condition was check:

$$\begin{aligned} \hat{g}(x) \cdot \hat{g}(x) &= [\hat{g}_A(x), \hat{g}_B(x)] \cdot [\hat{g}_A(x), \hat{g}_B(x)] = \\ &= [g_3(x) \cdot g_3(x) + g_+(x) \cdot g_-(x)] \cdot \hat{1} = \\ &= [1 + a_+(x) b_-(x)]^4 \cdot \exp[2b_3(x) - 2a_3(x)] \cdot \hat{1} = c \cdot \hat{1}. \end{aligned} \tag{3.65}$$

Indeed, C is a constant multiple of unity:

$$\frac{\partial}{\partial x} \left\{ [1 + a_+(x) b_-(x)]^4 \cdot \exp[2b_3(x) - 2a_3(x)] \right\} = 0. \tag{3.66}$$

From the normalization condition, $C = -\pi^2$, there follows for all x (up to a sign $\pm$ that is chosen to coincide with the bulk propagator):

$$\exp[b_3(x) - a_3(x)] = \frac{-\pi i}{[1 + a_+(x)b_-(x)]^2}. \tag{3.67}$$

Then the Eilenberger propagator may be parameterized in the form:

$$\hat{g}(x) = \frac{-\pi i}{1 + a(x) \cdot b(x)} \cdot \begin{bmatrix} 1 - a(x) \cdot b(x) & 2i \cdot a(x) \\ -2i \cdot b(x) & -1 + a(x) \cdot b(x) \end{bmatrix}. \tag{3.68}$$

Here and in the following were used notation $b_-(x) \equiv b(x)$ and $a_+(x) \equiv a(x)$, since the other functions $a_-(x)$, $a_3(x)$ and $b_+(x)$, $b_3(x)$ are obsolete for the parametrization of the Eilenberger propagator. It is remarkable that the solution to the Eilenberger equations (3.2) may be given a representation where it depends just on the solution of an initial value problem to a scalar differential equation of the Riccati type [Schopohl and Maki (1995)].

To integrate the Riccati equations, (3.44) and (3.54), in a stable manner suitable initial values for the functions $b(x)$ and $a(x)$ are needed. For $i\varepsilon_n$ situated in the upper half of the complex plane the function $a(x)$ may be found in a stable manner integrating Eq. (3.44) as an initial value problem from $x = -\infty$ towards increasing x-values, while the function $b(x)$ may be found integrating Eq. (3.54) as an initial value problem from $x = +\infty$ towards decreasing x-values. The initial values for $a(x)$ at $x = -\infty$ and $b(x)$ at $x = +\infty$ are

$$a(-\infty) = \frac{\Delta(-\infty)}{\varepsilon_n + \sqrt{\varepsilon_n^2 + |\Delta(-\infty)|^2}}, \tag{3.69}$$

$$b(+\infty) = \frac{\Delta^\dagger(+\infty)}{\varepsilon_n + \sqrt{\varepsilon_n^2 + |\Delta(+\infty)|^2}}, \tag{3.70}$$

provided ε_n is in the upper half of the complex plane.

The differential equations to be solved are:

$$\hbar v_F \frac{\partial}{\partial x} a(x) + [2\tilde{\varepsilon}_n + \Delta^\dagger(x) \cdot a(x)] \cdot a(x) - \Delta(x) = 0, \tag{3.71}$$

$$\hbar v_F \frac{\partial}{\partial x} b(x) - [2\tilde{\varepsilon}_n + \Delta(x) \cdot b(x)] \cdot b(x) + \Delta^\dagger(x) = 0. \tag{3.72}$$

Sometimes knowledge of just one of the functions, say $a(x)$, along a line $\mathbf{r}(x)$ (for $-\infty < x < +\infty$) suffices to fix the other function, $b(x)$, along the same line. An illustrative example is provided by a single cylindrically symmetric vortex line, orientated parallel to $\hat{\mathbf{c}}$, and centered at the origin of the ab-plane, say at **R = 0**. Due to energetic reasons, of course, only a single quantum of circulation, $\frac{h}{2m}$, is attached to the vortex. The corresponding pair potential becomes along the straight line $r(x) = r_a(x)\hat{\mathbf{a}} + r_b(x)\hat{\mathbf{b}}$ a function of x (and also of the impact parameter y) of the form:

$$\Delta(\mathbf{r}(x), \mathbf{p}_F) = F(\sqrt{x^2 + y^2}, \theta) \cdot \frac{x + iy}{\sqrt{x^2 + y^2}} \cdot e^{i\theta}. \tag{3.73}$$

The prefactor $F(\sqrt{x^2+y^2},\theta)$ is a suitable 'form factor' to shape the vortex core. It can be seen from Eqs. (3.71) and (3.72) that in the presence of such a vortex line, $b(x)$ is related to $a(x)$ by symmetry:

$$b(x) = -a(-x)e^{-2i\theta}. \tag{3.74}$$

Using Eq. (3.68) it follows that the corresponding Eilenberger propagator $\hat{g}$ for negative x is related to the propagator for positive x by the relation:

$$\hat{g}(-x) = -e^{i\theta\hat{\tau}_3}\cdot\hat{\tau}_2\cdot\hat{g}(x)\cdot e^{i\theta\hat{\tau}_3}. \tag{3.75}$$

To determine the local density of states one needs the retarded and the advanced propagator of the quasiclassical theory. Actually, in equilibrium, only the retarded (or advanced) propagator is needed in the calculations, since both propagators are related to each other by complex conjugation. A convenient numerical method for the calculation of the retarded propagator $\hat{g}^{(\mathrm{ret})}(\mathbf{r},\theta,E)$ is to replace the discrete Matsubara frequency $i\varepsilon_n$ according to the prescription $i\varepsilon_n \to E+i0^+$, and to solve the Riccati equations, Eqs. (3.71) and (3.72), as functions of the energy E and of the impact parameters y and z.

If the denominator of the quasiclassical propagator, $1+a(x)\cdot b(x)$, becomes equal to zero at a point $\mathbf{r}(x_0)$ for a characteristic energy $E=E_b$, it vanishes indeed for all x along the trajectory $\mathbf{r}(x)$:

$$[1+a(x)\cdot b(x)] = \exp[\frac{1}{\hbar v_F}\int_{x_0}^{x} ds(\Delta(s)b(s)-\Delta^\dagger(s)a(s))]\cdot[1+a(x_0)\cdot b(x_0)]. \tag{3.76}$$

A simple proof of this relation uses differentiation with respect to x, and Eqs. (3.71) and (3.72). So, if the denominator $1+a(x_0)\cdot b(x_0)$ of the quasiclassical propagator Eq. (3.68), considered as a function of energy E, displays a simple zero at $E=E_b$, this zero, E_b, has a natural interpretation as a bound state energy, provided there exists a finite residue of the retarded propagator at $E=E_b+i0^+$.

To obtain the quasiclassical Green function, the Riccati equations (3.71) and (3.72) are solved by the Fast Fourier Transform (FFT) method. Unlike the square vortex lattice studied in [Miranović and Machida (2003)], we consider a triangular vortex lattice, for which the wave vector mesh is transformed from square to hexagonal shape [Safonchik (2007)].

CHAPTER IV

Comments on the original publications

Paper 1. Quasiclassical Eilenberger approach to the vortex state in pnictide superconductors

Magnetism in the FeAs stoichiometric compounds and its interplay with superconductivity in vortex states was studied by solving self-consistently the Bogoliubov-de Gennes equations based on a two-orbital model with including the on-site interactions between electrons in the two orbitals [Jiang et al. (2009)]. It was revealed that for the parent compound, magnetism is caused by the strong Hund's coupling, and the Fermi-surface topology aids to select the spin-density-wave (SDW) pattern. The superconducting order parameter with $s^{\pm} = \Delta_0 \cos(k_x) \cos(k_y)$ symmetry was found to be the most favorable pairing for both the electron- and hole-doped cases while the local density of states exhibits the characteristic of nodal gap for the former and full gap for the latter. In the vortex state, the emergence of the field-induced SDW depends on the strength of the Hund's coupling and the Coulomb repulsions. The field-induced SDW gaps of the finite-energy contours on the electron- and hole-pocket sides lead to the dual structures with one reflecting the SC pairing and the other being related to the SDW order.

This model does not include the self-consistent calculation of the field distribution which is the aim of this theses. The study of the full solution of the Bogoliubov-de Gennes equations is time consuming [Atkinson and Sonier (2008)]. Therefore, a simplification of the model is needed. The current theoretical opinion on the SC order parameter has converged on a nodeless $s^{\pm}$ order parameter that changes sign between the electron (e) pockets and hole (h) pockets. This order parameter comes out of both the strong- and the weak-coupling pictures of the iron-based superconductors [Mazin et al. (2008); Chubukov et al. (2008); Stanev et al. (2008); Maier et al. (2009)] and owes its origin to the pnictide Fermi surface (FS) topology of h pockets at the Γ and e pockets at the X $(\pi, 0)/(0, \pi)$ point of the unfolded Brillouin zone. The dominant scattering contributions originate from h pocket scattering at Γ to e pockets at X, yielding the $s^{\pm}$ SC order parameter for the doped case and the collinear antiferromagnetic phase in the undoped case.

In **paper 1** we apply this $s^{\pm}$ two-band model to the vortex state and solve Eilenberger equations self-consistently. We neglect antiferromagnetic ordering in the vortex core (these effects will be discussed in the comments to **paper 3**) and small anisotropy of $s^{\pm}$ state in FS, i.e., $\cos(k_x)$ and $\cos(k_y)$ are approximated by ± 1 in different FS sheets. By fitting the calculated field distribution to Eq. (1) we can find the cutoff parameter ξ_h. To do that we need the penetration depth $\lambda(T)$

which was calculated in Ref. [Vorontsov et al. (2009)]. It scales as $1/\sqrt{\rho_S(T)}$, where $\rho_S(T)$ is the superfluid density. The latter is, up to a factor, the zero frequency value of the current-current correlation function and can be written in the form [Choi and Muzikar (1989)],

$$\frac{\rho_S(T)}{\rho_{S0}} = \pi T \sum_n \frac{\tilde{\Delta}_n^2}{(\tilde{\Delta}_n^2 + \tilde{\omega}_n^2)^{3/2}}, \tag{4.1}$$

where ρ_{S0} is the superfluid density at $T = 0$ in the absence of impurities. The integrand in Eq. (4.1) is defined in terms of impurity-renormalized Matsubara energy, $\tilde{\omega}_n$, and the superconducting vertex $\tilde{\Delta}_n$. In an $s^{\pm}$ superconductor the order parameters on the hole (c) and electron (f) FS pockets are related, $\tilde{\Delta}_n^c = -\tilde{\Delta}_n^f = \tilde{\Delta}_n$ and in Born approximation,

$$i\tilde{\omega}_n = i\omega_n - \Gamma_0 g^c(\tilde{\omega}_n, \tilde{\Delta}_n) - \Gamma_\pi g^f(\tilde{\omega}_n, \tilde{\Delta}_n), \tag{4.2}$$

$$\tilde{\Delta}_n = \Delta + \Gamma_0 f^c(\tilde{\omega}_n, \tilde{\Delta}_n) + \Gamma_\pi f^f(\tilde{\omega}_n, \tilde{\Delta}_n), \tag{4.3}$$

where $\omega_n = 2\pi(2n+1)$, $\Gamma_0 = \pi n_i N_F |u_0|^2$, and $\Gamma_\pi = \pi n_i N_F |u_\pi|^2$ are are the intra- and interband impurity scattering rates, respectively ($u_{0,\pi}$ are impurity scattering amplitudes with correspondingly small, or close to $\pi = (\pi, \pi)$, momentum transfer), Δ is the SC order parameter, and functions $g^{c,f}$ and $f^{c,f}$ are ξ-integrated normal and anomalous Green′s functions for holes and electrons,

$$\begin{aligned} g^c = g^f &= \frac{-i\tilde{\omega}_n}{\sqrt{\tilde{\omega}_n^2 + \tilde{\Delta}_n^2}}, \\ f^c = -f^f &= \frac{\tilde{\Delta}_n}{\sqrt{\tilde{\omega}_n^2 + \tilde{\Delta}_n^2}}. \end{aligned} \tag{4.4}$$

Since the f function has opposite signs in two bands, Γ_π has the same effect on anomalous self-energy as the scattering on magnetic impurities in an ordinary s-wave superconductor. Following the customary path one may introduce $\eta_n = \tilde{\omega}_n/\omega_n$ and $\bar{\Delta}_n = \tilde{\Delta}_n/\eta_n$ that satisfy

$$\eta_n = 1 + \frac{\Gamma_0 + \Gamma_\pi}{\sqrt{\bar{\Delta}_n^2 + \omega_n^2}}, \tag{4.5}$$

$$\bar{\Delta}_n = \Delta(T) - 2\Gamma_\pi \frac{\bar{\Delta}_n}{\sqrt{\bar{\Delta}_n^2 + \omega_n^2}}. \tag{4.6}$$

The order parameter $\Delta(T)$ is determined by the selfconsistent equation,

$$\Delta(T) = V^{SC} 2\pi T \sum_{0<\omega_n<\omega_c} f^c(\tilde{\omega}_n, \tilde{\Delta}_n) = \pi T \sum_{0<\omega_n<\omega_c} \frac{V^{SC}\bar{\Delta}_n}{\sqrt{\bar{\Delta}_n^2 + \omega_n^2}}, \tag{4.7}$$

where V^{SC} is the $s^{\pm}$ coupling constant and ω_c is the ultraviolet cutoff. Notice that the last expression contains $\bar{\Delta}_n$ and $bare$ Matsubara frequencies ω_n. Eqs. (4.2)-(4.7) can be extended to the case when the gaps on hole and electron FS have different magnitudes.

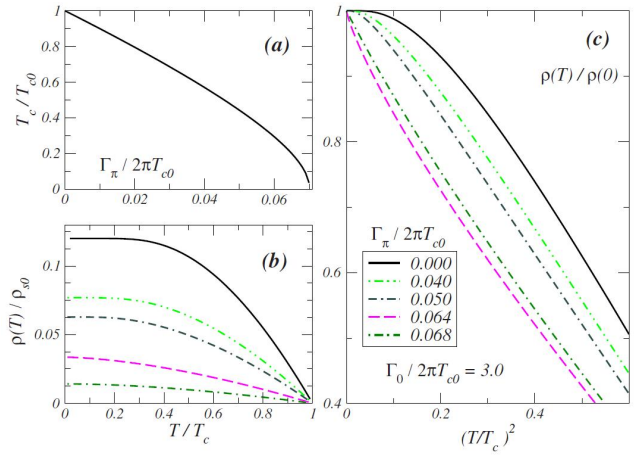

Figure 4.1: (a) Suppression of T_c by interband scattering in a two-band $(\Delta, -\Delta)$ model; (b) superfluid stiffness $\rho_S(T)$ in a dirty $s^{\pm}$ superconductor for fixed intraband impurity scattering $\Gamma_0/2\pi T_{c0} = 3$ and various interband scatterings $\zeta = \Gamma_\pi/2\pi T_{c0}$; and (c) low-$T$ plot of ρ_S vs T^2 showing near n=2 power law around onset of gapless regime [Vorontsov et al. (2009)].

Solutions of the system of Eqs. (4.6) and (4.7) give the values of $\Delta(T)$ and $\bar{\Delta}_n$. In particular, Eq. (4.6) is an algebraic equation (valid at any T) which expresses $\bar{\Delta}_n$ in terms of Δ. The latter itself depends on Γ_π because the self-consistent equation, Eq. (4.7), contains $\bar{\Delta}_n$. Without interband scattering ($\Gamma_\pi = 0$) the $\bar{\Delta}_n = \Delta = \Delta_0 = 1.76T_{c0}$, where T_{c0} and Δ_0 are the BCS transition temperature and the $T = 0$ gap in a clean superconductor. For $\Gamma_\pi \neq 0$, $\bar{\Delta}_n$ differs from Δ, and Δ differs from Δ_0. Converted to real frequencies, Eqs. (4.6) and (4.7) yield a complex function $\bar{\Delta}(\omega)$. For $2\Gamma_\pi \geq \Delta$, $\bar{\Delta}(\omega = 0)$ vanishes, i.e., superconductivity becomes gapless [Abrikosov and Gor'kov (1961)]. At the critical point $2\Gamma_\pi = \Delta$, $\bar{\Delta}(\omega) \propto (-i\omega)^{2/3}$ at small ω, at larger Γ_π, $\bar{\Delta}(\omega) = -i$ const $\omega + \boldsymbol{O}(\omega^2)$.

The results can be expressed using dimensionless parameter $\zeta = \Gamma_\pi/2\pi T_{c0}$. For equal gap magnitudes and $2\Gamma_\pi/\Delta < 1$, $y = \Delta/\Delta_0$ is the solution of $y = \exp[-\pi e^\gamma \zeta/y]$, where $\gamma \approx 0.577$ is the Euler constant [Skalski (1969)]. At a given T a gapless superconductivity emerges, when y becomes smaller than $4\zeta e^\gamma$, i.e., for $\zeta > (1/4)\exp[-(\gamma + \pi/4)] \approx 0.064$. The transition temperature obeys [Choi and Muzikar (1989); Skalski (1969)]

$$\ln(T_c/T_{c0}) = \Psi(1/2) - \Psi(1/2 + 2\zeta T_{c0}/T_c), \tag{4.8}$$

where $\Psi(x)$ is the di-Gamma function (Fig. 4.1 (a)). T_c decreases with ζ and vanishes at $\zeta_{cr} = e^{-\gamma}/8 \approx 0.07$ (i.e. $\Gamma_\pi/\Delta_0 = 1/4$). For $0.064 < \zeta < \zeta_{cr}$, $\bar{\Delta}(T, \omega) \propto i\omega$ for small ω, including $T = 0$, and thus even at $T = 0$ zero-energy density of states becomes finite and gapless superconductivity arises (at the onset, at $\zeta = 0.064$, $T_c \approx 0.22T_{c0}$, and $\Delta(0) = 0.46\Delta_0$). The ratio $2\Delta(0)/T_c$ increases with ζ and reaches 7.2 at the onset of the gapless behavior and 8.88 at $\zeta = \zeta_{cr}$ [Skalski (1969)]. A large value of $2\Delta(0)/T_c$ is often attributed to strong coupling [Scalapino (1969)] but, can also be due to impurities.

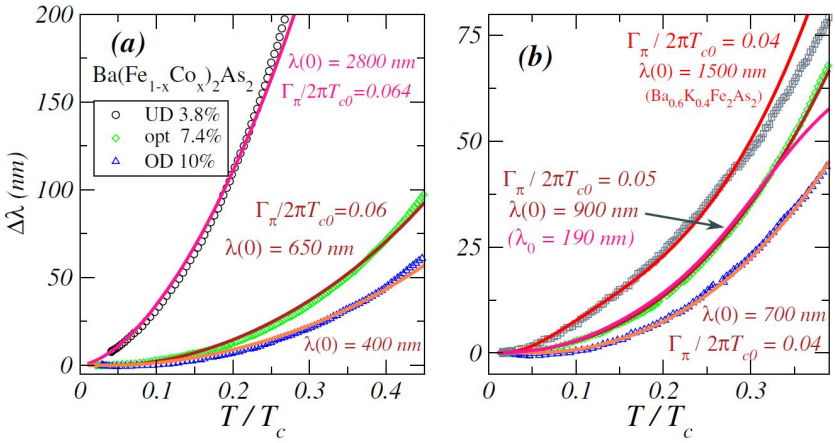

Figure 4.2: The fits to experimental data for $BaFe_2As_2$ [Martin et al. (2009)]. Only low-T data were used as at higher T the experimental $\lambda(T)$ may be influenced by sample geometry and fluctuations. (a) The data for electron-doped $BaFe_2As_2$ for optimally doped ($x = 7.4\%$) and overdoped ($x = 10\%$) samples can be fitted reasonably well using $(\Delta, -\Delta)$-model; (b) the fit of data for two Co-doped ($x = 7.3\%, 10\%$) and one K-doped samples with a phenomenological extension of the presented two-band model to the case of four gaps. The gaps are $(\Delta, -\Delta; \Delta, -\Delta_h)$ with $\Delta_h = \Delta/3, \Delta/2$. In this case the pairbreaking parameter does not need to be large. The fitting values of $T = 0$ penetration length are large, but for $x = 7.4\%$ sample a fit with inclusion of Fermi-liquid effects that reduces this parameter to $\lambda_{FL}(0) \equiv \lambda_0 \sim 190$ nm in agreement with experimental values is shown [Vorontsov et al. (2009)] .

In terms of auxiliary $\bar{\Delta}_n$ and η_n,

$$\frac{\rho_S(T)}{\rho_{S0}} = \pi T \sum_{\omega_n} \frac{\bar{\Delta}_n^2}{\eta_n (\bar{\Delta}_n^2 + \bar{\omega}_n^2)^{3/2}}. \tag{4.9}$$

In general, the value of $\rho_S(T = 0)$ and the functional form of $\rho_S(T)$ depend on both Γ_π and Γ_0 because Γ_0 is explicitly present in Eq. (4.9) via η_n given by Eq. (4.5). Impurity scattering amplitude is a decreasing function of momentum transfer, and, in general, $\Gamma_0 \gg \Gamma_\pi$, or $\Gamma_0 \gg \Delta$ (in the case of $\Gamma_\pi \sim \Delta$) and

$$\rho_S(T) \approx BT \sum_{\omega_n} \frac{\bar{\Delta}_n^2}{\bar{\Delta}_n^2 + \bar{\omega}_n^2}, \tag{4.10}$$

where $B = \pi\rho_{S0}/(\Gamma_0 + \Gamma_\pi)$. As can be seen, Γ_0 only affects the overall factor B, and all nontrivial T dependence comes from frequency and temperature dependence of $\bar{\Delta}_n$.

Several results for $\rho_S(T)$ given by Eq. (4.10) can be obtained analytically. First, near T_c, $\rho_S(T) \propto \Delta^2(T) \propto T_c - T$, i.e.,

$$\frac{\rho_S}{\rho_S(T = 0)} = B(\zeta)(1 - \frac{T}{T_c}), \tag{4.11}$$

where $\rho_S(T=0)$ is the actual zero-temperature value of ρ_S. In a clean BCS superconductor $B=2$. In the present dirty case ($\Gamma_0 \gg T_c, \Gamma_\pi$) $B(\zeta)$ is nonmonotonic in ζ and equals $B(\zeta \to 0) \approx 2.65$, $B(\zeta = 0.064) \approx 1.67$, and $B(\zeta \approx \zeta_{cr}) = 2.03$. This implies that a linear extrapolation of ρ_S from $T \approx T_c$ to $T = 0$ still yields a value significantly larger than the actual $\rho_S(0)$. Secondly, at $\zeta < 0.064$ the T dependence of $\rho_s(T)$ remains exponential at low T, $\rho_s(T) \propto e^{-\bar{\Delta}(\omega=0)/T}$ with $\bar{\Delta}(\omega=0) = \Delta_0[1-(\zeta/\zeta_{cr})^{2/3}]^{3/2}$, but at the onset of gapless superconductivity, when $\bar{\Delta}(\omega) \propto (-i\omega)^{2/3}$, $\rho_s(T) \propto T^{5/3}$ was obtained. Finally, in the gapless regime $0.064 < \zeta < \zeta_{cr}$, $\rho_s(T) \propto T^2$ was found at low T.

To obtain $\rho_S(T)$ at arbitrary T, the gap equation, Eq. (4.7), was numerically selfconsistently solved together with equations for the impurity self-energies, Eqs. (4.2) and (4.3), and the Green′s functions, Eq. (4.4); found $\Delta(T)$ and $\tilde{\omega}_n$, substituted them into Eq. (4.1), and obtained $\rho_S(T)$. Fig. 4.1 contains the results for several values of ζ.

Once the interband impurity scattering increases, the range of exponential behavior of $\rho_S(T)$ progressively shrinks to smaller T (Fig. 4.1 (b)). Outside this low T range, the temperature dependence of $\rho_S(T)$ strongly resembles T^2 behavior (see Fig. 4.1 (c)). The $T^{5/3}$ behavior at the onset of gapless superconductivity is difficult to see numerically as this power is confined to very low T, while for slightly larger T the behavior is again close to T^2. Overall, the behavior of the superfluid density in a relatively wide range of ζ is a power law T^n with n reasonably close to 2 down to quite low T.

Judging by the value of $2\Delta(0)/T_c$ [Malone et al. (2009)] , the material with the least amount of interband impurity scattering is $SmFeAsO_{1-x}F_x$, where $T_c \sim 55$K. In this compound it is difficult to expect a large ζ since the observed exponential BCS-type behavior of $\rho_S(T)$ at small T [Malone et al. (2009)] is consistent with extended s-wave gap and weak interband impurity scattering [Nagai et al. (2008)].

The data for electron- and hole-doped $BaFe_2As_2$ [Martin et al. (2009)] are fitted in Figs. 4.2 (a) and 4.1 (b). The measured $\rho_S(T)$ scales approximately as T^2, which is similar to behavior shown in Fig. 4.1 (c). Left panel of Figs. 4.2 is the fit assuming that the gaps on two electron FSs and two hole FSs are Δ and $-\Delta$; right panel is a more realistic fit assuming, guided by ARPES data [Evtushinsky et al. (2009a)], that the gaps on the inner hole and the two electron FS are the same, but the gap on the outer hole FS is two to three times smaller.

The values $\zeta = 0.04 - 0.06$ used in these fits correspond to $T_c/T_{c0} \sim 0.6 - 0.3$ which is consistent with the values of $T_c \sim 10 - 30$K in this material in the assumption that T_{c0} in the clean case is roughly the same as in SmFeAsO. The curves shown in Figs. 4.2 (a) and 4.2 (b) represent the best fits, but it is not needed to adjust ζ to get a T^2 behavior - it persists over a range of ζ (see Fig. 4.1 (c)). However, λ_0 used in the fits is rather large compared with the experimentally obtained values $\sim 200 - 300$ nm [Martin et al. (2009)]. This discrepancy may be due to the omission of Fermi-liquid effects. The qualitative argument, supported by numerical estimates, is as follows. Assume, by analogy with the cuprates, that fermion-fermion interactions renormalize $\omega \to \omega Z_\omega$, where Z_ω is a decaying function of frequency, and further assume that $Z_\omega \approx 1$ at energies comparable to Δ so that it does not affect the relation between $\Delta(0)$ and T_c. Then, the low-temperature dependence $f(T/T_c)$ of the penetration length is rescaled $\Delta\lambda/\lambda_0 \sim f(Z_0 T/T_c)$ and the value of the fitting parameter $\lambda_0 \equiv \lambda_{FL}(0)$ decreases compared to what is obtained without Fermi-liquid effects. This Z factor is particularly relevant in heavily underdoped regime where it increases because of spin-density wave (SDW) fluctuations. This is the reason why it is needed to use very large $\lambda_0 = 2800$ nm to fit the data. At larger dopings, Z is smaller, but according to ARPES, $Z \sim 2$ in optimally doped $Ba_{1-x}K_xFe_2As_2$. For $f \sim T^2$, from the analytic reasoning the effective λ_0 four times smaller

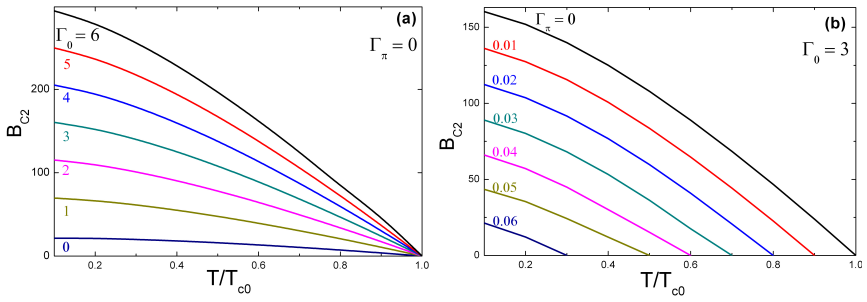

Figure 4.3: (a) The calculated temperature dependence of the upper critical field B_{c2} at interband scattering $\Gamma_\pi = 0$ with different values of intraband scattering values Γ_0. (b) The calculated temperature dependence of B_{c2} at intraband scattering rate $\Gamma_0 = 3$ with different values of interband scattering Γ_π.

than $\lambda(0)$ was chosen, reducing it to $\lambda_0 \sim 150 - 400$ nm, in the range of what is experimentally extracted. The numerical analysis confirms this, and for $Z = 2$ a fit for one of the electron-doped samples is shown, which gives a reasonable value for the zero-temperature penetration length. It can be concluded that the penetration depth data for 122 material can be fitted by a model of a dirty $s^{\pm}$ superconductor.

To study the obtained $\xi_h(B, T, \Gamma_0, \Gamma_\pi)$ dependences it is convenient to use the normalization to the GL coherence length ξ_{c2} determined from the upper critical field $B_{c2} = \Phi_0/2\pi\xi_{c2}^2$ (in our units $\xi_{c2} = 1/\sqrt{B_{c2}}$). Using the similarity to the model of spin-flip superconductors, $B_{c2}(T)$ for two dimensional $s^{\pm}$ pairing can be determined from the equations [Ovchinnikov and Kresin (1995)]

$$\ln(\frac{T_{c0}}{T}) = 2\pi T \sum_{n\geq 0} [\omega_n^{-1} - 2D_1(\omega_n, B_{c2})], \tag{4.12}$$

where

$$D_1(\omega_n, B_{c2}) = J(\omega_n, B_{c2}) \quad \times \quad [1 - 2(\Gamma_0 - \Gamma_\pi)J(\omega_n, B_{c2})]^{-1}, \tag{4.13}$$

$$J(\omega_n, B_{c2}) = (\frac{4}{\pi B_{c2}})^{1/2} \quad \times \quad \int_0^\infty dy \exp(-y) \arctan[\frac{(B_{c2}y)^{1/2}}{\alpha}], \tag{4.14}$$

where $\alpha = 2(\omega_n + \Gamma_0 + \Gamma_\pi)$.

Fig. 4.3 shows $B_{c2}(T)$ dependences at (a) $\Gamma_\pi = 0$, $\Gamma_0 = 0, 1, 2, 3, 4, 5, 6$ and (b) $\Gamma_0 = 3$, $\Gamma_\pi = 0.01, 0.02, 0.03, 0.04, 0.05, 0.06$ calculated from Eqs. (4.12-4.14). In Fig. 4.3 one can see the different influence of the intraband and interband scattering on $B_{c2}(T)$ dependence. The $B_{c2}(T)$ curve increases with Γ_0 (ξ_{c2} decreases with Γ_0), but Γ_π results in decreasing $B_{c2}(T)$ (increasing of ξ_{c2}).

Paper 2. Cutoff parameter of the field distribution in the mixed state of iron pnictides with $s^{\pm}$ and s_{++} pairing symmetries

Core structure of the vortices in iron pnictides has been studied in **paper 2** solving Eilenberger equations numerically. We consider $s^{\pm}$ symmetry (this mechanism is described in comments to

paper 1) and s_{++} symmetry without sign reversal in the FS, which is discussed below. Different impurity scattering rate dependences of cutoff parameter ξ_h have been found for these cases. In non-stoichiometric case, when intraband impurity scattering (Γ_0) is much larger than interband impurity scattering rate (Γ_π) the ξ_h/ξ_{c2} ratio is less in $s^\pm$ symmetry. When $\Gamma_0 \approx \Gamma_\pi$ (stoichiometric case) opposite tendencies has been found, in $s^\pm$ symmetry the ξ_h/ξ_{c2} goes upward from the "clean" case curve ($\Gamma_0 = \Gamma_\pi = 0$) while it goes downward in s_{++} case.

Regardless of the beauty of the $s^\pm$ mechanism, there are several serious discrepancies for the $s^\pm$-wave state. For example, although the $s^\pm$-wave state is expected to be very fragile against impurities due to the interband scattering [Onari and Kontani (2009)], the superconducting (SC) state is remarkably robust against impurities [Kawabata et al. (2008)] and α-particle irradiation [Tarantini et al. (2010)]. Moreover, clear 'resonancelike' peak structure observed by neutron scattering measurements [Christianson et al. (2008)] is reproduced by considering the strong correlation effect via quasiparticle damping, without the necessity of sign reversal in the SC gap [Onari et al. (2010)]. These facts indicate that a conventional s-wave state without sign reversal (s_{++}-wave state) is also a possible candidate for iron pnictides. Isotropic energy gaps found in angular-resolved photoemission spectroscopy [Borisenko et al. (2010)] of LiFeAs implies $s^\pm$ pairing state.

Then, a natural question is whether the electron-phonon (e-ph) interaction is important or not. Although first principle study predicts a small e-ph coupling constant $\lambda \sim 0.21$ [Boeri et al. (2008)], several experiments indicate the significance of the e-ph interaction. For example, the structural transition temperature T_S is higher than the Néel temperature in underdoped compounds, although the structural distortion is small. Also, prominent softening of the shear modulus is observed towards T_S or T_c in Ba122 [Fernandes et al. (2010)]. Raman spectroscopy [Rahlenbeck et al. (2009)] also indicates larger e-ph interaction.

Interestingly, there are several 'high-T_c' compounds with nodal superconducting gap structure, like $BaFe_2(As_{1-x}P_x)_2$ [Hashimoto et al. (2010)] and some 122 systems [Martin et al. (2010)]. Although the nodal $s^\pm$-wave state can appear in the spin-fluctuation scenario due to the competition between the dominant $\mathbf{Q} = (\pi, 0)$ and subdominant fluctuations [Kuroki et al. (2008); Maier et al. (2009)], the T_c is predicted to be very low. Thus, it is a crucial challenge to explain the rich variety of the gap structure in high-T_c compounds.

The five-orbital Hubbard-Holstein (HH) model for iron pnictides, considering the e-ph interaction by Fe-ion vibrations was introduced in Ref. [Kontani and Onari (2010)]. A relatively small e-ph interaction ($\lambda \lesssim 0.3$) induces the large orbital fluctuations, which can realize the high-T_c s_{++}-wave SC state. Moreover, the orbital fluctuations are accelerated by Coulomb interaction. In the presence of impurities, the s_{++}-wave state dominates the $s^\pm$-wave state for a wide range of parameters.

First, the e-ph iteration term was derived, considering only Einstein-type Fe-ion oscillations for simplicity. The d orbitals in the XYZ coordinate was described in Ref. [Kuroki et al. (2008)], which is rotated by $\pi/4$ from the xyz coordinate given by the Fe-site square lattice: the Z^2, XZ, YZ, $X^2 - Y^2$, and XY orbitals as 1, 2, 3, 4, and 5, respectively, can be written [Kuroki et al. (2008)]. The e-ph matrix elements due to the Coulomb potential was calculated, by following Ref. [Yada and Kontani (2008)]. The potential for a d electron at $\mathbf{r}$ (with the origin at the center of the Fe ion) due to the surrounding As^{3-}-ion tetrahedron is $U^\pm(\mathbf{r}; \boldsymbol{u}) = 3e^2 \sum_{s=1}^4 |\mathbf{r} + \mathbf{u} - \mathbf{R}_s^\pm|^{-1}$, where $\boldsymbol{u}$ is the displacement vector of the Fe ion, and $\mathbf{R}_s^\pm$ is the location of the surrounding As ions; $\sqrt{3}\mathbf{R}_s^+/R_{Fe-As} = (\pm\sqrt{2}, 0, 1)$ and $(0, \pm\sqrt{2}, -1)$ for $Fe^{(1)}$, and $\sqrt{3}\mathbf{R}_s^-/R_{Fe-As} = (\pm\sqrt{2}, 0, -1)$ and $(0, \pm\sqrt{2}, 1)$ for $Fe^{(2)}$ in the unit cell with two Fe-sites. Note that $u_{X,Y}$ and u_Z belong to E_g and B_{1g} phonons [Rahlenbeck et al. (2009)]. The $\boldsymbol{u}$ linear term of $U^\pm$, which gives the e-ph in-

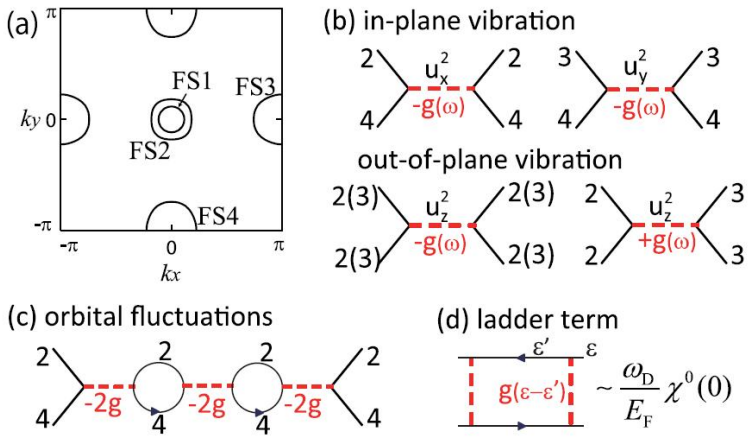

Figure 4.4: (a) FSs in the unfolded Brillouin zone. (b) Phonon-mediated electron-electron interaction. (c) A bubble-type diagram that induces the critical orbital fluctuations between (2,4) orbitals. (d) A ladder-type diagram that is ignorable when $\omega_D \ll E_F$ [Kontani and Onari (2010)].

teraction, is obtained as $V^{\pm}(\mathbf{r};\boldsymbol{u}) = \pm A[2XZu_X - 2YZu_Y + (X^2 - Y^2)u_Z] + O(\mathbf{r}^4)$, where $A = 30e^2/\sqrt{3}R^4_{Fe-As}$. Then, its nonzero matrix elements are given as

$$\begin{aligned}
\langle 2|V|4\rangle &= \pm 2a^2 A u_X/7, \\
\langle 2|V|2\rangle &= \pm 2a^2 A u_Z/7, \\
\langle 3|V|4\rangle &= \pm 2a^2 A u_Y/7, \\
\langle 3|V|3\rangle &= \pm 2a^2 A u_Z/7,
\end{aligned} \tag{4.15}$$

where a is the radius of the d orbital. Here, $\langle i|V|j\rangle$ is considered only for orbitals $i, j = 2-4$ that compose the Fermi surfaces (FSs) in Fig. 4.4 (a) [Kuroki et al. (2008)]. The obtained e-ph interaction does not couple to the charge density since $\langle i|V|j\rangle$ is traceless. Thus, the Thomas-Fermi screening for the coefficient A is absent. The local phonon Green function is $D(\omega_l) = 2\bar{u}_0^2\omega_D/(\omega_l^2 + \omega_D^2)$, which is given by the Fourier transformation of $\langle T_\tau u_\mu(\tau)u_\mu(0)\rangle(\mu = X, Y, Z)$. Here, $\bar{u}_0 = \sqrt{\hbar/2M_{Fe}\omega_D}$ is the position uncertainty of Fe ions, ω_D is the phonon frequency, and $\omega_l = 2\pi lT$ is the boson Matsubara frequency. Then, for both $\mathrm{Fe}^{(1)}$ and $\mathrm{Fe}^{(2)}$, the phonon-mediated interaction is given by

$$\begin{aligned}
V_{24,42} = V_{34,43} &= -(2Aa^2/7)^2 D(\omega_l) \equiv -g(\omega_l), \\
V_{22,22} = V_{33,33} &= -V_{22,33} = -g(\omega_l),
\end{aligned} \tag{4.16}$$

as shown in Fig. 4.4 (b). Note that $V_{ll',mm'}$ is symmetric with respect to $l \leftrightarrow l'$, $m \leftrightarrow m'$, and $(ll)' \leftrightarrow (mm)'$. In the case when $R_{Fe-As} \approx 2.4$Å, $a \approx 0.77$Å (Shannon crystal radius of Fe^{2+}), and $\omega_D \approx 0.018eV$, the $g(0) \approx 0.4eV$. The e-ph coupling was neglected due to $d-p$ hybridization [Yada and Kontani (2008)] considering the modest $d-p$ hybridization in iron pnictides [Singh (2009)]. Thus,

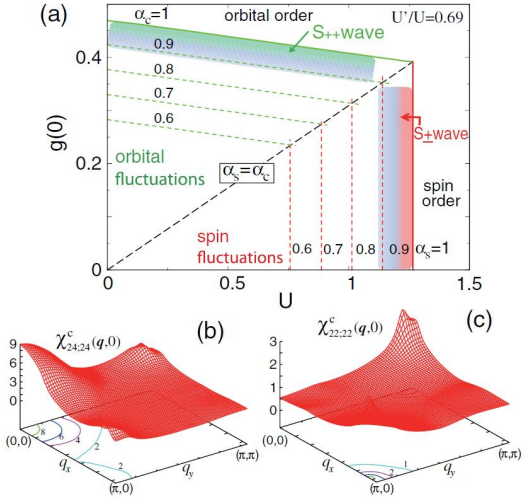

Figure 4.5: (a) Obtained $U - g(0)$ phase diagram. (b) Obtained $\chi^c_{24,42}(\mathbf{q}, 0)$ and $\chi^c_{22,22}(\mathbf{q}, 0)$ for $\alpha_c = 0.97$ [Kontani and Onari (2010)].

the multiorbital Hubbard-Holstein model for iron pnictides was obtained by combining Eq. (4.16) with the onsite Coulomb interaction; the intra- (inter-) orbital Coulomb U (U'), Hund coupling J, and pair hopping J'.

In this part, the rich electronic properties realized in the multiorbital Hubbard-Holstein model is studied [Capone et al. (2004)]. The irreducible susceptibility in the five-orbital model is given by $\chi^0_{ll',mm'}(q) = -(T/N)\sum_k G^0_{lm}(k+q)G^0_{m'l'}(k)$, where $\hat{G}^0(k) = [i\omega_n + \mu - \hat{H}^0_k]^{-1}$ is the d-electron Green function in the orbital basis: $q = (\mathbf{q}, \omega_l)$, $k = (\mathbf{k}, \omega_n)$ and $\omega_n = (2n+1)\pi T$ is the fermion Matsubara frequency, μ is the chemical potential, $\hat{H}^0_k$ is the kinetic term given in Ref. [Kuroki et al. (2008)]. Then, the susceptibilities for spin and charge sectors in the random phase approximation (RPA) are given as [Takimoto et al. (2002)]

$$\hat{\chi}^{s(c)}(q) = \hat{\chi}^0(q)[1 - \hat{\Gamma}^{s(c)}\hat{\chi}^0(q)]^{-1}. \tag{4.17}$$

For the spin channel, $\Gamma^s_{l_1l_2l_3l_4} = U, U', J$ and J' for $l_1 = l_2 = l_3 = l_4$, $l_1 = l_3 \neq l_2 = l_4$, $l_1 = l_2 \neq l_3 = l_4$ and $l_1 = l_4 \neq l_2 = l_3$, respectively [Kuroki et al. (2008)]. For the charge channel, $\hat{\Gamma}^c = -\hat{C} - 2\hat{V}(\omega_l)$, where $\hat{V}(\omega_l)$ is given in Eq. (4.16), and $C_{l_1l_2l_3l_4} = U, -U' + 2J, 2U' - J$ and J' for $l_1 = l_2 = l_3 = l_4$, $l_1 = l_3 \neq l_2 = l_4$, $l_1 = l_2 \neq l_3 = l_4$ and $l_1 = l_4 \neq l_2 = l_3$, respectively [Kuroki et al. (2008)]. Fig. 4.4 (c) shows one of the bubble diagrams for the (2,4)-channel due to the 'negative exchange coupling $V_{24,42}$' that leads to a critical enhancement of $\hat{\chi}^c(q)$ (the effect of Coulomb interaction on $\chi^c_{24,42}(\mathbf{q}, 0)$ is not large if $C_{ll',ll'} + C_{ll',l'l} = -U' + J + J'$ is small). The ladder diagrams given by $\hat{V}(\omega_l)$ in Fig. 4.4 (d) were neglected since $\omega_D \ll W_{band}$ [Boeri et al. (2008); Rahlenbeck et al. (2009)]. $\omega_D = 0.02eV$, $U'/U = 0.69$, $J/U = 0, 16$, and $J = J'$ were chosen and the electron number $n = 6.1$ (10% electron doping) was fixed; the density of states per spin is $N(0) = 0.66eV^{-1}$. Numerical results are not sensitive to these parameters, $128^2\mathbf{k}$ meshes, and 512 Matsubara frequencies were used. Hereafter, the unit of energy is eV.

Fig. 4.5 (a) shows the obtained $U-g(0)$ phase diagram. $\alpha_{s(c)}$ is the spin (charge) Stoner factor, given by the maximum eigenvalue of $\hat{\Gamma}^{s(c)}\hat{\chi}^0(\mathbf{q},0)$. Then, the enhancement factor for $\chi^{s(c)}$ is $(1-\alpha_{s(c)})^{-1}$, and $\alpha_{s(c)}=1$ gives the spin (orbital) order boundary. Because of the nesting of the FSs, the AFM fluctuation with $\mathbf{Q}\approx(\pi,0)$ develops as U increases, and s$\pm$-wave state is realized for $\alpha_s \lesssim 1$ [Kuroki et al. (2008)]. In contrast, the orbital fluctuations develop as $g(0)$ increases. For $U=1$, the critical value $g_{cr}(0)$ is 0.4 for $\alpha_c=1$, and the critical e-ph coupling constant is $\lambda_{cr}\equiv g_{cr}(0)N(0)=0.26$ (λ_i for orbital $i=2-4$ is $\lambda_i\approx -\Sigma_{j=2}^4 N_j(0)V_{ij,ij}(0)=N(0)g(0)$, where $N_j(0)$ is the partial DOS, then, $\lambda\approx N(0)g(0)$ in the band-diagonal basis). Since the obtained λ_{cr} is close to λ given by the first principle study [Boeri et al. (2008)], strong orbital fluctuations are expected to occur in iron pnictides. At fixed U, λ_{cr} decreases as J/U approaces zero.

Figs. 4.5 (b) and (c) show the obtained $\chi^c_{ll',mm'}(\mathbf{q},0)$ for $(ll',mm')=(24,42)$ and (22,22), respectively, for $U=1.14$ and $\alpha_c=0.97$ ($g(0)=0.40$): Both of them are the most divergent channels for electron-doped cases. The enhancement of (24, 42)-channel is induced by the multiple scattering by $V_{24,42}$. The largest broad peak around $\mathbf{q}=(0,0)$ originates from the forward scattering in the electron-pocket (FS3 or FS4) composed of 2-4 orbitals (FS1,2 are composed of only 2 and 3 orbitals.) These ferro-orbital fluctuations would induce the softening of shear modulus [Fernandes et al. (2010)], and also reinforce the ferro-orbital ordered state below T_S [Shimojima et al. (2010)] that had been explained by different theoretical approaches [Krüger et al. (2009)]: The divergence of $\chi^c_{24,42}$ ($\chi^c_{34,43}$) pushes the 2,4 (3,4) orbitals away from the Fermi level, and the Fermi surfaces in the ordered state will be formed only by 3 (2) orbital, consistently with Ref. [Shimojima et al. (2010)]. The lower peak around $\mathbf{Q}=(\pi,0)$ comes from the nesting between hole- and electron-pockets. Also, the enhancement of (22, 22)-channel for $\mathbf{Q}=(\pi,0)$ is induced by the nesting via multiple scattering by $V_{22,22}$ and $V_{22,33}$. In contrast, the charge susceptibility $\sum_{l,m}\chi^c_{ll,mm}(\mathbf{q},0)$ is finite even if $\alpha_c\to 1$ since $\chi^c_{22,33}\approx -\chi^c_{22,22}$.

The large orbital fluctuations, which are not considered in the first principle study of T_c [Boeri et al. (2008)], can induce the s_{++}-wave state when $g(0)>0$. The following linearized Eliashberg equation using the RPA [Kuroki et al. (2008)] was analyzed, by taking both the spin and orbital fluctuations into account on the same footing:

$$\lambda_E\Delta_{ll'}(k)=\frac{T}{N}\sum_{k',m_i}W_{lm_1,m_4l'}(k-k')G_{m_1m_2}(k')\Delta_{m_2m_3}(k')G_{m_4m_3}(-k'), \tag{4.18}$$

where $\hat{W}(q)=-\frac{3}{2}\hat{\Gamma}^s\hat{\chi}^s(q)\hat{\Gamma}^s+\frac{1}{2}\hat{\Gamma}^c\hat{\chi}^c(q)\hat{\Gamma}^c-\frac{1}{2}(\hat{\Gamma}^s-\hat{\Gamma}^c)$ for singlet states. The eigenvalue λ_E increases as $T\to 0$, and it reaches unity at $T=T_c$. In addition, the impurity effect was taken into consideration since many iron pnictides show relatively large residual resistivity. Here, the Fe-site substitution was assumed, where the impurity potential I is diagonal in the d-orbital basis [Onari and Kontani (2009)]. Then, the T matrix in the normal state is given by $\hat{T}(\epsilon_n)=[I^{-1}-N^{-1}\Sigma_{\mathbf{k}}\hat{G}(\mathbf{k},\epsilon_n)]^{-1}$ in the orbital basis [Onari and Kontani (2009)]. Then, the normal self-energy is $\hat{\Sigma}^n(\epsilon_n)=n_{imp}\hat{T}(\epsilon_n)$, where n_{imp} is the impurity concentration. Also, the linearized anomalous self-energy is given by

$$\Sigma^a_{ll'}(\epsilon_n)=\frac{n_{imp}}{N}\sum_{\mathbf{k},m_i}T_{lm_1}(\epsilon_n)G_{m_1m_2}(\mathbf{k},\epsilon_n)\Delta_{m_2m_3}(\mathbf{k},\epsilon_n)\times \times G_{m_4m_3}(-\mathbf{k},-\epsilon_n)T_{l'm_4}(-\epsilon_n). \tag{4.19}$$

Then, the Eliashberg equation for $n_{imp}\neq 0$ is given by using the full Green function $\hat{G}(k)=[i\epsilon_n+\mu-\hat{H}^0_k-\hat{\Sigma}^n(\epsilon_n)]^{-1}$ in Eqs. (4.18) and (4.19), and adding $\Sigma^a_{ll'}(\epsilon_n)$ to the right hand side of

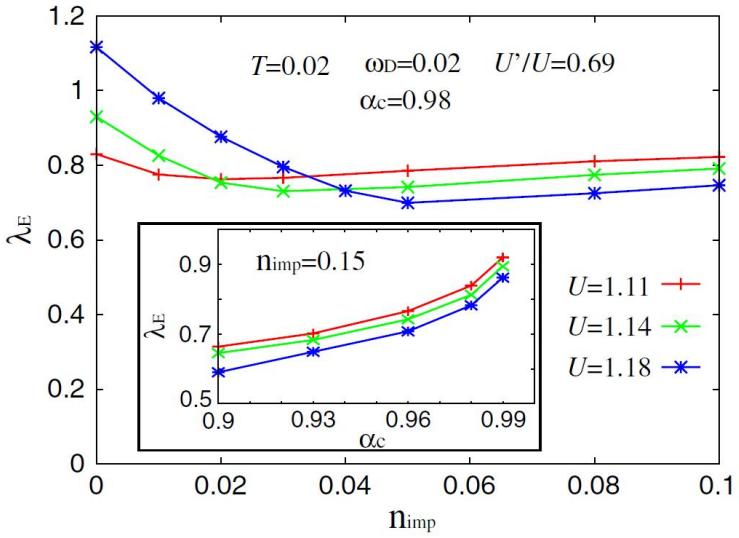

Figure 4.6: n_{imp} dependence of λ_E at $\alpha_c = 0.98$. For $g(0) = 0$ ($s^{\pm}$ state), λ_E at $n_{imp} = 0$ decreases by $0.1 \sim 0.15$, since the ferro-orbital fluctuations enhance both the s_{++} and $s^{\pm}$ wave states. Inset: α_c dependence of λ_E [Kontani and Onari (2010)].

Eq. (4.18). Hereafter, the equation was solved at relatively high temperature $T = 0.02$ since the number of **k** meshes (128^2) is not enough for $T < 0.02$.

Fig. 4.6 shows the n_{imp} dependence of λ_E at $\alpha_c = 0.98$, for $U = 1.11, 1.14$ and 1.18. Considering large $\lambda_E \gtrsim 0.8$ at $T = 0.02$, relatively high-T_c ($\lesssim 0.02$) is expected. For the smallest U ($U = 1.11$; $\alpha_s = 0.85$) the nearly isotropic s_{++}-wave state is realized; the obtained λ_E is almost independent of n_{imp}, indicating the absence of the impurity effect on the s_{++}-wave state, as discussed in Ref. [Onari and Kontani (2009)] (above T_c, λ_E slightly increases with n_{imp} in conventional s-wave superconductors, but never exceeds unity). For the largest U ($U = 1.18$; $\alpha_s = 0.91$), the $s^{\pm}$-wave state is realized at $n_{imp} = 0$; λ_E decreases slowly as n_{imp} increases from zero, whereas it saturates for $n_{imp} \geq 0.05$, indicating the smooth crossover from $s^{\pm}$- to s_{++}-wave states due to the interband impurity scattering. For $U = 1.14$ ($\alpha_s = 0.88$), the SC gap at $n_{imp} = 0$ is a hybrid of s_{++} and $s^{\pm}$; only Δ_{FS2} is different in sign.

The inset of Fig. 4.6 shows λ_E for the s_{++}-wave state in the presence of impurities: Since $\lambda_E(\alpha_c = 0.98)$ - $\lambda_E(\alpha_c = 0.9)$ is only ~ 0.15 for each value of U, relatively large T_c for s_{++}-wave state is realized even if orbital fluctuations are moderate. The obtained λ_E is almost constant for $\omega_D = 0.02 - 0.1$, suggesting the absence of isotope effect in the s_{++}-wave state due to the strong retardation effect [Yada and Kontani (2008)]. By the same reason, λ_E for the s_{++}-wave state is seldom changed if $U = 3$ is put in the Hartree-Fock term $\frac{1}{2}(\hat{\Gamma}^s - \hat{\Gamma}^c)$ in $W(q)$, indicating that the Morel-Anderson pseudopotential almost saturates.

Fig. 4.7 shows the SC gap on the FSs in the band representation for (a) $n_{imp} = 0$, (b) 0.03, and (c) 0.08. They satisfy the condition $N^{-1}\Sigma_{\mathbf{k},lm}|\Delta_{lm}(\mathbf{k})|^2 = 1$. The horizontal axis is the azimuth angle for the **k** point with the origin at Γ (M) point for FS1,2 (FS4); $\theta = 0$ corresponds to the k_x

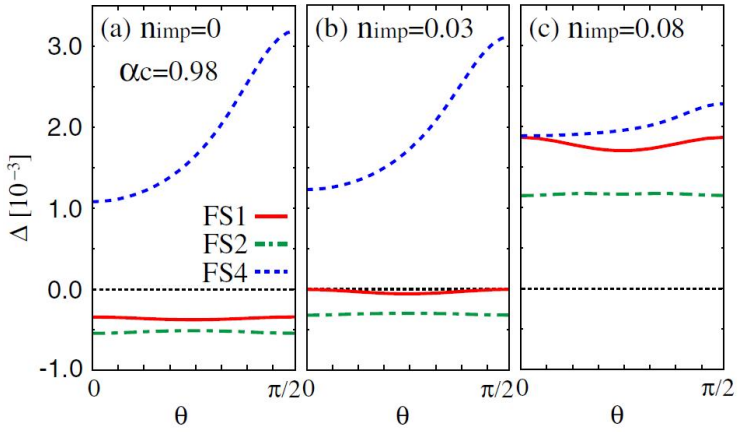

Figure 4.7: SC gap functions for $U = 1.18$ as functions of θ at (a) $n_{imp} = 0$, (b) 0.03, and (c) 0.08, respectively [Kontani and Onari (2010)].

direction. In case (a), the $s^{\pm}$ state with strong imbalance, $|\Delta_{FS1}|, |\Delta_{FS2}| \ll \Delta_{FS4}$, is realized, and Δ_{FS4} takes the largest value at $\theta = \pi/2$, where the FS is mainly composed of orbital 4. In case (c), the impurity-induced isotropic s_{++} state [Mishra et al. (2009)] with $\Delta_{FS1} \sim \Delta_{FS2} \sim \Delta_{FS4}$ is realized, consistently with many ARPES measurements [Evtushinsky et al. (2009b)]. In case (b), Δ_k on FS1 is almost gapless. However, considering the k_z dependence of the FSs, a (horizontal-type) nodal structure is expected to appear on FS1,2. In real compounds with $T_c \sim 50K$, the $s^{\pm} \to s_{++}$ crossover should be induced by small residual resistivity $\rho_{imp} \sim 20\mu\Omega$cm ($n_{imp} \sim 0.01$ for $I = 1$), as estimated in Ref. [Onari and Kontani (2009)].

At $n_{imp} = 0$, $s^{\pm}$-wave state is realized in the RPA even if $\alpha_s \lesssim \alpha_c$, due to factor 3 in front of $\frac{1}{2}\hat{\Gamma}^s\hat{\chi}^s\hat{\Gamma}^s$ in $W(q)$. For the same reason, however, reduction in α_s (or increment of U_{cr} for $\alpha_s = 1$) due to the 'selfenergy correction by U' is larger, which will be unfavorable for the $s^{\pm}$-wave state. Therefore, self-consistent calculation for the self-energy is required to discuss the value of $\alpha_{c,s}$ and the true pairing state.

Here, the location of real compounds in the $\alpha_s - \alpha_c$ phase diagram in Fig. 4.5 (a) is discussed. Considering the weak T dependence of $1/T_1T$ in electron-doped SC compounds [Nakai et al. (2010b)], it is expected that they belong to the area $\alpha_c \gg \alpha_s$. Then, the s_{++}-wave SC state will be realized without (or very low density) impurities, like the case of $U = 1.11$ or 1.14 in Fig. 4.6. On the other hand, impurity-induced $s^{\pm} \to s_{++}$ crossover may be realized in $BaFe_2(As_{1-x}P_x)_2$ (undoped) or $(Ba_{1-x}K_x)Fe_2As_2$ (hole-doped) SC compounds, where AFM fluctuations are rather strong.

The non-Fermi-liquid-like transport phenomena in iron pnictides is discussed. For example, the resistivity is nearly linear in T, and the Hall coefficient R_H increases at lower temperatures [Kawabata et al. (2008); Kasahara et al. (2010)]. Although the forward scattering induced by ferro-orbital fluctuations might be irrelevant, antiferro-orbital and AFM fluctuations with $\mathbf{Q} = (\pi, 0)$ are expected to cause the anomalous transport properties, due to the current vertex correction [Kontani (2008)].

A mechanism of the s_{++}-wave SC state induced by orbital fluctuations, due to the phonon-mediated

electron-electron interaction, was proposed. Three orbitals (XZ, YZ, and $X^2 - Y^2$) are necessary to lead the ferro-orbital fluctuations. The SC gap structure drastically changes depending on parameters α_s, α_c and n_{imp}, consistent with the observed rich variety of the gap structure that is a salient feature of iron pnictides. The orbital-fluctuation-mediated s_{++}-wave state is also obtained for hole-doped cases, although the antiferro-orbital fluctuations become stronger than the ferro-orbital ones.

The s-wave superconductivity induced by orbital fluctuations was discussed in Ref. [Takimoto et al. (2002)] for $U' > U$; this condition can be realized by including the A_{1g} phonon [Yanagi et al. (2010)]. In the present model, however, the A_{1g} phonon is negligible since $g_{cr}(0)$ given by the A_{1g} phonon is much greater than $g_{cr}(0) \sim 0.4$ in Fig. 4.5 (a): The ferro-obtital fluctuations in Fig. 4.5 (b) originate from the negative exchange interaction caused by the E_g phonon, as shown in Fig. 4.4 (c).

Paper 3. Effects of the order parameter symmetry on the vortex core structure in the iron pnictides

In **paper 3** is found that ξ_h/ξ_{c2} from (B/B_{c2}) dependence is nonuniversal, depending on the chosen parameter set it can reside both below and above AGL curve. Such behavior is quite different from that in s_{++} pairing symmetry where intraband and interband scattering rates act in similar way and ξ_h/ξ_{c2} decreases always with impurity scattering. It is found that intraband scattering (Γ_0) suppresses ξ_h/ξ_{c2} leading to values much less than unit at high Γ_0. The small value of ratio ξ_h/ξ_{c2} (~ 0.27) which is comparable with our theoretical prediction, Fig. 1 in **paper 3**, was obtained in μSR investigation of Co-doped $BaFe_2As_2$ [Sonier et al. (2011)]. The effects of interband impurity scattering (Γ_π) depend on the value of Γ_0: at small Γ_0 ξ_h/ξ_{c2} increases with Γ_π, but at high Γ_0 it decreases with Γ_π. The effects of interband impurity scattering at moderate Γ_0 depends on the field range resulting in increasing of ξ_h/ξ_{c2} at low fields, but suppressing it at high fields. The $\xi_h/\xi_{c2}(B/B_{c2})$ calculations for parameters of doped $BaFe_2As_2$ compounds [Vorontsov et al. (2009)], where $\Gamma_0 \gg \Gamma_\pi$, are done. These dependences demonstrate growing behavior defined by Γ_0 with values much less that one in whole field range, i.e. they are under the AGL curve of ξ_v. It should be noted that substantial deviation from the magnetic field distribution of a nearly perfect vortex lattice by field-induced magnetic order and strong vortex-lattice disorder can be also significant for iron-arsenic superconductors [Sonier et al. (2011)]. The influence of these effects to transverse-field muon spin rotation (TF μSR) is described below.

TF μSR is routinely used to determine the magnetic penetration depth λ of type-II superconductors in the vortex state, which provides indirect information on the energy gap structure [Sonier et al. (2000)]. The magnetic field distribution $n(B)$ in the sample is measured by detecting the decay positrons from implanted positive muons that locally probe the internal fields, and λ is subsequently determined by modeling the contribution of the vortex lattice (VL) to $n(B)$. However, even in conventional superconductors the VL contribution is not known *a priori*, and one must rely on phenomenological models to deduce what is really an 'effective' penetration depth $\tilde{\lambda}$. One reason is that only cumbersome microscopic theories account for the effects of low-energy excitations on $n(B)$ [Ichioka et al. (1999b)]. Extrapolating low-temperature measurements of $\tilde{\lambda}$ to zero field to eliminate intervortex quasiparticle transfer, nonlocal and/or nonlinear effects, has been demonstrated to be an accurate way of determining the 'true' λ [Sonier (2007); Sefat et al. (2008)]. Yet an underlying assumption is always that the VL is highly ordered and that other contributions to $n(B)$ are relatively

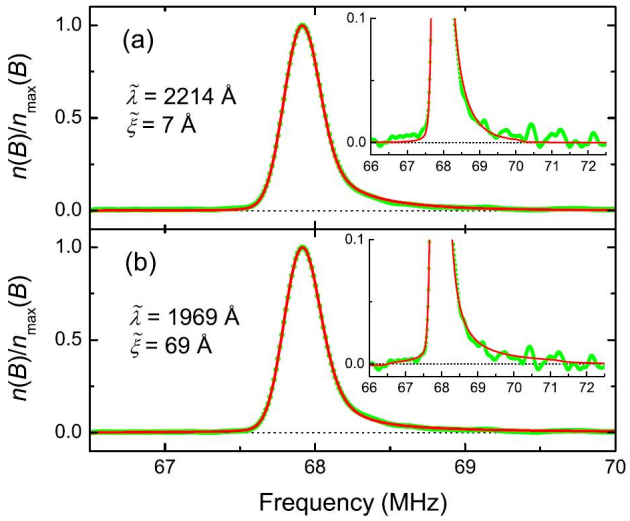

Figure 4.8: TF-μSR line shape of $BaFe_{1.82}Co_{0.18}As_2$ at $H = 0.5$ T and $T = 3.9$ K (green circles). (a) The red curve is the Fourier transform of a fit in the time domain assuming Eq. (4.21) [Sonier et al. (2011)]. In addition to the indicated values of $\tilde{\lambda}$ and $\tilde{\xi}$, the fit yields $\sigma = 0.265$ μs^{-1} and a PM shift of 8.6 G. (b) Fourier transform of a fit that assumes the model of field-induced AFM order described in the main text (red curve). The fit yields $\sigma = 0.251$ μs^{-1} and a PM shift of 9.2 G. Other fit parameters are shown in Fig. 4.10 [Sonier et al. (2011)].

minor. This is not the case in many of the recently discovered iron-arsenic superconductors, making a reliable determination of λ by TF μSR extremely difficult.

High-statistics TF-μSR spectra in $BaFe_{1.82}Co_{0.18}As_2$ ($T_c = 21$ K) single crystals [Sefat et al. (2008)] of 20×10^6 muon decay events were collected in magnetic fields $H = 0.02-0.5$ T applied transverse to the initial muon spin polarization $P(t = 0)$, and parallel to the c axis of the crystals. The TF-μSR signal is the time evolution of the muon spin polarization, and is related to $n(B)$ as follows:

$$P(t) = \int_0^\infty n(B) \exp(i\gamma_\mu B t) dB, \tag{4.20}$$

where γ_μ is the muon gyromagnetic ratio. Generally, the TF-μSSR signal is fit in the time domain, with the inverse Fourier transform or 'TF-μSR line shape' providing a visual approximation of the internal field distribution. For a perfectly ordered VL, $n(B)$ is characterized by sharp cutoffs at the minimum and maximum values of $B(\mathbf{r})$ and a sharp peak at the saddle-point value of $B(\mathbf{r})$ [Sonier et al. (2000)]. These features are observed in single crystals when the VL is highly ordered and other contributions to $n(B)$ are minor, but are not observed in polycrystalline samples, where the orientation of the crystal lattice varies with respect to H.

The TF-μSR spectra was fitted to a theoretical $P(t)$ that has been successfully applied to a wide variety of type-II superconductors, and utilized in some of the experiments on iron-arsenic superconductors. The spatial variation of the field, from which $n(B)$ is calculated, is modeled by the

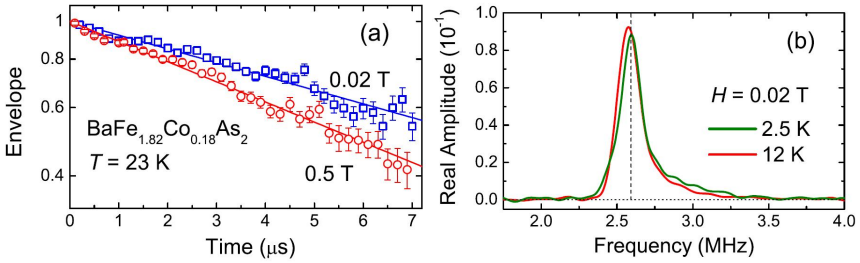

Figure 4.9: (a) Envelopes of TF-μSR spectra of $BaFe_{1.82}Co_{0.18}As_2$ in the normal state at $T = 23$ K. The solid curves are fits to a single exponential relaxation function $G(t) = \exp(-\Lambda t)$, yielding $\Lambda = 0.081 \pm 0.003$ μs^{-1} and $\Lambda = 0.119 \pm 0.003$ μs^{-1} at $H = 0.02$ T and $H = 0.5$ T, respectively. (b) TF-μSR line shapes of $BBaFe_{1.82}Co_{0.18}As_2$ below T_c at $H = 0.02$ T. The dashed vertical line corresponds to H [Sonier et al. (2011)].

analytical Ginzburg-Landau (GL) function [Sonier et al. (2000)]

$$B(\mathbf{r}) = B_0(1-b^4)\sum_{\mathbf{G}} \frac{e^{-i\mathbf{G}\mathbf{r}} u K_1(u)}{\tilde{\lambda}^2 G^2}, \tag{4.21}$$

where $\mathbf{G}$ are the reciprocal lattice vectors of a hexagonal VL, $b = B/B_{c2}$ is the reduced field, B_0 is the average internal magnetic field, $K_1(u)$ is a modified Bessel function, $u^2 = 2\tilde{\xi}^2 G^2(1+b^4)[1-2b(1-b)^2]$, and $\tilde{\xi}$ is the coherence length. As explained later, $P(t)$ is multiplied by a Gaussian depolarization function $\exp(-\sigma^2 t^2)$ to account for the effects of nuclear dipolar fields and frozen random disorder. The fitting parameters $\tilde{\lambda}$ and $\tilde{\xi}$ can deviate substantially from the 'true' λ and ξ if other contributions to $n(B)$ are significant. An important feature of Eq. (4.21) is that it accounts for the finite size of the vortex cores, by generating a 'high-field' cutoff in $n(B)$. The GL coherence length $\xi_{ab} \sim 26$ Å calculated from the upper critical field $H_{c2} \sim 50$ T of $BaFe_{1.84}Co_{0.16}As_2$ with $\mathbf{H}||c$ [Kano et al. (2009)] represents a lower limit for the vortex core radius [Sonier (2007)]. The core size can be much larger if there are spatially extended quasiparticle core states associated with either the existence of a second smaller superconducting gap [Callaghan et al. (2005)] or a single anisotropic gap [Sonier et al. (1999)]. Yet fits of the TF-μSR spectra of $BaFe_{1.82}Co_{0.18}As_2$ using Eq. (4.21) show no sensitivity to the vortex cores at any field and converge with values of $\tilde{\xi}$ approaching zero. Fig. 4.8 shows that even at 0.5 T, where the vortex density is highest, a high-field cutoff is not discernible in the TF-μSR line shape. There are two reasons responsible for this: magnetism and disorder.

a) Magnetism. The effective field $\mathbf{B}_\mu$ experienced by the muon is a vector sum of various contributions that may be static or fluctuating in time. With correlation times generally much longer than the muon lifetime, the nuclear moments constitute a dense static moment system that cause a Gaussian-like depolarization of the TF-μSR spectrum. Yet as shown in Fig. 4.9 (a),above T_c $BaFe_{1.82}Co_{0.18}As_2$ exhibits an exponential depolarization that is typical of dilute or fast fluctuating electronic moments [Uemura et al. (1985)]. The latter is consistent with the observation of a paramagnetic (PM) shift of the average internal field $\langle \mathbf{B}_\mu \rangle$ sensed by the muons below T_c. This is evident in Fig. 4.9 (b), where representative Fourier transforms of $P(t)$ at $H = 0.02$ T is shown.

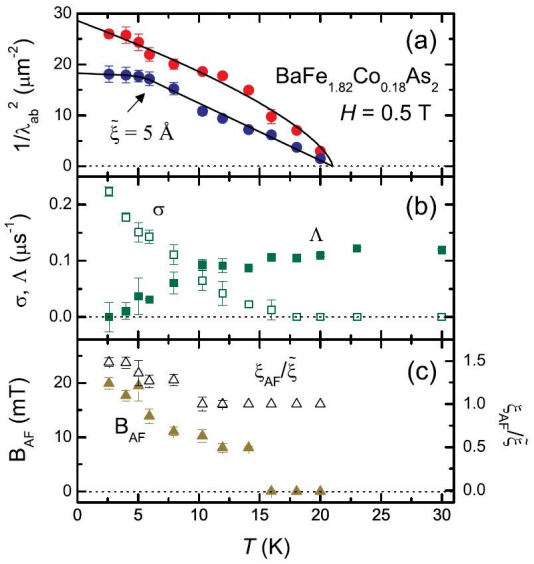

Figure 4.10: Results of fits of TF-μSR time spectra of $BaFe_{1.82}Co_{0.18}As_2$ at $H = 0.5$ T, assuming the model of magnetic order described in the main text. Temperature dependence of (a) $1/\tilde{\lambda}^2$, (b) the depolarization rates σ (Gaussian) and Λ (exponential), (c) B_{AFM} and the ratio $\xi_{AFM}/\tilde{\xi}$. Also shown in (a) results of fits without magnetic order but with $\tilde{\xi}$ fixed to be 5 Å (blue circles) [Sonier et al. (2011)].

Instead of the expected diamagnetic shift imposed by the superconducting state, $\langle \mathbf{B}_\mu \rangle$ exceeds H. The magnitude of the PM shift increases with increasing H and/or decreasing T.

The occurrence of a PM shift in the superconducting state of $BaFe_{2-x}Co_xAs_2$ and $SrFe_{2-x}Co_xAs_2$ has been reported by others [Khasanov et al. (2009b); Williams et al. (2010)] and implies an enhancement of $\langle \mathbf{B}_\mu \rangle$ from magnetic order occupying a large volume of the sample. Magnetic order exists in underdoped samples at $H = 0$ [Marsik et al. (2010)] and is apparently induced in overdoped samples by the applied field. Yet the effects of magnetism on the linewidth and functional form of $n(B)$ have not been considered. A strong relaxation of the TF-μSR signal occurs even in long-range magnetically ordered systems, and with decreasing temperature there must be an increased broadening of $n(B)$ associated with the growth of the correlation time for spin fluctuations.

Accounting for such magnetism is nontrivial because of the spatially varying superconducting order parameter and the likelihood that the field-induced magnetism occurs in a nematic phase [Chu et al. (2010)]. Even so excellent fits of the TF-μSR spectra of $BaFe_{1.82}Co_{0.18}As_2$ to polarization functions that incorporate enhanced magnetism in the vortex core region (e.g., commensurate spin-density wave, ferromagnetism, spin glass), where superconductivity is suppressed, were achieved. Here typical results for one model of magnetism are described: First, $P(t)$ is multiplied by an exponential depolarization function $\exp(-\Lambda t)$, as observed above T_c. In addition, enhanced magnetic order in

the vortex cores is modeled by adding the following term to Eq. (4.21):

$$B_{\text{AFM}}(\mathbf{r}) = B_{\text{AFM}} e^{-r^2/2\xi_{\text{AFM}}^2} \sum_{\mathbf{K}} (e^{-i\mathbf{K}\mathbf{r}} - e^{-i\mathbf{K}\mathbf{r}'}). \tag{4.22}$$

The **K** sum is the reciprocal lattice of an antiferromagnetic square iron sublattice of spacing $a = 2.8$ Å, B_{AFM} is the field amplitude, ξ_{AFM} governs the radial decay of B_{AFM} from the core center, and **r** and **r′** are the position vectors for 'up' and 'down' spins, respectively. This kind of magnetic order has the effect of smearing the high-field cutoff, and can even introduce a low-field tail in $n(B)$ [Sonier et al. (2007)]. As indicated by the large value of $\tilde{\xi}$ in Fig. 4.8 (b), fits to this model are sensitive to the vortex cores. With decreasing temperature, the magnetism induced relaxation evolves from exponential to Gaussian [see Fig. 4.10 (b)] and the magnetic order in the vortex cores is enhanced [see Fig. 4.10 (c)]. Consistent with behavior deduced from TF-μSR measurements on $BaFe_{1.772}Co_{0.228}As_2$ [Williams et al. (2010)], fits to a model without magnetism that is insensitive to the vortex cores (i.e., $\tilde{\xi}$ fixed to 5 Å) yield an unusual linear temperature dependence of $1/\tilde{\lambda}^2$ immediately below T_c and a saturation of $\tilde{\lambda}$ at low T [see Fig. 4.10 (a)]. In contrast, fits assuming magnetic order exhibit a linear temperature dependence well below T_c that is suggestive of gap nodes. However, these results simply demonstrate the ambiguity in modeling such data. Without knowledge of the precise form of the magnetism, this model cannot be deemed rigorously valid.

b) Disorder. Thus far TF μSR has been applied to iron-arsenic superconductors under the assumption that one is probing a fairly well-ordered hexagonal VL. Vortex imaging experiments on the RFeAs($0_{1-x}F_x$), $A_{1-x}B_xFe_2As_2$, and $AFe_{2-x}Co_xAs_2$ families all show a highly disordered VL indicative of strong bulk pinning [Eskildsen et al. (2009); Inosov et al. (2010b)]. In Fig. 4.11 the effect of such disorder on the ideal $n(B)$ is shown. Molecular dynamics to simulate $n(B)$ of the disordered VL was used. In particular, molecular dynamics iterations were performed until a radial distribution function closely resembling that observed in overdoped $BaFe_{1.81}Co_{0.19}As_2$ [Inosov et al. (2010b)] was achieved [see Fig. 4.11 (a)]. The vortex configuration at this point was then assumed to be static and $n(B)$ was calculated. Although the line shape of the disordered VL in Fig. 4.11 (b) is asymmetric, it is strongly smeared with a field variation greatly exceeding that of the perfect VL.

Small perturbations of the VL by random pinning can be handled by convoluting the ideal theoretical line shape with a Gaussian distribution of fields [Brandt (1988)]. This causes a Gaussian depolarization $\exp(-\sigma^2 t^2)$ of $P(t)$. But for polycrystalline samples, $n(B)$ is always nearly symmetric, so that the contribution from disorder cannot be isolated. Consequently, VL disorder has not been accounted for in TF-μSR studies of polycrystalline or powdered ironarsenic superconductors [Khasanov et al. (2008); Carlo et al. (2009)]. Given the severity of disorder in these materials and no knowledge about how this disorder evolves with temperature or doping, the accuracy of information deduced about λ is questionable. Since disorder of rigid flux lines broaden $n(B)$, such studies certainly underestimate λ.

While small perturbations of $B(r)$ by vortex pinning may be accounted for in measurements on single crystals, a Gaussian convolution of the ideal $n(B)$ becomes increasingly inadequate as the degree of disorder is enhanced [Menon et al. (2006)]. In Fig. 4.11 (b) is shown that Gaussian broadening of the ideal line shape does not precisely reproduce $n(B)$ of the disordered VL. Moreover, because the large disorder-induced broadening smears out the high-field cutoff, the fitting parameters $\tilde{\lambda}$ and $\tilde{\xi}$ are ambiguous. This is illustrated in Fig. 4.11 (c), where nearly identical Gaussian-broadened line shapes are obtained for very different values of these parameters. Hence substantial disorder introduces considerable uncertainty even in measurements on single crystals [Khasanov et al. (2009b); Williams et al. (2010); Khasanov et al. (2009a)].

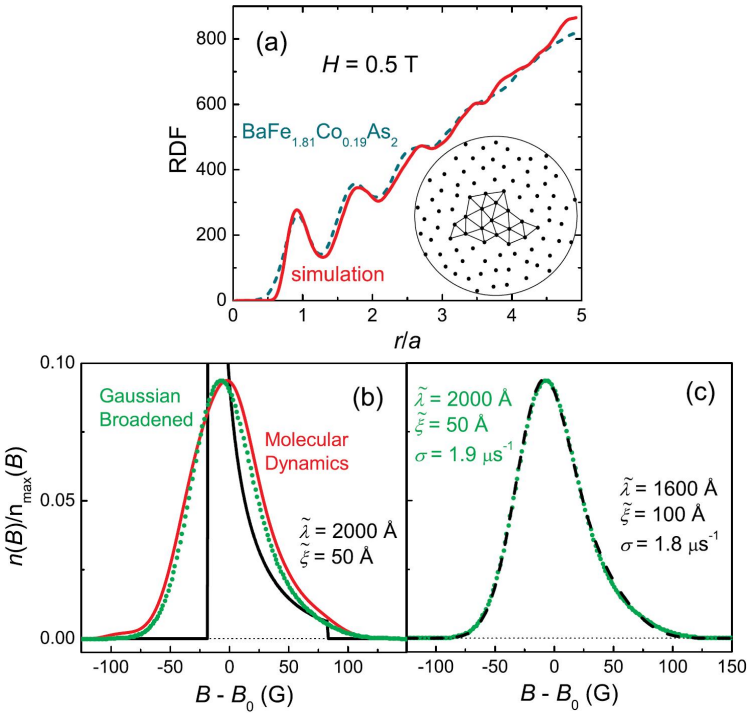

Figure 4.11: (a) Radial distribution function (RDF) of $BaFe_{1.81}Co_{0.19}As_2$ at $H = 0.5$ T from Ref. [Inosov et al. (2010b)] (dashed curve) and of the disordered VL shown in the lower right generated by molecular dynamics (MD). Note 5000 vortices were used in the MD simulation. The horizontal scale is normalized with respect to the intervortex spacing $a = 691$ Å of the perfect hexagonal VL. (b) Theoretical simulations of the TF-μSR line shape of the perfect VL (black curve) and of the disordered VL (red curve) corresponding to the RDF shown in (a). The green circles show the line shape of the perfect VL convoluted by a Gaussian distribution of fields, corresponding to $\sigma = 1.9$ μs^{-1}. All three simulations assume $\tilde{\lambda} = 2000$ Å and $\tilde{\xi} = 50$ Å. (c) Same Gaussian-broadened line shape as shown in (b) and a Gaussian-broadened ideal line shape with $\tilde{\lambda} = 1600$ Å, $\tilde{\xi} = 1000$ Å and $\sigma = 1.8$ μs^{-1}. The heights of the line shapes in (b) and (c) are normalized with respect to the height $n_{max}(B)$ of the ideal line shape [Sonier et al. (2011)].

The effects of magnetic order and/or random frozen VL disorder in iron-arsenic superconductors introduce considerable uncertainty in values of λ obtained by TF μSR. Unfortunately, these effects cannot be modeled in a reliable way. Compounding the problem is a lack of information on how these factors evolve with temperature. Consequently, caution is warranted in drawing conclusions about the anisotropy of the superconducting gap in these materials from TF-μSR measurements.

To summarize, three possible reasons (nonlocal effects in Eilenberger equations, Fig. 1 in **paper 3**, the core induced SDW and disorder effects in flux line lattice) can explain the TF μSR line shape of $BaFe_{1.82}Co_{0.18}As_2$ where impurity scattering rate is strong. The detail investigation the μSR results of whole field range can clarify the main origin of observed phenomena.

We study the case of weak intraband scattering which can be realized in stoichiometrical pnictides such as $LiFeAs$. The single absolute gap value is found in $LiFeAs$ and the high value $\xi_h(B \to 0, T = 0) = 9.8$ nm in comparison with $\xi_{c2}(T = 0) \approx 2 - 4$ nm is obtained in SANS measurements [Inosov et al. (2010c)], i.e. $\xi_h/\xi_{c2} \approx 3$. Fig. 2 in **paper 3** present the ξ_h/ξ_{c2} field dependence at $\Gamma_0 = \Gamma_\pi = \Gamma = 0, 0.05, 0.06, 0.065$ and $T/T_{c0} = 0.15$. As can be seen from this picture the shape of curve not change considerably, but the absolute values of ξ_h/ξ_{c2} depend crucially on it. At low values of Γ ξ_h/ξ_{c2} resides below the AGL curve and moves above it at high Γ (for gapless superconductivity case $\Gamma > 0.064$), opposite to the case of the strong intraband scattering considered in Fig. 1 in **paper 3**. Such behavior is quite different from that in s_{++} pairing symmetry where intraband and interband scattering rates act in similar way and ξ_h/ξ_{c2} decreases always with impurity scattering. The obtained $\xi_h(B \to 0)/\xi_{c2} = 1.75$ in the $s^{\pm}$ model is much more near to the experimental results [Inosov et al. (2010c)] than in the s_{++} model, where strong reduction of ξ_h is visible. But this requires too high value of $\Gamma_\pi > 0.064$, so the sample would be in the gapless state in this case. This contradicts to the observed value of gap by the ARPES measurements [Inosov et al. (2010c)].

Paper 4. Eilenberger and Ginzburg-Landau models of the vortex core in high κ-superconductors

The field distribution of the mixed state in dirty s-wave superconductors in wide temperature and field range is investigated in the framework of the Eilenberger theory in **paper 4**. The normalized dependences of the cutoff parameter $\xi_h/\xi_{c2}(B/B_{c2})$ responsible for the line shape of the μSR resonance are calculated. It is found that this dependence is nonuniversal and depends on temperature and on impurity scattering rate, Γ. This is different from the universal dependence expected from the GL theory. At high values of $\Gamma/2\pi T_{c0} \geq 0.5$ the dependence shows plateau in intermediate field range and the values $\xi_h(B)/\xi_{c2}$ are less than one. The strong suppression ξ_h/ξ_{c2} with Γ can qualitatively explain the μSR experimental results in some low-temperature superconductors V_3Si, $NbSe_2$ and $LuNi_2B_2C$ in high field range (see Fig. 7 in Ref. [Sonier (2007)]). For the quantitative comparison of the theory and experimental results the anisotropy of the Fermi surface should be taken into account. The coherence length ξ_{KZ} of the linearized Eilenberger equation was calculated for three-dimensional (3D) isotropic case of the Fermi sphere and two-dimensional (2D) isotropic materials, i.e. the Fermi cylinder [Kogan and Zhelezina (2005)]. A close-form equation for $\xi_{KZ}(B)$ was found for both Fermi surfaces. It was shown that the results can be represented in the reduced form as $\xi_{KZ}(B)/\xi_{c2}(B_{c2}) = U(B/B_{c2})$ with U being an universal function. The only difference between 2D and 3D situations is the numerical coefficient (α) in this universal function. We believe that the similar consideration about minor importance of the Fermi surface anisotropy can be

applied for our cutoff parameter ξ_h if it is presented in the reduced form $\xi_h/\xi_{c2}(B/B_{c2})$. Our microscopical model justified the empirical methods for the interpretation of the μSR [Sonier (2004, 2007)] and magnetization [Kogan et al. (2006)] investigations and shows that at least one parameter, different from GL theory, is needed for the explanation of the result even in the isotropic s-wave superconductors. It results in three-parameter ($\lambda(\Gamma,T)$, $B_{c2}(\Gamma,T)$, and $\xi_h/\xi_{c2}(\Gamma,B,T)$) model of the mixed state of s-wave superconductors. Absolute values of ξ_h and ξ_1 show different dependence on impurities: $\xi_h(B)$ curves decreases monotonously with impurity scattering rate, while $\xi_1(B)$ curves cross each other in this case.

The Ginzburg-Landau free energy per unit volume over cross-sectional area A in a plane perpendicular to the vortices, measured relative to that of the Meissner state, can be expressed in dimensionless form as [Hao et al. (1991)]

$$F = F_c + F_{kg} + F_{kj} + F_f, \tag{4.23}$$

where

$$F_c = \frac{1}{A}\int d^2\rho \frac{1}{2}(1-f^2)^2, \tag{4.24}$$

$$F_{kg} = \frac{1}{A}\int d^2\rho \frac{1}{\kappa^2}(\nabla f)^2, \tag{4.25}$$

$$F_{kj} = \frac{1}{A}\int d^2\rho f^2 \mathbf{a}_s^2, \qquad \mathbf{a}_s = \mathbf{a} + \frac{1}{\kappa}\nabla\gamma, \tag{4.26}$$

and

$$F_f = \frac{1}{A}\int d^2\rho \mathbf{b}^2, \tag{4.27}$$

are the condensation energy, kinetic energy associated with gradients in the magnitude of order parameter, kinetic energy associated with supercurrent, and magnetic field energy; f and γ are the normalized magnitude and phase of the order parameter $\Psi = \Psi_0 f e^{i\gamma}$ (Ψ_0 is the magnitude of order parameter in absence of field); $\mathbf{a}$ is the vector potential satisfying $\nabla\cdot\mathbf{a}=0$; $\mathbf{b}=\nabla\times\mathbf{a}$ is the local magnetic flux density; and the two-dimensional integral is taken over A.

The dimensionless units were used, which correspond to measuring the magnitude of the order parameter in units of Ψ_0, length in units of λ, magnetic field in units of $\sqrt{2}H_c = \kappa\Phi_0/2\pi\lambda^2$, vector potential in units of $\sqrt{2}H_c\lambda = \kappa\Phi_0/2\pi\lambda$, and energy in units of $H_c^2/4\pi$, where H_c is the thermodynamic critical field, and $\Phi_0 = hc/2e = 2.07\times10^{-7}$ G cm^2 is the flux quantum (Φ_0 corresponds to $2\pi/\kappa$ in the dimensionless expressions).

In Ginzburg-Landau theory, the temperature dependence of a superconductor is contained in the scaling factors, such as $\sqrt{2}H_c(T)$ and $\lambda(T)$, and therefore all physical quantities in their dimensionless form are independent of T, and the only parameter intrinsic to the sample is κ. The second Ginzburg-Landau equation is

$$\mathbf{j} = -f^2\mathbf{a}_s, \tag{4.28}$$

where **j** is the supercurrent density.

For a vortex centered on the z axis, in terms of cylindrical coordinates ρ, ϕ, and z, with unit vectors $\hat{\rho}$, $\hat{\phi}$, and $\hat{z}$, $\gamma = -\phi$, $\mathbf{b} = \hat{z}b_z(\rho)$, $\mathbf{j} = \hat{\phi}j_\phi(\rho)$, and $\mathbf{a} = \hat{\phi}a_\phi(\rho)$ the $\nabla\gamma = -\nabla\phi = -\hat{\phi}(1/\rho)$, $\mathbf{a}_s = \hat{\phi}(a_\phi - 1/\kappa\rho)$, and therefore

$$\nabla \times \mathbf{a}_s = \hat{\mathbf{z}}[b_z - \frac{2\pi}{\kappa}\delta(\rho)]. \tag{4.29}$$

For an array of vortices at positions ρ_i,

$$\nabla \times \mathbf{a}_s = \hat{\mathbf{z}}[b_z - \frac{2\pi}{\kappa}\sum_i \delta(\rho - \rho_i)], \tag{4.30}$$

where each term in the summation represents one vortex carrying one quantum of magnetic flux centered at ρ_i.

Using Eqs. (4.28) and (4.30), and with the help of Ampere's law $\mathbf{j} = \nabla \times \mathbf{b}$ and the divergence theorem, the electromagnetic free energy per unit volume $F_{em} = F_{kj} + F_j$ can be simply written as

$$F_{em} = Bb_z(0), \tag{4.31}$$

where $B = 2\pi/\kappa A_{cell}$ is the averaged magnetic flux density, A_{cell} is the unit-cell area of the flux-line lattice ($B = \Phi_0/A_{cell}$ in conventional units), and $b_z(0)$ is the local magnetic flux density at the center of a vortex resulting not only from the vortex's own field but also that of all surrounding vortices.

Then the superposition was applied

$$b_z(\rho) = \sum_i b_{0z}(\rho - \rho_i), \tag{4.32}$$

where $b_{0z}(\rho - \rho_i)$ is the magnetic flux density of an isolated vortex located at ρ_i, and the summation runs over all vortices; and to obtain b_{0z}, one should follow the procedure of Ref. [Clem (1975)] and take into account the effect of overlapping of vortices. For the order parameter a trial function

$$f = \frac{\rho}{(\rho^2 + \xi_v^2)^{1/2}} f_\infty, \tag{4.33}$$

where ξ_v and f_∞ are two variational parameters representing the effective core radius of a vortex and the depression in the order parameter due to overlapping of vortices, respectively. It is expected that $f_\infty \to 1$ as $B \to 0$ and $f_\infty \to 0$ as $B \to B_{c2}$ ($B_{c2} = H_{c2} = \kappa$ in the dimensionless units). Then, with the help of Ampere's law and $\mathbf{b} = \nabla \times \mathbf{a}$, the second Ginzburg-Landau equation can be solved analytically, and

$$b_{0z} = \frac{f_\infty K_0(f_\infty(\rho^2 + \xi_v^2)^{1/2})}{\kappa\xi_v K_1(f_\infty\xi_v)}, \tag{4.34}$$

where $K_n(x)$ is a modified Bessel function of *n*th order.

For a two-dimensional array of vortices at the positions $\rho_i = \mathbf{L}$, where **L** is a lattice vector, there is a corresponding two-dimensional reciprocal lattice of lattice vector **G** such that $e^{i\mathbf{G}\cdot\mathbf{L}} = 1$. The Fourier transform of b_{0z}, given by Eq. (4.34), is

$$\tilde{b}_{0z}(q) = \int d^2\rho b_{0z}(\rho)e^{i\mathbf{q}\cdot\rho} = \frac{2\pi f_\infty K_1(\xi_v(q^2 + f_\infty^2)^{1/2})}{\kappa(q^2 + f_\infty^2)^{1/2}K_1(f_\infty\xi_v)}, \tag{4.35}$$

where the below formulas were used [Abramowitz and Stegun (1964); Gradshteyn and Ryzhik (1965)]

$$\frac{1}{\pi}\int_0^{\pi} d\theta e^{ix\cos\theta} = J_0(x), \tag{4.36}$$

and

$$\int_0^{\infty} dx \cdot xJ_0(\beta x)K_0(\alpha(x^2+z^2)^{1/2}) = \frac{zK_1(z(\alpha^2+\beta^2)^{1/2})}{(\alpha^2+\beta^2)^{1/2}}. \tag{4.37}$$

(Note that $\tilde{b}_{0z}(0) = 2\pi/\kappa$ is the flux quantum). Then Eq. (4.32) becomes

$$b_z(\rho) = \sum_{\mathbf{L}} b_{0z}(\rho - \mathbf{L}) = \sum_{\mathbf{L}} \int \frac{d^2q}{(2\pi)^2}\tilde{b}_{0z}(q)e^{i(\rho-\mathbf{L})\cdot q} = \frac{1}{A_{cell}}\sum_{\mathbf{G}} \tilde{b}_{0z}(\mathbf{G})e^{i\rho\cdot\mathbf{G}}, \tag{4.38}$$

where the relation

$$A_{cell}\sum_{\mathbf{L}} e^{i\mathbf{L}\cdot q} = (2\pi)^2\sum_{\mathbf{G}}\delta(\mathbf{q}-\mathbf{G}), \tag{4.39}$$

has been used. Using the fact that $B = 2\pi/\kappa A_{cell}$ and separating the term with $\mathbf{G} = 0$ from the summation, the above equation becomes

$$b_z(\rho) = B[1 + \sum_{\mathbf{G}\neq 0}\frac{f_\infty K_1(\xi_v(\mathbf{G}^2+f_\infty^2)^{1/2})}{(\mathbf{G}^2+f_\infty^2)^{1/2}K_1(f_\infty\xi_v)}e^{i\rho\mathbf{G}}]. \tag{4.40}$$

The magnetic flux density at the vortex center is obtained by setting $\rho = 0$:

$$b_z(0) = B[1 + \sum_{\mathbf{G}\neq 0}\frac{f_\infty K_1(\xi_v(\mathbf{G}^2+f_\infty^2)^{1/2})}{(\mathbf{G}^2+f_\infty^2)^{1/2}K_1(f_\infty\xi_v)}]. \tag{4.41}$$

The summation approximation in **G** space by an integral taken over the outside of the first Brillouin zone is:

$$\sum_{\mathbf{G}\neq 0} \approx \frac{1}{A_{BZ}}\int_{G\geq G_{BZ}} d^2G, \tag{4.42}$$

where $A_{BZ} = \pi G_{BZ}^2 = (2\pi)^2/A_{cell}$ is the area of the first Brillouin zone, and the zone boundary has been approximated by a circle of radius G_{BZ}. That $B = 2\pi/\kappa A_{cell}$ gives $G_{BZ} = \sqrt{2B\kappa}$. Note that, although the approximation of Eq. (4.42) is valid only at low field when the reciprocal lattice spacing (which is inversely proportional to the vortex spacing) is small, for high field the error due to the approximation is reduced by the fact that the contribution of the sum becomes small compared to that of the $\mathbf{G} = 0$ term; therefore the approximation for the whole field region was used. Thus,

$$b_z(0) = B + \frac{f_\infty K_0(\xi_v(f_\infty^2+2B\kappa)^{1/2})}{\kappa\xi_v K_1(f_\infty\xi_v)}]. \tag{4.43}$$

The above equation shows the properties that $b_z(0) \to b_{0z}(0)$ when $B \to 0$ and $b_z(0) \to B$ when B becomes large.

Therefore, Eq. (4.31) becomes

$$F_{em} = B^2 + \frac{Bf_\infty K_0(\xi_v(f_\infty^2 + 2B\kappa)^{1/2})}{\kappa\xi_v K_1(f_\infty\xi_v)}]. \tag{4.44}$$

With f being given by Eq. (4.33), F_c and F_{kg} are calculated by taking the integral over one lattice cell, which is approximated by a circle centered at a vortex axis and having the same cell area. This approximation means that the energy differences between specific vortex structures (hexagonal, square, amorphous, ...) was neglected, which is expected to be only a few percent. So,

$$F_c = \frac{1}{2}(1 - f_\infty^2)^2 + \frac{B\kappa\xi_v^2 f_\infty^2}{2}[(1 - f_\infty^2)ln[\frac{2}{B\kappa\xi_v^2} + 1] + \frac{f_\infty^2}{2 + B\kappa\xi_v^2}], \tag{4.45}$$

and

$$F_{kg} = \frac{Bf_\infty^2(1 + B\kappa\xi_v^2)}{\kappa(2 + B\kappa\xi_v^2)^2}. \tag{4.46}$$

Now the variationally-calculated total free-energy density F is the sum of F_c,F_{kg}, and F_{em}, given by Eqs. (4.45), (4.46) and (4.44), where the variational parameters f_∞ and ξ_v satisfy

$$\frac{\partial F}{\partial f_\infty} = 0, \tag{4.47}$$

and

$$\frac{\partial F}{\partial \xi_v} = 0. \tag{4.48}$$

The thermodynamic magnetic field H is given by

$$H = \frac{1}{2}\frac{dF}{dB} = \frac{1}{2}[\frac{\partial F}{\partial B}]_{f_\infty,\xi_v}, \tag{4.49}$$

where the third part of the equation is obtained by using Eqs. (4.47) and (4.48). By a straightforward calculation,

$$\begin{aligned} H &= \frac{\kappa\xi_v^2 f_\infty^2}{2}[\frac{1 - f_\infty^2}{2}\ln[\frac{2}{B\kappa\xi_v^2 + 1}] - \frac{1 - f_\infty^2}{2 + B\kappa\xi_v^2} + \frac{f_\infty^2}{(2 + B\kappa\xi_v^2)^2}] + \frac{f_\infty^2(2 + 3B\kappa\xi_v^2)}{2\kappa(2 + B\kappa\xi_v^2)^3} + \\ &+ B + \frac{f_\infty}{2\kappa\xi_v K_1(f_\infty\xi_v)}[K_0(\xi_v(f_\infty^2 + 2B\kappa)^{1/2}) - \frac{B\kappa\xi_v K_1(\xi_v(f_\infty^2 + 2B\kappa)^{1/2})}{(f_\infty^2 + 2B\kappa)^{1/2}}], \end{aligned} \tag{4.50}$$

where the first two terms correspond to F_c and F_{kg}, respectively, and the last two terms correspond to F_{em}. The magnetization M is related to H by

$$-4\pi M = H - B. \tag{4.51}$$

Eqs. (4.50) and (4.51) give us the implicit function $M(H)$.

Note that H is the internal field, which is equal to the applied field only for a sample of zero demagnetization coefficient, but is approximately equal to the applied field when the demagnetization

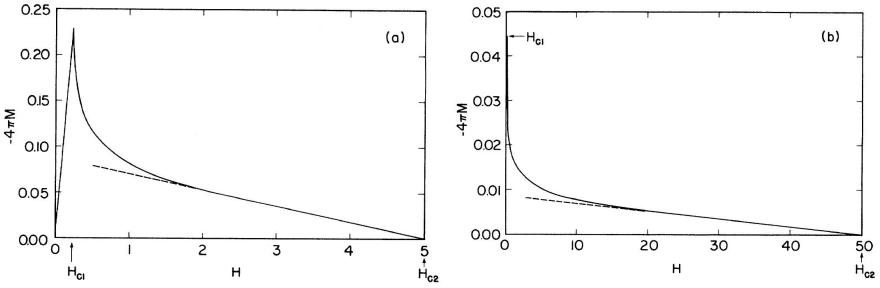

Figure 4.12: Calculated $-4\pi M$ vs H in dimensioneless units for (a) $\kappa = 5$ and (b) $\kappa = 50$, where the dashed lines are the corresponding Abrikosov high-field results [Hao et al. (1991)].

effect can be neglected. For the case when the demagnetization effect is important, H is equal to the applied field minus the field of demagnetization (see Ref. [Fetter and Hohenberg (1969)]).

H_{c1} is given by the limit of H as $B \to 0$.

$$H_{c1} = \frac{\kappa\xi_{v0}^2}{8} + \frac{1}{8\kappa} + \frac{K_0(\xi_{v0})}{2\kappa K_1(\xi_{v0})}, \tag{4.52}$$

where ξ_{v0} is the value of ξ_v at $B = 0$, which minimizes the free energy of a single vortex and satisfies

$$\kappa\xi_{v0} = \sqrt{2}[1 - \frac{K_0^2(\xi_{v0})}{K_1^2(\xi_{v0})}]^{1/2}. \tag{4.53}$$

The value of $\kappa\xi_{v0} \approx \sqrt{2}$ for $\kappa \gg 1$. Note that both Eqs. (4.52) and (4.53) have been obtained in Ref. [Clem (1975)], which are the limits of Eqs. (4.50) and (4.48) as $B \to 0$, as expected.

In principle, f_∞ and ξ_v are found for arbitrary B and κ by solving Eqs. (4.47) and (4.48) simultaneously, but this procedure involves numerical analysis and is not convenient in practical use. The approximation of $f_\infty(\kappa, B)$ and $\xi_v(\kappa, B)$ was used instead by some suitable functions. The following formulas are good approximations for the case of $\kappa > 10$:

$$f_\infty^2 = 1 - [\frac{B}{\kappa}]^4, \tag{4.54}$$

$$[\frac{\xi_v}{\xi_{v0}}]^2 = [1 - 2[1 - \frac{B}{\kappa}]^2\frac{B}{\kappa}][1 + [\frac{B}{\kappa}]^4]. \tag{4.55}$$

For smaller κ the above formulas need modification; for example, for $\kappa \approx 5$, ξ_v is better approximated by

$$[\frac{\xi_v}{\xi_{v0}}]^2 = 1 + [\frac{B}{\kappa}]^4, \tag{4.56}$$

with f_∞ remaining unchanged as given by Eq. (4.54).

The mixed-state diamagnetism can readily be measured, and, when compared to theory, can give the diamagnetic H_{c2}. Close enough to H_{c2}, the diamagnetism is given by

$$-4\pi M = \frac{H_{c2}(T) - H}{(2\kappa^2 - 1)\beta_A}, \tag{4.57}$$

where β_A is 1.16 for a hexagonal array. This suggests that a linear extrapolation of $M(H)$ or $M(T)$ data should determine $H_{c2}(T)$.

Curves of $-4\pi M(H)$ for the cases of $\kappa = 5$ and 50 are calculated using the above formulas and shown in Figs. 4.12 (a) and (b). Abrikosov's high-field results, Eq. (4.57) with $\beta_A = 1.16$, for the same values of κ are also shown for comparison. As can be seen, the results satisfy the qualitative properties of type-II superconductors: the slope $d(-4\pi M)/d(H)$ is infinite at H_{c1}; in the high-field region was covered the Abrikosov result that $-4\pi M$ decreases linearly as H increases and vanishes at H_{c2}.The magnitude of the limiting slope of $-4\pi M$ versus H obtained from Eqs. (4.50) and (4.51) is actually slightly less than that of the Abrikosov result [Eq. (4.57) with β_A is 1.16 for a hexagonal array] very close to H_{c2}, because of using of the circular cell approximation in Eqs. (4.45) and (4.46). Nevertheless, as seen from Figs. 4.12 (a) and (b), the results are practically indistinguishable from the linear Abrikosov curve over the field range $0.4H_{c2} < H < H_{c2}$. Quantitatively, as shown by the comparison with Abrikosov's high-field result, these results appear to be a good approximation to the solution of the Ginzburg-Landau equations.

Paper 5. Generalized London theory of the mixed state of high-κ superconductors as a projection of the quasiclassical Eilenberger approach

The field distribution of the mixed state in dirty s-wave superconductors in a wide temperature and field range is investigated in the framework of the nonlocal Eilenberger theory and projected on the London equation in **paper 5**. The normalized magnetic field dependences of the cutoff parameter $\xi_h/\xi_{c2}(B/B_{c2})$ responsible for the line shape of the μSR resonance are obtained. It is found that this dependence is nonuniversal and depends on the impurity scattering rate Γ and the temperature. At high enough values of $\Gamma/2\pi T_{c0} \geq 0.5$, the dependence plateaus in the intermediate field range and the low temperatures, and $\xi_h(B)/\xi_{c2}$ is of the order of 0.25. The strong suppression of ξ_h/ξ_{c2} with Γ and T can explain the experimental results in many low-temperature superconductors (V_3Si, $NbSe_2$ and $LuNi_2B_2C$ and iron pnictide superconductor $BaFe_{1.82}Co_{0.18}As$), where the values $\xi_h/\xi_{c2} < 1$ has been observed. It is connected with the nonlocal bound Andreev states of the vortex core. The obtained projection of the Eilenberger equations is compared with the nonlocal Kogan-Gurevich theory. The field dependence of the cutoff parameter changes the magnetization and the variance of the magnetic field. A difference is observed between $\xi_h(T)$ and nonlocal range $\rho(T)$ of the Kogan-Gurevich theory [Kogan et al. (1996b)], where only the contribution of the extended state is taken into account. A strong difference from the AGL theory and linearized Eilenberger approach (the Kogan-Zhelezina theory [Kogan and Zhelezina (2005)]) is found. This is explained by the Kramer-Pesch effect which is not taken into account in these theories.

The detailed microscopical approach to the Kramer-Pesch effect, i.e., the shrinking of the core radius upon lowering T (to be exact, an anomalous increase in the slope of the pair potential at the vortex center at low T) was obtained by Hayashi *et al.* [Hayashi et al. (1998)]. The Bogoliubov-de Gennes (BdG) equation, which is one of the most fundamental equation of superconductivity and

contains fully quantum effects, was self-consistently solved there. The starting point was the BdG equation for the quasiparticle wave functions $u_j(\mathbf{r})$ and $v_j(\mathbf{r})$ labeled by the quantum number j:

$$[\frac{-1}{2k_F\xi_0}\nabla^2 - E_F]u_j(\mathbf{r}) + \Delta(\mathbf{r})v_j(\mathbf{r}) = E_j u_j(\mathbf{r}),$$

$$-[\frac{-1}{2k_F\xi_0}\nabla^2 - E_F]v_j(\mathbf{r}) + \Delta^*(\mathbf{r})u_j(\mathbf{r}) = E_j v_j(\mathbf{r}), \tag{4.58}$$

in a dimensionless form, where $\Delta(\mathbf{r})$ is the pair potential and E_F ($= k_F\xi_0/2$) is the Fermi energy. The length (energy) scale is measured by $\xi_0(\Delta_0)$. For an isolated single vortex in an extreme type-II superconductor, the vector potential in Eq. (4.58) may be neglected. The pair potential is determined self-consistently by

$$\Delta(\mathbf{r}) = g\sum_{|E_j|\le\omega_D} u_j(\mathbf{r})v_j^*(\mathbf{r})(1-2f(E_j)), \tag{4.59}$$

with the Fermi function $f(E)$. Here, g is the coupling constant and $\omega_D = 10\Delta_0$ is the energy cutoff, which are related by the BCS relation via the transition temperature T_c and the gap Δ_0. The current density is given by

$$\mathbf{j(r)} \propto \mathtt{Im}\sum_j [f(E_j)u_j^*(\mathbf{r})\nabla u_j(\mathbf{r}) + (1-f(E_j))v_j(\mathbf{r})\nabla v_j^*(\mathbf{r})]. \tag{4.60}$$

An isolated vortex was considered under the following conditions: (a) The system is a cylinder with a radius R. (b) The Fermi surface is cylindrical, appropriate for the materials such as $NbSe_2$ and high-T_c cuprates. (c) The pairing has isotropic s-wave symmetry. Thus the system has a cylindrical symmetry. The eigenfunctions are

$$u_j(\mathbf{r}) = u_{n\mu}(r)\exp[i(\mu - \frac{1}{2})\theta], \tag{4.61}$$

and

$$v_j(\mathbf{r}) = v_{n\mu}(r)\exp[i(\mu + \frac{1}{2})\theta], \tag{4.62}$$

with $\Delta(\mathbf{r}) = \Delta(r)\exp[-i\theta]$ in polar coordinates, where n is a radial quantum number and the angular momentum $|\mu| = \frac{1}{2}, \frac{3}{2}, \frac{5}{2}, ...$ The eigenfunctions were expanded in terms of the Bessel functions $J_m(r)$ as

$$u_{n\mu}(r) = \sum_i c_{ni}\phi_{i|\mu-\frac{1}{2}|}(r), \tag{4.63}$$

and

$$v_{n\mu}(r) = \sum_i d_{ni}\phi_{i|\mu+\frac{1}{2}|}(r), \tag{4.64}$$

with

$$\phi_{im}(r) = [\sqrt{2}/RJ_{m+1}(\alpha_{im})]J_m(\alpha_{im}r/R), \tag{4.65}$$

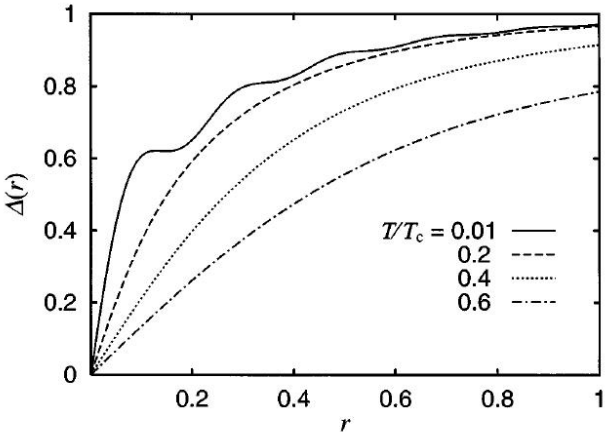

Figure 4.13: The spatial variation of the pair potential $\Delta(r)$ normalized by Δ_0 around the vortex for several temperatures and $k_F\xi_0 = 16$. The length r is measured by ξ_0 [Hayashi et al. (1998)].

[$i = 1, 2, ..., N$, and α_{im} is the ith zero of $J_m(R)$]. The BdG is reduced to a $2N \times 2N$ matrix eigenvalue problem [Gygi and Schlüter (1991)]. This system is characterized by $k_F\xi_0$, which is a key parameter of the present problem.

In Fig. 4.13, the calculated spatial variation of $\Delta(r)$ is displayed for various T. It is seen that as T decreases, the core size ξ_1 defined by $\xi_1^{-1} = \lim_{r\to 0} \Delta(r)/r$ shrinks and the oscillatory spatial variation with a wave length $\sim 1/k_F$ becomes evident in $\Delta(r)$ [Kramer and Pesch (1974); Gygi and Schlüter (1991)]. The physical reason for this Friedel-like oscillation lies in the following facts. All eigenfunctions $u_{n\mu}(r)$ and $v_{n\mu}(r)$ contain a rapid oscillation component with $1/k_F$. At lower T the lowest bound states, whose oscillation amplitude is large near the core, dominate physical quantities. The oscillatory behavior always appears at sufficiently low T irrespective of values of $k_F\xi_0$. A similar oscillatory spatial variation around a vortex core in the Bose condensate of ^{4}He is found theoretically, due to the roton excitations [Giorgini et al. (1997)].

The associated supercurrent $j_\theta(r)$ and the field $H(r)$ are shown in Fig. 4.14. Reflecting the above oscillation, $j_\theta(r)$ also exhibits a weak oscillation around $r = (0.2 - 0.5)\xi_0$. It is difficult to see the oscillation in $H(r)$, because it is obtained by integrating $j_\theta(r)$ via the Maxwell equation $\nabla \times \mathbf{H} = \frac{4\pi}{c}\mathbf{j(r)}$, resulting in a smeared profile. It is also seen that the position of the maximum of $j_\theta(r)$ becomes shorter as T decreases. These features quite differ from those obtained within the Ginzburg-Landau framework [Fetter and Hohenberg (1969); Brandt (1997)].

The T dependence of $\xi_1(T)$ for various $k_F\xi_0$ values is shown in Fig. 4.15. Coinciding with Kramer and Pesch [Kramer and Pesch (1974)] for the s-wave pair and Ichioka *et al.* [Ichioka et al. (1996)] for the d-wave pair, $\xi_1(T)$ decreases almost linearly with T; that is, $\xi_1(T)/\xi_0 \sim T/T_c$ except at extremely low T. An important difference from these quasiclassical theories [Kramer and Pesch (1974); Ichioka et al. (1996)] appears at lower T. At a lower $T < T_0 \simeq T_c/(k_F\xi_0)$, where the quantum limit is realized, the shrinkage of the core size stops to saturate, and the saturated value is estimated as $\xi_1/\xi_0 \sim (k_F\xi_0)^{-1}$.

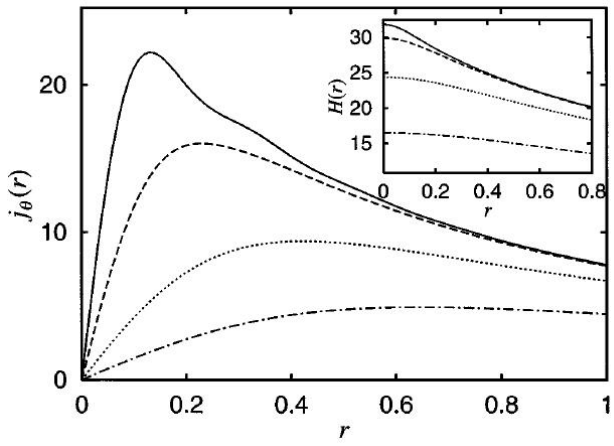

Figure 4.14: The current distribution normalized by $c\phi_0/(8\pi^2\xi_0^3\kappa^2)$ for several temperatures, where ϕ_0 is the flux quantum and κ ($\gg 1$) is the GL parameter. The inset shows the field distribution normalized by $\phi_0/(2\pi\xi_0^2\kappa^2)$. The temperatures are the same as in Fig. 4.13, and $k_F\xi_0 = 16$ [Hayashi et al. (1998)].

According to the μSR experimental data [Sonier et al. (1997a,b)], the core radius in $NbSe_2$ shows a strong T dependence, while that in YBCO with $T_c = 60$ K is almost T independent below $\sim 0.6T_c$. This seemingly contradicting result can be understood as follows. The strong T dependence in $NbSe_2$ is the usual Kramer and Pesch (KP) effect [Kramer and Pesch (1974); Gygi and Schlüter (1991); Volovik (1993); Ichioka et al. (1996)] corresponding to the curves for larger $k_F\xi_0$ in Fig. 4.15. At T below T_0 estimated as ~ 100 mK ($k_F\xi_0 \sim 70$), the shrinkage must saturate (the above experiment is done above ~ 2 K). As for the YBCO data, since the estimated $k_F\xi_0$ is small (~ 4 [Maggio-Aprile et al. (1995)] for YBCO with $T_c = 90$ K), the saturation is already attained at a relatively high T such as shown in Fig. 4.15. Thus the absence or weakness of the KP effect in YBCO is simply attributable to the fact that the quantum-limit temperature T_0 is quite high.

Reflecting the shrinkage of the core radius, the boundstate energies E_μ increase as T decreases. This T-dependent E_μ shift, due to the KP effect, and its saturation at lower T may lead to a nontrivial T dependence in thermodynamic and transport properties.

In Fig. 4.16, the energy levels E_μ of the low-lying bound states ($\mu = \frac{1}{2}, \frac{3}{2}, ..., \frac{13}{2}$) are presented as a function of $k_F\xi_0$, at sufficiently low T ($T/T_c = 0.01$) where increasing of the energy levels saturates. It is seen that in the large $k_F\xi_0$ region, the bound states densely pack inside the gap Δ_0, allowing us to regard them as continuous ones. This is the case where the quasiclassical approximation [Kramer and Pesch (1974); Ichioka et al. (1996)] validates. It is found that even for small $|\mu|$, the spacing between the energy levels E_μ is not constant, but rather becomes narrower as $|\mu|$ increases. The often adopted formula $E_\mu/\Delta_0 = 2\mu/(k_F\xi_0)$ or $2\mu/(k_F\xi_1)$ due to Caroli *et al.* [Caroli and Matricon (1964)], or $E_\mu/\Delta_0 = (2\mu/k_F\xi_0)\ln[\xi_0/2\xi_1]$ by Kramer and Pesch in the limit $\xi_1 \ll \xi_0$ [Kramer and Pesch (1974)] do not satisfactorily explain the self-consistent results. Instead, the result is empirically fitted to a formula $E_{1/2}/\Delta_0 = (0.5/k_F\xi_0)\ln[k_F\xi_0/0.3]$ for large $k_F\xi_0$ as shown in the

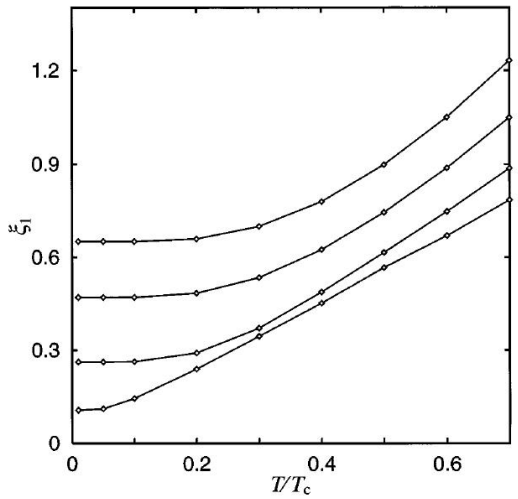

Figure 4.15: The T dependence of the vortex radius ξ_1 normalized by ξ_0 for several $k_F\xi_0$ $(= 1.2, 2, 4,$ and 16 from top to bottom) [Hayashi et al. (1998)].

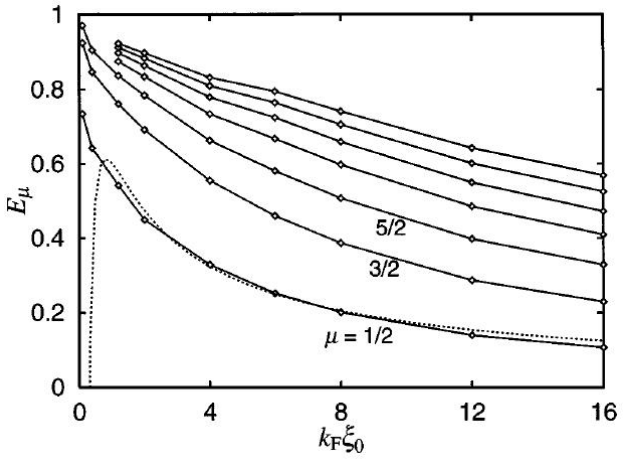

Figure 4.16: The lowest seven bound-state energies E_μ, normalized by Δ_0, as a function of $k_F\xi_0$, with $\mu = 1/2, 3/5, 5/2, ..., 13/2$ at enough low temperature $T/T_c = 0.01$. The dotted line is a fitting curve (see the text) [Hayashi et al. (1998)].

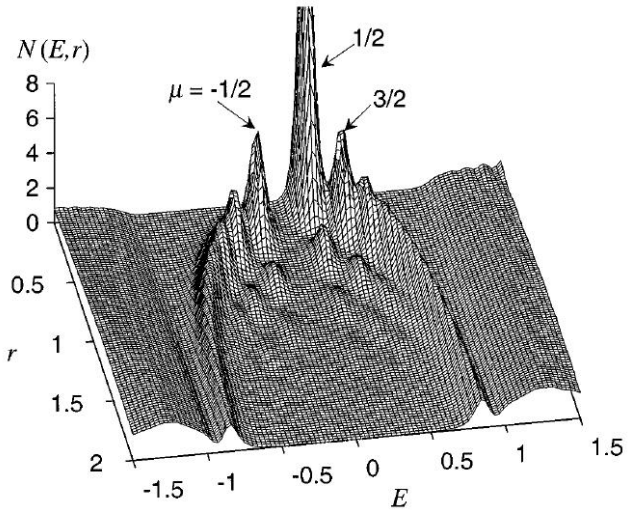

Figure 4.17: The spectral evolution $N(E, r)$ at $T/T_c = 0.05$ and $k_F\xi_0 = 8$. It is normalized by the normal-state density of states at the Fermi surface. E and r are measured by Δ_0 and ξ_0, respectively [Hayashi et al. (1998)].

dotted curve in Fig. 4.16.

In Fig. 4.17, the spectral evolution, i.e., the spatial variation of local density of states, which is calculated by $N(\mathbf{r}, E) \propto \sum_j [|u_j(\mathbf{r})|^2 f'(E-E_j) + |v_j(\mathbf{r})|^2 f'(E+E_j)]$, is shown for $k_F\xi_0 = 8$ at low temperature $T = 0.05T_c$. It is well contrasted with that of the higher T case by Gygi and Schlüter [Gygi and Schlüter (1991)] (see, for comparison, Fig. 15 in Ref. [Gygi and Schlüter (1991)], where $k_F\xi_0 = 70$ and $T = 0.13T_c$, calculated under the two-dimensional Fermi surface). As one lower T, because of the quantum effects, the thermally smeared spectral structure drastically changes and becomes far finer around the vortex. The spectra are discretized inside the gap and consist of several isolated peaks, each of which precisely corresponds to the bound states E_μ ($|\mu| = \frac{1}{2}, \frac{3}{2}, ...,$). Reflecting the oscillatory nature of the eigenfunctions $u_\mu(r)$ and $v_\mu(r)$ with the period $1/k_F$, the spectral evolution also exhibits the Friedel-like oscillation as seen in Fig. 4.17.

To show clearly the particle-hole asymmetry of the local density of states of Fig. 4.17, the spectra at the vortex center $r = 0$ and $0.2\xi_0$ is presented in Fig. 4.18. At the center $r = 0$, the bound-state peak with $E_{1/2}$, which comes from $u_{1/2}$ and $v_{-1/2}$, appears on the $E > 0$ side and other peaks for $|E_\mu| < \Delta_0$ (which include $E_{-1/2}$) vanish at $r = 0$, because only $u_{1/2}(r)$ and $v_{-1/2}(r) \propto J_0(r = 0) \neq 0$. The particle-hole asymmetry in the vortex bound states appears even if the normal-state density of states is symmetric. These features are subtle [Gygi and Schlüter (1991)] or absent [Hayashi et al. (1996)] in the previous calculations. This asymmetry around the vortex is quite distinctive, should be checked by STM experiments, and may be crucial for the Hall conductivity in the mixed state.

The lowest bound state level $E_{1/2}/\Delta_0$ is estimated by Maggio-Aprile *et al.* [Maggio-Aprile et al. (1995)] for YBCO with $T_c = 90$ K ($E_{1/2} = 5.5$ meV and $\Delta_0 = 20$ meV), yielding $k_F\xi_0 \sim 4$. Since it implies that ξ_0 is only of the order of the crystal-lattice constant, it should be mentioned that

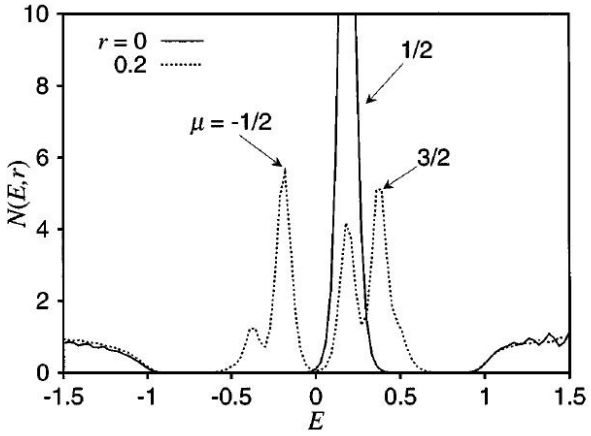

Figure 4.18: The local density of states $N(E, r)$ at $r = 0$ (solid line) and $0.2\xi_0$ (dotted line). $T/T_c = 0.05$ and $k_F\xi_0 = 8$ [Hayashi et al. (1998)].

Maggio-Aprile *et al.* [Maggio-Aprile et al. (1995)] take their data for the spectral evolution every 10 Å apart near the core; thus the important spatial information on the local density of states might be lost. So far the existing STM data [Maggio-Aprile et al. (1995); Hess et al. (1989); Wilde et al. (1997)] taken at the vortex center are almost symmetric about $E = 0$, e.g., on $NbSe_2$ at $T = 50$ mK [Hess et al. (1989)]. The reason why the so-called zero-bias peak is centered just symmetrically at $E = 0$ is that $k_F\xi_0$ is large and T is too high to observe the quantum effects. In any clean s-wave type-II superconductors at appropriately low T [$< T_0 \simeq T_c/(k_F\xi_0)$], one can observe these eminent characteristics associated with the quantum effects.

Paper 6. Coherence length of magnetic field in the mixed state of type-II superconductors

Although the main superconductivity research in the last few years has been dominated by the study of iron-pnictides, there exist unresolved issues concerning conventional superconductors. $NbSe_2$ is particularly well suited for a μSR study of the vortex state since the geometry of the vortex lattice is well established - thus removing one of the largest experimental uncertainties. Scanning tunneling microscopy (STM) measurements at the surface [Hartmann et al. (1993); Hess et al. (1989, 1992)] and small angle neutron scattering (SANS) measurements in the bulk [Gammel et al. (1994)] have produced high quality images of a nearly perfect triangular lattice with long range order. Also the coherence length and the magnetic penetration depth in $NbSe_2$ are nearly ideal for a μSR investigation of the vortex cores. In particular, the large coherence length and correspondingly small value of H_{c2} ($< 4T$) imply a large signal from the vortex-core regions at moderate magnetic fields.

Nearly universal field dependence with a minimum near critical temperature in clean superconductors is found in **paper 6**. A similar slope $d(\xi_h/\xi_{c2})/d(B/B_{c2})$ at $B/B_{c2} = 1$ weakly dependent on temperature and scattering rate is discovered. Quasiparticle scattering by impurities and lower-

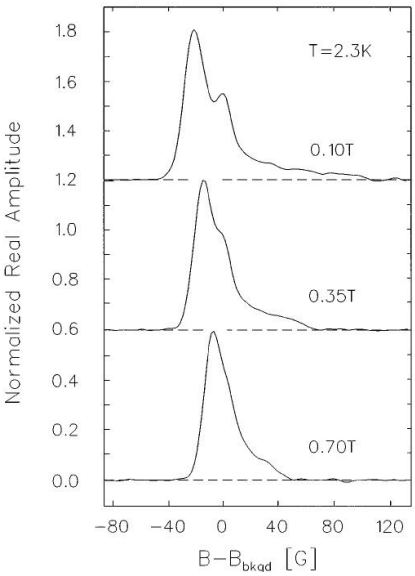

Figure 4.19: The Fourier transforms of the muon spin precession signal in $NbSe_2$ after field cooling to $T = 0.33T_c$ in magnetic fields of $H = 0.1$, 0.35, and 0.7 T. The average magnetic field of the residual background signal is denoted as B_{bkgd} [Sonier et al. (1997b)].

ing of the temperature reduce the value of ξ_h shifting it considerably downward from the analytical Ginzburg-Landau curve and at low temperatures strong influence of the Kramer-Pesch effect is found. It can explain muon spin rotation experimental results in some low temperature superconductors, where the ratio $\xi_h/\xi_{c2} \ll 1$ [Sonier (2007)] is observed in intermediate fields. A comparison with the behavior of the order parameter coherence length ξ_1 and another theories is done. It is found that impurities influence by different way on ξ_h and ξ_1. A clear impurity dependence of the ξ_h/ξ_{c2} value even at high temperatures (compare Fig. 1 (a) and Fig. 1 (b) in **Paper 6**) can not be explained by the local Usadel theory, where scaling $\xi_h/\xi_{c2} = Const$ (independent on Γ) is expected [Golubov and Hartmann (1994)].

Most theoretical calculations have modeled the core structure using Ginzburg-Landau (GL) theory, which is strictly valid only near the superconducting phase boundary. The field dependence of the vortex-core radius has been determined deep in the superconducting state from the microscopic theory in the dirty limit, by Golubov and Hartmann [Golubov and Hartmann (1994)] solving the Usadel equation. The vortex-core radius was found to decrease monotonically with increasing applied magnetic field due to the increased strength of the vortex-vortex interactions. Although the authors reported good agreement with STM measurements [Hartmann et al. (1993)] at the surface of $NbSe_2$ at $T = 0.6T_c$, ρ_0 was somewhat arbitrarily defined and the uncertainty in the measurements was large. The results were relatively surprising since $NbSe_2$ is a clean superconductor - the ratio of the coherence length to the mean free path in the $\hat{a} - \hat{b}$ plane is $\xi_0/l \sim 0.15$ [Takita and Masuda (1985)]. Muon-spin rotation spectroscopy has been used to measure the internal magnetic field distribution in $NbSe_2$ for $H_{c1} < H < 0.25H_{c2}$ [Sonier et al. (1997b)]. The deduced profiles of

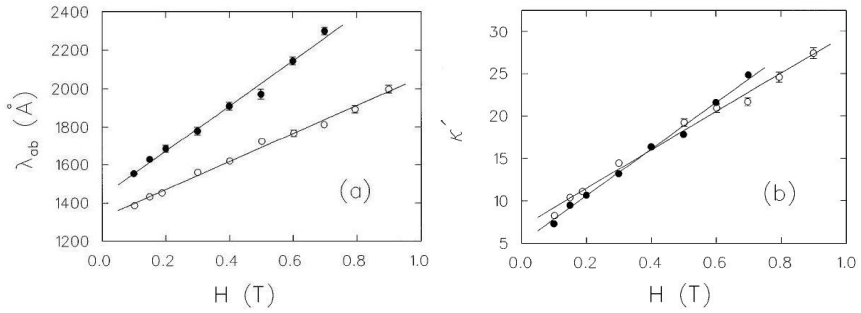

Figure 4.20: The magnetic field dependence of (a) $\lambda_{ab}(H)$ and (b) $\kappa'(H) = \lambda_{ab}(H)/\rho_0(H)$ in the vortex state of $NbSe_2$ at $T = 0.33T_c$ (open circles) and $T = 0.6T_c$ (solid circles). The solid line fits are described in the text [Sonier et al. (1997b)].

the supercurrent density J_s indicate that the vortex-core radius ρ_0 in the bulk decreases sharply with increasing magnetic field. This effect, which is attributed to increased vortex-vortex interactions, does not agree with the local Usadel theory.

In Fig. 4.19 the Fourier transforms of the muon precession signal in $NbSe_2$ are shown for different fields at $T = 0.33T_c$. The real amplitude of the Fourier transforms is a good representation of the internal magnetic field distribution from the vortex lattice convoluted with small nuclear dipolar fields. Note the small peak near zero in the top panel of Fig. 4.19. This is due to a small (2%) residual background signal due to muons which miss the sample. Line shapes have been renormalized to the same maximum amplitude. The sharp features expected for a perfect triangular vortex lattice, such as the Van Hove singularity at the saddle point, are obscured partly by the broadening effects of the finite Fourier transform and by flux-line lattice disorder. Nevertheless there is a clear high-field cutoff observed in the μSR line shape originating from the finite size of the vortex cores. The effect of increasing H on the high-field cutoff is clearly seen in Fig. 4.19. At all of the magnetic fields the signal-to-noise ratio of the highfield tail is so large that one can unambiguously extract the vortex-core radius. In order to test the strength of the pinning forces on the vortex lattice the sample was cooled in an applied field of 0.5 T to 2.3 K, after which the field was decreased by 7.5 mT.

The μSR spectra was fitted in the time domain, where there are no complications associated with fitting finite Fourier transforms [Sonier et al. (1997a)]. The distribution of muon precession frequencies from the vortex lattice was modeled with a theoretical field distribution generated from a GL model [Hao et al. (1991)]. The local field at any point in the $\hat{a} - \hat{b}$ plane is given in a suitable approximation by [Yaouanc et al. (1997)]

$$B(\rho) = B_0(1 - b^4) \sum_{\mathbf{G}} \frac{e^{-i\mathbf{G}\rho} u K_1(u)}{\lambda_{ab}^2 G^2}, \tag{4.66}$$

with

$$u^2 = 2\xi_{ab}^2 G^2 (1 + b^4)[1 - 2b(1 - b)^2].$$

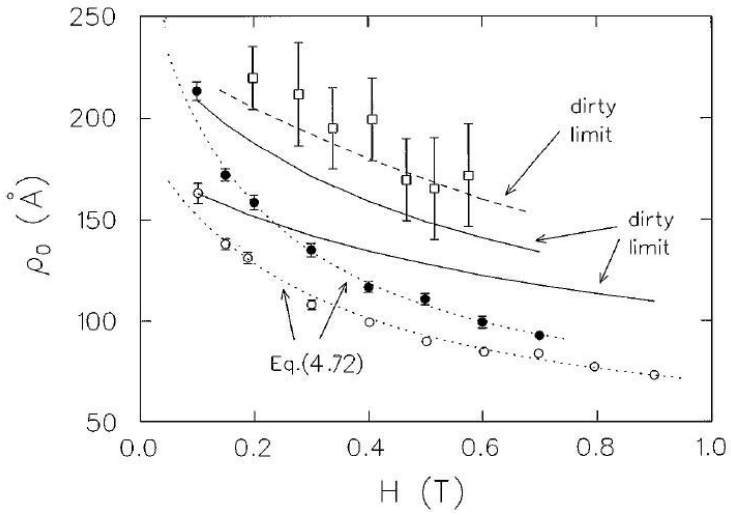

Figure 4.21: The magnetic field dependence of the vortex-core radius in $NbSe_2$ determined by STM [Hartmann et al. (1993)] at $T = 0.6T_c$ (open squares) and by μSR at $T = 0.33T_c$ (open circles) and $0.6T_c$(solid circles). The solid lines are from calculations of supercurrent density $J_s(\rho)$ profiles using $H_{c2}(0) = 3.5$ T, $H_{c2}(0.33T_c) = 2.9$ T, and $H_{c2}(0.6T_c) = 1.9$ T from magnetization. The dotted lines through the μSR data are from Eq. (4.72) [Sonier et al. (1997b)].

Here, B_0 is the average magnetic field, **G** are the reciprocal lattice vectors, $b = B_0/B_{c2}$, ξ_{ab} is the GL coherence length, and $K_1(u)$ is a modified Bessel function. The cutoff factor $uK_1(u)$ accounts for the finite size of the vortex core, whereas, in the London model, $B(\rho)$ diverges logarithmically as $\rho \to 0$. Recently, Yaouanc et al. [Yaouanc et al. (1997)] showed that $uK_1(u)$ is a good approximation of the cutoff factor determined from the exact numerical solutions of the GL equations [Brandt (1997)] at low reduced fields b.

The theoretical muon polarization function was generated by assuming the field profile of Eq. (4.66) and then multiplying by a Gaussian relaxation function $e^{-\sigma^2 t^2/2}$ to take into account any residual disorder in the flux-line lattice and the contribution of the nuclear dipolar moments to the internal field distribution. The residual background signal was fitted assuming a Gaussian broadened distribution of fields. All fitted parameters were treated as independent variables. From the fitted values of σ, the root-mean-square deviation of the vortices from their ideal positions in the triangular lattice was determined to be less than 3% of the intervortex spacing over the entire field range studied. This small disorder is consistent with STM and SANS imaging experiments on $NbSe_2$.

The magnetic field dependence of λ_{ab} is shown in Fig. 4.20 (a). Contrary to the Meissner state, a linear-H dependence is observed in the field range studied. A fit to the linear relation $\lambda_{ab}(H) = \lambda_{ab}(0)[1 + \beta h]$, where $h = H/H_{c2}(T)$, gives $\lambda_{ab}(0)$ = 1323 Å and $\beta = 1.61$ at $T = 0.33T_c$ and $\lambda_{ab}(0)$ = 1436 Å and $\beta = 1.56$ at $T = 0.6T_c$. Note that $d[\Delta\lambda/\lambda(0)]/d(H/H_{c2})$ is considerably weaker than for $YBa_2Cu_3O_{6.95}$ (Ref. [Sonier et al. (1997a)]), in which there is strong evidence for

line nodes in the superconducting energy gap function.

An effective vortex-core radius ρ_0 is defined as the distance from the vortex center for where the supercurrent density $J_s(\rho)$ reaches its maximum value. $J_s(\rho)$ was obtained from fits of the data to Eq. (4.66) and the Maxwell relation $\mathbf{J}(\rho) = \nabla \times \mathbf{B}(\rho)$. In Fig. 4.21, μSR measurements of ρ_0 are shown as a function of H at $T = 0.33T_c$ (open circles) and $0.6T_c$ (solid circles), along with the STM measurements (open squares) of Ref. [Hartmann et al. (1993)]. The smaller error bars and reduced scatter in the μSR data reflect the statistical improvement of a μSR experiment which samples a large number of vortices in the bulk of the crystal, as opposed to STM which averages the radius of only a few vortices at the surface. The dashed line drawn through the STM results comes from tunneling current $I(\rho)$ profiles calculated from the Usadel equations, as explained in Ref. [Golubov and Hartmann (1994)]. To generate $J_s(\rho)$ profiles from Usadel's dirty-limit theory the work of Ref. [Golubov and Hartmann (1994)] was extended to include the self-consistency equation for the vector potential $A(\rho)$. In cylindrical coordinates the equation of motion is [Kramer et al. (1974)]

$$\frac{1}{\rho}\frac{d}{d\rho}(\rho\frac{d\theta}{d\rho}) = \bar{\kappa}^{-2}A^2\sin\theta\cos\theta - \Delta\cos\theta + \omega\sin\theta, \tag{4.67}$$

where θ parametrizes Usadel's normal ($G = \cos\theta$) and anomalous ($F = \sin\theta$) Green's functions [Usadel (1970)], $\Delta(\rho)$ is the order parameter, $\omega = (T/T_c)(2l+1)$ is the Matsubara frequency and $\bar{\kappa} = [4\pi^5/7\zeta(3)]^{1/2}$ (where $\kappa = \lambda/\xi$). Eq. (4.67) is supplemented by the following selfconsistency equations:

$$\Delta\ln(T/T_c) = -2(T/T_c)\sum_{\omega}[\Delta/\omega - \sin\theta], \tag{4.68}$$

$$J_s(\rho) = \frac{d}{d\rho}\frac{1}{\rho}(\frac{d}{d\rho}\rho A) = 16\pi\bar{\kappa}^{-2}(T/T_c)A\sum_{\omega}\sin^2\theta, \tag{4.69}$$

and the boundary conditions for singly quantized vortices with a Wigner-Seitz cell radius $\rho_s = (\Phi_0/\pi H)^{1/2}$,

$$\begin{aligned}\Delta(0) = \theta(\omega,0) = 0,\\ \Delta'(\rho_s) = \theta'(\omega,\rho_s) = 0,\end{aligned} \tag{4.70}$$

$$\begin{aligned}A(\rho\to 0) \to -\bar{\kappa}/\rho,\\ A(\rho_s) = 0.\end{aligned} \tag{4.71}$$

Eq. (4.67), subject to these boundary conditions, was solved numerically for $\theta(\omega,\rho)$ starting with the initial trial potentials $\Delta(\rho) = \Delta_0\tanh(\rho)$ and $A(\rho) = \bar{\kappa}(1/\rho - \rho/\rho_s^2)$. Improved values of $\Delta(\rho)$ and $A(\rho)$ were obtained by including the self-consistent conditions (4.68) and (4.69). The parameter κ in Eqs. (4.67) and (4.69) was determined from fits to the data. κ was found to be nearly temperature independent at all fields studied, which is consistent with the original definition of κ near T_c in GL theory [Ginzburg and Landau (1950)]. The deduced values of ρ_0 were not very sensitive to κ. In Fig. 4.20 (b) $\kappa' = \lambda_{ab}/\rho_0$ was defined, where $\kappa'(H) = 1.06\kappa(H) - 1.98$ and $\kappa'(H) = 1.12\kappa(H) - 1.26$ at $T = 0.33T_c$ and $T = 0.6T_c$, respectively. At both temperatures,

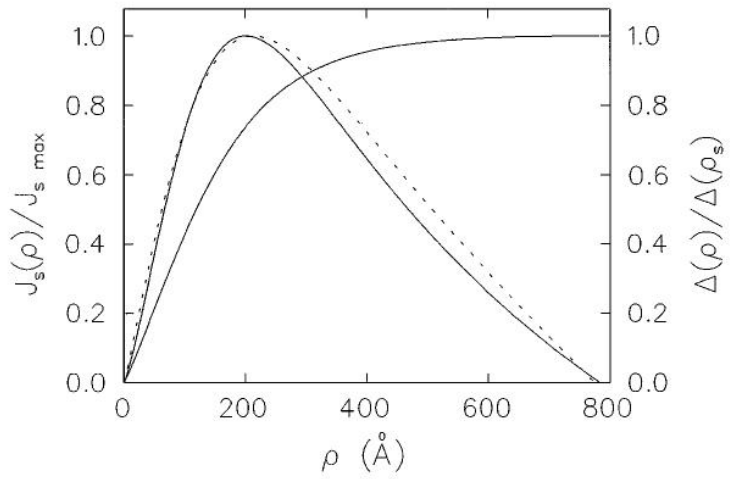

Figure 4.22: The current density and order parameter for $T = 0.6T_c$ and $H/H_{c2}(0.6T_c) = 0.053$. The solid lines are from the dirty-limit microscopic theory while the dashed line is the supercurrent density from a μSR measurement of the field distribution in $NbSe_2$ [Sonier et al. (1997b)].

κ' (and hence κ) increases linearly with H. Fitting to the linear relation $\kappa'(H) = \kappa'(0)[1 + \gamma h]$, $\kappa'(0) = 6.9$ and $\gamma = 9.5$ at $T = 0.33T_c$ and $\kappa'(0) = 5.1$ and $\gamma = 10.2$ at $T = 0.6T_c$ were obtained.

Fig. 4.22 shows the theoretical $J_s(\rho)$ and $\Delta(\rho)$ profiles together with the $J_s(\rho)$ profile obtained from experiment for a particular T and H. The vortex-core radius taken from the $J_s(\rho)$ profiles of the dirty-limit theory are shown as solid lines in Fig. 4.21. Not surprisingly, there is poor agreement with the μSR data at $T = 0.33T_c$, where thermal smearing of the bound states in the vortex core is negligible. Contrary to the STM results [Hartmann et al. (1993)], however, there is also poor agreement at $T = 0.6T_c$ - suggesting that the dirty-limit theory does not adequately describe the shrinking of the vortex-core radius with increasing H. In the STM experiment it was necessary to arbitrarily define ρ_0 as the radius in which the tunneling current decreased to 36% of $I_{max} - I_{min}$ and $\Delta(\rho)/\Delta(\rho_s) = 1/\sqrt{2}$. However, the $J_s(\rho)$ profiles generated from the dirty-limit theory do not peak exactly at a radius corresponding to $\Delta(\rho)/\Delta(\rho_s) = 1/\sqrt{2}$ for all values of T/T_c and H/H_{c2}. Thus, the previous definition of ρ_0 should provide a better description of the true H dependence of the vortex-core radius. The STM data may also be influenced somewhat by the discontinuity in the energy spectrum of the vortex cores which occurs at the sample surface. It has been suggested that the effect may be an enlargement of ρ_0 [Klein (1990)].

On the other hand, the μSR results fit well (see dotted lines in Fig. 4.21) to the phenomenological equation,

$$\rho_0(H) = \frac{\lambda_{ab}(H)}{\kappa'(H)} = \rho_0(0)\frac{[1 + \beta h]}{[1 + \gamma h]}, \tag{4.72}$$

where $\rho_0(0) = \lambda_{ab}(0)/\kappa'(0)$. From the fits to $\lambda_{ab}(H)$ and $\kappa'(H)$, $\rho_0(0) = 191$ and 282 Å at $T = 0.33T_c$ and $0.6T_c$, respectively. For a triangular vortex lattice $H \cong B_0 = 3\Phi_0/\sqrt{2}L^2$, where L

is the intervortex spacing. Thus, for a given temperature, Eq. (4.72) may be rewritten as a function of the distance between vortices.

In **paper 6** we do not consider the field dependence of penetration depth nor take its value as in the Meissner state. This dependence can be introduced by the separation of the extended states contribution by considering the nonlocal London equation. This method is described in **paper 5**. It is shown that it does not give the essential improvement of the fitting, i.e., microscopical determination of the cutoff parameter is needed.

As is shown in [Kadono et al. (2004)] that the vortex core radius ξ_2 (or ρ_0 in notation to Fig. 4.21) is strongly correlated with cutoff parameter ξ_h. In the case of strong impurity scattering ξ_2/ξ_{c2} and ξ_h/ξ_{c2} are much less than one and order parameter coherence length ξ_1/ξ_{c2} (Fig. 3 in **paper 6**). This can explain the difference between characteristic lengths measured by μSR and STM experiments presented in Fig. 4.21. Nonlocal Eilenberger approach should be used in first case. As it noted in **paper 4** the symmetry $\xi_2 \approx \xi_1$ can be broken by strong impurity scattering in Eilenberger theory.

CHAPTER V

Conclusions

The field distribution of the mixed state in type-II superconductors with different pairing symmetries is investigated in the framework of the Eilenberger theory and projected on the London equation in wide temperature and field range. The normalized dependences of the cutoff parameter $\xi_h/\xi_{c2}(B/B_{c2})$ responsible for the line shape of the μSR resonance are calculated. It is found that this dependence is nonuniversal and depends on temperature and on impurity scattering rate, Γ. This is different from the universal dependence expected from the Ginzburg-Landau theory.

Core structure of the vortices in iron pnictides have been studied using $s^{\pm}$ symmetry (connected with antiferromagnetic spin fluctuation mechanism) and s_{++} symmetry (mediated by moderate electron-phonon interaction due to Fe-ion oscillation and the critical orbital fluctuation). Different impurity scattering rate dependences of cutoff parameter ξ_h have been found for these cases. In nonstoichiometric case, when intraband impurity scattering (Γ_0) is much larger than interband impurity scattering rate (Γ_π) the ξ_h/ξ_{c2} ratio is less in $s^{\pm}$ symmetry. When $\Gamma_0 \approx \Gamma_\pi$ (stoichiometric case) opposite tendencies has been found, in $s^{\pm}$ symmetry the ξ_h/ξ_{c2} goes upward from the "clean" case curve ($\Gamma_0 = \Gamma_\pi = 0$) while it goes downward in s_{++} case.

Low temperature s-wave superconductors are also considered. At high enough values of $\Gamma \geq 0.5$, the dependence plateaus in the intermediate field range and the low temperatures, and $\xi_h(B)/\xi_{c2}$ is of the order of 0.25. The strong suppression of ξ_h/ξ_{c2} with Γ and T can explain the experimental results in many low-temperature superconductors (V_3Si, $NbSe_2$ and $LuNi_2B_2C$), where the values $\xi_h/\xi_{c2} < 1$ has been observed. It is connected with the nonlocal bound Andreev states of the vortex core. The obtained projection of the Eilenberger equations is compared with the nonlocal Kogan-Gurevich theory. The field dependence of the cutoff parameter changes the magnetization and the variance of the magnetic field. A difference is observed between $\xi_h(T)$ and nonlocal range $\rho(T)$ of the Kogan-Gurevich theory, where only the contribution of the extended state is taken into account. A strong difference from the analytical Ginzburg-Landau theory and linearized Eilenberger approach (the Kogan-Zhelezina theory) is found. This is explained by the Kramer-Pesch effect which is not taken into account in these theories.

Abramowitz, M., Stegun, I. A., 1964. Handbook of Mathematical Functions (National Bureau of Standards, Washington, DC), p. 360.

Abrikosov, A. A., Gor'kov, L. P., 1961. Zh. Eksp. Teor. Fiz. 39, 1781.

Anderson, P. W., Morel, P., 1961. Phys. Rev. 123, 1911.

Andreev, A. F., 1964. Sov. Phys. JETP 19, 1228.

Atkinson, W. A., Sonier, J. E., 2008. Phys. Rev. B 77, 024514.

Bardeen, J., Cooper, L. N., Schrieffer, J. R., 1957. Phys. Rev. 108, 1175.

Bardeen, J., Kümmel, R., Jacobs, A. E., Tewordt, L., 1969. Phys. Lett. 187, 556.

Bardeen, J., Stephen, M. J., 1965. Phys. Rev. 140, A1197.

Basov, D., Chubukov, A., 2011. Nature Physics 7, 241.

Bednorz, J. G., Muller, K. A., 1986. Zeitschrift für Physik B Condensed Matter 64, 189.

Boeri, L., Dolgov, O. V., Golubov, A. A., 2008. Phys. Rev. Lett. 101, 026403.

Bogolyubov, N. N., Tolmachev, V., Shirkov, D., 1958. New Methods in the Theory of Superconductivity, Academy of Science, Moscow.

Borisenko, S. V., Zabolotnyy, V. B., Evtushinsky, D. V., Kim, T. K., Morozov, I. V., Yaresko, A. N., Kordyuk, A. A., Behr, G., Vasiliev, A., Follath, R., Büchner, B., 2010. Phys. Rev. Lett. 105, 067002.

Brandt, E. H., 1988. Phys. Rev. B 37, 2349.

Brandt, E. H., 1997. Phys. Rev. Lett. 78, 2208.

Brydon, P. M. R., Daghofer, M., Timm, C., van den Brink, J., 2011. Phys. Rev. B 83, 060501.

Callaghan, F. D., Laulajainen, M., Kaiser, C., Sonier, J. E., 2005. Phys. Rev. Lett. 95, 197001.

Capone, M., Fabrizio, M., Castellani, C., Tosatti, E., 2004. Phys. Rev. Lett. 93, 047001.

Carlo, J. P., Uemura, Y. J., Goko, T., MacDougall, G. J., Rodriguez, J. A., Yu, W., Luke, G. M., Dai, P., Shannon, N., Miyasaka, S., Suzuki, S., Tajima, S., Chen, G. F., Hu, W. Z., Luo, J. L., Wang, N. L., 2009. Phys. Rev. Lett. 102, 087001.

Caroli, C., deGennes, P. G., Matricon, J., 1964. Phys. Lett. 9, 307.

Caroli, C., deGennes, P. G., Matricon, J., 1965. Phys. Kondens. Mater. 3, 380.

Caroli, C., Matricon, J., 1964. Phys. Lett. 9, 307.

Chen, G. F., Chen, Z. G., Dong, J., Hu, W. Z., Li, G., Zhang, X. D., Zheng, P., Luo, J. L., Wang, N. L., 2009. Phys. Rev. B 79, 140509(R).

Chen, G. F., Li, Z., Wu, D., Li, G., Hu, W. Z., Dong, J., Zheng, P., Luo, J. L., Wang, N. L., 2008a. Phys. Rev. Lett. 100, 247002.

Chen, X. H., Wu, T., Wu, G., Liu, R. H., Chen, H., Fang, D. F., 2008b. Nature 453, 761.

Choi, C. H., Muzikar, P., 1989. Phys. Rev. B 39, 11296.

Christianson, A. D., Goremychkin, E. A., Osborn, R., Rosenkranz, S., Lumsden, M. D., Malliakas, C. D., Todorov, I. S., Claus, H., Chung, D. Y., Kanatzidis, M. G., Bewley, R. I., Guidi, T., 2008. Nature (London) 456, 930.

Chu, J.-H., Analytis, J., Press, D., Greve, K. D., Ladd, T., Yamamoto, Y., Fisher, I., 2010. Phys. Rev. B 81, 214502.

Chubukov, A. V., 2009. Physica C 469, 640.

Chubukov, A. V., 2012. Condensed Matter Physics 3, 57.

Chubukov, A. V., Efremov, D. V., Eremin, I., 2008. Phys. Rev. B 78, 134512.

Clem, J. R., 1975. J. Low Temp. Phys. 18, 427.

Dong, J. K., Zhou, S. Y., Guan, T. Y., Zhang, H., Dai, Y. F., Qiu, X., Wang, X. F., He, Y., Chen, X. H., Li, S. Y., 2010. Phys. Rev. Lett. 104, 087005.

Eilenberger, G., 1968. Z. Physik 214, 195.

Eskildsen, M. R., Vinnikov, L. Y., Blasius, T. D., Veshchunov, I. S., Artemova, T. M., Densmore, J. M., Dewhurst, C. D., Ni, N., Kreyssig, A., Bud'ko, S. L., Canfield, P. C., Goldman, A. I., 2009. Phys. Rev. B 79, 100501(R).

Evtushinsky, D. V., Inosov, D. S., Zabolotnyy, V. B., Koitzsch, A., Knupfer, M., Buchner, B., Viazovska, M. S., Sun, G. L., Hinkov, V., Boris, A. V., Lin, C. T., Keimer, B., Varykhalov, A., Kordyuk, A. A., Borisenko, S. V., 2009a. Phys. Rev. B 79, 054517.

Evtushinsky, D. V., Inosov, D. S., Zabolotnyy, V. B., Viazovska, M. S., Khasanov, R., Amato, A., Klauss, H.-H., Luetkens, H., Niedermayer, C., Sun, G. L., Hinkov, V., Lin, C. T., Varykhalov, A., Koitzsch, A., Knupfer, M., Buchner, B., Kordyuk, A. A., Borisenko, S. V., 2009b. New J. Phys. 11, 055069.

Fernandes, R. M., VanBebber, L. H., Bhattacharya, S., Chandra, P., Keppens, V., Mandrus, D., McGuire, M. A., Sales, B. C., Sefat, A. S., Schmalian, J., 2010. Phys. Rev. Lett. 105, 157003.

Fetter, A. L., Hohenberg, P. C., 1969. in Superconductivity, edited by R. D. Parks (Marcel Dekker Inc., New York), p. 817.

Fletcher, J. D., Serafin, A., Malone, L., Analytis, J. G., Chu, J.-H., Erickson, A. S., Fisher, I. R., Carrington, A., 2009. Phys. Rev. Lett. 102, 147001.

Gammel, P. L., Huse, D. A., Kleiman, R. N., Batlogg, B., Oglesby, C. S., Bucher, E., Bishop, D. J., Mason, T. E., Mortensen, K., 1994. Phys. Rev. Lett. 72, 278.

Ginzburg, V. L., Landau, L. D., 1950. Zh. Eksp. Teor. Fiz. 20, 1064.

Giorgini, S., Boronat, J., Casulleras, J., 1997. Phys. Rev. Lett. 77, 2754.

Goldman, A., Argyriou, D., Ouladdiaf, B., Chatterji, T., Kreyssig, A., Nandi, S., Ni, N., Bud'ko, S., Canfield, P., McQueeney, R., 2008. Phys. Rev. B 78, 100506(R).

Golubov, A. A., Hartmann, U., 1994. Phys. Rev. Lett. 72, 3602.

Gradshteyn, I. S., Ryzhik, I. M., 1965. Tables of Integrals, Series, and Products (Academic, New York), p. 706.

Guo, J., Jin, S., Wang, G., Wang, S., Zhu, K., Zhou, T., He, M., Chen, X., 2010. Phys. Rev. B 82, 180520(R).

Gygi, F., Schluter, M., 1990. Phys. Rev. B 41, 822.

Gygi, F., Schlüter, M., 1991. Phys. Rev. B 43, 76092.

Hanaguri, T., Niitaka, S., Kuroki, K., Takagi, H., 2010. Science 328, 474.

Hao, Z., Clem, J. R., McElfresh, M. W., Civale, L., Malozemoff, A. P., Holtzberg, F., 1991. Phys. Rev. B 43, 2844.

Hartmann, U., Drechsler, T., Heiden, C., 1993. SPIE Conf. Proc 1885, 140.

Hashimoto, K., Yamashita, M., Kasahara, S., Senshu, Y., Nakata, N., Tonegawa, S., Ikada, K., Serafin, A., Carrington, A., Terashima, T., Ikeda, H., Shibauchi, T., Matsuda, Y., 2010. Phys. Rev. B 81, 220501(R).

Hayashi, N., Ichioka, M., Machida, K., 1996. Phys. Rev. Lett. 77, 4074.

Hayashi, N., Isoshima, T., Ichioka, M., Machida, K., 1998. Phys. Rev. Lett. 80, 2912.

Hess, H. F., Murray, C. A., Waszczak, J. V., 1992. Phys. Rev. Lett. 69, 2138.

Hess, H. F., Robinson, R. B., Dynes, R. C., Valles, J. M., Waszczaks, J. V., 1989. Phys. Rev. Lett. 62, 214.

Huang, Q., Qiu, Y., Bao, W., Green, M., Lynn, J., Gasparovic, Y., Wu, T., Wu, G., Chen, X., 2008. Phys. Rev. Lett. 101, 257003.

Ichioka, M., Hasegawa, A., Machida, K., 1999a. Phys. Rev. B 59, 8902.

Ichioka, M., Hasegawa, A., Machida, K., 1999b. Phys. Rev. B 59, 184.

Ichioka, M., Hayashi, N., Enomoto, N., Machida, K., 1996. Phys. Rev. B 53, 15316.

Inosov, D. S., Park, J. T., Bourges, P., Sun, D. L., Sidis, Y., Schneidewind, A., Hradil, K., Haug, D., Lin, C. T., Keimer, B., Hinkov, V., 2010a. Nature Physics 6, 178.

Inosov, D. S., Shapoval, T., Neu, V., Wolff, U., White, J. S., Haindl, S., Park, J. T., Sun, D. L., Lin, C. T., Forgan, E. M., Viazovska, M. S., Kim, J. H., Laver, M., Nenkov, K., Khvostikova, O., Kuhnemann, S., Hinkov, V., 2010b. Phys. Rev. B 81, 014513.

Inosov, D. S., White, J. S., Evtushinsky, D. V., Morozov, I. V., Cameron, A., Stockert, U., Zabolotnyy, V. B., Kim, T. K., Kordyuk, A. A., Borisenko, S. V., Forgan, E. M., Klingeler, R., Park, J. T., Wurmehl, S., Vasiliev, A. N., Behr, G., Dewhurst, C. D., Hinkov, V., 2010c. Phys. Rev. Lett. 104, 187001.

Jiang, H.-M., Li, J.-X., Wang, Z. D., 2009. Phys. Rev. B 80, 134505.

Johnston, D., 2010. Advances in Physics 59, 803.

Kadono, R., Higemoto, W., Koda, A., Larkin, M. I., Luke, G. M., Savici, A. T., Uemura, Y. J., Kojima, K. M., Okamoto, T., Kakeshita, T., Uchida, S., Ito, T., Oka, K., Takigawa, M., Ichioka, M., Machida, K., 2004. Phys. Rev. B 69, 104523.

Kamihara, Y., Watanabe, T., Hirano, M., Hosono, H., 2006. J. Am. Chem. Soc. 128, 10012.

Kamihara, Y., Watanabe, T., Hirano, M., Hosono, H., 2008. J. Am. Chem. Soc. 130, 3296.

Kano, M., Kohama, Y., Graf, D., Balakireva, F., andM. A. Mcguire, A. S. S., Sales, B. C., Mandrus, D., Tozer, S. W., 2009. J. Phys. Soc. Jpn. 78, 084719.

Kasahara, S., Shibauchi, T., Hashimoto, K., Ikada, K., Tonegawa, S., Okazaki, R., Shishido, H., Ikeda, H., Takeya, H., Hirata, K., Terashima, T., Matsuda, Y., 2010. Phys. Rev. B 81, 184519.

Kawabata, A., Lee, S. C., Moyoshi, T., Kobayashi, Y., Sato, M., 2008. J. Phys. Soc. Jpn. 77, 103704.

Khasanov, R., Evtushinsky, D. V., Amato, A., Klauss, H., Luetkens, H., Niedermayer, C., Buchner, B., Sun, G. L., Lin, C. T., Park, J. T., Inosov, D. S., Hinkov, V., 2009a. Phys. Rev. Lett. 102, 187005.

Khasanov, R., Luetkens, H., Amato, A., Klauss, H.-H., Ren, Z.-A., Yang, J., Lu, W., Zhao, Z.-X., 2008. Phys. Rev. B 78, 092506.

Khasanov, R., Maisuradze, A., Maeter, H., Kwadrin, A., Luetkens, H., Amato, A., Schnelle, W., Rosner, H., Leithe-Jasper, A., Klauss, H., 2009b. Phys. Rev. B 103, 067010.

Klein, U., 1990. Phys. Rev. B 41, 4819.

Kogan, V. G., Gurevich, A., Cho, J. H., Johnston, D. C., Xu, M., Thompson, J. R., Martynovich, A., 1996a. Phys. Rev. B 54, 12386.

Kogan, V. G., Gurevich, A., Cho, J. H., Johnston, D. C., Xu, M., Thompson, J. R., Martynovich, A., 1996b. Phys. Rev. B 54, 12386.

Kogan, V. G., Prozorov, R., Bud'ko, S. L., Canfield, P. C., Thompson, J. R., Karpinski, J., Zhigadlo, N. D., Miranović, P., 2006. Phys. Rev. B 74, 184521.

Kogan, V. G., Zhelezina, N. V., 2005. Phys. Rev. B 71, 134505.

Kohn, W., Luttinger, J. M., 1965. Phys. Rev. Lett. 15, 524.

Kontani, H., 2008. Rep. Prog. Phys. 71, 026501.

Kontani, H., Onari, S., 2010. Phys. Rev. Lett. 104, 157001.

Kortus, J., Mazin, I. I., Belashchenko, K. D., Antropov, V. P., Boyer, L. L., 2001. Phys. Rev. Lett. 86, 4656.

Kramer, L., Pesch, W., 1974. Z. Phys. 269, 59.

Kramer, L., Pesch, W., Watts-Tobin, R. J., 1974. J. Low Temp. Phys 14, 29.

Krüger, F., Kumar, S., Zaanen, J., Brink, J., 2009. Phys. Rev. B 80, 064509.

Kuroki, K., Onari, S., Arita, R., Usui, H., Tanaka, Y., Kontani, H., Aoki, H., 2008. Phys. Rev. Lett. 101, 087004.

Kuroki, K., Usui, H., Onari, S., Arita, R., Aoki, H., 2009. Phys. Rev. B 79, 224511.

Laiho, R., Safonchik, M., Traito, K. B., 2007. Phys. Rev. B 76, 140501(R).

Laiho, R., Safonchik, M., Traito, K. B., 2008. Phys. Rev. B 78, 064521.

Larkin, A. I., Ovchinnikov, Y. N., 1969. Soviet Physics Journal of Experimental and Theoretical Physics 28, 1200.

Lee, P. A., Wen, X.-G., 2008. Phys. Rev. B 78, 144517.

Louca, D., Horigane, K., Llobet, A., Arita, R., Ji, S., Katayama, N., Konbu, S., Nakamura, K., Koo, T.-Y., Tong, P., Yamada, K., 2010. Phys. Rev. B 81, 134524.

Loudon, J., Bowell, C., Gillett, J., Sebastian, S., Midgleyu, P., 2010. Phys. Rev. B 81, 214111.

Lynn, J., Dai, P., 2009. Physica C 469, 469.

Ma, C., Yang, H., Tian, H., Shi, H., Lu, J., Wang, Z., Zeng, L., Chen, G., Wang, N., Li, J., 2009. Phys. Rev. B 79, 060506(R).

Maggio-Aprile, I., Renner, C., Erb, A., Walker, E., Fischer, Ø., 1995. Phys. Rev. Lett. 77, 2754.

Maier, T. A., Graser, S., Scalapino, D. J., Hirschfeld, P. J., 2009. Phys. Rev. B 79, 224510.

Malone, L., Fletcher, J. D., Serafin, A., Carrington, A., Zhigadlo, N. D., Bukowsk, Z., Katrych, S., Karpinski, J., 2009. Phys. Rev. B 79, 140501(R).

Marsik, P., Kim, K. W., Dubroka, A., Rossle, M., Malik, V. K., Schulz, L., Wang, C. N., Niedermayer, C., Drew, A. J., Willis, M., Wolf, T., Bernhard, C., 2010. Phys. Rev. Lett. 105, 057001.

Martin, C., Gordon, R. T., Tanatar, M. A., Kim, H., Ni, N., Bud'ko, S. L., Canfield, P. C., Luo, H., Wen, H. H., Wang, Z., Vorontsov, A. B., Kogan, V. G., Prozorov, R., 2009. Phys. Rev. B 80, 020501(R).

Martin, C., Kim, H., Ni, R. T. G. N., Kogan, V. G., Bud'ko, S. L., Canfield, P. C., Tanatar, M. A., Prozorov, R., 2010. Phys. Rev. B 81, 060505(R).

Mazin, I., 2010. Nature 464, 183.

Mazin, I., Schmalian, J., 2009. Physica C 468, 614.

Mazin, I. I., Singh, D. J., Johannes, M. D., Du, M. H., 2008. Phys. Rev. Lett. 101, 057003.

Menon, G. I., Drew, A., Divakar, U. K., Lee, S. L., Gilardi, R., Mesot, J., Ogrin, F. Y., Charalambous, D., Forgan, E. M., Momono, N., Oda, M., Dewhurst, C., Baines, C., 2006. Phys. Rev. Lett. 197, 177004.

Miranović, P., Machida, K., 2003. Phys. Rev. B 67, 092506.

Mishra, V., Boyd, G., Graser, S., Maier, T., Hirschfeld, P. J., Scalapino, D. J., 2009. Phys. Rev. B 79, 094512.

Nagai, Y., Hayashi, N., Naka, N., Nakamura, H., Okumura, M., Machida, M., 2008. New J. Phys. 10, 103026.

Nakai, Y., Iye, T., Kitagawa, S., Ishida, K., Ikeda, H., Kasahara, S., Shishido, H., Shibauchi, T., Matsuda, Y., Terashima, T., 2010a. Phys. Rev. Lett. 105, 107003.

Nakai, Y., Iye, T., Kitagawa, S., Ishida, K., Kasahara, S., Shibauchi, T., Matsuda, Y., Terashima, T., 2010b. Phys. Rev. B 81, 020503(R).

Nath, R., Singh, Y., Johnston, D., 2009. Phys. Rev. B 79, 174513.

Ni, N., Nandi, S., Kreyssig, A., Goldman, A., Mun, E., Bud'ko, S., Canfield, P., 2008. Phys. Rev. B 78, 014523.

Ni, N., Thaler, A., Yan, J. Q., Kracher, A., Colombier, E., Bud'ko, S. L., Canfield, P. C., 2010. Phys. Rev. B 82, 024519.

Onari, S., Kontani, H., 2009. Phys. Rev. Lett. 103, 177001.

Onari, S., Kontani, H., Sato, M., 2010. Phys. Rev. B 81, 060504(R).

Ovchinnikov, Y. N., Kresin, V. Z., 1995. Phys. Rev. B 52, 3075.

Qian, T., Wang, X.-P., Jin, W.-C., Zhang, P., Richard, P., Xu, G., Dai, X., Fang, Z., Guo, J.-G., Chen, X.-L., Ding, H., 2011. Phys. Rev. Lett. 106, 187001.

Rahlenbeck, M., Sun, G. L., Sun, D. L., Lin, C. T., Keimer, B., Ulrich, C., 2009. Phys. Rev. B 80, 064509.

Rainer, D., Sauls, J. A., 1995. in Superconductivity: From Basic Physics to Latest Developments, Singapore: World Scientific Publishers.

Renner, C., Ø. Fischer, 1995. Phys. Rev. Lett. 51, 9208.

Rotter, M., Hieke, C., Johrendt, K., 2010. Phys. Rev. B 82, 014513.

Rotter, M., Tegel, M., Johrendt, D., 2011. Phys. Rev. Lett. 101, 107006.

Safonchik, M., 2007. PhD thesis. Turku University.

Sato, T., Nakayama, K., Sekiba, Y., Richard, P., Xu, Y.-M., Souma, S., Takahashi, T., Chen, G. F., Luo, J. L., Wang, N. L., Ding, H., 2009. Phys. Rev. Lett. 103, 047002.

Scalapino, D. J., 1969. in Superconductivity, edited by R. D. Parks (Marcel Dekker Inc., New York) Vol.1, p. 449.

Schopohl, N., Maki, K., 1995. Phys. Rev. B 52, 490.

Sefat, A. S., Jin, R., McGuire, M. A., Sales, B. C., Singh, D. J., Mandrus, D., 2008. Phys. Rev. Lett. 101, 117004.

Shimojima, T., Ishizaka, K., Ishida, Y., Katayama, N., Ohgushi, K., Kiss, T., Okawa, M., Wang, T. T. X.-Y., Chen, C.-T., Watanabe, S., Kadota, R., Oguchi, T., Chainani, A., Shin, S., 2010. Phys. Rev. Lett. 104, 057002.

Singh, D., 2009. Physica C 469, 418.

Skalski, S., 1969. in Superconductivity, edited by R. D. Parks (Marcel Dekker Inc., New York) Vol. 2, p. 1035.

Sonier, J. E., 2004. J. Phys.: Condens. Matter 16, S4499.

Sonier, J. E., 2007. Rep. Prog. Phys. 70, 1717.

Sonier, J. E., Brewer, J. H., Kiefl, R. F., 2000. Rev. Mod. Phys. 72, 769.

Sonier, J. E., Brewer, J. H., Kiefl, R. F., Bonn, D. A., Dunsiger, S. R., Hardy, W. N., Liang, R., MacFarlane, W. A., Miller, R. I., Riseman, T. M., Noakes, D. R., Stronach, C. E., White, M. F., 1997a. Phys. Rev. Lett. 79, 2875.

Sonier, J. E., Brewer, J. H., Kiefl, R. F., Morris, G. D., Miller, R. I., Bonn, D. A., Chakhalian, J., Heffner, R. H., Hardy, W. N., Liang, R., 1999. Phys. Rev. Lett. 83, 4156.

Sonier, J. E., Callaghan, F. D., Ando, Y., Kiefl, R. F., Brewer, J. H., Kaiser, C. V., Pacradouni, V., Sabok-Sayr, S. A., Sun, X. F., Komiya, S., Hardy, W. N., Bonn, D. A., Liang, R., 2007. Phys. Rev. B 76, 064522.

Sonier, J. E., Huang, W., Kaiser, C. V., Cochrane, C., Pacradouni, V., Sabok-Sayr, S. A., Lumsden, M. D., Sales, B. C., McGuire, M. A., Sefat, A. S., Mandrus, D., 2011. Phys. Rev. Lett. 106, 127002.

Sonier, J. E., Kiefl, R. F., Brewer, J. H., Chakhalian, J., Dunsiger, S. R., MacFarlane, W. A., Miller, R. I., Wong, A., Luke, G. M., Brill, J. W., 1997b. Phys. Rev. Lett. 79, 1742.

Stanev, V., Kang, J., Tesanovic, Z., 2008. Phys. Rev. B 78, 184509.

Takahashi, H., Igawa, K., Arii, K., Kamihara, Y., Hirano, M., Hosono, H., 2008. Nature 453, 376.

Takimoto, T., Hotta, T., Maehira, T., Ueda, K., 2002. J. Phys.: Condens. Matter 14, L369.

Takita, K., Masuda, K., 1985. J. Low Temp. Phys 58, 127.

Tanatar, M., Kreyssig, A., Nandi, S., Ni, N., Bud'ko, S., Canfield, P., Goldman, A., Prozorov, R., 2009. Phys. Rev. B 79, 180508(R).

Tarantini, C., Putti, M., Gurevich, A., Shen, Y., Singh, R. K., Rowell, J. M., Newman, N., Larbalestier, D. C., Cheng, P., Y.Jia, Wen, H.-H., 2010. Phys. Rev. Lett. 104, 087002.

Thuneberg, E., Kurkijärvi, J., D.Rainer, 1982. Phys. Rev. Lett. 48, 1853.

Uemura, Y. J., Yamazaki, T., Harshman, D. R., Senba, M., Ansaldo, E. J., 1985. Phys. Rev. B 31, 546.

Usadel, K. D., 1970. Phys. Rev. Lett. 25, 507.

Volovik, G. E., 1993. JETP Lett. 58, 455.

Vorontsov, A. B., Vavilov, M. G., Chubukov, A. V., 2009. Phys. Rev. B 79, 140507(R).

Wang, Z., Yang, H., Ma, C., Tian, H., Shi, H., Lu, J., Zeng, L., Li, J., 2009. J. Phys.: Condens. Matter 21, 495701.

Wilde, Y. D., Iavarone, M., Welp, U., Metlushko, V., Koshelev, A. E., Aranson, I., Crabtree, G. W., 1997. Phys. Rev. Lett. 78, 4273.

Williams, T. J., Aczel, A. A., Baggio-Saitovitch, E., Bud'ko, S. L., Canfield, P. C., Carlo, J. P., Goko, T., Kageyama, H., Kitada, A., Munevar, J., Ni, N., Saha, S. R., Kirschenbaum, K., Paglione, J., Sanchez-Candela, D. R., Uemura, Y. J., Luke, G. M., 2010. Phys. Rev. B 82, 094512.

Wilson, S., Yamani, Z., Rotundu, C., Freelon, B., Bourret-Courchesne, E., Birgeneau, R., 2009. Phys. Rev. B 79, 184519.

Yada, K., Kontani, H., 2008. Phys. Rev. B 77, 184521.

Yanagi, Y., Yamakawa, Y., Ōno, Y., 2010. Phys. Rev. B 81, 054518.

Yaouanc, A., Reotier, P. D., Brandt, E. H., 1997. Phys. Rev. B 55, 11107.

Yin, W., Lee, C. C., Ku, W., 2010. Phys. Rev. Lett. 105, 107004.

PART II: PUBLICATIONS

PUBL. 1

P. Belova, M. Safonchik, K. B. Traito and E. Lähderanta, Quasiclassical Eilenberger approach to the vortex state in pnictide superconductors, *Journal of Physics: Conference Series*, **303**, 012113, 2011.

Joint European Magnetic Symposia – JEMS 2010 IOP Publishing
Journal of Physics: Conference Series **303** (2011) 012113 doi:10.1088/1742-6596/303/1/012113

Quasiclassical Eilenberger approach to the vortex state in pnictide superconductors

P. Belova[1,2], M. Safonchik[1,3], K. B. Traito[1], E. Lähderanta[1]

[1] Lappeenranta University of Technology, P.O.Box 20, FI-53851, Lappeenranta, Finland
[2] Petrozavodsk State University, Lenin str. 33, RU-185640, Petrozavodsk, Russia
[3] A. F. Ioffe Physico-Technical Institute, St. Petersburg, 194021, Russia

E-mail: Polina.Belova@lut.fi

Abstract. Quasiclassical Eilenberger equations are solved for $s^{\pm}$-wave superconductors in the mixed state. This symmetry has been proposed for multiband superconductors as pnictides. This mechanism can be realized because of Umklapp scattering between the electron and the hole Fermi surface pockets resulting in opposite sign of pairing gap in these pockets. The applicability of the phenomenological Hao-Clem theory is investigated. Magnetic, temperature and impurity scattering rate dependencies of vortex core size are calculated. It is found that the accuracy of the effective London model gets better with the presence of the impurity scattering and even near the second critical field it is below 6%. The model with the parameters of intraband and interband impurity scattering, describing well superfluid density in $BaFe_2As_2$, is also considered.

The discoveries of the superconductivity in the layered FeP [1] and $FeAs$ [2] systems have ignited tremendous research activities for understanding of the superconductivity in Fe pnictides. The superconducting transition temperature T_c of electron-doped $LaFeAsO_{1-x}F_x$ ("1111") reaches 43 K under pressure [3], and $NdFeAsO_{1-x}F_x$ and $SmFeAsO_{1-x}F_x$ show T_c higher than 40 K at ambient pressure [4]. $BaFe_2As_2$ ("122") also shows superconductivity by hole doping with the highest T_c of 38 K in $(Ba,K)Fe_2As_2$ [5] and by electron doping with the highest T_c of 25 K in $Ba(Fe,Co)_2As_2$ [6]. Stoichiometric iron pnictides such as $LiFeAs$ or $NaFeAs$ ("111") are also interesting because they become superconducting without doping [7]. These Fe pnictides commonly have the $FeAs$ layers, where the Fe ions form a square lattice and each Fe ion is tetrahedrally coordinated by four As ions.

One key feature for understanding the origin of the high critical temperature and the pairing mechanism in superconductors is the symmetry of the order parameter. For iron pnictides, one of the attractive idea is that antiferromagnetic spin fluctuations mediate interband pairing. The sign of the Umklapp scattering between the electron and the hole Fermi surface, which is responsible for the superconducting pairing, is positive and the order parameter is fully gapped but changes sign between different Fermi sheets [8]. This situation is referred to as the extended $s^{\pm}$ symmetry. Using an $s^{\pm}$ model for the superconducting gap, a good explanation of experimental results on penetration depth in electron-doped and hole-doped $BaFe_2As_2$ pnictides has been obtained [9, 10]. In this model the Fermi surface is approximated by two cylindrical pockets centered at Γ (hole) and M (electron) points of the Fermi surface, i.e. two dimensional limit of five-band model is proposed. Recently, strong evidence of the $s^{\pm}$ symmetry in iron pnictides has been found by scanning tunneling microscopic measurements [11]. In spite of

success of $s^{\pm}$ model, there are some indications, e.g. weak sensitivity of T_c to the impurity concentration [12], that a conventional s-wave state without sign reversal (so called s_{++}-wave state) is also possible candidate for iron pnictides. It has been proposed that the moderate electron-phonon interaction due to Fe-ion oscillation can induce the critical orbital fluctuation, without being prohibited by the Coulomb interaction. These fluctuations give rise to the strong pairing interactions for the s_{++}-wave superconductivity [13].

The aim of our paper is to apply quasiclassical Eilenberger approach to the vortex state of stoichiometric and nonstoichiometric iron pnictides considering $s^{\pm}$ and s_{++} pairing symmetries as presumable states [9] and to calculate magnetic coherence length ξ_h [14, 15]. As described in Ref. [16], ξ_h is important for the description of the muon spin rotation (μSR) experiments and can be directly measured. On theoretical ground, the magnetic coherence length can be found from the fitting of the calculated magnetic field distribution $h_E(\mathbf{r})$ to the Eilenberger - Ginzburg-Landau field distribution $h_{EGL}(\mathbf{r})$ [14, 15]

$$h_{EGL}(\mathbf{r}) = \frac{\phi_0}{S}\sum_{\mathbf{G}}\frac{F(G)e^{i\mathbf{G}\mathbf{r}}}{1+\lambda^2 G^2}, \tag{1}$$

where $F(\mathbf{G}) = uK_1(u)$, $K_1(u)$ is the modified Bessel function, $u = \xi_h G$, $\mathbf{G}$ is a reciprocal lattice vector and S is the area of the vortex lattice unit cell. It is important to note that ξ_h in Eq. (1) is obtained from solving the Eilenberger equations and doesn't coincide with the variational parameter ξ_v (analytical Ginzburg-Landau (AGL) model), "improved" analytical GL solution [17] or numerical GL solution [18]. We will call the obtained field distribution as an Eilenberger - Ginzburg-Landau field distribution $h_{EGL}(\mathbf{r})$. Using the GL type of the field distribution does not mean direct connection to the GL theory and it is taken as a reasonable starting point of the investigation similar to the empirical approach to the problem [16, 19]. In Eq. (1) $\lambda(T)$ is calculated in Ref. [9]

$$\frac{\lambda_{L0}^2}{\lambda^2(T)} = 2\pi T\sum_{\omega_n>0}\frac{\bar{\Delta}_n^2}{\eta_n(\bar{\Delta}_n^2+\omega_n^2)^{3/2}}, \quad \eta_n = 1+2\pi\frac{\Gamma_0+\Gamma_\pi}{\sqrt{\bar{\Delta}_n^2+\omega_n^2}}, \tag{2}$$

where λ_{L0} is the London penetration depth at $T = 0$ K in the absence of the impurities. Here, $\bar{\Delta}_n = \Delta(T) - 4\pi\Gamma_\pi\bar{\Delta}_n/\sqrt{\bar{\Delta}_n^2+\omega_n^2}$ for the $s^{\pm}$ pairing and $\bar{\Delta}_n = \Delta(T)$ for the s_{++} pairing symmetry. The order parameter $\Delta(T)$ is determined by the selfconsistent equation

$$\Delta(T) = 2\pi T\sum_{0<\omega_n<\omega_c}\frac{V^{SC}\bar{\Delta}_n}{\sqrt{\bar{\Delta}_n^2+\omega_n^2}}. \tag{3}$$

With the Riccati transformation of the Eilenberger equations quasiclassical Green functions f and g can be parameterized via functions a and b [20]

$$\bar{f} = \frac{2a}{1+ab}, \quad f^{\dagger} = \frac{2b}{1+ab}, \quad g = \frac{1-ab}{1+ab}, \tag{4}$$

satisfying the nonlinear Riccati equations. In Born approximation for impurity scattering we have

$$\mathbf{u}\cdot\nabla a = -a[2(\omega_n+G)+i\mathbf{u}\cdot\mathbf{A}] + (\Delta+F) - a^2(\Delta^*+F^*), \tag{5}$$

$$\mathbf{u}\cdot\nabla b = b[2(\omega_n+G)+i\mathbf{u}\cdot\mathbf{A}] - (\Delta^*+F^*) + b^2(\Delta+F), \tag{6}$$

where $\omega_n = \pi T(2n+1)$, $G = 2\pi \langle g \rangle(\Gamma_0 + \Gamma_\pi) \equiv 2\pi \langle g \rangle \Gamma^*$, $F = 2\pi \langle f \rangle(\Gamma_0 - \Gamma_\pi)$ for $s^{\pm}$ pairing symmetry and $F = 2\pi \langle f \rangle \Gamma^*$ for the s_{++} pairing symmetry. Here, $\Gamma_0 = \pi n_i N_F |u_0|^2$ and $\Gamma_\pi = \pi n_i N_F |u_\pi|^2$ are the intra- and interband impurity scattering rates, respectively ($u_{0,\pi}$ are impurity scattering amplitudes with correspondingly small, or close to $\pi = (\pi, \pi)$, momentum transfer) and $\mathbf{u}$ is a unit vector of the Fermi velocity. The FLL create the anisotropy of the electron spectrum. Therefore the impurity renormalization correction in Eq. (5) and (6), averaged over Fermi surface, can be reduced to averages over the polar angle θ, i.e. $\langle \ldots \rangle = (1/2\pi) \int \ldots d\theta$. To take into account the influence of screening the vector potential $\mathbf{A}(\mathbf{r})$ in Eqs. (5) and (6) is obtained from the equation $\nabla \times \nabla \times \mathbf{A_E} = \frac{4}{\kappa^2}\mathbf{J}$, where the supercurrent $\mathbf{J}(\mathbf{r})$ is given in terms of $g(\omega_n, \theta, \mathbf{r})$ by

$$\mathbf{J}(\mathbf{r}) = 2\pi T \sum_{\omega_n > 0} \int_0^{2\pi} \frac{d\theta}{2\pi} \frac{\hat{\mathbf{k}}}{i} g(\omega_n, \theta, \mathbf{r}). \tag{7}$$

Here $\mathbf{A}$ and $\mathbf{J}$ are measured in units of $\phi_0/2\pi\xi_0$ and $2ev_F N_0 T_c$, respectively. The self-consistent condition for the pairing potential $\Delta(\mathbf{r})$ is given by

$$\Delta(\mathbf{r}) = V^{SC} 2\pi T \sum_{\omega_n > 0} \int_0^{2\pi} \frac{d\theta}{2\pi} f(\omega_n, \theta, \mathbf{r}), \tag{8}$$

where V^{SC} is the coupling constant and ω_c is the ultraviolet cutoff determining T_{c0} [15].

All over this paper the energy, the temperature and the length are measured in units of T_{c0} and the coherence length $\xi_0 = v_F/T_{c0}$, where v_F is the Fermi velocity. The magnetic field $\mathbf{h}$ is given in units of $\phi_0/2\pi\xi_0^2$. The impurity scattering rates are in units of $2\pi T_{c0}$. In calculations the ratio $\kappa = \lambda_{L0}/\xi_0 = 10$ is used. It corresponds to $\kappa_{GL} = 43.3$ [20]. To obtain the quasiclassical Green function, the Riccati equations [Eq. (5, 6)] are solved by the Fast Fourier Transform (FFT) method for triangular FLL [15]. This method is reasonable for dense FLL discussed in this paper. In high field the pinning effects are weak and they are not considered in our paper. To study high field regime we should calculate upper critical field $B_{c2}(T)$. It can be found from the similarity of the considered model to the model of spin-flip superconductors [21].

Solid lines in Fig. 1 demonstrate magnetic field dependence $\xi_h(B)$ in reduced units for superconductors with impurity scattering at $T/T_{c0} = 0.5$ with $\Gamma_0 = \Gamma_\pi = 0$; $\Gamma_0 = 3$, $\Gamma_\pi = 0.03$ and $\Gamma_0 = 0.5$, $\Gamma_\pi = 0.01$. Dash line demonstrates the result of the AGL theory for ξ_v[22]

$$\xi_v = \xi_{c2}(\sqrt{2} - \frac{0.75}{\kappa_{GL}})(1 + b^4)^{1/2}[1 - 2b(1-b)^2]^{1/2}, \tag{9}$$

where ξ_{c2} is determined from the relation $B_{c2} = \Phi_0/2\pi\xi_{c2}^2$ (in our units $\xi_{c2} = 1/\sqrt{B_{c2}}$). This dependence with ξ_{c2} as a fitting parameter is used often for the description of the μSR experimental results [16, 19]. As can be seen from Fig. 1 (a) the magnetic field dependence of ξ_h/ξ_{c2} is nonuniversal because it depends not only from B/B_{c2} (as in the AGL theory, dash line in Fig. 1 (a)), but also on interband and intraband impurity scattering parameters. In the case when, $\Gamma_0 = \Gamma_\pi = 0$, the results are the same for $s^{\pm}$ and s_{++} pairing symmetries. We mark this curve as "clean" one. In this figure is considered the case $\Gamma_0 \gg \Gamma_\pi$ and the value of ξ_h is reduced considerably in comparison with clean case. One can compare the observed behavior with that in s_{++} pairing model. In s_{++} pairing symmetry the intraband and interband scattering rates act in similar way and ξ_h/ξ_{c2} decreases always with impurity scattering. In contrast, in $s^{\pm}$ model $\xi_h/\xi_{c2}(B/B_{c2})$ dependences show different behavior with Γ_π: ξ_h/ξ_{c2} increases with Γ_π at $B/B_{c2} < 0.8$ and decreases at higher fields, i.e. the curves are getting more flat. A crossing point appears in the dependences $\xi_h/\xi_{c2}(B/B_{c2})$ for $s^{\pm}$ and s_{++} pairing. This can be explained by the fact that in superconductors without interband pair breaking the increasing in high field is

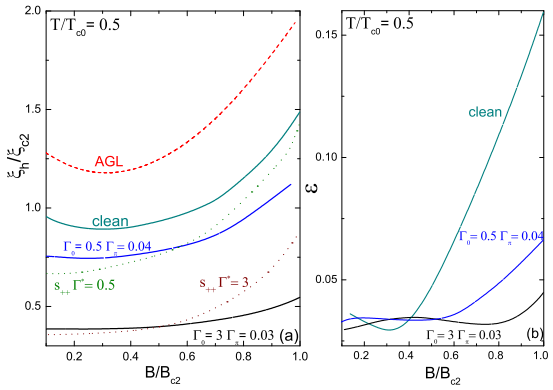

Figure 1. (a) The magnetic field dependence of ξ_h/ξ_{c2} for superconductors with impurity scattering. Dashed line demonstrates the result of the AGL theory for ξ_v from Eq. 9. Solid lines represent our solution of Eilenberger equations at $T/T_{c0} = 0.5$ for the "clean" case ($\Gamma_0 = \Gamma_\pi = 0$) and $s^\pm$ model ($\Gamma_0 = 0.5$, $\Gamma_\pi = 0.04$ and $\Gamma_0 = 3$, $\Gamma_\pi = 0.03$). Dotted lines show result for s_{++} model ($\Gamma^* = 0.5$ and $\Gamma^* = 3$). (b) Magnetic field dependence of mean square deviation of the h_{EGL} distribution from the Eilenberger distribution normalized by the variance of the Eilenberger distribution, ε, for $T/T_{c0} = 0.5$ for the "clean" case, $\Gamma_0 = 3$, $\Gamma_\pi = 0.03$ and $\Gamma_0 = 0.5$, $\Gamma_\pi = 0.04$ for the $s^\pm$ model.

connected with field-dependent pair breaking under approaching to the upper critical field. We also calculate magnetic field dependence of mean square deviation of the h_{EGL} distribution of the magnetic field from the Eilenberger distribution normalized by the variance of the Eilenberger distribution $\varepsilon = \sqrt{\overline{(h_E - h_{EGL})^2}/\overline{(h_E - B)^2}}$, where $\overline{\cdots}$ is average over unit vortex cell. Fig. 1 (b) demonstrates $\varepsilon(B)$ dependence for $T/T_{c0} = 0.5$ at $\Gamma_0 = 0$, $\Gamma_\pi = 0$; $\Gamma_0 = 3$, $\Gamma_\pi = 0.03$ and $\Gamma_0 = 0.5$, $\Gamma_\pi = 0.04$. It can be seen from this figure that accuracy of effective London model getting worse with increasing magnetic field, but in superconductors with impurity scattering the accuracy is below 6% even near the second critical field (Fig. 1 (b)).

The superfluidity density in pnictides shows often a power law dependence with exponent approximately equal to two at low temperatures [9, 10]. This law was explained by $s^\pm$ model with parameters $\Gamma_0 = 3$ and $\Gamma_\pi = 0.04 - 0.06$. Fig. 2 (a) shows $\xi_h/\xi_{c2}(B/B_{c2})$ dependence with $\Gamma_0 = 3$ and $\Gamma_\pi = 0.06$ at different temperatures. All curves demonstrate growing behavior with values much less that one in whole field range, i.e. they are under the AGL curve of ξ_v. This shows strong effect of interband scattering. The inset to Fig. 2 (a) presents $\xi_h/\xi_{c2}(B/B_{c2})$ results for $\Gamma_0 = 3$, $\Gamma_\pi = 0.06$ ($s^\pm$ pairing) and $\Gamma^* = 3$ (s_{++} pairing) at $T/T_{c0} = 0.15$. This type of the behavior is cut off by the impurity pair breaking and introducing characteristic field B^* in the field dependence by the substitution $B/B_{c2} \to (B + B^*(\Gamma_\pi))/B_{c2}(\Gamma_\pi)$. There is additional low-field crossing point between $s^\pm$ and s_{++} curves in this low-temperature case comparing with $T/T_{c0} = 0.5$ (Fig. 1 (a)). It can be explained by the restoration of the Usadel dirty limit behavior (where $\Gamma \gg 1$ and monotonously decreasing $\xi_h(B)$ is expected [20, 23]) which is not realized for $s^\pm$ symmetry due to the pair breaking there. Opposite, slowly increasing $\xi_h/\xi_{c2}(B/B_{c2})$ function is obtained for $s^\pm$ case in low-field range (Fig. 2 (a) main plot). It can be explained by the field-dependent splitting of the low-energy spectrum of bound state in the vortex core similar to the case of the surface bound states in d-wave superconductors [24]. The same effect is realized for extended state in high-field (for $B/B_{c2} > 0.5$ in Fig. 2 (a)).

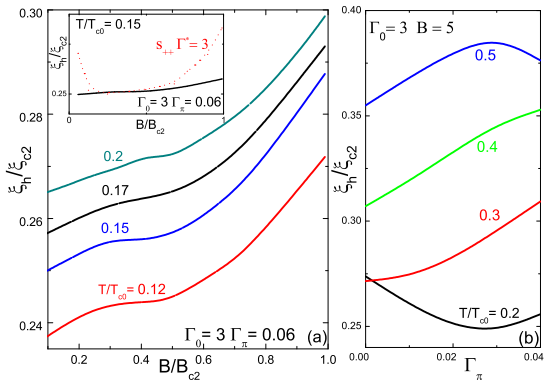

Figure 2. (a) The magnetic field dependence of coherence length ξ_h with different temperatures T_c/T_{c0} for $\Gamma_0 = 3$, $\Gamma_\pi = 0.06$. The inset shows the magnetic field dependence of ξ_h/ξ_{c2} for $s^{\pm}$ model ($\Gamma_0 = 3$, $\Gamma_\pi = 0.06$) and s_{++} model ($\Gamma^* = 3$, dotted line) at $T/T_{c0} = 0.15$. (b) The interband scattering Γ_π dependence of ξ_h/ξ_{c2} at different temperatures T/T_{c0} (intraband scattering $\Gamma_0 = 3$ and $B = 5$) for the $s^{\pm}$ pairing.

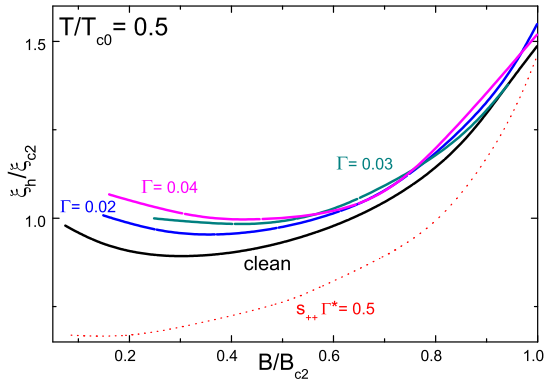

Figure 3. The magnetic field dependence of coherence length at $T/T_{c0} = 0.5$ with the similar values of intraband Γ_0 and interband Γ_π scattering Γ ($\Gamma = 0$ for "clean" case and $\Gamma = 0.02, 0.03, 0.04$ for the $s^{\pm}$ pairing). Dotted line shows result for s_{++} model ($\Gamma^* = 0.5$).

Study of the field dependence $\xi_h/\xi_{c2}(B/B_{c2})$ can clarify the both branches [25] of the energetic spectrum of the mixed state which can not be done in the phenomenological GL theory. Thus, the field-dependent suppression of ξ_h/ξ_{c2} is expected in $s^{\pm}$ model in comparison to s_{++} one in nonstoichiometric iron pnictides with high Γ_π (like doped 122 compounds). Also nonmonotonous $\xi_h/\xi_{c2}(\Gamma_\pi)$ dependence is possible in general as is shown in Fig. 2 (b).

We also study the case of weak intraband scattering. This case can be realized in stoichiometric pnictides such as $LiFeAs$. Fig. 3 presents the ξ_h/ξ_{c2} magnetic field dependence with scattering parameters $\Gamma_0 = \Gamma_\pi = \Gamma$ equal to 0, 0.02, 0.03 and 0.04. Dotted line shows the result for s_{++} model ($\Gamma^* = 0.5$). The $\xi_h(B)$ dependence shifts upward from the "clean" curve and have higher values in $s^{\pm}$ model. In contrast, ξ_h/ξ_{c2} curve shifts downward with impurity

scattering in s_{++} model. The high values of ξ_h observed in μSR measurements in $LiFeAs$ [7] supports the $s^{\pm}$ pairing.

To conclude, Eilenberger equations have been solved in the mixed state for superconductors with $s^{\pm}$ pairing symmetry. This symmetry is proposed to realize in iron pnictide superconductors. Effects of interband (Γ_0) and intraband (Γ_π) impurity scattering on coherence length ξ_h are investigated. It is found that $\xi_h/\xi_{c2}(B/B_{c2})$ dependence is nonuniversal and different from the GL theory prediction. In the case of intraband scattering ξ_h/ξ_{c2} decreases with Γ_0. The effects of interband scattering on ξ_h depends on Γ_0. The predictions for $\xi_h/\xi_{c2}(B/B_{c2})$ for doped 122 compounds (nonstoichiometric iron pnictides), where $\Gamma_0 \gg \Gamma_\pi$, are done. These dependencies demonstrate growing behavior defined by Γ_0 with values much less that one in whole field range, i.e. they are under the "clean" ($\Gamma_0 = \Gamma_\pi = 0$) curve. In the case of weak impurity scattering, $\Gamma_0 = \Gamma_\pi \ll 1$, the $\xi_h/\xi_{c2}(B/B_{c2})$ dependence shifts upward from the "clean" curve. This case can be realized in stoichiometric 111 compounds. A comparison with s_{++} pairing model is done. Opposite tendencies with interband scattering for $\xi_h/\xi_{c2}(B/B_{c2})$ dependences are found for $s^{\pm}$ and s_{++} models for stoichiometric and nonstoichiometric iron pnictides. The predictions can be tested by μSR experiments.

This work was supported by the Finnish Cultural Foundation.

References

[1] Kamihara Y, Hiramats H, Hirano M, Kawamura R, Yanagi H, Kamiya T and Hosono H 2006 *J. Am. Chem. Soc.* **128** 10012
[2] Kamihara Y, Watanabe T, Hirano M and Hosono H 2008 *J. Am. Chem. Soc.* **130** 3296
[3] Takahashi H, Igawa K, Arii K, Kamihara Y, Hirano M and Hosono H 2008 *Nature (London)* **453** 376
[4] Chen G F, Li Z, DWu, GLi, ZHu W, Dong J, Zheng P, Luo J L and Wang N L 2008 *Phys. Rev. Lett.* **100** 247002
[5] Rotter M, Tegel M and Johrendt D 2008 *Phys. Rev. Lett.* **101** 107006
[6] Sefat A S, Jin R, McGuire M A, Sales B C, Singh D J and Mandrus D 2008 *Phys. Rev. Lett.* **101** 117004
[7] Inosov D S, White J S, Evtushinsky D V, Morozov I V, Cameron A, Stockert U, Zabolotnyy V B, Kim T K, Kordyuk A A, Borisenko S V, Forgan E M, Klingeler R, Park J T, Wurmehl S, Vasiliev A N, Behr G, Dewhurst C D and Hinkov V 2010 *Phys. Rev. Lett.* **104** 187001
[8] Mazin I I, Singh D J, Johannes M D and Du M H 2008 *Phys. Rev. Lett.* **101** 057003
[9] Vorontsov A B, Vavilov M G and Chubukov A V 2009 *Phys. Rev. B* **79** 140507(R)
[10] Martin C, Gordon R T, Tanatar M A, Kim H, Ni N, Bud'ko S L, Canfield P C, Luo H, Wen H H, Wang Z, Vorontsov A B, Kogan V G and Prozorov R 2009 *Phys. Rev. B* **80** 020501(R)
[11] Hanaguri T, Niitaka S, Kuroki K and Takagi H 2010 *Science* **328** 474
[12] Tanatar M A, Reid J P, Shakeripour H, Luo X G, Doiron-Leyraud N, Ni N, Bud'ko S L, Canfield P C, Prozorov R and Taillefer L 2010 *Phys. Rev. Lett.* **104** 067002
[13] Kontani H and Onari S 2010 *Phys. Rev. Lett.* **104** 157001
[14] Laiho R, Safonchik M and Traito K B 2007 *Phys. Rev. B* **76** 140501(R)
[15] Laiho R, Safonchik M and Traito K B 2008 *Phys. Rev. B* **78** 064521
[16] Sonier J E 2007 *Rep. Prog. Phys.* **70** 1717
[17] Pogosov W V, Kugel K I, Rakhmanov A L and Brandt E H 2001 *Phys. Rev. B* **64** 064517
[18] de Oliveira I G and Thompson A M 1998 *Phys. Rev. B* **57** 7477
[19] Sonier J E 2004 *J. Phys.: Condens. Matter* **16** S4499
[20] Miranović P, Ichioka M and Machida K 2004 *Phys. Rev. B* **70** 104510
[21] Ovchinnikov Y N and Kresin V Z 1995 *Phys. Rev. B* **52** 3075
[22] Hao Z, Clem J R, McElfresh M W, Civale L, Malozemoff A P and Holtzberg F 1991 *Phys. Rev. B* **43** 2844
[23] Sonier J E, Kiefl R F, Brewer J H, Chakhalian J, Dunsiger S R, MacFarlane W A, Miller R I, Wong A, Luke G M and Brill J W 1997 *Phys. Rev. Lett.* **79** 1742
[24] Zare A, Markowsky A, Dahm T and Schopohl N 2008 *Phys. Rev. B* **78** 104524
[25] Gygi F and Schlüter M 1991 *Phys. Rev. B* **43** 7609

PUBL. 2

P. Belova, M. Safonchik, K. B. Traito and E. Lähderanta, Cutoff parameter of the field distribution in the mixed state of iron pnictides with $s^{\pm}$ and s_{++} pairing symmetries, *Physical Review B*, **83**, 104518, 2011.

PHYSICAL REVIEW B **83**, 104518 (2011)

Cutoff parameter of the field distribution in the mixed state of iron pnictides with $s_{\pm}$ and s_{++} pairing symmetries

P. Belova,[1,2,*] M. Safonchik,[1,3,†] K. B. Traito,[1] and E. Lähderanta[1]
[1]*Lappeenranta University of Technology, P.O. Box 20, FI-53851, Lappeenranta, Finland*
[2]*Petrozavodsk State University, Lenin Strasse 33, RU-185640, Petrozavodsk, Russia*
[3]*A. F. Ioffe Physico-Technical Institute, RU-194021, St. Petersburg, Russia*
(Received 21 October 2010; revised manuscript received 24 January 2011; published 25 March 2011)

The effects of the pairing symmetries ($s_{\pm}$ and s_{++}) on the cutoff parameter of field distribution, ξ_h, in stoichiometric (like LiFeAs) and nonstoichiometric (like doped $BaFe_2As_2$) iron pnictides have been investigated using Eilenberger quasiclassical equations. Magnetic field, temperature, and impurity scattering dependencies of ξ_h have been calculated. Two opposite behaviors have been discovered. The ξ_h/ξ_{c2} ratio is less in $s_{\pm}$ symmetry when the intraband impurity scattering (Γ_0) is much larger than 1 and is much larger than the interband impurity scattering (Γ_π), i.e., in nonstoichiometric iron pnictides. In contrast, the value ξ_h/ξ_{c2} is higher in the $s_{\pm}$ case and the field-dependent curve is shifted upward from the "clean" case ($\Gamma_0 = \Gamma_\pi = 0$) for stoichiometric iron pnictides ($\Gamma_0 = \Gamma_\pi \ll 1$). Results can be tested in muon spin rotation measurements.

DOI: 10.1103/PhysRevB.83.104518 PACS number(s): 74.20.Rp, 74.20.Fg, 74.25.Op

The discovery of superconductivity ($T_c = 26K$) in fluorine-doped LaFeAsO ("1111")[1] has generated remarkable interest in the community. This interest has lead to the discovery of other oxyarsenides having critical temperatures exceeding 55 K.[2] Later, superconductivity, with T_c as high as 38 K, was discovered in $Ba_{1-x}K_xFe_2As_2$ (Ref. 3) and in $Ba(Fe_{1-x}Co_x)_2As_2$ (Ref. 4) with $T_c = 23$ K. These "122" compounds are not oxides, downplaying the role of oxygen in the mechanism of high-temperature superconductivity. Stoichiometric iron pnictides such as LiFeAs or NaFeAs (111 pnictides) are also interesting because they become superconducting without doping.[5] Close proximity to a magnetic state could imply the importance of magnetic fluctuations for pairing and may be reflected in the symmetry of the superconducting gap. At the same time, band-structure calculations and angle resolved photoemission spectroscopy experiments[6] show that multiple bands cross the Fermi level, opening a possibility for multiband superconductivity.

The results of scanning tunneling microscopy[7] indicate that the sign is reversed between the hole and the electron Fermi-surface pockets ($s_{\pm}$ wave), favoring the unconventional pairing mechanism associated with spin fluctuations. The order parameter is fully gapped but changes sign between different Fermi sheets.[8] This situation is referred to as the extended $s_{\pm}$ symmetry. Using an $s_{\pm}$ model for the superconducting gap, a good explanation of experimental results on penetration depth in electron-doped and hole-doped $BaFe_2As_2$ pnictides has been obtained.[9,10] In this model the Fermi surface is approximated by two cylindrical pockets centered at Γ (hole) and M (electron) points of the Fermi surface; i.e., a two-dimensional limit of a five-band model is proposed. Recently, strong support for the $s_{\pm}$ symmetry in iron pnictides has been found by scanning tunneling microscopic measurements.[7] Despite the success of the $s_{\pm}$ model, there are some indications that a conventional s-wave state without sign reversal (s_{++}-wave state) is also a possible candidate for iron pnictides. It has been proposed that the moderate electron-phonon interaction due to Fe-ion oscillation can induce the critical orbital fluctuation, without being prohibited by the Coulomb interaction. These fluctuations give rise to the strong pairing interactions for the s_{++}-wave superconductivity.[11] A resonancelike peak structure observed by neutron scattering measurements[12] is reproduced by considering the strong correlation effect via quasiparticle damping, without the necessity of sign reversal in the superconducting gap.[13] The $s_{\pm}$-wave state is expected to be very fragile against impurities due to the interband scattering,[14] and the superconducting state is remarkably robust against impurities and α-particle irradiation.[15]

The aim of our paper is to apply a quasiclassical Eilenberger approach to the vortex state of iron pnictides considering $s_{\pm}$ and s_{++} pairing symmetries as presumable states[9] for the different levels of impurity scattering rates Γ^* and to calculate the cutoff parameter ξ_h.[16,17] As described in Ref. 18, ξ_h is important for the description of the muon spin rotation (μSR) experiments and can be directly measured.

The London model used for the analysis of the experimental data does not account for the spatial dependence of the superconducting order parameter and it breaks down at distances on the order of coherence length from the vortex core center, i.e., $B(r)$ logarithmically diverges as $r \to 0$. To correct this, the $\mathbf{G}$ sum in the expression for vortex lattice free energy can be truncated by multiplying each term by the cutoff function $F(G)$. Here, $\mathbf{G}$ is a reciprocal vortex lattice vector and G is its module. In this method the sum is cut at high $G_{\max} \approx 2\pi/\xi_h$, where ξ_h is the cutoff parameter. The characteristic length ξ_h accommodates a number of inherent uncertainties of the London approach, the question discussed originally by de Gennes[19] and in some detail in Ref. 20. It is important to stress that the appropriate form of $F(G)$ depends on the precise spatial dependence of the order parameter in the vortex core region, and this in general depends on temperature and magnetic field.

A smooth Gaussian cutoff factor $F(G) = \exp(-\alpha G^2\xi^2)$ was phenomenologically suggested. Here, ξ is the Gizburg-Landau coherence length. If there is no dependence of the superconducting coherence length on temperature and magnetic field, then changes in the spatial dependence of the

order parameter around a vortex correspond to changes in α. By solving the Ginzburg-Landau (GL) equations, Brandt determined that $\alpha = 1/2$ at fields near B_{c2} (Ref. 21) and arbitarily determined that $\alpha \approx 2$ at fields immediately above B_{c1}.[22] For an isolated vortex in an isotropic extreme (the GL parameter $\kappa_{\rm GL} \gg 1$) s-wave superconductor, α was obtained by numerical calculation of GL equations. It was found that α decreases smoothly from $\alpha = 1$ at B_{c1} to $\alpha \approx 0.2$ at B_{c2}.[23] The analytical GL expression was obtained by Clem[24] for isotropic superconductors at low inductions $B \ll B_{c2}$. Using a Lorentzian trial function for the order parameter of an isolated vortex, Clem[24] found for large $\kappa_{\rm GL} \gg 1$ that $F(G)$ is proportional to the modified Bessel function. Hao *et al.*[25] extended the model[24] to larger magnetic fields up to B_{c2} through the linear superposition of the field profiles of individual vortices. In this model, the Clem trial function[24] is multiplied by a second variational parameter, f_α, to account for the suppression of the order parameter due to the overlapping vortex cores. This model gave the method to calculate the magnetization of type-II superconductors in the full range $B_{c1} < B < B_{c2}$. Their analytical formula is in a good agreement with the well-known Abrikosov high-field result and corrected the results obtained with exponential cutoff function at low field considerably.[26] This approximation was widely used for the analysis of the experimental data on magnetization of type-II superconductors (see Refs. 27–29 in Ref. 27). The improved approximate GL solution for the regular flux-line lattice using a circular cell method was obtained in Ref. 27. It gives better coincidence with numerical solution of GL equations.

Strictly speaking, GL theory is valid only near T_c but it is often used in whole temperature range taking the cutoff parameter and penetration depth λ as fitting parameters. Recently an effective London model with the effective cutoff parameter $\xi_h(B)$ as a fitting parameter was obtained for clean[16] and dirty[17] superconductors, using a self-consistent solution of quasiclassical nonlinear Eilenberger equations. In this approach λ is not a fitting parameter but is calculated from the microscopical theory of the Meissner state. This consideration implies only one fitting parameter for analysis of experimental data, i.e., $f_\alpha = 1$, similar to the theory used for the explanation of the magnetization experiments.[28] As was shown in Ref. 29 the reduction of the amount of the fitting parameters to one simplified considerably the fitting procedure. In this method the cutoff parameter obtained from the GL model is extended over the whole field and temperature range. In this case the effects of bound states in the vortex cores leading to the Kramer-Pesch effect,[30] their delocalization between the vortices[31,32] and nonlocal electrodynamic[33] are self-consistently included.

Following the microscopical Eilenberger theory, ξ_h can be found from the fitting of the calculated magnetic field distribution $h_E(\mathbf{r})$ to the Eilenberger–Ginzburg-Landau (EGL) field distribution $h_{\rm EGL}(\mathbf{r})$[16,17]:

$$h_{\rm EGL}(\mathbf{r}) = \frac{\phi_0}{S}\sum_{\mathbf{G}}\frac{F(G)e^{i\mathbf{G}\mathbf{r}}}{1+\lambda^2 G^2}, \tag{1}$$

where $F(G) = uK_1(u)$, where $K_1(u)$ is modified Bessel function; $u = \xi_h G$; and S is the area of the vortex lattice unit cell. It is important to note that ξ_h in Eq. (1) is obtained from solving the Eilenberger equations and doesn't coincide with the variational parameter ξ_v [analytical Ginzburg-Landau (AGL) model]. We call the obtained field distribution an EGL field distribution, $h_{\rm EGL}(\mathbf{r})$. Using the GL type of the field distribution does not mean direct connection to the GL theory. It can be taken as a reasonable starting point of the investigation similar to the empirical approach to the problem.[18,34] In Eq. (1), $\lambda(T)$ is the penetration depth in the Meissner state. It is calculated in Ref. 9 as

$$\frac{\lambda_{L0}^2}{\lambda^2(T)} = 2\pi T\sum_{\omega_n>0}\frac{\bar{\Delta}_n^2}{\eta_n\left(\bar{\Delta}_n^2+\omega_n^2\right)^{3/2}}, \tag{2}$$

where λ_{L0} is the London penetration depth at $T = 0$ K in the absence of the impurities and $\eta_n = 1 + 2\pi * (\Gamma_0 + \Gamma_\pi)/(\sqrt{\bar{\Delta}_n^2+\omega_n^2})$. Here, $\Gamma_0 = \pi n_i N_F |u_0|^2$ and $\Gamma_\pi = \pi n_i N_F |u_\pi|^2$ are the intra- and interband impurity scattering rates, respectively ($u_{0,\pi}$ are impurity scattering amplitudes with correspondingly small, or close to $\pi = (\pi,\pi)$, momentum transfer). In this work, we investigate the field distribution in the vortex lattice by systematically changing the impurity concentration in the Born approximation and analyze the field dependence of the cutoff parameter. In particular, we consider two limits: small $\Gamma^* \ll 1$ (calling it as "stoichiometric" case) and relatively high $\Gamma^* \geqslant 1$ ("nonstoichiometric" case). Here, Γ^* is measured in units of $2\pi T_{c0}$.

In Eq. (2), $\bar{\Delta}_n = \Delta(T) - 4\pi\Gamma_\pi\bar{\Delta}_n/\sqrt{\bar{\Delta}_n^2+\omega_n^2}$ for the $s_\pm$ pairing and $\bar{\Delta}_n = \Delta(T)$ for the s_{++} pairing symmetry. The order parameter $\Delta(T)$ in the Meissner state is determined by the self-consistent equation

$$\Delta(T) = 2\pi T\sum_{0<\omega_n<\omega_c}\frac{V^{\rm SC}\bar{\Delta}_n}{\sqrt{\bar{\Delta}_n^2+\omega_n^2}}. \tag{3}$$

Experimentally, $\lambda(T)$ can be obtained by radio-frequency measurements[35] and magnetization measurements of nanoparticles.[36] With the Riccati transformation of the Eilenberger equations, quasiclassical Green's functions f and g can be parametrized via functions a and b (Ref. 37):

$$\bar{f} = \frac{2a}{1+ab}, \quad f^\dagger = \frac{2b}{1+ab}, \quad g = \frac{1-ab}{1+ab}, \tag{4}$$

satisfying the nonlinear Riccati equations. In the Born approximation for impurity scattering we have

$$\mathbf{u}\cdot\nabla a = -a\left[2(\omega_n+G)+i\mathbf{u}\cdot\mathbf{A}\right] + (\Delta+F) - a^2(\Delta^*+F^*), \tag{5}$$

$$\mathbf{u}\cdot\nabla b = b\left[2(\omega_n+G)+i\mathbf{u}\cdot\mathbf{A}\right] - (\Delta^*+F^*) + b^2(\Delta+F), \tag{6}$$

where $\omega_n = \pi T(2n+1)$, $G = 2\pi\langle g\rangle(\Gamma_0+\Gamma_\pi) \equiv 2\pi\langle g\rangle\Gamma^*$, $F = 2\pi\langle f\rangle(\Gamma_0-\Gamma_\pi)$ for $s_\pm$ pairing symmetry, and $F = 2\pi\langle f\rangle\Gamma^*$ for the s_{++} pairing symmetry. Here, $\mathbf{u}$ is a unit vector of the Fermi velocity. The flux line lattice (FLL) creates the anisotropy of the electron spectrum. Therefore, the impurity renormalization correction in Eqs. (5) and (6), averaged over the Fermi surface, can be reduced to averages over the polar angle θ, i.e., $\langle\cdots\rangle = (1/2\pi)\int\ldots d\theta$. To take into account the influence of screening the vector potential, $\mathbf{A}(\mathbf{r})$ in Eqs. (5) and (6) is obtained from the equation $\nabla\times\nabla\times\mathbf{A}_{\mathbf{E}} = \frac{4}{\kappa^2}\mathbf{J}$, where

the supercurrent $\mathbf{J}(\mathbf{r})$ is given in terms of $g(\omega_n,\theta,\mathbf{r})$ by

$$\mathbf{J}(\mathbf{r}) = 2\pi T \sum_{\omega_n>0} \int_0^{2\pi} \frac{d\theta}{2\pi} \frac{\hat{\mathbf{k}}}{i} g(\omega_n,\theta,\mathbf{r}). \quad (7)$$

Here $\mathbf{A}$ and $\mathbf{J}$ are measured in units of $\phi_0/2\pi\xi_0$ and $2ev_F N_0 T_c$, respectively. The self-consistent condition for the pairing potential $\Delta(\mathbf{r})$ in the vortex state is given by $\Delta(\mathbf{r}) = V^{\rm SC} 2\pi T \sum_{\omega_n>0} \int_0^{2\pi} \frac{d\theta}{2\pi} f(\omega_n,\theta,\mathbf{r})$, where $V^{\rm SC}$ is the coupling constant and ω_c is the ultraviolet cutoff determining T_{c0}.[17] All over our paper the energy, the temperature, and the length are measured in units of T_{c0}, and the coherence length $\xi_0 = v_F/T_{c0}$, where v_F is the Fermi velocity. The magnetic field $\mathbf{h}$ is given in units of $\phi_0/2\pi\xi_0^2$. The impurity scattering rates are in units of $2\pi T_{c0}$. In calculations the ratio $\kappa = \lambda_{L0}/\xi_0 = 10$ is used. It corresponds to $\kappa_{\rm GL} = 43.3$.[37]

To obtain the quasiclassical Green's function, the Riccati equations [Eqs. (5), (6)] are solved by the fast Fourier transform (FFT) method for the triangular FLL.[17] This method is reasonable for the dense FLL discussed in this paper. In high field the pinning effects are weak and they are not considered in our paper. To study a high field regime we should calculate upper critical field $B_{c2}(T)$. It could be found from the similarity of the considered model to the model of spin-flip superconductors.[38]

Figure 1(a) shows magnetic field dependence $\xi_h(B)$ in reduced units at $T/T_{c0} = 0.5$ for the $s_\pm$ pairing with $\Gamma_0 = 3$, $\Gamma_\pi = 0.02$ and $\Gamma_0 = 0.5$, $\Gamma_\pi = 0.03$ and the "clean" case (solid lines) and for the s_{++} pairing with $\Gamma^* = 0.5$ and $\Gamma^* = 3$ (dotted lines). The dashed line shows the analytical solution

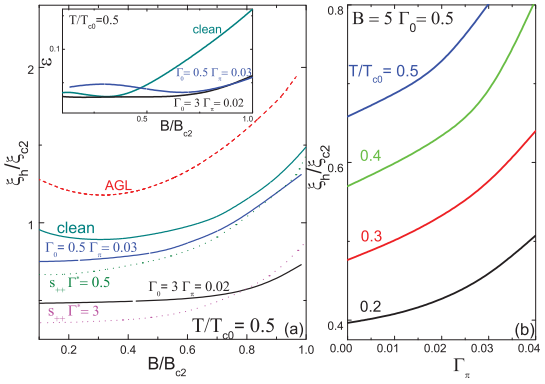

FIG. 1. (Color online) (a) The magnetic field dependence of ξ_h/ξ_{c2} for superconductors with impurity scattering. Solid lines represent our solution of Eilenberger equations at $T/T_{c0} = 0.5$ for the "clean" case ($\Gamma_0 = \Gamma_\pi = 0$) and $s_\pm$ model ($\Gamma_0 = 0.5$, $\Gamma_\pi = 0.03$ and $\Gamma_0 = 3$, $\Gamma_\pi = 0.02$). Dotted lines show results for the s_{++} model ($\Gamma^* = 0.5$ and $\Gamma^* = 3$). The dashed line demonstrates the result of the AGL theory for ξ_v from Eq. (8). The inset shows magnetic field dependence of mean square deviation of the $h_{\rm EGL}$ distribution from the Eilenberger distribution normalized by the variance of the Eilenberger distribution, ε, for $T/T_{c0} = 0.5$ at $\Gamma_0 = \Gamma_\pi = 0$ (clean); $\Gamma_0 = 3$, $\Gamma_\pi = 0.02$ and $\Gamma_0 = 0.5$, $\Gamma_\pi = 0.03$. (b) The interband scattering Γ_π dependence of ξ_h/ξ_{c2} at different temperatures T/T_{c0} (intraband scattering $\Gamma_0 = 0.5$ and $B = 5$) for the $s_\pm$ pairing.

of the AGL theory[25]

$$\xi_v = \xi_{c2}\left(\sqrt{2} - \frac{0.75}{\kappa_{\rm GL}}\right)(1+b^4)^{1/2}[1-2b(1-b)^2]^{1/2}. \quad (8)$$

This dependence with ξ_{c2} as a fitting parameter is often used for the description of the experimental μSR results.[18,34] As can be seen from Fig. 1(a), the magnetic field dependence of ξ_h/ξ_{c2} is nonuniversal because it depends not only on B/B_{c2} [as in the AGL theory, dashed line in Fig. 1(a)] but also on interband and intraband impurity scattering parameters. In the case when $\Gamma_0 = \Gamma_\pi = 0$, the results are the same for $s_\pm$ and s_{++} pairing symmetries. We mark this curve as the clean one. In this figure the case $\Gamma_0 \gg \Gamma_\pi$ is considered and the value of ξ_h is reduced considerably in comparison with the clean case. One can compare the observed behavior with that in the s_{++} pairing model. In s_{++} pairing symmetry the intraband and interband scattering rates act in a similar way and ξ_h/ξ_{c2} decreases always with impurity scattering. In contrast, in the $s_\pm$ model $\xi_h/\xi_{c2}(B/B_{c2})$ dependencies show different behavior with Γ_π. Here, ξ_h/ξ_{c2} increases with Γ_π at $B/B_{c2} < 0.8$ and decreases at higher fields; i.e., the curves are getting more flat. A crossing point appears in the dependencies $\xi_h/\xi_{c2}(B/B_{c2})$ for $s_\pm$ and s_{++} pairings. We also calculate magnetic field dependence of the mean square deviation of the $h_{\rm EGL}$ distribution of the magnetic field from the Eilenberger distribution normalized by the variance of the Eilenberger distribution $\varepsilon = \sqrt{\overline{(h_E - h_{\rm EGL})^2}/\overline{(h_E - B)^2}}$, where $\overline{\cdots}$ is the average over the unit vortex cell. The inset to Fig. 1(a) demonstrates the $\varepsilon(B)$ dependence for $T/T_{c0} = 0.5$ at $\Gamma_0 = 0$, $\Gamma_\pi = 0$; $\Gamma_0 = 3$, $\Gamma_\pi = 0.02$; and $\Gamma_0 = 0.5$, $\Gamma_\pi = 0.03$. From this figure it can be seen that the accuracy of the effective London model is getting worse with the increasing magnetic field, but in superconductors with impurity scattering the accuracy is below 6% even near with second critical field [the inset to Fig. 1(a)].

In Fig. 1(b) the interband scattering Γ_π dependencies of ξ_h are presented in low fields for the $s_\pm$ pairing at different temperatures T. As can be seen ξ_h/ξ_{c2} increases with the interband scattering rate Γ_π. Strong decreasing of ξ_h/ξ_{c2} with decreasing of temperature can be explained by the Kramer-Pesch effect.[30] It should be noted that the normalization constant ξ_{c2} increases with Γ_π because Γ_π suppress T_c similar to superconductors with spin-flip scattering (violation of the Anderson theorem). Thus, the growing ξ_h/ξ_{c2} implies more strong growth of ξ_h than ξ_{c2} (from GL theory one can expect $\xi_h/\xi_{c2} = $ Const.). Qualitatively, it can be explained by the strong temperature dependence of $\xi_h(B,T/T_c)$ connected with the Kramer-Pesch effect.[30] Increasing Γ_π results in suppression of T_c, i.e., effective increasing of T and $\xi_h(T/T_c)$. $\xi_{c2}(T/T_c)$ has not so strong T_c dependence leading to the increasing of the ration ξ_h/ξ_{c2} with Γ_π.

The superfluidity density in pnictides shows often power law dependence with an exponent approximately equal to 2 at low temperatures.[9,10] This law was explained by the $s_\pm$ model with parameters $\Gamma_0 = 3$ and $\Gamma_\pi = 0.04$–0.06. Figure 2 shows $\xi_h/\xi_{c2}(B/B_{c2})$ dependence with $\Gamma_0 = 3$ and $\Gamma_\pi = 0.04$ at different temperatures. All curves demonstrate growing behavior with values much less than 1 in the whole field range; i.e., they are under the AGL curve of ξ_v. This shows

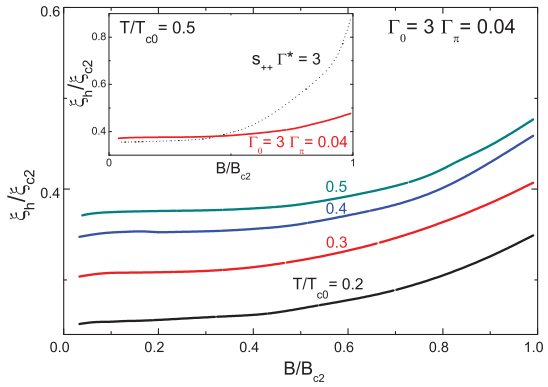

FIG. 2. (Color online) The magnetic field dependence of cutoff parameter ξ_h/ξ_{c2} with different temperatures ($T/T_{c0} = 0.2,0.3,0.4,0.5$) for $s_\pm$ pairing with $\Gamma_0 = 3$, $\Gamma_\pi = 0.04$. The inset shows the magnetic field dependence of ξ_h/ξ_{c2} for the $s_\pm$ model ($\Gamma_0 = 3$, $\Gamma_\pi = 0.04$, solid line) and the s_{++} model ($\Gamma^* = 3$, dotted line) at $T/T_{c0} = 0.5$.

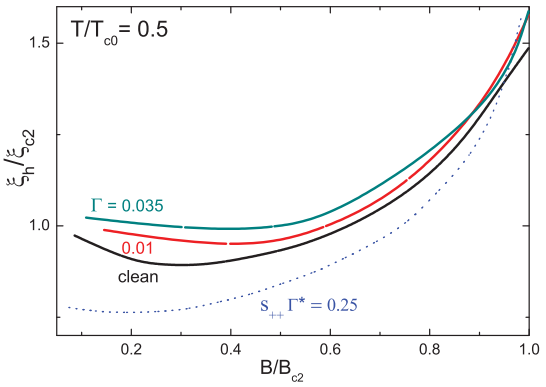

FIG. 3. (Color online) The magnetic field dependence of the cutoff parameter at $T/T_{c0} = 0.5$ with the same values of intraband Γ_0 and interband Γ_π scattering Γ ($\Gamma = 0$ for the clean case and $\Gamma = 0.01,0.035$ for the $s_\pm$ pairing). The dotted line shows result for the s_{++} model ($\Gamma^* = 0.25$).

a strong effect of interband scattering. The inset to Fig. 2 shows $\xi_h/\xi_{c2}(B/B_{c2})$ for $\Gamma_0 = 3$, $\Gamma_\pi = 0.04$ ($s_\pm$ pairing) and $\Gamma^* = 3$ (s_{++} pairing). It can be seen from the inset that ξ_h/ξ_{c2} is strongly suppressed in the $s_\pm$ pairing with comparison to the s_{++} pairing. This can be explained by the fact that in superconductors without interband pair breaking the increase in the high field is connected with field-dependent pair breaking when approaching the upper critical field. This type of behavior is cut off by the impurity pair breaking and by introducing characteristic field B^* in the field dependence by the substitution $B/B_{c2} \to [B + B^*(\Gamma_\pi)]/B_{c2}(\Gamma_\pi)$. The crossing point between the $s_\pm$ and s_{++} curves depends on Γ_π and it shifts to the lower field in comparison with the case $\Gamma_\pi = 0.02$ shown in Fig. 1(a).

We also study the case of weak intraband scattering. This case can be realized in stoichiometrical pnictides such as LiFeAs. Figure 3 presents the ξ_h/ξ_{c2} magnetic field dependence with scattering parameters $\Gamma_0 = \Gamma_\pi = \Gamma$ equal to 0, 0.01, and 0.035. The dotted line shows the results for the s_{++} model ($\Gamma^* = 0.25$). The $\xi_h(B)$ dependence shifts upward from the clean curve and has higher values in the $s_\pm$ model. In contrast, the ξ_h/ξ_{c2} curve shifts downward with impurity scattering in the s_{++} model. The high values of ξ_h observed in μSR measurements in LiFeAs (Ref. 5) support the $s_\pm$ pairing.

To conclude, the core structures of the vortices in iron pnictides have been studied using $s_\pm$ symmetry (connected with antiferromagnetic spin fluctuation mechanism) and s_{++} symmetry (mediated by moderate electron-phonon interaction due to Fe-ion oscillation and the critical orbital fluctuation). Different impurity scattering rate dependencies of the cutoff parameter ξ_h have been found for these cases. In the nonstoichiometric case, when the intraband impurity scattering (Γ_0) is much larger than the interband impurity scattering rate (Γ_π), the ξ_h/ξ_{c2} ratio is less in $s_\pm$ symmetry. When $\Gamma_0 \approx \Gamma_\pi$ (the stoichiometric case) opposite tendencies have been found, in $s_\pm$ symmetry the ξ_h/ξ_{c2} goes upward from the clean case curve ($\Gamma_0 = \Gamma_\pi = 0$) while it goes downward in the s_{++} case.

This work was supported by the Finnish Cultural Foundation.

*polina.belova@lut.fi
†miksaf@gmail.com

[1] Y. Kamihara, T. Watanabe, M. Hirano, and H. Hosono, J. Am. Chem. Soc. **130**, 3296 (2008).
[2] C. Wang, L.-J. Li, S. Chi, Z.-W. Zhu, Z. Ren, Y.-K. Li, Y.-T. Wang, X. Lin, Y.-K. Luo, S. Jiang *et al.*, Europhys. Lett. **83**, 67006 (2008).
[3] M. Rotter, M. Tegel, D. Johrendt, I. Schellenberg, W. Hermes, and R. Pottgen, Phys. Rev. B **78**, 020503(R) (2008).
[4] P. C. Canfield, S. L. Bud'ko, N. Ni, J. Q. Yan, and A. Kracher, Phys. Rev. B **80**, 060501(R) (2009).
[5] D. S. Inosov, J. S. White, D. V. Evtushinsky, I. V. Morozov, A. Cameron, U. Stockert, V. B. Zabolotnyy, T. K. Kim, A. A. Kordyuk, S. V. Borisenko *et al.*, Phys. Rev. Lett. **104**, 187001 (2010).
[6] C. Liu, G. D. Samolyuk, Y. Lee, N. Ni, T. Kondo, A. F. Santander-Syro, S. L. Bud'ko, J. L. McChesney, E. Rotenberg, T. Valla *et al.*, Phys. Rev. Lett. **101**, 177005 (2008).
[7] T. Hanaguri, S. Niitaka, K. Kuroki, and H. Takagi, Science **328**, 474 (2010).
[8] I. I. Mazin, D. J. Singh, M. D. Johannes, and M. H. Du, Phys. Rev. Lett. **101**, 057003 (2008).
[9] A. B. Vorontsov, M. G. Vavilov, and A. V. Chubukov, Phys. Rev. B **79**, 140507(R) (2009).
[10] C. Martin, R. T. Gordon, M. A. Tanatar, H. Kim, N. Ni, S. L. Bud'ko, P. C. Canfield, H. Luo, H. H. Wen, Z. Wang *et al.*, Phys. Rev. B **80**, 020501(R) (2009).
[11] H. Kontani and S. Onari, Phys. Rev. Lett. **104**, 157001 (2010).

[12]A. D. Christianson, E. A. Goremychkin, R. Osborn, S. Rosenkranz, M. D. Lumsden, C. D. Malliakas, I. S. Todorov, H. Claus, D. Y. Chung, M. G. Kanatzidis *et al*., Nature (London) **456**, 930 (2008).
[13]S. Onari, H. Kontani, and M. Sato, Phys. Rev. B **81**, 060504(R) (2010).
[14]S. Onari and H. Kontani, Phys. Rev. Lett. **103**, 177001 (2009).
[15]C. Tarantini, M. Putti, A. Gurevich, Y. Shen, R. K. Singh, J. M. Rowell, N. Newman, D. C. Larbalestier, P. Cheng, Y. Jia *et al*., Phys. Rev. Lett. **104**, 087002 (2010).
[16]R. Laiho, M. Safonchik, and K. B. Traito, Phys. Rev. B **76**, 140501(R) (2007).
[17]R. Laiho, M. Safonchik, and K. B. Traito, Phys. Rev. B **78**, 064521 (2008).
[18]J. E. Sonier, Rep. Prog. Phys. **70**, 1717 (2007).
[19]P. de Gennes, *Superconductivity of Metals and Alloys* (Addison–Wesley, New York, 1989).
[20]V. G. Kogan, A. Gurevich, J. H. Cho, D. C. Johnston, M. Xu, J. R. Thompson, and A. Martynovich, Phys. Rev. B **54**, 12386 (1996).
[21]E. H. Brandt, Phys. Rev. B **37**, 2349(R) (1988).
[22]E. H. Brandt, Physica C **195**, 1 (1992).
[23]I. G. de Oliveira and A. M. Thompson, Phys. Rev. B **57**, 7477 (1998).
[24]J. R. Clem, J. Low Temp. Phys. **18**, 427 (1975).
[25]Z. Hao, J. R. Clem, M. W. McElfresh, L. Civale, A. P. Malozemoff, and F. Holtzberg, Phys. Rev. B **43**, 2844 (1991).
[26]A. Yaouanc, P. Dalmas de Reotier, and E. H. Brandt, Phys. Rev. B **55**, 11107 (1997).
[27]W. V. Pogosov, K. I. Kugel, A. L. Rakhmanov, and E. H. Brandt, Phys. Rev. B **64**, 064517 (2001).
[28]V. G. Kogan and N. V. Zhelezina, Phys. Rev. B **71**, 134505 (2005).
[29]A. Maisuradze, R. Khasanov, A. Shengelaya, and H. Keller, J. Phys. Condens. Matter **21**, S075701 (2009).
[30]L. Kramer and W. Pesch, Z. Phys. **269**, 59 (1974).
[31]M. Ichioka, A. Hasegawa, and K. Machida, Phys. Rev. B **59**, 8902 (1999).
[32]M. Ichioka, A. Hasegawa, and K. Machida, Phys. Rev. B **59**, 184 (1999).
[33]V. G. Kogan, A. Gurevich, J. H. Cho, D. C. Johnston, M. Xu, J. R. Thompson, and A. Martynovich, Phys. Rev. B **54**, 12386 (1996).
[34]J. E. Sonier, J. Phys. Condens. Matter **16**, S4499 (2004).
[35]W. A. Huttema, J. S. Bobowski, P. J. Turner, R. Liang, W. N. Hardy, D. A. Bonn, and D. M. Broun, Phys. Rev. B **80**, 104509 (2009).
[36]V. G. Fleisher, Y. P. Stepanov, K. B. Traito, E. Lähderanta, and R. Laiho, Physica C **264**, 295 (1996).
[37]P. Miranović, M. Ichioka, and K. Machida, Phys. Rev. B **70**, 104510 (2004).
[38]Y. N. Ovchinnikov and V. Z. Kresin, Phys. Rev. B **52**, 3075 (1995).

PUBL. 3

P. Belova, I. Zakharchuk, K. B. Traito and E. Lähderanta, Effects of the order parameter symmetry on the vortex core structure in the iron pnictides, *Journal of Physics: Conference Series*, in press.

Effects of the order parameter symmetry on the vortex core structure in the iron pnictides

P. Belova[1,2], I. Zakharchuk[1,3], K. B. Traito[1], E. Lähderanta[1]

[1] Lappeenranta University of Technology, P.O.Box 20, FI-53851, Lappeenranta, Finland
[2] Petrozavodsk State University, Lenin str. 33, RU-185640, Petrozavodsk, Russia
[3] Saint-Petersburg Electrotechnical University, Popov str. 5, RU-197376, St.Petersburg, Russia

E-mail: Polina.Belova@lut.fi

Abstract. Effects of the order parameter symmetry on the cutoff parameter ξ_h (determining the magnetic field distribution) in the mixed state are investigated in framework of quasiclassical Eilenberger theory for isotropic $s^{\pm}$ and for s_{++} pairing symmetries of superconductors using computational methods. In $s^{\pm}$ pairing symmetry the gap function has opposite sign and equal absolute values of the electron and hole pockets of the Fermi surface and in s_{++} pairing symmetry the gap function has the same sign of the electron and hole pockets of the Fermi surfaces. The $s^{\pm}$ pairing symmetry results in different effects of intraband (Γ_0) and interband (Γ_π) impurity scattering on ξ_h. It is found that ξ_h/ξ_{c2} decreases with the Γ_0 leading to values much less than those predicted by the analytical Ginzburg-Landau (AGL) theory for high Γ_0. At very high Γ_0 the interband scattering suppresses ξ_h/ξ_{c2} considerably less than the one in the whole field range making it flat. If Γ_0 and Γ_π are small and equal then the $\xi_h/\xi_{c2}(B/B_{c2})$ dependence behaves like that of the AGL model and shows a minimum with value much more than that obtained for s_{++} superconductors. With high Γ_π the dependence of $\xi_h/\xi_{c2}(B/B_{c2})$ resides above the AGL curve. Such behavior is quite different from that in s_{++} pairing symmetry where intraband and interband scattering rates act in a similar way and ξ_h/ξ_{c2} decreases monotonously with impurity scattering and resides below the AGL curve.

Since the discovery of superconductivity of iron pnictides with high transition temperature next to high-T_c cuprates, the structure of the superconducting gap has been studied very intensively. The angle resolved photoemission spectroscopy (ARPES) and Andreev spectroscopy measurements show that pnictide superconductors have the gap without nodes. Electronic band configuration of the pnictides assumes two hole pockets centered at the Γ point, $q = (0, 0)$, and two electron pockets centered at the M points, $(0, \pi)$ and $(\pi, 0)$, in the unfolded Brillouin zone. The sign of the Umklapp scattering between the electron and the hole Fermi surfaces, which is responsible for the superconducting pairing, is positive and the gap function has opposite sign on the electron and hole pockets ($s^{\pm}$ symmetry) [1]. By applying a magnetic field to break the time-reversal symmetry, the relative sign of the superconducting gap can be determined from the magnetic field dependence of quasiparticle impurity scattering amplitudes. The results of scanning tunneling microscopy [2] indicate that the sign is reversed between the hole and the electron Fermi-surface pockets ($s^{\pm}$-wave), favoring the unconventional pairing mechanism associated with the spin fluctuations.

In spite of success of $s^{\pm}$ model, there are some indications that a conventional s-wave state without sign reversal (s_{++}-wave state) is also a possible candidate for iron pnictides. For example, resonancelike peak structure observed by neutron scattering measurements is

reproduced by considering the strong correlation effect via quasiparticle damping, without the necessity of sign reversal in the SC gap [3]. Additionally, the $s^{\pm}$-wave state is expected to be very fragile against impurities due to the interband scattering [4]. In the same time s_{++} gap is much more steady with impurity scattering [4] consistently with the experiments. Even if spin fluctuation mechanism dominates in clean superconductors impurities can induce transition between $s^{\pm}$ and s_{++} symmetries [5].

We solve the quasiclassical self-consistent Eilenberger equations for triangular flux line lattice (FLL) for $s^{\pm}$ and s_{++}-wave pairing symmetries. With the Riccati transformation of the Eilenberger equations, quasiclassical Green functions f and g can be parameterized via functions a and b [6]

$$\bar{f} = \frac{2a}{1+ab}, \quad f^{\dagger} = \frac{2b}{1+ab}, \quad g = \frac{1-ab}{1+ab}, \tag{1}$$

satisfying the nonlinear Riccati equations. In Born approximation for impurity scattering we have

$$\mathbf{u} \cdot \nabla a = -a[2(\omega_n + G) + i\mathbf{u} \cdot \mathbf{A}] + (\Delta + F) - a^2(\Delta^* + F^*), \tag{2}$$

$$\mathbf{u} \cdot \nabla b = b[2(\omega_n + G) + i\mathbf{u} \cdot \mathbf{A}] - (\Delta^* + F^*) + b^2(\Delta + F), \tag{3}$$

where $\omega_n = \pi T(2n+1)$, $F = 2\pi \langle f \rangle(\Gamma_0 - \Gamma_\pi)$ and $G = 2\pi \langle g \rangle(\Gamma_0 + \Gamma_\pi)$. Here, $\Gamma_0 = \pi n_i N_F |u_0|^2$ and $\Gamma_\pi = \pi n_i N_F |u_\pi|^2$ are the intra- and interband impurity scattering rates, respectively ($u_{0,\pi}$ are impurity scattering amplitudes with correspondingly small, or close to $\pi = (\pi, \pi)$, momentum transfer) and $\mathbf{u}$ is a unit vector of the Fermi velocity. The FLL creates the anisotropy of the electron spectrum. Therefore the impurity renormalization correction in Eqs. (2) and (3) averaging over Fermi surface can be reduced to averages over the polar angle θ, $\langle \ldots \rangle = (1/2\pi) \int \ldots d\theta$. Since the f function has opposite signs in two bands, Γ_π has the opposite effect on normal and anomalous self-energy. To take into account the influence of screening the vector potential $\mathbf{A}(\mathbf{r})$ in Eqs. (2) and (3) is obtained from the equation $\nabla \times \nabla \times \mathbf{A_E} = \frac{4}{\kappa^2}\mathbf{J}$, where the supercurrent $\mathbf{J}(\mathbf{r})$ is given in terms of $g(\omega_n, \theta, \mathbf{r})$ from Ref. [6]. There $\mathbf{A}$ and $\mathbf{J}$ are measured in units of $\Phi_0/2\pi\xi_0$ and $2ev_F N_0 T_c$, respectively. The spatial variation of the internal field $h_E(\mathbf{r})$ is determined through $\nabla \times \mathbf{A} = \mathbf{h_E}(\mathbf{r})$. The pairing potential $\Delta(\mathbf{r})$ is expressed through the Green function f. All over the paper the energy, the temperature, and the length are measured in units of T_{c0} and the coherence length $\xi_0 = v_F/T_{c0}$, where v_F is the Fermi velocity. The magnetic field $\mathbf{h}$ is given in units of $\Phi_0/2\pi\xi_0^2$. In equations impurities are in a units of T_{c0}, but in the plots impurities are in units of $2\pi T_{c0}$. In computations the ratio $\kappa = \lambda_{L0}/\xi_0 = 10$ is used. To obtain the quasiclassical Green function, the Riccati equations [Eqs. (2, 3)] are solved by the Fast Fourier Transform (FFT) method for triangular FLL [7]. This method is reasonable for dense FLL discussed in this paper. In high field the pinning effects are weak and not considered in our paper.

The investigation of experimental results of field distribution in mixed state of type-II superconductors is usually done [8] in the framework of the Hao-Clem theory (analytical solution of the Ginzburg-Landau theory, AGL [9]). Strictly speaking, Ginzburg-Landau theory is valid only near T_c but it is often used in whole temperature range taking the cutoff parameter ξ_v and penetration depth λ as fitting parameters. Recently an effective London model with the effective cutoff parameter $\xi_h(B)$ as a fitting parameter was obtained for clean [10] and dirty [7] superconductors, using self-consistent solution of quasiclassical nonlinear Eilenberger equations. To emphasize the differences between calculated cutoff parameter and variational parameter of the AGL we changed the notations $\xi_v \to \xi_h$. In this approach the cutoff parameter obtained from the Ginzburg-Landau model is extended over the whole field and temperature range. In this case the effects of bound states in the vortex cores are leading to Kramer-Pesch effect and

their delocalization between the vortices [11] are self-consistently included. In this model the magnetic field distribution is given [7]

$$h_{EHC}(\mathbf{r}) = \frac{\Phi_0}{S}\sum_{\mathbf{G}}\frac{F(G)e^{i\mathbf{Gr}}}{1+\lambda^2 G^2}, \tag{4}$$

where $F(\mathbf{G}) = uK_1(u)$, $K_1(u)$ is the modified Bessel function, $u = \xi_h G$, $\mathbf{G}$ is a reciprocal lattice vector and S is the area of the vortex lattice unit cell. Because the magnetic field distribution is similar to the GL model we will call this approach as Eilenberger-Ginzburg-Landau model and ξ_h as a GL cutoff parameter. Here, λ is not a fitting parameter but is calculated from the microscopical theory of the Meissner state and ξ_h is calculated from Eilenberger theory of the mixed state.

After solving the Eilenberger equations the obtained magnetic field distribution $h_E(\mathbf{r})$ is fitted with the London field distribution $h_{EHC}(\mathbf{r})$ (Eq. (4)) with $\lambda(T)$ calculated from isotropic $s^{\pm}$ model [1]. To study the obtained $\xi_h(B, T, \Gamma_0, \Gamma_\pi)$ dependences it is convenient to use the normalization to the coherence length ξ_{c2} determined from the upper critical field $B_{c2} = \Phi_0/2\pi\xi_{c2}^2$ (in our units $\xi_{c2} = 1/\sqrt{B_{c2}}$). Using the similarity to the model of spin-flip superconductors $B_{c2}(T)$ for two dimensional, $s^{\pm}$ pairing can be determined from the equations [12]. The superfluidity density in pnictides often shows the power shape dependence with

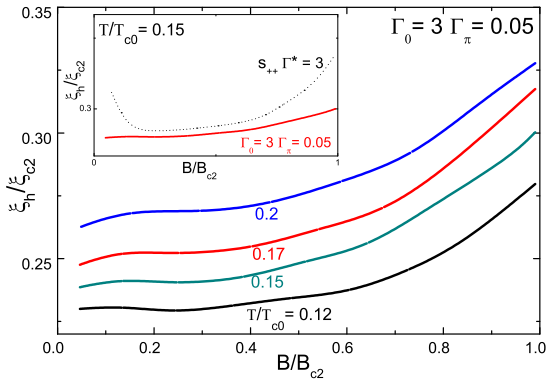

Figure 1. The magnetic field dependence of ξ_h/ξ_{c2} with different temperatures for $\Gamma_0 = 3$ and $\Gamma_\pi = 0.05$ for $s^{\pm}$ model. The inset shows the magnetic field dependence ξ_h/ξ_{c2} for $s^{\pm}$ model ($\Gamma_0 = 3, \Gamma_\pi = 0.05$) and s_{++} model ($\Gamma^* = 3$, dotted line) at $T/T_{c0} = 0.15$.

exponent approximately equal to two at low temperatures. This law was explained by $s^{\pm}$ model with the parameters $\Gamma_0 = 3$ and $\Gamma_\pi = 0.04 - 0.06$ [1]. Fig. 1 shows $\xi_h/\xi_{c2}(B/B_{c2})$ dependence with the parameters $\Gamma_0 = 3$ and $\Gamma_\pi = 0.05$ at different temperatures. All curves demonstrate growing behavior with values much less that one in whole field range. The small value of ratio ξ_h/ξ_{c2} (~ 0.27) which is comparable with our theoretical prediction, Fig. 1, was obtained in μSR investigation of Co-doped $BaFe_2As_2$ [13]. We also study the case of weak intraband scattering. This case can be realized in stoichiometrical pnictides such as $LiFeAs$. Fig. 2 presents the ξ_h/ξ_{c2} magnetic field dependence at $\Gamma_0 = \Gamma_\pi = \Gamma = 0, 0.05, 0.06, 0.065$ and $T/T_{c0} = 0.15$. Dashed line demonstrates the result of the AGL theory for ξ_v [9]

$$\xi_v = \xi_{c2}(\sqrt{2} - \frac{0.75}{\kappa_{GL}})(1+b^4)^{1/2}[1-2b(1-b)^2]^{1/2}, \tag{5}$$

where ξ_{c2} is determined from the relation $B_{c2} = \Phi_0/2\pi\xi_{c2}^2$ (in our units $\xi_{c2} = 1/\sqrt{B_{c2}}$). This dependence with ξ_{c2} as a fitting parameter is often used for the description of the μSR experimental results [8]. As can be seen from this picture the shape of curve does not change

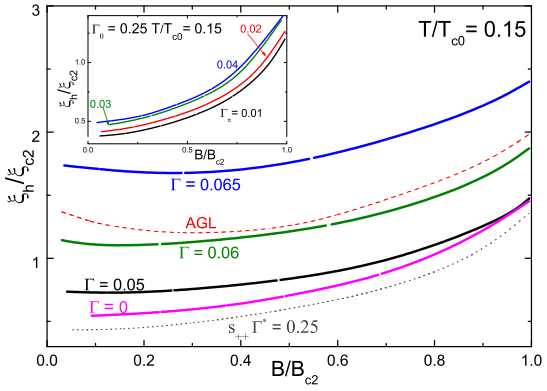

Figure 2. The magnetic field dependence of ξ_h/ξ_{c2} at $T/T_{c0} = 0.15$ with the same values of intraband Γ_0 and interband Γ_π scattering Γ ($\Gamma = 0, 0.05, 0.06, 0.065$). Dotted lines show the magnetic field dependence of ξ_h/ξ_{c2} for s_{++} model ($\Gamma^* = 0.25$). Dashed line demonstrates the result of the AGL theory for ξ_v from Eq. 5. The inset shows the magnetic field dependence of ξ_h/ξ_{c2} for $\Gamma_0 = 0.25$, $\Gamma_\pi = 0.01, 0.02, 0.03, 0.04$ at $T/T_{c0} = 0.15$.

considerably, but the absolute values of ξ_h/ξ_{c2} depend crucially on it. At low Γ values, ξ_h/ξ_{c2} resides below the AGL curve and moves above it at high Γ, opposite to the case of the strong intraband scattering considered in Fig. 2. Such behavior is quite different from that in s_{++} pairing symmetry where intraband and interband scattering rates act in similar way and ξ_h/ξ_{c2} decreases always with impurity scattering.

To conclude, Eilenberger equations have been solved for superconductors with isotropic $s^{\pm}$ and s_{++} pairing symmetries in the mixed state. These symmetries are proposed for the pairing state of the Fe-pnictides. Effects of interband and intraband impurity scattering on Hao-Clem cutoff parameter ξ_h are investigated. It is found that ξ_h/ξ_{c2} from (B/B_{c2}) dependence is nonuniversal, depending on the chosen parameter set it can reside both below and above AGL curve. Such behavior is quite different from that in s_{++} pairing symmetry where intraband and interband scattering rates act in similar way and ξ_h/ξ_{c2} decreases always with impurity scattering. It is found that intraband scattering (Γ_0) suppresses ξ_h/ξ_{c2} leading to values much less than unit at high Γ_0. The effects of interband impurity scattering (Γ_π) depend on the value of Γ_0: at small Γ_0 ξ_h/ξ_{c2} increases with Γ_π, but at high Γ_0 it decreases with Γ_π. The effects of interband impurity scattering at moderate Γ_0 depends on the field range resulting in increasing of ξ_h/ξ_{c2} at low fields, but suppressing it at high fields. The $\xi_h/\xi_{c2}(B/B_{c2})$ calculations for parameters of doped $BaFe_2As_2$ compounds [1], where $\Gamma_0 \gg \Gamma_\pi$, are done. These dependences demonstrate growing behavior defined by Γ_0 with values much less that one in whole field range, i.e. they are under the AGL curve of ξ_v.

This work was supported by Finnish Cultural Foundation.

References

[1] Vorontsov A B, Vavilov M G and Chubukov A V 2009 *Phys. Rev. B* **79** 140507(R)
[2] Hanaguri T, Niitaka S, Kuroki K and Takagi H 2010 *Science* **328** 474
[3] Onari S, Kontani H and Sato M 2010 *Phys. Rev. B* **81** 060504(R)
[4] Onari S and Kontani H 2009 *Phys. Rev. Lett.* **103** 177001
[5] Kontani H and Onari S 2010 *Phys. Rev. Lett.* **104** 157001
[6] Miranović P, Ichioka M and Machida K 2004 *Phys. Rev. B* **70** 104510
[7] Laiho R, Safonchik M and Traito K B 2008 *Phys. Rev. B* **78** 064521
[8] Sonier J E 2007 *Rep. Prog. Phys.* **70** 1717
[9] Hao Z, Clem J R, McElfresh M W, Civale L, Malozemoff A P and Holtzberg F 1991 *Phys. Rev. B* **43** 2844
[10] Laiho R, Safonchik M and Traito K B 2007 *Phys. Rev. B* **76** 140501(R)
[11] Ichioka M, Hasegawa A and Machida K 1999 *Phys. Rev. B* **59** 8902
[12] Ovchinnikov Y N and Kresin V Z 1995 *Phys. Rev. B* **52** 3075
[13] Sonier J E, Huang W, Kaiser C V, Cochrane C, Pacradouni V, Sabok-Sayr S A, Lumsden M D, Sales B C, McGuire M A, Sefat A S and Mandrus D 2011 *Phys. Rev. Lett.* **106** 127002

PUBL. 4

P. Belova, K. B. Traito and E. Lähderanta, Eilenberger and Ginzburg-Landau models of the vortex core in high κ-superconductors, *Journal of applied physics*, **110**, 033911, 2011.

Eilenberger and Ginzburg-Landau models of the vortex core in high κ-superconductors

P. Belova,[1,2,a)] K. B. Traito,[1] and E. Lähderanta[1]
[1]*Lappeenranta University of Technology, P.O. Box 20, Lappeenranta FI-53851, Finland*
[2]*Petrozavodsk State University, Lenin str. 33, Petrozavodsk RU-185640, Russia*

(Received 17 May 2011; accepted 11 June 2011; published online 9 August 2011)

Eilenberger approach to the cutoff parameter, ξ_h, of the field distribution in the mixed state of high κ-superconductors is developed. It is found that normalized value of ξ_h/ξ_{c2} decreases both with temperature (due to Kramer-Pesch effect) and with impurity scattering rate Γ. Our theory explains μSR experiments in some low-field superconductors and different ξ_h values from the Ginzburg-Landau theory predictions in isotropic s-wave superconductors. A comparison with another characteristic length ξ_1, describing the gradient of the order parameter in the vortex center, is done. They have very different Γ-dependences: monotonous suppression of $\xi_h(B)$ values and crossing behavior of the $\xi_1(B)$ curves at various Γ. This is explained by the nonlocal effects in the Eilenberger theory. © *2011 American Institute of Physics*. [doi:10.1063/1.3610502]

I. INTRODUCTION

Much attention has been focused on a vortex structure in high κ-superconductors. It is explained by many predicted remarkable phenomenon in the vortex core physics: induced superconducting order parameter of other symmetries;[1,2] induced antiferromagnetic order parameter in high-T_c superconductors;[3–5] current-carrying bound states resulting in Kramer-Pesch effect;[6–8] Majorana states in topological superconductors;[9,10] and the quasiparticle transfer between vortices, i.e, the vortex lattice effects.[1] Experimentally, several important means to probe the vortex structure are now available, such as muon spin resonance[11–13] (μSR), nuclear magnetic resonance,[5] and small-angle neutron scattering[14,15] through the field distribution, heat transport[16] or by scanning tunneling microscopy[17–19] through the local density of states in various superconductors, including high-T_c superconductors.

The analysis of the experimental data in the mixed state depends on the theoretical model of the distribution function of local fields $P(B)$ in the vortex lattice.[16,20] One of the most widely used models is an approximation of the analytical Ginzburg-Landau theory (the AGL theory).[21,22] For the dense vortex lattice ($B \gg B_{c1}$) and high-κ ($\kappa_{GL} > 10$) superconductors, the AGL theory prediction for the Fourier components of the magnetic field is

$$B_z(\mathrm{G}) = \frac{\phi_0}{S}\frac{f_\infty^2}{\lambda^2 G^2}(\xi_v G)K_1(\xi_v G), \qquad (1)$$

where $K_1(x)$ is a modified Bessel function, G is a reciprocal-lattice vector, S is the area of the vortex lattice unit cell, and ξ_v and f_∞ are variation parameters representing the effective core radius of a vortex and the depression of the order parameter due to the overlap of vortex cores, respectively. They have simple functional dependences on $b = B/B_{c2}$ and κ_{GL}:

$$\xi_v = \xi_{c2}\left(\sqrt{2} - \frac{0.75}{\kappa_{GL}}\right)(1+b^4)^{1/2}[1-2b(1-b)^2]^{1/2} \qquad (2)$$

and $f_\infty^2 = 1 - b^4$. Here, ξ_{c2} and κ_{GL} are GL coherence length and GL parameter, respectively. ξ_{c2} can be found from the value of the upper critical field $B_{c2} = \phi_0/2\pi\xi_{c2}^2$. In Eq. (1), $\phi_0/S = B = bB_{c2}$ is the mean induction. It is important to note that, in this approximation, $\xi_v(B)$ is determined only by ξ_{c2} and the ratio B/B_{c2}. It implies that ξ_v/ξ_{c2} (B/B_{c2}) is a universal function. One can consider Eq. (1) as a solution of the modified London equation (with cutoff ξ_v and effective penetration depth $\lambda_{eff} = \lambda/f_\infty$.)[21] The comparison between the variation and the exact numerical solution shows that the accuracy of the AGL theory is in the order of 10%.[21]

In the analysis of the experimental data λ and ξ_v are often considered as fitting parameters. To emphasize that ξ_v is a fitting parameter, we will use another notation in the following consideration for it, ξ_h, and leave ξ_v notation for the prediction of AGL theory. While the fitting analysis of the μSR data is performed entirely in time domain, one can reconstruct $B(r)$ by Eq. (1), using the physical parameters deduced from the fitting analysis. Using the reconstructing field distribution and Maxwell equations, the supercurrent density $J(\vec{r})$ and the core radius ξ_2 defined by $J(\vec{\xi}_2) = J_{max}$ (where J_{max} denotes the current modulus maximum of $J(\vec{r})$) can be obtained.[23] In the AGL theory, the equality $\xi_h = \xi_1$ is suggested. Here, the order characteristic length ξ_1, determined as $1/\xi_1 = (\partial|\Delta(r)|/\partial r)_{r=0}/|\Delta_{NN}|$, where $|\Delta_{NN}|$ is the maximum value of the order parameter along the nearest-neighbor direction, which is the direction of taking the derivative. The length ξ_1 is directly connected with the length ξ_3 responsible for the density of states and STM measurements description.[24] The microscopic theory valid in the whole temperature range is the quasiclassical Eilenberger theory. The characteristic lengths ξ_1 and ξ_2 were calculated.[8,24,25] The similarity $\xi_1(B) \approx \xi_2(B)$ was found for clean superconductors.[24] However, the case of dirty superconductors was not considered in the details.

a)Author to whom correspondence should be addressed. Electronic mail: polina.belova@lut.fi.

Using this method, the experimental muon spin resonance (μSR) results in V_3Si, Nb_3Sn, $NbSe_2$, YNi_2BC, and $LuNi_2B_2C$ in intermediate magnetic fields (where contribution of the weak superconducting gap is suppressed) and, at low temperatures, showed that ξ_h is much less than ξ_v of the prediction of AGL theory.[16,20] Theoretical consideration is needed for explanation of this experimental fact. Simultaneous experimental determination of λ_{eff} and ξ_h without any restrictions is very problematic, regardless of the model used to describe the vortex state.[26] It has been suggested that $P(B)$ of flux-line lattice (FLL) can be explained using only one fitting parameter.[27] The magnetic-field penetration depth $\lambda(T)$ is assumed to be field independent and have the same value as in the Meissner state, i.e., $f_\infty = 1$. In this approach, all field dependent effects are taken into account in $\xi_h(B)$ dependence. This is equivalent to the use of the effective critical field B^*_{c2} for the description of the mixed state. It will be impurity scattering (by a different way than B_{c2}) and field dependent in this case. In this model, the field dependence of the cutoff parameter was introduced phenomenologically for explanation of deviations in $M(\ln B)$ from linear behavior prescribed by the London model. It was used for explanation of deviation of field dependence flux flow resistivity from Bardeen-Stephen law.[28] Deviations from the London model description were also found in the investigation of magnetization of superconductor nanoparticles in the mixed state.[29,30]

Recently, an effective London model with the $\xi_h(B)$ as a fitting parameter has been obtained for clean[31] and dirty[32] superconductors, using self-consistent solution of quasiclassical nonlocal Eilenberger equations. Such a theory looks appropriate for the description of the vortex core, where strong nonlinear and nonlocal effects are expected. In this approach, the analysis of the coherence length ξ_{c2}, obtained from the Ginzburg-Landau model, is extended over the whole field and temperature range. The Fourier components of magnetic field in this model are described by Eq. (1) with $f_\infty = 1$ and $\lambda_{eff} = \lambda$:

$$h_{EGL}(\mathrm{r}) = \frac{\phi_0}{S}\sum_{\mathrm{G}}\frac{F(G)e^{i\mathrm{Gr}}}{1+\lambda^2 G^2}, \tag{3}$$

where $F(\mathrm{G}) = \xi_h G K_1(\xi_h G)$. It is important to note that ξ_h in Eq. (3) is obtained from solving the Eilenberger equations and does not coincide with the variational parameter ξ_v of the AGL model. We will call the field distribution (3) as an Eilenberger-Ginzburg-Landau field distribution h_{EGL} (r). In Eq. (3) $\lambda(T)$ is calculated from microscopic theory for the Meissner state and renormalized by impurity scattering.[33] In dirty superconductors, the value of λ increases considerably and it is the main effect of impurities in the field distribution (Eq. (3)), suppressing deviation of the field from the mean value B.

Thus, in this model, there are only one fitting parameter for the description of the vortex state, ξ_h, similar to Kogan *et al.* in Ref. 27, and two GL parameters $\lambda(T)$ and $B_{c2}(T)$ (three-parameter Eilenberger-Ginzburg-Landau model). Using the Hao-Clem type of the field distribution does not mean direct connection to the GL theory, and it is taken as a reasonable starting point of the investigation, similar to the empirical approach to the problem.[16,20]

It was recently demonstrated by the μSR measurements that the variance of the magnetic field, σ, at $T \to 0$ can be fitted by GL theory using two fitting parameters λ and B_{c2}.[34–36] Moreover, the value of B_{c2}, evaluated in such a way, coincides with the result of magnetization measurements. This coincidence proves that the theoretical $\sigma(B)$ dependence calculated in the framework of the GL theory can indeed be used for quantitative analysis of isothermal experimental data, even at temperatures $T \ll T_c$. It is most probable that the distribution of the magnetic induction in the sample ($P(B)$) is different from predictions of microscopic theory, while a, as a more integral characteristic of this distribution, remains practically the same.[36] The doubts were expressed in the expediency to use phenomenological field dependent λ and B_{c2} in Ref. 36. The authors asserted also that, if the conventional GL theory cannot describe the μSR results and if all other possibilities (such as polycrystalline samples of anisotropic superconductors) for this disagreement are excluded, one may conclude that this superconductor is unconventional. For example, such conclusion was done in μSR investigation of $P_rPt_4Ge_{12}$.[11]

The aim of our paper is to numerically calculate $\xi_h(B)/\xi_{c2}$ dependences (characterizing line shape of the μSR data, local field, and current distributions) at different temperatures and impurity scattering rates in the framework of the Eilenberger theory. In this way, one can check the reliability of the GL theory in the whole parameter range and claim the signatures about unconventional superconductivity: if the ratio ξ_h/ξ_{c2} can be much different from one, even in isotropic s-wave superconductors, such statements should be taken very carefully. Such consideration can also help to clarify the value of the vortex core radius ρ_v.[16,20]

II. THE MODEL

With the Riccati transformation of the Eilenberger equations, quasiclassical Green functions f and g can be parameterized via functions a and b:[25]

$$\bar{f} = \frac{2a}{1+ab}, \quad f^\dagger = \frac{2b}{1+ab}, \quad g = \frac{1-ab}{1+ab}, \tag{4}$$

satisfying the nonlinear Riccati equations. In Born approximation for the nonmagnetic impurity scattering, we have

$$\mathbf{n}\cdot\nabla a = -a[2(\omega_n + G) + i\mathbf{n}\cdot\mathbf{A}] + (\Delta + F) - a^2(\Delta^* + F^*), \tag{5}$$

$$\mathbf{n}\cdot\nabla b = b[2(\omega_n + G) + i\mathbf{n}\cdot\mathbf{A}] - (\Delta^* + F^*) + b^2(\Delta + F), \tag{6}$$

where $\omega_n = \pi T(2n+1)$, $F = 2\pi\langle f\rangle\cdot\Gamma$, and $G = 2\pi\langle g\rangle\cdot\Gamma$. Here, $\Gamma = \pi n_i N_F |u|^2$ is the impurity scattering rate (u is impurity scattering amplitude) and $\mathbf{n}$ is a unit vector of the Fermi velocity. The FLL create the anisotropy of the electron spectrum.[24] Therefore, the impurity renormalization correction in Eqs. (5) and (6) are averaged over Fermi surface and can be reduced to averages over the polar angle θ, i.e., $\langle\ldots\rangle = (1/2\pi)\int\cdots d\theta$.

To take into account the influence of screening, the vector potential $\mathbf{A}(\mathbf{r})$ in Eqs. (5) and (6) is obtained from the equation $\nabla \times \nabla \times \mathbf{A}_\mathbf{E} = \frac{4}{\kappa^2}\mathbf{J}$, where the supercurrent J(r) is given in terms of $g(\omega_n, \theta, r)$ by

$$\mathbf{J}(\mathbf{r}) = 2\pi T \sum_{\omega_n>0}^{\omega_c} \int_0^{2\pi} \frac{d\theta}{2\pi} \frac{\hat{\mathbf{k}}}{i} g(\omega_n, \theta, \mathbf{r}). \quad (7)$$

Here, $\mathbf{A}$ and $\mathbf{J}$ are measured in units of $\phi_0/2\pi\xi_0$ and $2ev_F N_0 T_c$, respectively. The self-consistent condition for the pairing potential $\Delta(\mathbf{r})$ is given by

$$\Delta(\mathbf{r}) = V^{SC} 2\pi T \sum_{\omega_n>0}^{\omega_c} \int_0^{2\pi} \frac{d\theta}{2\pi} f(\omega_n, \theta, \mathbf{r}), \quad (8)$$

where V^{SC} is the superconducting coupling constant and ω_c is the ultraviolet cutoff frequency determining T_{c0}.[32] All over our paper, the energy, the temperature, and the length are measured in units of T_{c0} and the characteristic length $\xi_0 = v_F/T_{c0} = \xi_{BCS}\pi\Delta_0/T_{c0}$. Here, $\xi_{BCS} = v_F/\pi\Delta_0$, where v_F is the Fermi velocity and Δ_0 is the temperature dependent uniform gap. The magnetic field h is given in units of $\phi_0/2\pi\xi_0^2$. The impurity scattering rates are in units of $2\pi T_{c0}$. In computations, the ratio $\kappa = \lambda_{L0}/\xi_0 = 10$ is used. It corresponds to $\kappa_{GL} = 43.3$.[25] The Riccati equations [Eqs. (5) and (6)] are solved by the fast Fourier transform (FFT) method.[32] This method is reasonable for dense FLL discussed in this paper. After solving the Eilenberger equations, the obtained magnetic field distribution h_E(r) is fitted with the London field distribution h_{EGL}(r) (Eq. (3)). In high field, the pinning effects are weak and not considered in our paper. To study the obtained $\xi_h(B,T,\Gamma)$ dependences, it is convenient to use the normalization to the coherence length ξ_{c2}, determined from the upper critical field $B_{c2} = \phi_0/2\pi\xi_{c2}^2$ (in our units $\xi_{c2} = 1/\sqrt{B_{c2}}$). Figure 1(a) shows $B_{c2}(T)$ dependences, and $\xi_{c2}(T)$ dependences are shown in Fig. 1(b) with $\Gamma = 0$, 1, 2, 3, 4, 5, and 6, calculated from the model of two dimensional s-wave superconductors[37]

$$\ln\left(\frac{T_{c0}}{T}\right) = 2\pi T \sum_{n\geq 0} [\omega_n^{-1} - 2D_1(\omega_n, B_{c2})], \quad (9)$$

where

$$D_1(\omega_n, B_{c2}) = J(\omega_n, B_{c2})[1 - 2\Gamma J(\omega_n, B_{c2})]^{-1}, \quad (10)$$

$$J(\omega_n, B_{c2}) = \left(\frac{4}{\pi B_{c2}}\right)^{1/2} \int_0^\infty dy \exp(-y) \arctan\left[\frac{(B_{c2}y)^{1/2}}{\alpha}\right], \quad (11)$$

where $\alpha = 2(\omega_n + \Gamma)$.

III. RESULTS AND DISCUSSIONS

A. Comparison with the AGL theory

Figure 2 shows the calculated ξ_h/ξ_{c2} values at different temperatures. Strong decreasing of ξ_h/ξ_{c2} with decreasing of temperature is clearly visible in Fig. 2. It can be explained by Kramer-Pesch effect.[6–8] Similar effect was observed in

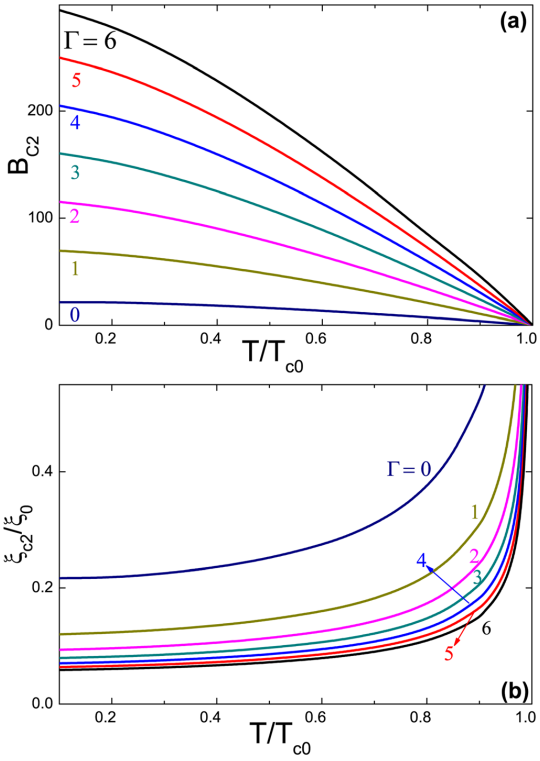

FIG. 1. (Color online) (a) The temperature dependence of the upper critical field B_{c2} with different values of scattering rates Γ. (b) The temperature dependence of ξ_{c2}/ξ_0 with different values of scattering rates Γ.

μSR investigation of the $NbSe_2$ single crystal.[16] Because Kramer-Pesch effect says ξ_h/ξ_{BCS} decreases with temperature, the results with another normalization constant ξ_{BCS} are presented in the insets to this figure. Since ξ_h/ξ_{BCS} is temperature dependent, it results in a minor difference between the values of ξ_h/ξ_{c2} and ξ_h/ξ_{BCS} taken with the different temperatures. Our calculations show that, in clean superconductors $\xi_h(B)$ dependence has minimum, which disappears at low temperatures. Surprisingly, a qualitative similarity is observed with the AGL model (dashed line in Fig. 2), which is supposed to be noncorrect.[38] The absolute values of ξ_h are considerably less than those of the AGL theory predictions because the Kramer-Pesch effect is not included in the phenomenological GL theory. With increasing temperature, magnetic field dependence of ξ_h moves to higher values, toward the AGL theory predictions (Fig. 2(a)). It looks like the restoration of Ginzburg-Landau behavior at high temperatures. In the presence of impurity scattering, the same tendency is also visible (Fig. 2(b)), but shifting of ξ_h to the direction of the AGL curve is slower. It should be noted that the normalization constant ξ_{c2} used in Fig. 2 is strongly dependent on Γ. Some other explanation is needed.

In Fig. 3(a) at $T/T_{c0} = 0.5$, the change of the shape of the $\xi_h(B)$ curve in low fields with increasing of scattering rate Γ

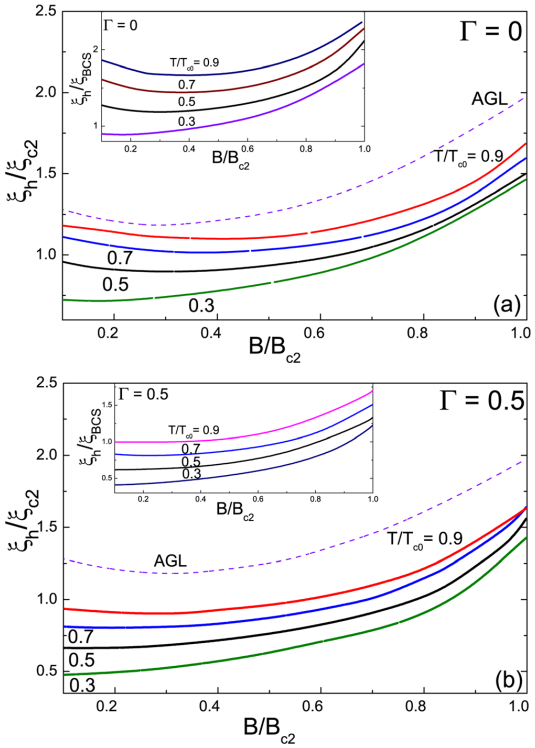

FIG. 2. (Color online) (a) The magnetic field dependence of the calculated ξ_h/ξ_{c2} values at different temperatures with impurity scattering rate $\Gamma = 0$. The inset shows the magnetic field dependence of the calculated ξ_h/ξ_{BCS} values at different temperatures with impurity scattering rate $\Gamma = 0$. (b) The magnetic field dependence of the calculated ξ_h/ξ_{c2} values at different temperatures with impurity scattering rate $\Gamma = 0.5$. The inset shows the magnetic field dependence of the calculated ξ_h/ξ_{BCS} values at different temperatures with impurity scattering rate $\Gamma = 0.5$. Dashed lines demonstrate the result of the AGL theory for ξ_v taken from Ref. 22.

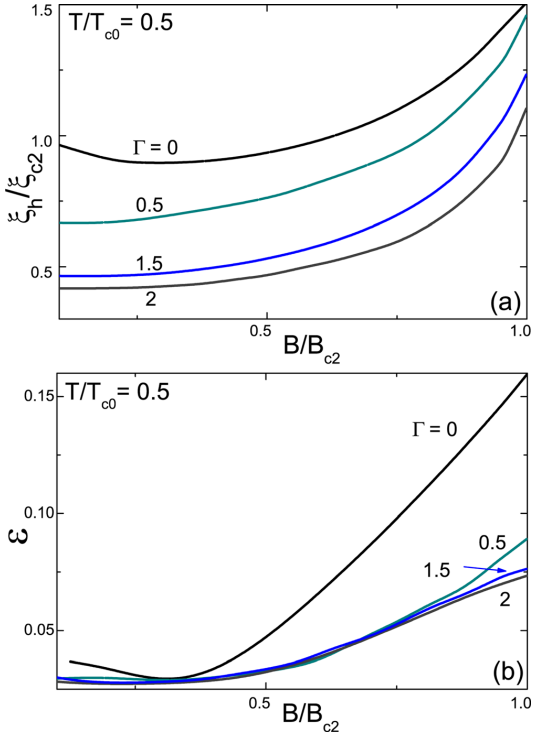

FIG. 3. (Color online) (a) The magnetic field dependence of ξ_h/ξ_{c2} at $T/T_{c0} = 0.5$ with different impurity scattering rate Γ. (b) Magnetic field dependence of mean square deviation, ϵ, of the London distribution from the Eilenberger distribution, normalized by the variance of the Eilenberger distribution for $T/T_{c0} = 0.5$ with different impurity scattering rate Γ.

is shown. Strong suppression of the ξ_h/ξ_{c2} values to values much less than one is visible at increasing Γ. The obtained small ξ_h/ξ_{c2} values are consistent with the experimental observation in some high-κ, low-T_c superconductors.[16,20] Such strong suppression of ξ_h/ξ_{c2} values in dirty superconductors is similar to that obtained in Ref. 39. But authors of this paper used semianalytical methods, while we obtained numerical solution of the full self-consistent Eilenberger theory. We also calculate magnetic field dependence of mean square deviation of h_{EGL} distribution of the magnetic field from the Eilenberger distribution, $\varepsilon = \left(\overline{(h_E - h_{EGL})^2}/\overline{(h_E - B)^2}\right)^{1/2}$, where normalization is done by the variance of the Eilenberger distribution and $\overline{\cdots}$ is average over vortex unit cell. Figure 3(b) shows $\varepsilon(B)$ dependence at different impurity scattering Γ. It can be seen that accuracy of the EGL model is getting better, with increasing impurity scattering and saturates at the $\Gamma \approx 2$.

With high Γ, it is well known that $\xi_{c2} \sim \sqrt{1/\Gamma} \sim \sqrt{l}$, where l is the mean-free path. The decreasing of the ξ_h/ξ_{c2} ratio implies stronger dependence of ξ_h on l. It is found that, in dirty superconductors, ξ_h can be scaled with relaxation time τ, $\xi_h(B,T,\tau) = \xi_{pure}(B,T)/(1 + \tau_0(B,T)/\tau)$, where $\xi_{\text{pure}}(B,T)$ is the cutoff parameter in clean superconductors[31] and τ_0 is a characteristic relaxation time. It results in $\xi_h \xi\, 1$ dependence at high Γ similar to the behavior of nonlocality radius,[40] ρ, resulting in decreasing of ξ_h/ξ_{c2} at high Γ, observed in Fig. 3(a). Thus, Figs. 2 and 3 demonstrate the strong differences between the nonlocal Eilenberger and the local GL theories. With nonlocality effects, the field distribution should contain the new characteristic field $B_0 \sim \phi_0/\rho^2$ instead of $B_{c2} \sim \phi_0/\xi_{c2}^2$.[40] Because of $\rho(\Gamma,T) \neq \xi_{c2}(\Gamma,T)$, the limit $\xi_h(B \to B_{c2})$ is different from ξ_{c2}, which is visible at Figs. 2 and 3. We also note the difference between AGL theory and our calculation in the limit of $B \to B_{c2}$. In our methods, there is only one fitting parameter ξ_h, while in the AGL theory, there are two of them, ξ_v and $f_\infty (f_\infty \equiv 1$, in our case). Because of the boundary condition of the field distribution ($h(r) \to B$ at $B \to B_{c2}$), ξ_h is the growing function of B at the high fields, resulting in the appearance of the minimum in the field dependence and the inequality of the ξ_h and ξ_{c2} at $B \to B_{c2}$. In the AGL theory, the boundary condition is satisfied by the limit $f_\infty \to 0$ at $B \to B_{c2}$, so the behavior of $\xi_v(B)$ dependence is not predetermined.[38]

B. Characteristics' lengths of the vortex core in the mixed state

For the convenience of the reader, we summarized the definitions of all characteristics' lengths of the vortex core used in our paper. Characteristics' lengths of the vortex core in the mixed state: • ξ_v, the AGL cutoff parameter (Eq. (2)) • ξh, the Eilenberger cutoff parameter, (Eq. (3)) • ξ_0, the characteristic scale in the calculation, v_F/T_c • ξ_1, the order parameter coherence length, $1/\xi_1 = (\partial|\Delta(r)|/\partial r)_{r=0}/|\Delta_{NN}|$ • ξ_2, the core radius, where the superconductor current around the vortex has its maximum • ξ_3, the STM vortex core radius, $\xi_3 = 0.35[(N(0)/N_0)/(H/H_{c2})]^{1/2}$ (see Ref. 24) • ξ_{BCS}, the BCS coherence length, $\xi_{BCS} = v_F/\pi\Delta_0$• ξ_{c2}, the GL coherence length, $\xi_{c2} = \sqrt{\phi_0/2\pi B_{c2}}$• ξ_{KZ}, the coherence length of the linearized Eilenberger equation (see Ref. 39).

Fast decreasing of ξ_h can be compared with the behavior of another characteristic length ξ_1, which is determined as $1/\xi_1 = (\partial|\Delta(r)|/\partial r)_{r=0}/|\Delta_{NN}|$, where $|\Delta_{NN}|$ is the maximum value of the order parameter along the nearest-neighbor direction, which is the direction of taking the derivative.[25] This length is important for the description of the scanning tunneling microscopy experiments.[24] At low temperatures, impurity scattering suppresses Kramer-Pesch effect in $\xi_1(T)$ dependence, resulting in nonmonotonous behavior of $\xi_1(\Gamma)$. This is shown in Fig. 4, where normalization constant ξ_{BCS} is used (ξ_{BCS} is not depending on Γ). It is clearly visible that magnetic field dependence of ξ_h decreases monotonously with Γ (Fig. 4(a)) in contrast to crossing behavior of $\xi_1(B)$ dependences for different Γ reported in Ref. 25 (Fig. 4(b)). Different impurity induced behavior of ξ_h and ξ_1 is also visible when using Γ-dependent normalization constant ξ_{c2} (Fig. 5). The $\xi_h/\xi_{c2}(B/B_{c2})$ curve shifts downward with Γ, while $\xi_1/\xi_{c2}(B/B_{c2})$ curve moves in the opposite direction. In the same time, lowering of the temperature reduces both ξ_h/ξ_{c2} and ξ_1/ξ_{c2} values. The dependences of ξ_h/ξ_{c2} from $1/\Gamma$ at different temperatures are shown in Fig. 6 in detail. A strong suppression of the ξ_h/ξ_{c2} with temperatures and scattering time is clearly visible in this figure.

The similar tendencies in the temperature and impurity scattering dependences are found for current characteristic length ξ_2: its value decreases monotonously with reducing T and $1/\Gamma$. It can be seen from Fig. 7, where $\xi_h/\xi_2(B/B_{c2})$ are shown for different T and Γ. It is important to note that, in the absence of impurity scattering, the value of ξ_2 is scaled with that of ξ_1 and they have the same field dependences: decreasing and increasing functions of B at $T/T_{c0} = 0.5$ and $T/T_{c0} = 0.2$, respectively. Impurity scattering breaks the scaling between $\xi_2(B)$ and $\xi_1(B)$. It means that different methods of vortex core investigation, such as μSR experiments (connected with ξ_h and ξ_2) and STM studies (connected with ξ_3 and ξ_1), can give different results for characteristic length of the vortex core. The different vortex core sizes have been found in μSR and STM investigations of $NbSe_2$ single crystals.[41,42] But because these crystals are two-band superconductors, they cannot be described quantitatively by our one-band model. We also note the strong different values of ξ_2/ξ_{c2} for high and low temperatures (compare curve for $T/T_{c0} = 0.9$ and $T/T_{c0} = 0.2$). This means that using the Ginzburg-Landau value for the cutoff parameter ξ_v (approximately

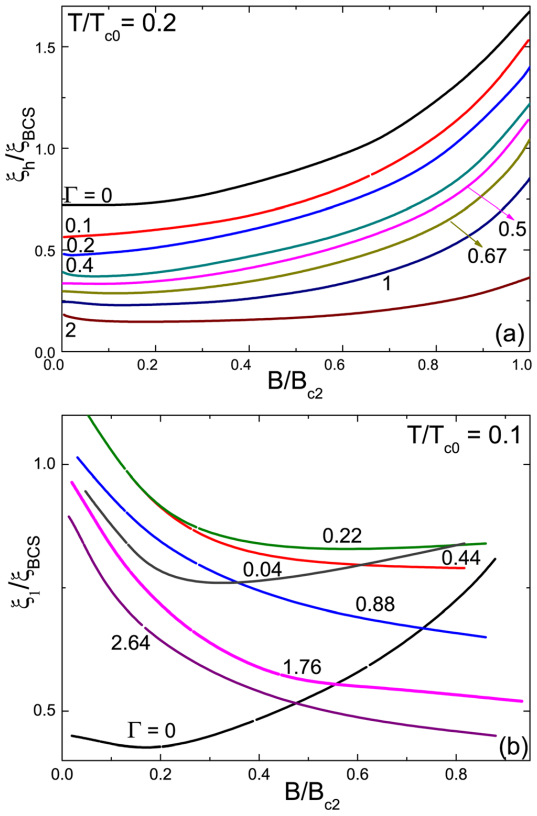

FIG. 4. (Color online) (a) The magnetic field dependence of ξ_h/ξ_{BCS} at $T/T_{c0} = 0.2$ with different impurity scattering rate Γ ($\Gamma = 0$, 0.1, 0.2, 0.4, 0.5, 0.67, 1, and 2). (b) The magnetic field dependence of ξ_1/ξ_{BCS} at $T/T_{c0} = 0.1$ with different impurity scattering rate Γ taken from Ref. 25.

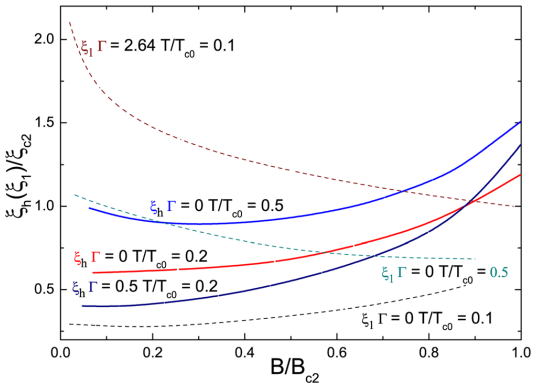

FIG. 5. (Color online) Comparison of field dependences of ξ_h/ξ_{c2} (at $T/T_{c0} = 0.2$, $\Gamma = 0$; 0.5 and $T/T_{c0} = 0.5$, $\Gamma = 0$, solid lines) and ξ_1/ξ_{c2} (at $T/T_{c0} = 0.1$, $\Gamma = 0$ and $T/T_{c0} = 0.1$, $\Gamma = 2.64$ from Ref. 25 and $T/T_{c0} = 0.5$, $\Gamma = 0$ from Ref. 24, dotted lines).

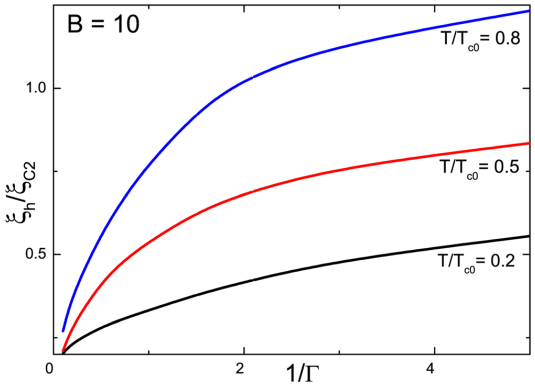

FIG. 6. (Color online) The impurity scattering rate $1/\Gamma$ dependence of ξ_h/ξ_{c2} at different temperatures T/T_{c0} ($T/T_{c0} = 0.2$, 0.5, and 0.8) with $B = 10$.

valid at high temperatures), instead of the microscopic value of ξ_h, can give a nonadequate description of the FLL local properties, in contrast to average over FLL units characteristics, such as the variance of the magnetic field.[34–36]

Thus, for the descriptions of the vortex core, two degrees of freedom are needed, ξ_h (connected with the field distribution) and ξ_1 (connected with the order parameter). This is characteristic of the nonlocal problems of the vortex matter. For example, to describe the ac response of the vortex lattice, two modes are needed: one is connected to the displacements of the vortex cores and another determines the perturbation of the magnetic field, resulting in two-mode electrodynamics.[43–45] In ac response, the nonlocality appears from the wave-dependent elastic moduli,[46] while in the considered case, it is connected with the finite size of the Cooper pair.[33]

We believe that ξ_h behavior is connected with the nature of the current-carrying quantum states of the quasi-particles in the vortex core (formed due to particle-holed coherence and Andreev reflection[6]). The current distribution can be decomposed in terms of bound states and extended states

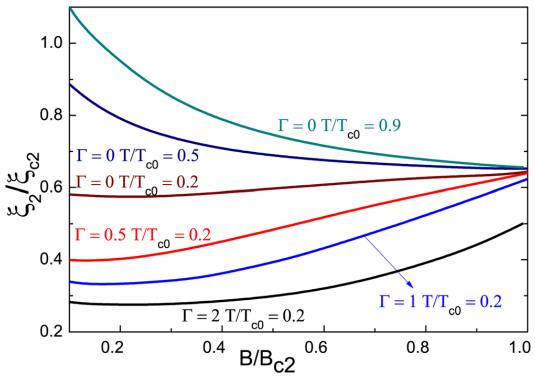

FIG. 7. (Color online) The magnetic field dependence of ξ_2/ξ_{c2} at different temperatures and with different impurity scattering rates Γ ($\Gamma = 0$, $T/T_{c0} = 0.2$, 0.5, and 0.9 and $T/T_{c0} = 0.2$, $\Gamma = 0.5$, 1, and 2).

contributions.[47] Close to the vortex core, the current density arises mainly from the occupation of the bound states. The effect of extended states becomes important only at distances larger than the coherence length. The bound states and the extended states contributions to the current density have opposite signs. The current density originating from the bound states is paramagnetic, whereas extended states contribute a diamagnetic term. At distance larger than the penetration depth, the paramagnetic and diamagnetic parts essentially cancel, resulting in exponential decay of the total current density. The similar paramagnetic current of Andreev bound states has been found at the surface of *d*-wave superconductors.[48] At low temperatures, the current rises to its maximum over a distance of the order of ξ_2, which is consistent with the sharp rise of the pair potential in the same region. In this region, the current is mainly carried by the lowest bound state. As discussed in Ref. 49, for the proper description of the bound states, quantum mechanical nonlocal approach is needed, and the strong difference between the nonlocal Eilenberger and the local Doppler-shift method has been found. It is well known that nonlocal effects and current-carrying states are suppressed strongly by impurity scattering.[6,40] It results in decreasing of the ξ_2/ξ_{c2} value and restoration of the local behavior for ξ_1/ξ_{c2} (Fig. 5, upper curve).

IV. CONCLUSIONS

The field distribution of the mixed state in dirty *s*-wave superconductors in wide temperature and field range is investigated in the framework of the Eilenberger theory. The normalized dependences of the cutoff parameter $\xi_h/\xi_{c2}(B/B_{c2})$ responsible for the line shape of the μSR resonance are calculated. It is found that this dependence is nonuniversal and depends on temperature and on impurity scattering rate, Γ. This is different from the universal dependence expected from the GL theory. At high values of $\Gamma/2\pi T_{c0} \geq 0.5$, the dependence shows a plateau in intermediate field range, and the values $\xi_h(B)/\xi_{c2}$ are less than one. The strong suppression ξ_h/ξ_{c2} with Γ can qualitatively explain the μSR experimental results in some low-temperature superconductors, V_3Si, $NbSe_2$, and $LuNi_2B_2C$, in high field range (see Fig. 7 in Ref. 16). For the quantitative comparison of the theory and experimental results, the anisotropy of the Fermi surface should be taking into account. The coherence length ξ_{KZ} of the linearized Eilenberger equation was calculated for three-dimensional (3D) isotropic case of the Fermi sphere and two-dimensional (2D) isotropic materials, i.e., the Fermi cylinder.[39] A close-form equation for $\xi_{KZ}(B)$ was found for both Fermi surfaces. It was shown that the results can be represented in the reduced form as $\xi_{KZ}(B)/\xi_{c2}(B_{c2}) = U(B/B_{c2})$, with U being a universal function. The only difference between 2D and 3D situations is the numerical coefficient (α) in this universal function. We believe that the similar consideration about minor importance of the Fermi surface anisotropy can be applied for our cutoff parameter ξ_h if it is presented in the reduced form $\xi_h/\xi_{c2}(B/B_{c2})$. Our microscopic model justified the empirical methods for the interpretation of the μSR[16,20] and magnetization[27]

investigations and shows that at least one parameter, different from GL theory, is needed for the explanation of the result, even in the isotropic *s*-wave superconductors. It results in a three-parameter $(\lambda(\Gamma,T), B_{c2}(\Gamma,T),$ and $\xi_h/\xi_{c2}(\Gamma,B,T))$ model of the mixed state of *s*-wave superconductors. Absolute values of ξ_h and ξ_1 show different dependence on impurities: $\xi_h(B)$ curves decrease monotonously with impurity scattering rate, while $\xi_1(B)$ curves cross each other in this case.

ACKNOWLEDGMENTS

This work was supported by the Finnish Cultural Foundation.

[1]M. Ichioka, A. Hasegawa, and K. Machida, Phys. Rev. B **59**, 8902 (1999).
[2]Y. Tanuma, N. Hayashi, Y. Tanaka, and A. A. Golubov, Phys. Rev. Lett. **102**, 117003 (2009).
[3]E. Demler, W. Hanke, and S.-C. Zhang, Rev. Mod. Phys. **76**, 909 (2004).
[4]Y. Gao, H.-X. Huang, C. Chen, C. S. Ting, and W.-P. Su, Phys. Rev. Lett. **106**, 027004 (2011).
[5]A. M. Mounce, S. Oh, S. Mukhopadhyay, W. P. Halperin, A. P. Reyes, P. L. Kuhns, K. Fujita, M. Ishikado, and S. Uchida, Phys. Rev. Lett. **106**, 057003 (2011).
[6]A. Gumann, S. Graser, T. Dahm, and N. Schopohl, Phys. Rev. B **73**, 104506 (2006).
[7]N. Hayashi, Y. Kato, and M. Sigrist, J. Low Temp. Phys. **139**, 79 (2005).
[8]N. Nakai, P. Miranovic, M. Ichioka, and K. Machida, Phys. Rev. B **73**, 172501 (2006).
[9]R. Roy, Phys. Rev. Lett. **105**, 186401 (2010).
[10]T. Neupert, S. Onoda, and A. Furusaki, Phys. Rev. Lett. **105**, 206404 (2010).
[11]A. Maisuradze, M. Nicklas, R. Gumeniuk, C. Baines, W. Schnelle, H. Rosner, A. Leithe-Jasper, Y. Grin, and R. Khasanov, Phys. Rev. Lett. **103**, 147002 (2009).
[12]R. Khasanov, M. Bendele, A. Amato, K. Conder, H. Keller, H.- H. Klauss, H. Luetkens, and E. Pomjakushina, Phys. Rev. Lett. **104**, 087004 (2010).
[13]T. J. Williams, A. A. Aczel, E. Baggio-Saitovitch, S. L. Bud'ko, P. C. Canfield, J. P. Carlo, T. Goko, J. Munevar, N. Ni, Y. J. Uemura, W. Yu, and G. M. Luke, Phys. Rev. B **80**, 094501 (2009).
[14]D. S. Inosov, J. S. White, D. V. Evtushinsky, I. V. Morozov, A. Cameron, U. Stockert, V. B. Zabolotnyy, T. K. Kim, A. A. Kordyuk, S. V. Borisenko, E. M. Forgan, R. Klingeler, J. T. Park, S. Wurmehl, A. N. Vasiliev, G. Behr, C. D. Dewhurst, and V. Hinkov, Phys. Rev. Lett. **104**, 187001 (2010).
[15]L. DeBeer-Schmitt, C. D. Dewhurst, B. W. Hoogenboom, C. Petrovic, and M. R. Eskildsen, Phys. Rev. Lett. **97**, 127001 (2006).
[16]J. E. Sonier, Rep. Prog. Phys. **70**, 1717 (2007).
[17]Y. Yin, M. Zech, T. L. Williams, X. F. Wang, G. Wu, X. H. Chen, and J. E. Hoffman, Phys. Rev. Lett. **102**, 097002 (2009).
[18]T. Hanaguri, S. Niitaka, K. Kuroki, and H. Takagi, Science **328**, 474 (2010).
[19]O. Fischer, M. Kugler, I. Maggio-Aprile, C. Berthod, and C. Renner, Rev. Mod. Phys. **79**, 353 (2007).
[20]J. E. Sonier, J. Phys.: Condens. Matter **16**, S4499 (2004).
[21]A. Yaouanc, P. D. de Reotier, and E. H. Brandt, Phys. Rev. B **55**, 11107 (1997).
[22]Z. Hao, J. R. Clem, M. W. McElfresh, L. Civale, A. P. Malozemoff, and F. Holtzberg, Phys. Rev. B **43**, 2844 (1991).
[23]R. Kadono, W. Higemoto, A. Koda, M. I. Larkin, G. M. Luke, A. T. Savici, Y. J. Uemura, K. M. Kojima, T. Okamoto, T. Kakeshita, S. Uchida, T. Ito, M. Takigawa, M. Ichioka, and K. Machida, Phys. Rev. B **69**, 104523 (2004).
[24]M. Ichioka, A. Hasegawa, and K. Machida, Phys. Rev. B **59**, 184 (1999).
[25]P. Miranović, M. Ichioka, and K. Machida, Phys. Rev. B **70**, 104510 (2004).
[26]A. Maisuradze, R. Khasanov, A. Shengelaya, and H. Keller, J. Phys.: Condens. Matter **21**, S075701 (2009).
[27]V. G. Kogan, R. Prozorov, S. L. Bud'ko, P. C. Canfield, J. R. Thompson, J. Karpinski, N. D. Zhigadlo, and P. Miranovic, Phys. Rev. B **74**, 184521 (2006).
[28]A. A. Gapud, S. Moraes, R. P. Khadka, P. Favreau, C. Henderson, P. C. Canfield, V. G. Kogan, A. P. Reyes, L. L. Lumata, D. K. Christen and J. R. Thompson, Phys. Rev. B. **80**, 134524 (2009).
[29]E. V. Blinov, V. G. Fleisher, R. Laiho, E. Lahderanta, Y. P. Stepanov, and K. B. Traito, Physica C **281**, 17 (1997).
[30]E. V. Blinov, R. Laiho, A. G. Lyublinski, E. Lahderanta, and K. B. Traito, Physica C **316**, 45 (1999).
[31]R. Laiho, M. Safonchik, and K. B. Traito, Phys. Rev. B **76**, 140501(R) (2007).
[32]R. Laiho, M. Safonchik, and K. B. Traito, Phys. Rev. B **78**, 064521 (2008).
[33]T. Lemberger, D. Ginsberg, and G. Rickayzen, Phys. Rev. B **18**, 6057 (1978).
[34]R. Khasanov, I. Landau, C. Baines, F. L. Mattina, A. Maisuradze, K. Togano, and H. Keller, Phys. Rev. B **73**, 214528 (2006).
[35]R. Khasanov, P. W. Klamut, A. Shengelaya, Z. Bukowski, I. M. Savic, C. Baines, and H. Keller, Phys. Rev. B **78**, 014502 (2008).
[36]I. Landau and H. Kelle, Physica C **466**, 131 (2007).
[37]Y. N. Ovchinnikov and V. Z. Kresin, Phys. Rev. B **52**, 3075 (1995).
[38]W. V. Pogosov, K. I. Kugel, A. L. Rakhmanov, and E. H. Brandt, Phys. Rev. B **64**, 064517 (2001).
[39]V. G. Kogan and N. V. Zhelezina, Phys. Rev. B **71**, 134505 (2005).
[40]V. G. Kogan, A. Gurevich, J. H. Cho, D. C. Johnston, M. Xu, J. R. Thompson, and A. Martynovich, Phys. Rev. B **54**, 12386 (1996).
[41]A. A. Golubov and U. Hartmann, Phys. Rev. Lett. **72**, 3602 (1994).
[42]J. E. Sonier, R. F. Kiefl, J. H. Brewer, J. Chakhalian, S. R. Dunsiger, W. A. MacFarlane, R. I. Miller, A. Wong, G. M. Luke, and J. W. Brill, Phys. Rev. Lett. **79**, 1742 (1997).
[43]B. Placais, P. Mathieu, Y. Simon, E. Sonin, and K. Traito, Phys. Rev. B **54**, 13083 (1996).
[44]E. B. Sonin, A. K. Tagantsev, and K. B. Traito, Phys. Rev. B **46**, 5830 (1992).
[45]N. Lutke-Entrup, B. Placais, P. Mathieu, and Y. Simon, Phys. Rev. Lett. **79**, 2538 (1997).
[46]E. Brandt, J. Low Temp. Phys. **26**, 709 (1977).
[47]F. Gygi and M. Schluter, Phys. Rev. B **43**, 7609 (1991).
[48]M. Fogelstom, D. Rainer, and J. A. Sauls, Phys. Rev. Lett. **79**, 281 (1997).
[49]T. Dahm, S. Graser, C. Iniotakis, and N. Schopohl, Phys. Rev. B **66**, 144515 (2002).

PUBL. 5

P. Belova, I. Zakharchuk,, M. Safonchik, K. B. Traito and E. Lähderanta, Generalized London theory of the mixed state of high-κ superconductors as a projection of the quasiclassical Eilenberger approach, *Physica C: Superconductivity and its Applications*, **476**, 1, 2012.

Physica C 476 (2012) 1–9

Contents lists available at SciVerse ScienceDirect

Physica C

journal homepage: www.elsevier.com/locate/physc

Generalized London theory of the mixed state of high-κ superconductors as a projection of the quasiclassical Eilenberger approach

P. Belova [a,b,*], I. Zakharchuk [a,c], M. Safonchik [a,d], K.B. Traito [a], E. Lähderanta [a]

[a] Lappeenranta University of Technology, P.O. Box 20, FI-53851 Lappeenranta, Finland
[b] Petrozavodsk State University, Lenin Str. 33, RU-185640 Petrozavodsk, Russia
[c] Saint-Petersburg Electrotechnical University, Popov Str. 5, RU-197376 St. Petersburg, Russia
[d] A.F. Ioffe Physico-Technical Institute, St. Petersburg 194021, Russia

ARTICLE INFO

Article history:
Received 12 January 2012
Accepted 31 January 2012
Available online 10 February 2012

Keywords:
Quasiclassic
Mixed state
Eilenberger
Kramer–Pesch

ABSTRACT

The generalized London equation in the mixed state of high-κ *s*-wave pairing superconductors with impurities is considered as a projection of the quasiclassical nonlocal nonlinear Eilenberger theory. Only one fitting parameter – the cutoff parameter ξ_h – is used in the theory. The distribution of the magnetic field is calculated self-consistently. Both nonlocal effects originated from extended states between the vortices and bound Andreev states in the vortex are taken into account. Comparison with different analytical nonlocal linear approaches (the Kogan–Gurevich, Amin–Franz–Affleck, Kogan–Zhelezina models) including only extended states is done. The importance of the Kramer–Pesch nonlinear effect and the field dependence of the cutoff parameter is emphasized and their strong influence on the variance of the magnetic field is found. The influence of the impurities on the ratio of the cutoff parameter ξ_h and the Ginzburg–Landau coherence length ξ_{c2} is considered. Quasiparticle scattering by impurities and lowering of the temperature reduces the value of ξ_h to the values much less than ξ_{c2}. This is different from the prediction of the local Ginzburg–Landau theory where ξ_h is scaled by ξ_{c2}. It is found that impurities influence by different way on the cutoff parameter ξ_h and the order parameter coherence length ξ_1. The ξ_h decreases monotonously with the impurity scattering time in contrast to the nonmonotonous behavior of ξ_1. The results can be used for analysis of the μSR experimental data.

1. Introduction

Recently, the field dependence and other properties of the vortex structure in the conventional *s*-wave superconductors and in high-T_c superconductors have attracted much attention. Several important means to probe the vortex structure are available experimentally in various superconductors. Specific heat experiments [1] give information of low-energy excitations. Muon spin resonance (μSR) [2,3] and small-angle neutron scattering [4] measurements investigate the internal field distribution of the vortex structure. Scanning tunneling microscopy (STM) [5] directly observes the local density of states. The vortex core size is determined from the μSR measurements by fitting it into a theoretical function for $B(r)$ that includes a cutoff function $F(\mathbf{G}, \xi_h)$, where $\mathbf{G}$ refers to the reciprocal lattice vectors. The parameter ξ_h is the cutoff $\mathbf{G}_{\max}$ of the sum over the reciprocal lattice. This removes the divergence of the sum over the $\mathbf{G}$ in the expression for the field distribution in the London approach. The cutoff cannot be improved within the London theory; to this end, one should use a theory which is able to handle the core structure properly [6]. The functional form of $F(\mathbf{G}, \xi_h)$ depends on the spatial dependence of the superconducting order parameter $\Delta(r)$ in the core region. The cutoff parameter ξ_h is directly connected with the microscopical length ξ_2 defined as the distance where the screening current around the vortex has its maximum [7]. Cutoff function $F(\mathbf{G}, \xi_h)$ was obtained in the variational approach of the Ginzburg–Landau (GL) equations [8] (the Hao–Clem theory (HC), the analytical GL theory (AGL)) and the field dependence of ξ_h was calculated (ξ_v in a notation of the AGL theory). In this model, ξ_h/ξ_{c2} is a universal function of B/B_{c2}. Here, ξ_{c2} is the GL coherence length determined from the relation $B_{c2} = \Phi_0/2\pi\xi_{c2}^2$, where B_{c2} is an upper critical field and Φ_0 is a flux quantum. The GL theory was carefully reanalyzed in Ref. [12], where strong deviation from the AGL theory and the values of the variational parameters were found *i.e.*, the AGL model can be considered as a very approximative and qualitative. But it can be used for the description of the field distribution with ξ_h obtained by fitting to the numerical solution of the GL [13]. In this method the HC type of the field distribution is conserved, but $\xi_h(B) \neq \xi_v(B)$ is found. In the same way, in analysis of experimental data the functional form of $F(\mathbf{G}, \xi_h)$ is often taken in the form of the HC

* Corresponding author at: Lappeenranta University of Technology, P.O. Box 20, FI-53851 Lappeenranta, Finland. Tel.: +358 466166615.
E-mail address: Polina.Belova@lut.fi (P. Belova).

0921-4534/$ - see front matter © 2012 Elsevier B.V. All rights reserved.
doi:10.1016/j.physc.2012.01.019

Table 1
Characteristics lengths of the vortex core in the mixed state.

Length	Definition
ξ_h	Cutoff parameter in the field distribution $h_{EHC}(\mathbf{r})$, (Eq. (1))
k_1	The cutoff parameter in the field distribution $\tilde{h}_{EHC}(\mathbf{r})$, (Eq. (13))
ξ_v	AGL cutoff parameter, (Eq. (18))
ξ_0	Characteristic scale in the calculation, v_F/T_c
ξ_1	Order parameter coherence length, $1/\xi_1 = (\partial\lvert\Delta(r)\rvert/\partial r)_{r=0}/\lvert\Delta_{NN}\rvert$
ξ_2	Core radius, where the superconductor current around the vortex has its maximum
ξ_3	STM vortex core radius [9], $\xi_3 = 0.35[(N(0)/N_0)/(H/H_{c2})]^{1/2}$
ξ_{BCS}	BCS coherence length, $\xi_{BCS} = v_F/\pi\Delta_0$
ξ_{c2}	GL coherence length, $\xi_{c2} = \sqrt{\Phi_0/2\pi B_{c2}}$
ξ_{KZ}	Coherence length of the linearized Eilenberger equations [10]
ρ	The nonlocality range [11]
λ	Magnetic field penetration depth in the Meissner state, (Eq. (2))
λ_{eff}	Effective penetration depth in the mixed state, (Eq. (16))

model in all temperature range with ξ_h as a fitting parameter. This is explained by historical reasons and its convenience for the fitting. It is important that connection between ξ_h and ξ_2 does not depend strongly on fitting procedure [14] and does not include any microscopical parameters. Using of any other fitting methods could not change the conclusions about the microscopical length ξ_2.

Analyzed with this method, μSR experimental results in V_3Si, $NbSe_2$, and $LuNi_2B_2C$ in intermediate magnetic fields and low temperatures showed that $\xi_h/\xi_{c2}(\sim 0.7) < 1$ (see Fig. 7 on page 1731 in Ref. [3]). Similar effect has been observed also in iron pnictide superconductor $BaFe_{1.82}Co_{0.18}As$ where $\xi_h/\xi_{c2}(\sim 0.4) < 1$ [15]. These small values are quite different from the prediction of the AGL theory ($\xi_v/\xi_{c2} = \sqrt{2}$), which needs explanations.

In the AGL theory, the equality $\xi_h = \xi_1$ is suggested. Here, the order parameter coherence length ξ_1 is determined as $1/\xi_1 = (\partial|\Delta(r)|/\partial r)_{r=0}/|\Delta_{NN}|$, where $|\Delta_{NN}|$ is maximum value of the order parameter along the nearest-neighbor direction which is the direction of taking the derivative. The length ξ_1 is directly connected with the length ξ_3 responsible for the density of states and STM measurements description [16]. For the convenience of the reader we summarized the definitions of all characteristics lengths of the vortex core used in our paper in Table 1.

The measurements of the reversible magnetization of type-II superconductors in the mixed state is also powerful method to investigate of the characteristic lengths such as λ and ξ_{c2}. The AGL model gives the possibility to calculate the magnetization of type-II superconductors in the full range $B_{c1} < B < B_{c2}$. The analytical formula is in a good agreement with the well-known Abrikosov high-field result. The Hao–Clem model was further extended to include anisotropy. This approximation was widely used for the analysis of the experimental data on magnetization of type-II superconductors (see references 27–29 in Ref. [12]). While at high temperatures, the analysis of data for Tl − 2223 and Hg − 1201 produced a well-behaved $H_{c2} \propto (T_c - T)$ [17], the method failed when applied to low T. Extensive magnetization data on Bi − 2212 [18] analyzed with the help of AGL approach have generated a nearly constant $B_{c2}(T)$ between 35 and 70 K, whereas the standard Helfand–Werthamer estimate predicts a reduction by a factor of 3 or 5. This difficulty motivated Kogan and Gurevich to review the microscopic derivation of the London equations and to obtain corrections due to the basic nonlocality of the relation between current density and the vector potential (the KG theory) [11]. In this theory the field B enters M in the combination B/B_0 instead of the standard London or GL ratio B/B_{c2}. The field B_0 of a given sample increases with T; at a given T, B_0 of a set of samples increases fast with shorter mean-free path l. The characteristic field B_0 is related to the nonlocality range ρ. This theory reasonably explains the magnetization data for strongly anisotropic compounds (Bi − 2212, Tl − 2212, Hg − 1201) [11] and for nearly isotropic borocarbides [19,20].

The scaling field B_0 is found to be nearly proportional to the field B_2 at which the vortex lattice undergoes the symmetry change in high-quality crystals of borocarbides (the "square-to-hexagonal" transition) under reducing the field [21,22]. Anisotropic nonlocal corrections to the London model were used to describe vortex lattices in tetragonal $LuNi_2B_2C$ [23]. The nonlocal corrections are expected to introduce a fourfold anisotropy as a function of the magnetic field orientation within the $a - b$ plane [24]. Studies of single crystal YNi_2B_2C revealed a fourfold anisotropy of the equilibrium magnetization in the square crystallographic basal plane [25]. This $\pi/2$ periodicity occurs deep in the superconducting mixed state. The experimental results were well described by generalized London theory incorporating nonlocal electrodynamics [24].

The nonlocal generalized London equation was also developed to the description of the mixed state in high-T_c superconductors such as $YBa_2Cu_3O_{7-\delta}$ compounds (the Amin–Franz–Affleck (AFA) model) [26,27]. In this case fourfold anisotropy arises from d-wave pairing. This theory was applied for investigation of the flux line lattice (FLL) structures [28] and effective penetration depth measured by μSR experiments [29]. Deviations from the London model description were also found in the investigation of magnetization of YBaCuO superconductor nanoparticles in the mixed state [30,31]. Detailed investigations of YBaCuO nanoparticles was done in Refs. [32,33].

In the KG and AFA models the cutoff function was introduced phenomenologically. The attempt to describe the vortex core microscopically was made in Ref. [10] (the Kogan–Zhelezina (KZ) model). In this model the linearized Eilenberger equations (EEs) have been solved and uniform magnetic field has been suggested. The obtained field dependence of the coherence length ξ_{KZ} looked similar to that observed experimentally but the temperature dependence has opposite tendency, *i.e.*, Kramer–Pesch effect is absent in this theory [2,3].

In spite of the nonlocal generalized London models look quite attractive and convenient for analysis of the experimental data their applicability is not clear because of using only partly Eilenberger theory results. The bridge between the full self-consistent solution and phenomenologically renormalized London models is needed.

The aim of this paper is to project the Eilenberger theory solution to the London model leaving only minimal possible amount of parameters and to check the applicability of the above methods. To do that, we will use two presentations of the field distribution $h_{EHC}(\mathbf{r})$ and $\tilde{h}_{EHC}(\mathbf{r})$. In both methods the Hao–Clem cutoff function with one fitting parameter ξ_h or k_1, respectively, will be used. In the second case the contribution of the extended electronic case outside the vortex core will be separated obviously.

2. Model

The microscopical theory valid in the whole temperature range is the quasiclassical Eilenberger theory. The cutoff parameter can be found from the fitting of the calculated magnetic field distribution obtained from the EE to the Hao–Clem type field distribution [34,35]

$$h_{EHC}(\mathbf{r}) = \frac{\Phi_0}{S}\sum_{\mathbf{G}}\frac{F(G)e^{i\mathbf{G}\mathbf{r}}}{1+\lambda^2 G^2}, \tag{1}$$

where $F(\mathbf{G}) = uK_1(u)$, $K_1(u)$ is the modified Bessel function, $u = \xi_h G$ and S is the area of the vortex lattice unit cell. In Eq. (1), $\lambda(T)$ is calculated from microscopical theory and renormalized by nonmagnetic impurity scattering [36]. So that,

$$\frac{\lambda^2}{\lambda_0^2} = \left(2\pi T\sum_{n\geq 0}\frac{1}{\tilde{\Delta}_n\left(1+u_n^2\right)^{3/2}}\right)^{-1}, \tag{2}$$

where

$$\widetilde{\Delta}_n = \Delta + \frac{2\pi\Gamma}{\sqrt{u_n^2+1}}. \quad (3)$$

Here, $\lambda_0 = \left(c^2/4\pi^2 e^2 v_F^2 N_0\right)^{(1/2)}$ is the London penetration depth at $T = 0K$, N_0 is the density of states at the Fermi surface, $\Gamma = \pi n_i N_F |u|^2$ is the impurity scattering rate (u is impurity scattering amplitude), $u_n = w_n/\Delta$ and $\omega_n = (2n+1)\pi T$ is the fermionic Matsubara frequency. Fig. 1 shows the temperature dependence of the $\lambda_0^2/\lambda^2(T)$ with different values of the impurity scattering rates Γ. Within this approach the London penetration depth is field independent. Assuming a field dependent λ would have changed the London equation *per se*: the quantity $\lambda^2(H)$ cannot be taken out of differentiation operators. There is no microscopic justification for a field dependent λ (in nonmagnetic superconductors). In other words, the London theory is rigid with respect to a constancy of λ, unlike the case of ξ_h [37]. Additionally, simultaneous experimental determination of λ_{eff} (depending on the magnetic field) and ξ_h without any restrictions is very problematic, regardless of the model used to describe the vortex state [38].

It is important to note that ξ_h in Eq. (1) is obtained from solving the EE and ξ_h does not coincide with the variational parameter of the AGL theory, the improved analytical GL solution [12] or the numerical GL solution [13]. We will call the obtained field distribution as an Eilenberger–Hao–Clem (EHC) field distribution $h_{EHC}(\mathbf{r})$. Using the HC type of the field distribution does not mean direct connection to the GL theory and it is taken as a reasonable starting point of the investigation similar to the empirical approach to the problem [2,3]. This approach allows to take into account the different symmetries of the order parameter which ware demonstrated in our investigation of iron pnictides superconductors [39]. The main effect of the impurity scattering in this theory is the renormalization of $\lambda(T)$. In this paper the next order correction which is described by $\xi_h(\lambda)$ dependence is studied.

We solve the quasiclassical self-consistent EE for triangular FLL and *s*-wave pairing symmetry. Quasiclassical Green functions f and g can be parameterized with the Riccati transformation of the EE via functions a and b [40]

$$\bar{f} = \frac{2a}{1+ab}, \quad f^{\dagger} = \frac{2b}{1+ab}, \quad g = \frac{1-ab}{1+ab}, \quad (4)$$

satisfying the nonlinear Riccati equations. In Born approximation for the nonmagnetic impurity scattering we have

$$\mathbf{n}\cdot\nabla a = -a[2(\omega_n + G) + i\mathbf{n}\cdot\mathbf{A}] + (\Delta + F) - a^2(\Delta^* + F^*), \quad (5)$$

$$\mathbf{n}\cdot\nabla b = b[2(\omega_n + G) + i\mathbf{n}\cdot\mathbf{A}] - (\Delta^* + F^*) + b^2(\Delta + F), \quad (6)$$

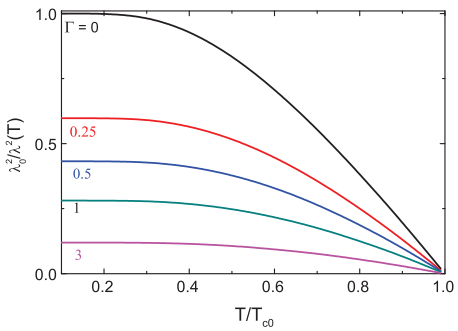

Fig. 1. The temperature dependence of the $\lambda_0^2/\lambda^2(T)$ with different values of the impurity scattering rates Γ.

where $F = 2\pi\langle f\rangle \cdot \Gamma$, $G = 2\pi\langle g\rangle \cdot \Gamma$ and $\mathbf{n}$ is a unit vector of the Fermi velocity. The impurity renormalization correction in Eqs. (5) and (6) are averaged over Fermi surface and can be reduced to averages over the polar angle θ, *i.e.*, $\langle\ldots\rangle = (1/2\pi)\int\ldots d\theta$.

To take into account the influence of screening, the vector potential $\mathbf{A}(\mathbf{r})$ in Eqs. (5) and (6) is obtained from the equation $\nabla\times\nabla\times\mathbf{A}_E = \frac{4}{\kappa^2}\mathbf{J}$, where the supercurrent $\mathbf{J}(\mathbf{r})$ is given in terms of $g(\omega_n, \theta, \mathbf{r})$ by

$$\mathbf{J}(\mathbf{r}) = 2\pi T \sum_{\omega_n>0}^{\omega_c} \int_0^{2\pi} \frac{d\theta}{2\pi} \frac{\hat{\mathbf{k}}}{i} g(\omega_n, \theta, \mathbf{r}). \quad (7)$$

Here $\mathbf{A}$ and $\mathbf{J}$ are measured in units of $\Phi_0/2\pi\xi_0$ and $2eV_F N_0 T_c$, respectively. The spatial variation of the internal field $h_E(\mathbf{r})$ is determined through $\nabla\times\mathbf{A} = \mathbf{h_E}(\mathbf{r})$. The self-consistent condition for the pairing potential $\Delta(\mathbf{r})$ is given by

$$\Delta(\mathbf{r}) = V^{SC} 2\pi T \sum_{\omega_n>0}^{\omega_c} \int_0^{2\pi} \frac{d\theta}{2\pi} f(\omega_n, \theta, \mathbf{r}), \quad (8)$$

where V^{SC} is the superconducting coupling constant and ω_c is the ultraviolet cutoff frequency determining T_{c0} [35]. All over our paper, the energy, the temperature, and the length are measured in units of T_{c0} and the characteristic length $\xi_0 = v_F/T_{c0} = \xi_{BCS}\pi\Delta_0/T_{c0}$. Here $\xi_{BCS} = v_F/\pi\Delta_0$, where v_F is the Fermi velocity and Δ_0 is temperature dependent uniform gap. The magnetic field $\mathbf{h_E}$ is given in units of $\Phi_0/2\pi\xi_0^2$. The impurity scattering rates are in units of $2\pi T_{c0}$. In computations the ratio $\kappa = \lambda_0/\xi_0 = 10$ is used. It corresponds to $\kappa_{GL} = 43.3$ [40]. The Riccati equations (Eqs. (5 and 6)) are solved by the Fast Fourier Transform (FFT) method [35]. This method is reasonable for dense FLL discussed in this paper. In high field the pinning effects are weak and not considered in our paper. After solving the EE the obtained magnetic field distribution $h_E(\mathbf{r})$ is fitted with the Eilenberger–Hao–Clem field distribution $h_{EHC}(\mathbf{r})$ finding the fitting parameter ξ_h. The normalized difference between these fields corresponding to $\Gamma = 0$, $B = 1$ and $T/T_{c0} = 0.5$ is shown in Fig. 2. The accuracy of the fitting exceeds 1%. To study high field regime we should calculate upper critical field $B_{c2}(T)$ [41].

3. Nonlocal effects in generalized London equation

The change of the shape of $\xi_h(B)$ curve in different fields with increasing scattering rate Γ is shown in details in Fig. 3 at

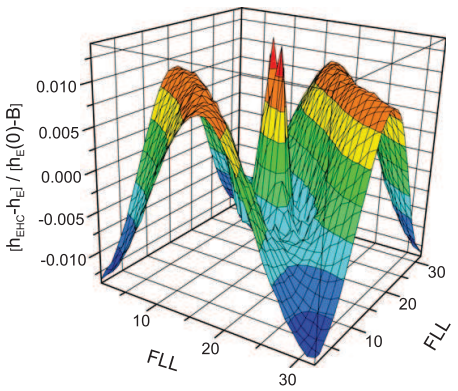

Fig. 2. Normalized differences between the fields h_{EHC} and h_E calculated with the generalized London model and with the Eilenberger equation, respectively, for $\Gamma = 0$, $B = 1$ and $T/T_{c0} = 0.5$. The scales of the lengths are those of the flux line lattice unit vectors.

$T/T_{c0} = 0.5$. Strong suppression of ξ_h/ξ_{c2} to values much lower than 1 at an increasing scattering rates Γ is also visible from this figure.

In Fig. 3, the normalization constant ξ_{c2} depends on the impurity scattering rate Γ. It is well known that at a high Γ, the $\xi_{c2} \sim \sqrt{1/\Gamma} \sim \sqrt{l}$. Therefore, the decreasing of the ratio ξ_h/ξ_{c2} with Γ implies a strong dependence of ξ_h on l. It is found that ξ_h in dirty superconductors can be scaled with the relaxation time τ, $\xi_h(B,T,\tau) = \xi_{pure}(B,T)/\left(1+\frac{\tau_0(B,T)}{\tau}\right)$, where $\xi_{pure}(B, T)$ is the effective coherence length in clean superconductors [35] and τ_0 is a characteristic relaxation time. This results in $\xi_h \sim l$ dependence at a high Γ similar to the behavior of the nonlocality range $\rho(\Gamma, T)$ [11] resulting in the decrease of ξ_h/ξ_{c2} versus B/B_{c2} at a high Γ, as shown in Fig. 3. It means that the nonlocal effects are important for the description of the vortex core even in the "dirty" limit. The low obtained ξ_h/ξ_{c2} values are consistent with the experimental observation in some high-κ low-T_c superconductors [3] and iron pnictide superconductors [15]. The nonlocality of the Bardeen–Cooper–Schrieffer (BCS) electrodynamics has been studied extensively. Even before BCS, the nonlocal relation between the current density **j** and the vector potential **A** was suggested by Pippard [42] to explain data on the penetration depth. The physics of nonlocality originates in a finite size, ξ_{BCS} at $T = 0$, of Cooper pairs: **j** at a given point is determined by the vector potential **A** within a domain $\sim\xi_{BCS}(T = 0)$ around this point. Instead of local relations between **j** and **A** of the GL or London theories, BCS provide an integral equation with a kernel $\widehat{Q}$ extending to distances $\sim\xi_{BCS}(T = 0)$. In Fourier space this relation is of the form $\mathbf{j}(\mathbf{k}) \propto \widehat{Q}(\mathbf{k})\mathbf{A}(\mathbf{k})$ with the Fourier transform of $\widehat{Q}$ explicitly depending on **k**.

Traditionally, it was widely thought that nonlocality effects should be significant only in materials with a Ginzburg–Landau parameter $\kappa_{GL} = \lambda/\xi_{GL} \sim 1$. Those materials, e.g., *Nb*, were clean enough to have $l \gg \xi_{GL}$, but the large vortex cores with $\xi_{GL} \approx \lambda$ make theoretical analysis very difficult. The tractable nonlocal London formalism was developed [11] for understanding these intermediate-to-high κ materials (the KG model). In this theory the term $\lambda^2 G^2$ in the denominator of the Eq. (1) was replaced by the anisotropic term $\widehat{Q}_{ij}G_iG_j$. In isotropic case this term was expanded up to fourth-order of G. This gave the additional term $\rho^2\lambda^2G^4$ in denominator of Eq. (1), where $\rho^2(T) = \frac{\hbar^2v^2}{16\Delta_0^2(0)}\gamma(T)$. Parameter γ which determine the temperature dependence of nonlocality range ρ was calculated from microscopical BCS theory in the Meissner state [11].

The inset of Fig. 4 shows the dependence of the nonlocality radius ρ/ξ_{c2} on the different scattering rates Γ in two-dimensional superconductors [11] similar to ξ_h/ξ_{c2} in Fig. 3. In this theory, in addition to B_{c2}, a characteristic field $B_0 = \frac{B_{c2}}{\sqrt{3}\pi}\left(\frac{\xi_{c2}}{\rho}\right)^2$ related to the nonlocality range enters the free energy and the magnetization reads

$$-\frac{M}{M_0} = \ln\left(\frac{B_0}{B}+1\right) - \frac{B_0}{B_0+B} + \zeta(T), \tag{9}$$

$$\zeta(T) = \eta_1 - \ln\left(\frac{B_0}{\eta_2 B_{c2}}+1\right), \tag{10}$$

Here, $M_0 = \Phi_0/32\pi^2\lambda^2$. The constant $\eta_1 \sim 1$ was introduced to account for the uncertainty in defining the core size in an estimation for the core contribution in the free energy; the constant $\eta_2 \sim 1$ accommodates the uncertainty in the cutoff of the field distribution. The quantity ζ slowly decreases with temperature due to the second term. The leading term in $M(B)$ of Eq. (10) is $\ln(H_0/B)$, corrected with terms on the order B/H_0, which are impurity scattering dependent and small in high-Γ limit. For three-dimensional situation, which is more suitable for the description of the borocarbides, the nonlocality range was calculated in Ref. [20]. The nonlocal London model describes qualitatively and consistently the whole set of $M(T, H)$ data in high quality single crystals of $Lu(Ni_{1-x}Co_x)_2B_2C$ with $x = 0 - 0.09$ and, in particular, its temperature and the mean-free path dependence [20].

In spite of good agreement between the prediction of the KG theory (Eq. (9)) in experiments [19,20] the theoretical basis of this model is lacking. Indeed, microscopically this theory takes into account only nonlocal effects outside the vortex core but short-scaled effects are included only phenomenologically by using fitting parameters η_1 and η_2. Additionally, the KG model is a linear theory with respect to the magnetic field and nonlinear effects are neglected. A priori, it is not clear which effects are more effective.

In Fig. 5 we compare the prediction of the KG theory for $M(B)$ (the main panel) and the numerical solution of the EE [43] (the inset) with different temperatures at $\kappa_{GL} = 49$. According the KG assumption $\zeta(T)$ is not dependent function from the magnetic field and $\zeta(T)$ is found from the boundary condition $M(T_c) = 0$. It can be seen from this figure that the KG and Eilenberger theories have quite different shape of the curves. In the later case there is a crossing point of the curves but this point is absent in the first case. It results from the neglecting of η_1 and η_2 field dependences which present in $\xi_h(B)$ for the EHC theory (see Figs. 3 and 4). It can be also noted that instead of the standard slope $\partial M/\partial \ln B = M_0$ there is $\partial M/\partial \ln B = M_0/(1 + B/B_0)^2$, *i.e.*, the slope $\partial M/\partial \ln B$ decreases with B in the KG theory. It is worth recalling that in the Abrikosov solution

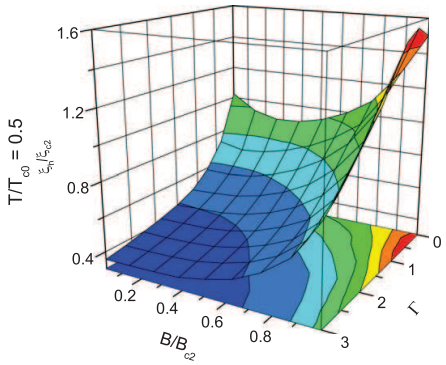

Fig. 3. The magnetic field dependence of ξ_h/ξ_{c2} with different impurity scattering values Γ at the temperature $T/T_{c0} = 0.5$.

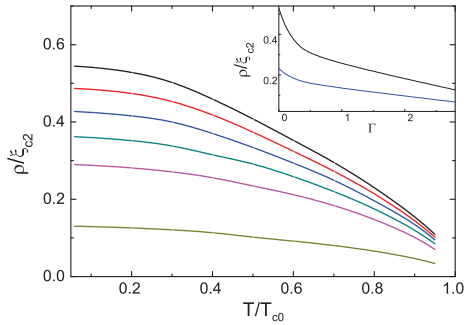

Fig. 4. The temperature dependence of the nonlocality radius ρ/ξ_{c2} for the scattering rates $\Gamma = 0$ (the upper curve), 0.057, 0.14, 0.28, 0.56 and 2.8 (the bottom curve) from Ref. [11]. The inset shows the scattering rates Γ dependence of the nonlocality radius ρ/ξ_{c2} for the temperature $T/T_{c0} = 0.2$ (the upper curve) and 0.8 (the bottom curve).

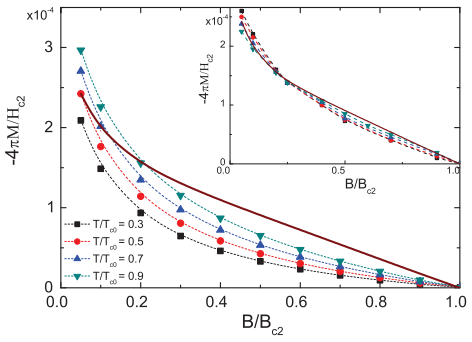

Fig. 5. The magnetization by supercurrent as a function of B/B_{c2} in the clean s-wave superconductors. The temperatures are $T/T_{c0} = 0.9$, 0.7, 0.5, and 0.3 (dashed lines from bottom to top). The inset shows the magnetization by supercurrent as a function of B/B_{c2} in the clean s-wave superconductors from Ref. [43]. The temperatures are $T/T_{c0} = 0.9$, 0.7, 0.5, and 0.3 (dashed lines from top to bottom). The solid lines show the numerical solution of the GL equations.

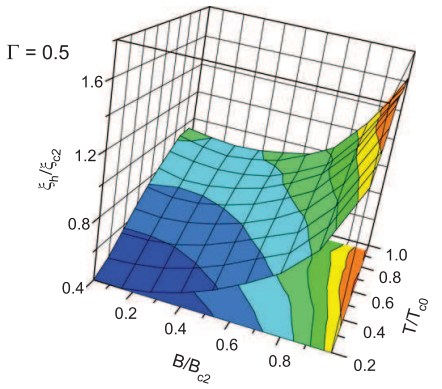

Fig. 6. The magnetic field dependence of ξ_h/ξ_{c2} at different temperatures with impurity scattering value $\Gamma = 0.5$.

of the GL theory there is the linear domain $4\pi M = (B - B_{c2})/\,2\beta_A\kappa_{GL}^2$ near $B_{c2}(T)$ for large κ (see Ref. [44]), where $\beta_A = 1.16$ is an Abrikosov parameter for the triangular FLL. Then the slope is $\partial M/\partial \ln B = B\partial M/\partial B = B/8\pi\beta_A\kappa_{GL}^2$, *i.e.*, here the slope $\partial M/\partial \ln B$ increases with B. Thus, in the KG theory the linear part of $M(B)$ is discarded altogether. It was proposed there that the Abrikosov region of $M(B)$ curve is narrow for high-κ superconductors and can be often negligible in the analysis of experimental data. However, the full self-consistent solution of EE shows clearly this linear Abrikisov part in high-κ superconductors [45]. As can been seen from the inset to Fig. 5, the linear slope of $M(B)$ curve near B_{c2} is temperature dependent. This is described by the introduction the Maki parameter $\kappa_2(T)$ instead of κ_{GL} ($\kappa_2(T) = \kappa_{GL}$ at $T = T_c$ and increases with lowering the temperature [44]).

It is instructive to compare the solution of the EE with that of the GL theory. A good fit of the numerical GL solution in the spirit of the logarithmic approximation is

$$-\frac{4\pi M}{B_{c2}} = \frac{1}{4\kappa_{GL}^2}\ln\left[1 + \frac{1-b}{b}f_2(b)\right], \tag{11}$$

$$f_2(b) = 0.357 + 2.890b - 1.581b^2, \tag{12}$$

where $b = B/B_{c2}$ [46]. This dependence is shown in the inset to Fig. 5 with $\kappa_{GL} = 49$ as a solid line. In reduced units used in Fig. 5 the GL curve is a universal one and depends only on κ_{GL}. The deviation of the EE solution from the GL curve is connected with the Kramer–Pesch effect at low temperatures and effective field dependence of κ_{GL} which results in the appearance of the crossing point in this inset. Obviously, the GL curve is the closest to the EE solution at highest temperature ($T/T_{c0} = 0.9$ in this plot).

4. Influence of the Andreev bound states and Kramer–Pesch effect on the cutoff parameter

A strong decrease in ξ_h/ξ_{c2} with decreasing temperature is clearly visible in Fig. 6 at $\Gamma = 0.5$. This can be explained by the Kramer–Pesch effect [1], which was observed in the μSR investigation of the $NbSe_2$ single crystal [3].

Such behavior is quite different from that of $\rho(T)$ which is not dependent from T at low temperatures and decreases slowly at high temperatures (the main panel in Fig. 4 [11]). The reason for this is that in the KG model the nonlocality is described in the same way as in the Meissner state, where only extended states exist in s-wave superconductors. In contrast, low temperature physics of the vortex state is connected with the nature of the current-currying quantum states of the quasiparticles in the vortex core (formed due to particle-holed coherence and Andreev reflection [47]). The current distribution can be decomposed in terms of bound states and extended states contributions [48]. Close to the vortex core, the current density arises mainly from the occupation of the bound states.

The effect of extended states becomes important only at distances larger than the coherence length. The bound states and the extended states contributions to the current density have opposite signs. The current density originating from the bound states is paramagnetic, whereas extended states contribute a diamagnetic term. At distance larger than the penetration depth, the paramagnetic and diamagnetic parts essentially cancel, resulting in exponential decay of the total current density. Similar paramagnetic current of Andreev bound states has been found at the surface of d-wave superconductors [49].

While all other length scales describing the superconducting state, especially the London penetration depth and the coherence length, reach a saturation value with decreasing temperature, this investigation introduced a new length scale in the discussion of the vortex state of clean superconductors. It can be defined as the inverse of the slope of the pairing potential at the vortex center (the length $\xi_1(T)$) and describes not only the spatial variation of the gap function but also the maximum height of the supercurrent density around the vortex center and thus measures the size of the vortex core (the length $\xi_2(T)$). In a clean superconductor without impurity scattering this length ξ_v decreases linearly with temperature, tending to zero for $T \to 0$ (the Kramer–Pesch effect) [47]. At low temperatures, the current rises to its maximum over a distance of the order of ξ_2, which is consistent with the sharp rise of the pair potential in the same region. In this region, the current is mainly carried by the lowest bound state. As discussed in Ref. [51] for the proper description of the bound states quantum mechanical nonlocal approach is needed and the strong difference between the nonlocal Eilenberger and the local Doppler-shift method has been found.

The Kramer–Pesch effect depends strongly on the impurity scattering rate. The decrease of ξ_h/ξ_{c2} in dirty superconductors can be compared with the behavior of another characteristic length ξ_1/ξ_{c2}. It has been found that at low temperatures impurity scattering suppresses Kramer–Pesch effect in $\xi_1(T)$ dependence, resulting in the nonmonotonous behavior of $\xi_1(\Gamma)$. This can be seen from Fig. 7, where the normalization constant ξ_{BCS} is used (ξ_{BCS} is not dependent on Γ). It is apparent that ξ_h monotonously decreases with $1/\Gamma$ (Fig. 7a) in contrast to the nonmonotonous behavior of

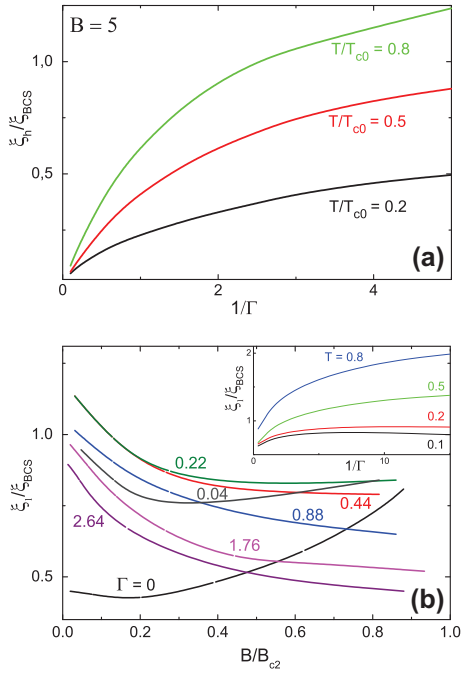

Fig. 7. (a) The magnetic field dependence of ξ_h/ξ_{BCS} at $B = 5$ at different temperatures. (b) The magnetic field dependence of ξ_1/ξ_{BCS} at $T/T_{c0} = 0.1$ with different impurity scattering rate Γ taken from Ref. [40]. The inset shows the magnetic field dependence of ξ_1/ξ_{BCS} at different temperatures from Ref. [50].

ξ_1 for a single vortex obtained from Ref. [50] (inset to Fig. 7b). The nonmonotonous behavior of ξ_1 is also visible in its field dependence. This is shown in the main panel Fig. 7b, which presents the curves $\xi_1/\xi_{BCS}(B/B_{c2})$ at $T/T_{c0} = 0.1$ with different impurity scattering rates [40].

The difference between $\xi_1(B)$ and $\xi_h(B)$ can be explained by the following reasons. According to the definition, $\xi_1(B)$ depends on Δ_{NN} (which is decreasing function of the field [16]) and, correspondingly, on extended states. The core physics for this length is descried by the derivative $(\partial|\Delta(r)|/\partial r)_{r=0}$ which is also decreasing function of the field [1]. Therefore, the field dependence of ξ_1 is determined by the competition between $(\partial|\Delta(r)|/\partial r)_{r=0}(B)$ and $\Delta_{NN}(B)$. The cutoff parameter ξ_h is directly connected with the microscopical length ξ_2 defined as the one where the screening current around the vortex has its maximum [7]. Because this maximum is located in the core center $\xi_h(B)$ is related mainly with core Andreev bound states.

We also note that indirect connection between the superconductor current and the modulus of the order parameter occurs often in the different nonlocal microscopical theories. For example, the screening current in the Meissner state can even change the sign near the surface in the type-I superconductors (overscreening) while the order parameter is practically constant [42]. In this case the effective penetration depth of the magnetic field and the region of the shielding current are less than the coherence length of the order parameter. This is similar to the results presented at Fig. 7 where ξ_h can be much less than ξ_1, *i.e.*, the "effective" type-I superconductor is realized in the vortex core.

Likewise, the current flowing opposite to the screening current appears at the *d*-wave high-κ superconductors surface [52]. In this case the electron reflecting from the surface feels the pairing potential with opposite signs in its trajectory. It results in creating of the bound Andreev states. With the anomalous Meissner current flowing, the magnetic field initially increases before the normal Meissner screening sets in and eventually screens out the magnetic field exponentially. This situation is similar to that of the Andreev bound states forming in the vortex core where the order parameter changes its sign at the opposite side of the vortex because of the π-phase altering.

5. Vortex core effects on the variance of the magnetic field and effective penetration depth in the mixed state

To demonstrate the importance of core effects obviously one can detach the contribution of the nonlocality of the extended electronic state outside the vortex core in the EHC theory similar to the KG method and project the solution of the EE to the nonlocal generalized London equation (NGLE) [53]. In this presentation the magnetic field distribution for clean superconductors is given as

$$\tilde{h}_{EHC}(\mathbf{r}) = \frac{\Phi_0}{S}\sum_{\mathbf{G}}\frac{F(G)e^{i\mathbf{G}\mathbf{r}}}{1+L_{ij}(\mathbf{G})G_iG_j}, \tag{13}$$

where

$$L_{ij}(\mathbf{G}) = \frac{Q_{i,j}(\mathbf{G})}{det\widehat{Q}(\mathbf{G})}. \tag{14}$$

The anisotropic electromagnetic response tensor is defined as

$$Q_{ij}(\mathbf{G}) = \frac{4\pi T}{\lambda_0^2}\sum_{\omega_n>0}\int_0^{2\pi}\frac{d\theta}{2\pi}\times\frac{\bar{\Delta}(\theta)^2\hat{v}_{Fi}\hat{v}_{Fj}}{\sqrt{\omega_n^2+\bar{\Delta}(\theta)^2}\left[\omega_n^2+\bar{\Delta}(\theta)^2+\gamma_G^2\right]}, \tag{15}$$

where $\gamma_G = \boldsymbol{v}_F\mathbf{G}/2$. In Eq. (15) the term including γ_G describes the nonlocal correction to the London equation. With $\gamma_G = 0$ we obtain the London result $L_{ij}(G) = \lambda(T)^2\delta_{ij}$. In Eq. (13) the cutoff function is written in the form of $F(\mathbf{G}) = u\,K_1(u)$. The cutoff parameter k_1 can be found by comparison of the solution of the EE with the Eq. (13). For $\tilde{h}_{EHC}$ we used the same shape of the cutoff function as for h_{EHC} but values of the cutoff parameters are different because of fitting to various field distributions. In presentation $\tilde{h}_{EHC}$ anisotropy effects of Eilenberger theory remained. To show the influence of the magnetic field and temperature dependence of k_1 we calculate the values of $\langle\delta\tilde{h}^2\rangle$ using the field distribution obtained in the Eq. (13).

Fig. 8 shows the field dependence of the ratio $\langle\delta\tilde{h}^2\rangle$ with the cutoff parameter obtained from the solution of the EE to that with $k_1 = 1$. As one can find from the data presented in Fig. 8, this ratio deviates considerably from unity when the temperature is lowered pointing on the importance of the proper determine value of the cutoff parameter.

This consideration proves that the nonlocal generalized London model with $\tilde{h}_{EHC}(\mathbf{r})$ distribution also needs the proper determined cutoff parameter k_1, *i.e.*, introducing only nonlocal extended electronic states does not allow to avoid the problem of vortex core solving.

In the analysis of the μSR and SANS experimental data the field dependent penetration depth $\lambda_{eff}(B)$ is often introduced [3]. It has physical sense if it is not dependent from core effects, *i.e.*, it should be invariant of the cutoff parameter. One of such way to do that was suggested in AFA model [27,29]:

$$\frac{\lambda_{eff}}{\lambda} = \left(\frac{\left|\delta h_0^2\right|}{\left|\delta\tilde{h}_{EHC}^2\right|}\right)^{1/4}. \tag{16}$$

Here, $\left|\delta h_0^2\right|$ is the variance of the magnetic field $h_0(\mathbf{r})$ obtained by applying the ordinary London model with the same average field B and λ and with the same cutoff parameter as in the field distribution $\tilde{h}_{EHC}(\mathbf{r})$.

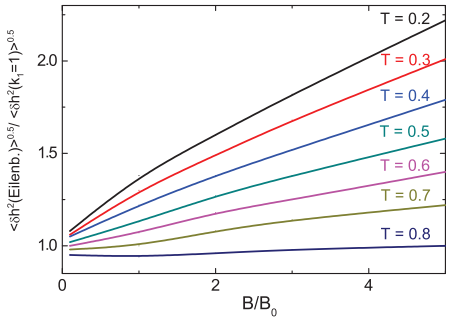

Fig. 8. The magnetic field dependence of the ratio of the second moment of the magnetic field distributions obtained from the solution of the EE to that of the nonlocal generalized London model with the parameter $k_1 = 1$ for $T = 0.2$ (the upper curve), 0.3, 0.4, 0.5, 0.6, 0.7, 0.8 (the bottom curve). Here $B_0 = \Phi_0/2\pi\xi_0^2$.

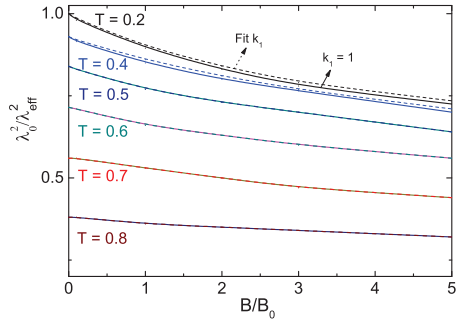

Fig. 9. The magnetic field dependence of the ratio $\lambda_0^2/\lambda_{eff}^2$ calculated from the nonlocal generalized London equation with $k_1 = 1$ (solid lines) and Fit k_1 from the solution of EE (dotted lines) for the different temperatures ($T = 0.2$ (the upper curve), 0.4, 0.5, 0.6, 0.7, 0.8 (the bottom curve)). Here $B_0 = \Phi_0/2\pi\xi_0^2$.

In Fig. 9 is shown the magnetic field dependence of the ratio $\lambda_0^2/\lambda_{eff}^2$ calculated from the $\tilde{h}_{EHC}$ distribution with $k_1 = 1$ and with Fit k_1 from the solution of EE for the different temperatures. The obtained $\lambda_{eff}(B)$ dependences are quite similar in these cases. The low-field result ($B/B_0 = 0.1$) for λ_{eff} is close to $\lambda(T)$ in the Meissner state. This demonstrates that λ_{eff} is determined by a large scale of the order of FLL period and is not very sensitive to details of the microscopical core structure and the cutoff parameter. Thus, our microscopical consideration justify the phenomenological AFA model. The AFA model was originally developed for the explanation of the structural transition in FLL in *d*-wave superconductors where anisotropy and nonlocal effects arise from nodes of the gap at the Fermi surface and appearing there of the long extending electronic states [28]. They result also in the field dependent flattening of $\lambda_{eff}(B)$ at low temperatures [29]. In this case the separation between localized and extended states looks quite reasonably. The obtained anisotropy of superconducting current around the single vortex in AFA theory agrees well with that found from the EE [54]. Also $\lambda_{eff}(B, T)$ is not strongly dependent on the core effects [55]. However, it was shown that full self-consistent quasiclassical approach is needed when gap and Fermi surface anisotropies exist simultaneously [45]. Recently, the measurements of the angle resolved specific heat in a field rotated around the *c* axis in *d*-wave pairing $CeCoIn_5$ ($T_c = 2.3K$) down to a very low temperature, $0.05T_c$, were done. And a sign reversal of the fourfold angular oscillation was observed [56]. This low temperature "quasiclassical" regime was explained by Eilenberger theory.

The field dependence of λ_{eff} in *s*-wave superconductors (Fig. 9) results from the nonlinear dependence of the zero-energy density of states $N(0)(B)$ even in the isotropic superconductors [16]. The contribution of the extended states is essential even in the small *B* region, meaning that vortex cores are overlapped there (vortex lattice effect [16]) [57]. This invalidates rigid normal core picture [6]. This is qualitatively similar to the *d*-wave superconductors where nonlinear effects are stronger due to nodes in the gap and $N(0)(B) \sim B^{1/2}$. The introduction of $\lambda_{eff}(B)$ results in the transformation of the NGLE to usual local London equation but with two field-dependent parameters $\lambda_{eff}(B)$ and $k_1(B)$. This consideration gives the way for the fitting of the experimental results: firstly, to find $\lambda_{eff}(B)$ using Eq. (16), secondly, to find $k_1(B)$ from the absolute value of variance of the magnetic field. With this route one can avoid the problems of two-parameter fitting discussed in Ref. [38]. We note that $\lambda_{eff}(B)$ (like k_1 and ξ_h) is effective parameter and does not have fundamental physical sense like λ in the Meissner state where it is connected with the superconducting electron density [58]. Both fitting procedures are possible with parameters $\lambda_{eff}(B)$, $k_1(B)$ or $\lambda(T)$ (from the Meissner state), $\xi_h(B)$. The accuracy is the neglecting of the anisotropy effect.

6. High-field effects: comparison of Kogan–Zhelezina and analytical Ginzburg–Landau models

The microscopical model which allows to obtain analytical solution for $\xi_h(B)$ has been suggested in Ref. [10] (the KZ model). In this model linearized EE has been solved and uniform magnetic field has been suggested. It means than Kramer–Pesch effect is not included in the consideration. Also the distribution of the magnetic field is not calculated self-consistently. The exact form equation of $\xi_h(B)$ for the zero-*T* clean case for both Fermi sphere and cylinder has been obtained. The result can be represented as $\xi_{KZ}(B)/\xi_{c2}(B_{c2}) = U(B/B_{c2})$ with *U* being an universal function. The most important features of the KZ model and $\xi_{KZ}(B)$ dependence are as follows: (i) this dependence is weakened by scattering and disappears in the dirty limit; (ii) the *B* dependence of ξ vanishes as $T \to T_c$; (iii) in reduced variables, the dimensionless coherence length $\xi^* = \xi_{KZ}/\xi_{c2}$ should be nearly universal function of the reduced field $b = B/B_{c2}$ for clean materials in high fields and low temperatures; and (iv) for materials on the clean side ($\Gamma < 1$) the low-*T* slope $d\xi^*/d\, b^{(-1/2)}$ is nearly universal in high fields ($b \to 1$).

The data in Fig. 10a and b demonstrate nearly universal behavior near T_c and small scattering rates: (i) a nonmonotonous field dependence with a minimum and (ii) a similar slope $d(\xi_h/\xi_{c2})/db$ at $b = 1$ which is weakly dependent on temperature and scattering rate. But the results are very different from the prediction of the KZ theory because of neglecting of the Kramer–Pesch effect there. This can be seen from Fig. 10c, where predictions of KZ theory for different scattering rates and temperatures are presented. As is visible from this figure, the clean limit results are not compatible with the prediction of Kramer and Pesch that the core size of an isolated vortex goes to zero as $T \to 0$. In contrast, the strong suppression of ξ_h (Fig. 10a and b) and ξ_1 [1,50] with temperature lowering is obtained in the self-consistent Eilenberger theory. This difference points out at the importance of Kramer–Pesch effect. But impurity induced behavior is similar for ξ_h/ξ_{c2} and ξ_{KZ}/ξ_{c2}: both decreases with increasing impurity rates.

The analysis of the experimental data in the mixed state depends on the theoretical model of the distribution function of local fields $P(B)$ in the vortex lattice [2,3]. One of the most widely used model is an approximation of the analytical Ginzburg–Landau theory (the AGL theory) [8,59]. For the dense vortex lattice ($B \gg B_{c1}$) and high-κ ($\kappa_{GL} > 10$) superconductors the AGL theory prediction for the Fourier components of the magnetic field is

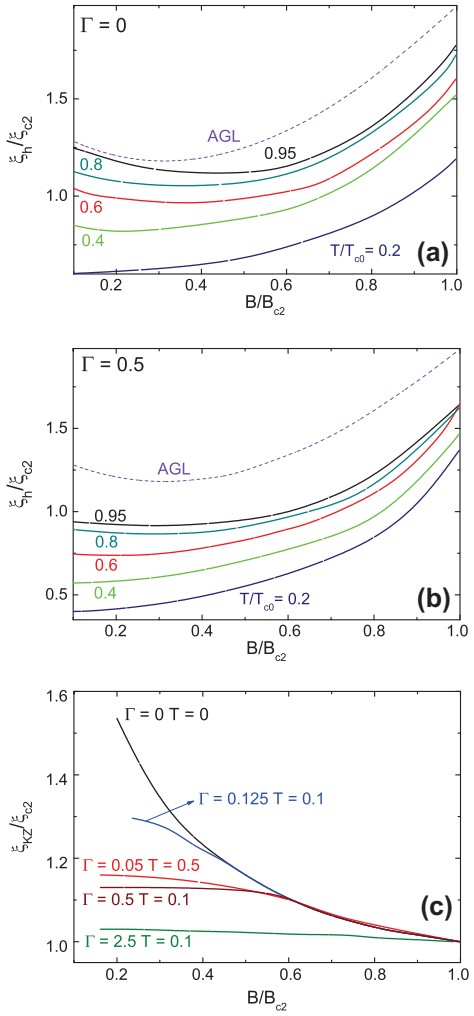

Fig. 10. The magnetic field dependence of ξ_h/ξ_{c2} at different temperatures (a) with impurity scattering $\Gamma = 0$ (b) with impurity scattering $\Gamma = 0.5$. Dashed lines show the result of the AGL theory for ξ_v from Ref. [8]. (c) The magnetic field dependences of ξ_{KZ}/ξ_{c2} (at $T = 0$, $\Gamma = 0$; $T = 0.1$, $\Gamma = 0.25$; $T = 0.5$, $\Gamma = 0.05$; $T = 0.5$, $\Gamma = 0.1$ and $T = 0.1$, $\Gamma = 2.5$ from Ref. [10]).

$$B_z(\mathbf{G}) = \frac{\phi_0}{S}\frac{f_\infty^2}{\lambda^2 G^2}(\xi_v G)K_1(\xi_v G), \tag{17}$$

where $K_1(x)$ is a modified Bessel function, $\mathbf{G}$ is a reciprocal-lattice vector, S is the area of the vortex lattice unit cell, ξ_v and f_∞ are variation parameters representing the effective core radius of a vortex and the depression of the order parameter due to the overlap of vortex cores, respectively. They have simple functional dependences on $b \equiv B/B_{c2}$ and κ_{GL}:

$$\xi_v = \xi_{c2}\left(\sqrt{2} - \frac{0.75}{\kappa_{GL}}\right)(1+b^4)^{1/2} \times [1 - 2b(1-b)^2]^{1/2}, \tag{18}$$

and $f_\infty^2 = 1 - b^4$. Here, $b = B/B_{c2}$ is the reduced magnetic induction in the units of upper critical field. It is important to note that in this approximation $\xi_v(B)$ is determined only by ξ_{c2} and the ratio B/B_{c2}. It implies that $\xi_v/\xi_{c2}(B/B_{c2})$ is an universal function. One can consider Eq. (17) as a solution of the modified London equation with cutoff ξ_v and effective penetration depth $\lambda_{eff} = \lambda/f_\infty$ [59]. The comparison between the variation and the exact numerical solution shows that the accuracy of the AGL theory is the order of 10% [59]. The dashed lines in Fig. 10 shows the prediction of the AGL theory for ξ_v.

The absolute values of ξ_h are considerably less than those of the AGL theory predictions because the Kramer–Persh effect is not included in the phenomenological GL theory. With increasing temperature the magnetic field dependence of ξ_h moves to higher values, towards the AGL theory predictions (Fig. 10a). It looks like the restoration of Ginzburg–Landau behavior at high temperatures. In the presence of impurity scattering the same tendency is also visible (Fig. 10b), but shifting of ξ_h to direction of AGL curve is slower. It was recently demonstrated by the μSR measurements that the variance of the magnetic field, σ, at $T \to 0$ can be fitted by GL theory using two fitting parameters λ and B_{c2} [58,60,61]. Moreover, the value of B_{c2}, evaluated in such a way, coincides with the result of magnetization measurements. This coincidence proves that the theoretical $\sigma(B)$ dependence calculated in framework of the GL theory can indeed be used for quantitative analysis of isothermal experimental data even at temperatures $T \ll T_c$. It is most probable that the distribution of the magnetic induction in the sample ($P(B)$) is different from predictions of microscopical theory, while σ, as a more integral characteristic of this distribution, remains practically the same [58].

7. Conclusions

The field distribution of the mixed state in dirty *s*-wave superconductors in a wide temperature and field range is investigated in the framework of the nonlocal Eilenberger theory and projected on the London equation. The normalized magnetic field dependences of the cutoff parameter ξ_h/ξ_{c2} (B/B_{c2}) responsible for the line shape of the μSR resonance are obtained. It is found that this dependence is nonuniversal and depends on the impurity scattering rate Γ and the temperature. At high enough values of $\Gamma/2\pi T_{c0} \geqslant 0.5$, the dependence plateaus in the intermediate field range and the low temperatures, and $\xi_h(B)/\xi_{c2}$ is of the order of 0.25. The strong suppression of ξ_h/ξ_{c2} with Γ and T can explain the experimental results in many low-temperature superconductors (V_3Si, $NbSe_2$ and $LuNi_2B_2C$ and iron pnictide superconductor $BaFe_{1.82}Co_{0.18}As$), where the values $\xi_h/\xi_{c2} < 1$ has been observed. It is connected with the nonlocal bound Andreev states of the vortex core. The obtained projection of the EE is compared with the nonlocal KG theory. The field dependence of the cutoff parameter changes the magnetization and the variance of the magnetic field. A difference is observed between $\xi_h(T)$ and nonlocal range $\rho(T)$ of the KG theory, where only the contribution of the extended state is taken into account. A strong difference from the AGL theory and linearized Eilenberger approach (the KZ theory) is found. This is explained by the Kramer–Pesch effect which is not taken into account in these theories.

References

[1] N. Nakai, P. Miranović, M. Ichioka, K. Machida, Phys. Rev. B 73 (2006) 172501.
[2] J.E. Sonier, J. Phys.: Condens. Matter 16 (2004) S4499.
[3] J.E. Sonier, Rep. Prog. Phys. 70 (2007) 1717.
[4] L. DeBeer-Schmitt, C.D. Dewhurst, B.W. Hoogenboom, C. Petrovic, M.R. Eskildsen, Phys. Rev. Lett. 97 (2006) 127001.
[5] A.A. Golubov, U. Hartmann, Phys. Rev. Lett. 72 (1994) 3602.
[6] P.D. Gennes, Superconductivity of Metals and Alloys, Addison-Wesley, New York.
[7] R. Kadono, W. Higemoto, A. Koda, M.I. Larkin, G.M. Luke, A.T. Savici, Y.J. Uemura, K.M. Kojima, T. Okamoto, T. Kakeshita, S. Uchida, T. Ito, K. Oka, M. Takigawa, M. Ichioka, K. Machida, Phys. Rev. B 69 (2004) 104523.

[8] Z. Hao, J.R. Clem, M.W. McElfresh, L. Civale, A.P. Malozemoff, F. Holtzberg, Phys. Rev. B 43 (1991) 2844.
[9] M. Ichioka, A. Hasegawa, K. Machida, Phys. Rev. B 59 (1999) 8902.
[10] V.G. Kogan, N.V. Zhelezina, Phys. Rev. B 71 (2005) 134505.
[11] V.G. Kogan, A. Gurevich, J.H. Cho, D.C. Johnston, M. Xu, J.R. Thompson, A. Martynovich, Phys. Rev. B 54 (1996) 12386.
[12] W.V. Pogosov, K.I. Kugel, A.L. Rakhmanov, E.H. Brandt, Phys. Rev. B 64 (2001) 064517.
[13] I.G. de Oliveira, A.M. Thompson, Phys. Rev. B 57 (1998) 7477.
[14] W.A. Atkinson, J.E. Sonier, Phys. Rev. B 77 (2008) 024514.
[15] J.E. Sonier, W. Huang, C.V. Kaiser, C. Cochrane, V. Pacradouni, S.A. Sabok-Sayr, M.D. Lumsden, B.C. Sales, M.A. McGuire, A.S. Sefat, D. Mandrus, Phys. Rev. Lett. 106 (2011) 127002.
[16] M. Ichioka, A. Hasegawa, K. Machida, Phys. Rev. B 59 (1999) 184.
[17] J.R. Thompson, J.G. Ossandon, D.K. Christen, B.C. Chakoumakos, Y.R. Sun, M. Paranthaman, J. Brynestad, Phys. Rev. B 48 (1993) 14031.
[18] J.H. Cho, Z. Hao, D.C. Johnston, Phys. Rev. B 46 (1992) 8679.
[19] K.J. Song, J.R. Thompson, M. Yethiraj, D.K. Christen, C.V. Tomy, D.M. Paulr, Phys. Rev. B 59 (1999) R6620.
[20] V.G. Kogan, S.L. Bud'ko, I.R. Fisher, P.C. Canfield, Phys. Rev. B 62 (2000) 9077.
[21] M.R. Eskildsen, P.L. Gammel, B.P. Barber, U. Yaron, A.P. Ramirez, D.A. Huse, D.J. Bishop, C. Bolle, C.M. Lieber, S. Oxx, K.M.S. Sridhar, N.H. Andersen, P.C. Canfield, Phys. Rev. Lett. 78 (1997) 1968.
[22] Y.D. Wilde, M. Iavarone, U. Welp, V. Metlushko, A.E. Koshelev, I. Aranson, G.W. Crabtree, P. Canfield, Phys. Rev. Lett. 78 (1997) 4273.
[23] V.G. Kogan, M. Bullock, B. Harmon, P. Miranović, L. Dobrosavljevic-Grujic, P.L. Gammel, D.J. Bishop, Phys. Rev. B 55 (1997) R8693.
[24] V.G. Kogan, S.L. Bud'ko, P. Canfield, P. Miranović, Phys. Rev. B 60 (1999) R12577.
[25] L. Civale, A.V. Silhanek, J.R. Thompson, K.J. Song, C.V. Tomy, D.M. Paul, Phys. Rev. Lett. 83 (1999) 3920.
[26] I. Affleck, M. Franz, M.H.S. Amin, Phys. Rev. B 55 (1997) R704.
[27] M.H.S. Amin, I. Affleck, M. Franz, Phys. Rev. B 58 (1998) 5848.
[28] M. Franz, I. Affleck, M.H.S. Amin, Phys. Rev. Lett. 79 (1997) 1555.
[29] M.H.S. Amin, M. Franz, I. Affleck, Phys. Rev. Lett. 84 (2000) 5864.
[30] E.V. Blinov, V.G. Fleisher, R. Laiho, E. Lähderanta, Y.P. Stepanov, K.B. Traito, Physica C 281 (1997) 17.
[31] E.V. Blinov, R. Laiho, A.G. Lyublinski, E. Lähderanta, K.B. Traito, Physica C 316 (1999) 45.
[32] V. Fleisher, E. Lähderanta, R. Laiho, Y.P. Stepanov, Physica C 170 (1990) 161.
[33] E.V. Blinov, E. Lähderanta, R. Laiho, Y.P. Stepanov, Physica C 199 (1992) 201.
[34] R. Laiho, M. Safonchik, K.B. Traito, Phys. Rev. B 76 (2007) R140501.
[35] R. Laiho, M. Safonchik, K.B. Traito, Phys. Rev. B 78 (2008) 064521.
[36] T. Lemberger, D. Ginsberg, G. Rickayzen, Phys. Rev. B 18 (1978) 6057.
[37] V.G. Kogan, R. Prozorov, S.L. Bud'ko, P.C. Canfield, J.R. Thompson, J. Karpinski, N.D. Zhigadlo, P. Miranović, Phys. Rev. B 74 (2006) 184521.
[38] A. Maisuradze, R. Khasanov, A. Shengelaya, H. Keller, J. Phys.: Condens. Matter 21 (2009) S075701.
[39] P. Belova, M. Safonchik, K.B. Traito, E. Lähderanta, Phys. Rev. B 83 (2011) 104518.
[40] P. Miranović, M. Ichioka, K. Machida, Phys. Rev. B 70 (2004) 104510.
[41] Y.N. Ovchinnikov, V.Z. Kresin, Phys. Rev. B 52 (1995) 3075.
[42] M. Tinkham, Introduction to Superconductivity, McGraw-Hill, New York, 1996.
[43] K. Watanabe, T. Kita, M. Arai, Phys. Rev. B 71 (2005) 144515.
[44] T. Kita, Phys. Rev. B 68 (2003) 184503.
[45] H. Adachi, P. Miranović, M. Ichioka, K. Machida, Phys. Rev. Lett. 94 (2005) 067007.
[46] E.H. Brandt, Phys. Rev. B 68 (2003) 054506.
[47] A. Gumann, S. Graser, T. Dahm, N. Schopohl, Phys. Rev. B 73 (2006) 104506.
[48] F. Gygi, M. Schlüter, Phys. Rev. B 43 (1991) 7609.
[49] M. Fogelström, D. Rainer, J.A. Sauls, Phys. Rev. Lett. 79 (1997) 281.
[50] N. Hayashi, Y. Kato, M. Sigrist, J. Low Temp. Phys. 139 (1995) 79.
[51] T. Dahm, S. Graser, C. Iniotakis, N. Schopohl, Phys. Rev. B 66 (2002) 144515.
[52] A. Zare, A. Markowsky, T. Dahm, N. Schopohl, Phys. Rev. B 78 (2008) 104524.
[53] R. Laiho, M. Safonchik, K.B. Traito, Phys. Rev. B 75 (2007) 174524.
[54] R. Laiho, E. Lähderanta, M. Safonchik, K.B. Traito, Phys. Rev. B 71 (2005) 024521.
[55] R. Laiho, M. Safonchik, K.B. Traito, Phys. Rev. B 73 (2006) 024507.
[56] K. An, T. Sakakibara, R. Settai, Y. Onuki, M. Hiragi, M. Ichioka, K. Machida, Phys. Rev. Lett. 104 (2010) 037002.
[57] N. Nakai, P. Miranović, M. Ichioka, K. Machida, Phys. Rev. B 70 (2004) R100503.
[58] I. Landau, H. Kelle, Physica C 466 (2007) 131.
[59] A. Yaouanc, P.D. de Reotier, E.H. Brandt, Phys. Rev. B 55 (1997) 11107.
[60] R. Khasanov, I. Landau, C. Baines, F.L. Mattina, A. Maisuradze, K. Togano, H. Keller, Phys. Rev. B 73 (2006) 214528.
[61] R. Khasanov, P.W. Klamut, A. Shengelaya, Z. Bukowski, I.M. Savic, C. Baines, H. Keller, Phys. Rev. B 78 (2008) 014502.

PUBL. 6

P. Belova, M. Safonchik, K. B. Traito and E. Lähderanta, Coherence length of magnetic field in the mixed state of type-II superconductors, *Journal of Physics: Conference Series*, **303**, 012114, 2011.

Joint European Magnetic Symposia – JEMS 2010 IOP Publishing
Journal of Physics: Conference Series **303** (2011) 012114 doi:10.1088/1742-6596/303/1/012114

Coherence length of magnetic field in the mixed state of type-II superconductors

P. Belova[1,2], M. Safonchik[1,3], K. B. Traito[1], E. Lähderanta[1]

[1] Lappeenranta University of Technology, P.O.Box 20, FI-53851, Lappeenranta, Finland
[2] Petrozavodsk State University, Lenin str. 33, RU-185640, Petrozavodsk, Russia
[3] A. F. Ioffe Physico-Technical Institute, St. Petersburg, 194021, Russia

E-mail: Polina.Belova@lut.fi

Abstract. Influence of impurities on coherence length ξ_h in the mixed state of s-wave superconductors is investigated in framework of quasiclassical Eilenberger theory. The increasing of impurity scattering rate results in decreasing of ξ_h. The obtained field dependence of ξ_h for clean superconductors has a minimum and it is similar to that in Hao-Clem and Miranović-Ichioka-Machida theories for order parameter of coherence length. It is found that growing behavior of ξ_h with magnetic field in dirty superconductors is different from order parameter coherence length determining by pairing potential near with vortex core. The magnetic field dependence of coherence length in normalized units, $\xi_h/\xi_{c2}(B/B_{c2})$, is nonuniversal and depends on impurity scattering potential.

Last ten years much attention has been paid to the investigation of the field distribution in high-κ superconductors [1–3]. On the theoretical level, there are four widely used methods: solving of the Bogoliubov-de Geenes (BdG) equations [4], the quasiclassical nonlocal Eilenberger theory [5–7] (this is the quasiclassical limit of the BdG theory for $k_F\xi_{BCS} \gg 1$), solving of the Usadel theory [8] (this is the dirty local limit of the Eilenberger equations with the strong impurity scattering rates ($\Gamma/T_c \gg 1$)) and the phemenological Ginzburg-Landau (GL) theory [9–13] which is valid near T_c. Because BdG method is very time consuming for the self-consistent numerical calculation [4], the Eilenberger or Usadel theories are used in the microscopical consideration. In analysis of the experimental data, the analytical GL model (AGL) with penetration depth λ and cutoff parameter ξ_h as a fitting parameters is used very often. The cutoff parameter ξ_h (in the notation of the AGL ξ_v) is connected with GL coherence length ξ_{c2}, determined by the relation $B_{c2} = \Phi_0/2\pi\xi_{c2}^2$. From theoretical reasons (see discussion in Ref. [14]), λ can not be taken arbitrarily and should be taken as a differential operator L_{ij} [15], for the description of the nonlocal effects giving the additional field dependence in the mixed state, or its local limit obtained from microscopical consideration of the Meissner state [16] independent on the magnetic field.

There is no consensus about the meaning of ξ_h, the problem was discussed originally by de Geenes group [17]. There are several proposes for the value of ξ_h: it can be taken as a coherence length ξ_{c2} with some numerical coefficient [18], or as the order parameter coherence length ξ_1, or as a proportional to the superconducting current coherence length ξ_2. Characteristic length ξ_1 is determined as $1/\xi_1 = (\partial|\Delta(r)|/\partial r)_{r=0}/|\Delta_{NN}|$, where $|\Delta_{NN}|$ is the maximum value of the order parameter along the nearest-neighbor direction which is the direction of taking the derivative [19] and ξ_2 is determined by maximum of screening current around the vortex [20].

But connections between ξ_h, ξ_1 and ξ_2 is not investigated in detail yet. The microscopical model allowing to obtain analytical solution for $\xi_h(B)$ has been suggested in Ref. [21] (the KZ model). In this model linearized Eilenberger equation has been solved and uniform magnetic field has been suggested. It means than Kramer-Pesch effect is not included in the consideration. The exact form equation of $\xi_h(B)$ for the zero-T clean case for both Fermi sphere and cylinder has been obtained. The result can be represented as $\xi_{KZ}(B)/\xi_{c2}(B_{c2}) = U(B/B_{c2})$ with U being an universal function. The most important features of the KZ model and $\xi(B)$ dependence are as follows: (i) this dependence is weakened by scattering and disappears in the dirty limit; (ii) the B dependence of ξ vanishes as $T \to T_c$; (iii) in reduced variables, the dimensionless coherence length $\xi^* = \xi/\xi_{c2}$ should be nearly universal function of the reduced field $b = B/B_{c2}$ for clean materials in high fields and low temperatures; and (iv) for materials on the clean side ($\Gamma < 1$) the low-T slope $d\xi^*/db^{(-1/2)}$ is nearly universal in high fields ($b \to 1$). It is found that the microscopical calculations of ξ_1 [5] do not agree with the KZ theory. In particular, these calculations don't confirm the KZ assertion about weakening of the field dependence of the core size with the increasing scattering. As noted in Ref. [14] the question still remains: which of these two theoretical approaches, Ref. [5] or Ref. [21], describes better various data on $\xi_h(B)$? It is important to note also that the GL theory predictions is not reproduced by the KZ theory.

Recently, an effective London model with the magnetic coherence length $\xi_h(B)$ as a fitting parameter has been obtained for clean [22] and dirty [23] superconductors, using self-consistent solution of quasiclassical nonlocal Eilenberger equations. Such theory looks appropriate for the description of the vortex core where strong nonlinear and nonlocal effects are expected. In this approach the coherence length obtained from the Ginzburg-Landau model is extended over the whole field and temperature range. The Fourier components of magnetic field in this model are described by London equation with GL type cutoff function

$$h_{EGL}(\mathbf{r}) = \frac{\phi_0}{S} \sum_{\mathbf{G}} \frac{F(G) e^{i\mathbf{G}\mathbf{r}}}{1 + \lambda^2 G^2}, \tag{1}$$

where $F(\mathbf{G}) = uK_1(u)$, $u = \xi_h G$. It is important to note that ξ_h in Eq. (1) is obtained by solving the Eilenberger equations and ξ_h doesn't coincide with the variational parameter of the AGL model. We will call obtained field distribution as an Eilenberger - Ginzburg-Landau field distribution $h_{EGL}(\mathbf{r})$. In Eq. (1) $\lambda(T)$ is calculated from microscopical theory for the Meissner state and renormalized by impurity scattering [24]. In dirty superconductors the value of λ increases considerable and gives the main effect of impurities in the field distribution (Eq. (1)) suppressing deviation of the field from the mean value B. Thus, in this model there is only one fitting parameter for the description of the vortex state, ξ_h, similar to Ref. [14].

The aim of our paper is to calculate $\xi_h(B)$ in the framework of the Eilenberger theory and to study the applicability of the above mentioned theories in wide temperature range and at different impurity scattering rates. In particular, we are interested in looking for possible predicted universal behavior. With the Riccati transformation of the Eilenberger equations, quasiclassical Green functions f and g can be parameterized via functions a and b [5]

$$\bar{f} = \frac{2a}{1+ab}, \quad f^\dagger = \frac{2b}{1+ab}, \quad g = \frac{1-ab}{1+ab}, \tag{2}$$

satisfying the nonlinear Riccati equations. In Born approximation for impurity scattering we have

$$\mathbf{u} \cdot \nabla a = -a[2(\omega_n + G) + i\mathbf{u} \cdot \mathbf{A}] + (\Delta + F) - a^2(\Delta^* + F^*), \tag{3}$$

$$\mathbf{u} \cdot \nabla b = b[2(\omega_n + G) + i\mathbf{u} \cdot \mathbf{A}] - (\Delta^* + F^*) + b^2(\Delta + F), \tag{4}$$

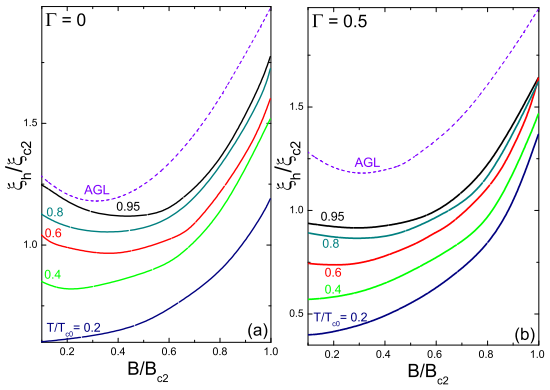

Figure 1. The magnetic field dependence of ξ_h/ξ_{c2} at different temperatures (a) with impurity scattering $\Gamma = 0$ (b) with impurity scattering $\Gamma = 0.5$. Dashed lines dshow the result of the AGL theory for ξ_v from Ref. [9].

where $\omega_n = \pi T(2n+1)$, $F = 2\pi \langle f \rangle \cdot \Gamma$ and $G = 2\pi \langle g \rangle \cdot \Gamma$. Here, $\Gamma = \pi n_i N_F |u|^2$ is the impurity scattering rate, u is impurity scattering amplitude and $\mathbf{u}$ is a unit vector of the Fermi velocity. The FLL create the anisotropy of the electron spectrum [19]. Therefore the impurity renormalization correction in Eq. (3) and (4) are averaged over Fermi surface and can be reduced to averages over the polar angle θ, i.e. $\langle \ldots \rangle = (1/2\pi) \int \ldots d\theta$.

To take into account the influence of screening the vector potential $\mathbf{A}(\mathbf{r})$ in Eqs. (3) and (4) is obtained from the equation $\nabla \times \nabla \times \mathbf{A_E} = \frac{4}{\kappa^2}\mathbf{J}$, where the supercurrent $\mathbf{J}(\mathbf{r})$ is given in terms of $g(\omega_n, \theta, \mathbf{r})$ by

$$\mathbf{J}(\mathbf{r}) = 2\pi T \sum_{\omega_n > 0} \int_0^{2\pi} \frac{d\theta}{2\pi} \frac{\hat{\mathbf{k}}}{i} g(\omega_n, \theta, \mathbf{r}). \tag{5}$$

Here $\mathbf{A}$ and $\mathbf{J}$ are measured in units of $\phi_0/2\pi\xi_0$ and $2ev_F N_0 T_c$, respectively. The self-consistent condition for the pairing potential $\Delta(\mathbf{r})$ is given by

$$\Delta(\mathbf{r}) = V^{SC} 2\pi T \sum_{\omega_n > 0} \int_0^{2\pi} \frac{d\theta}{2\pi} f(\omega_n, \theta, \mathbf{r}), \tag{6}$$

where V^{SC} is the superconducting coupling constant and ω_c is the ultraviolet cutoff determining T_{c0}[23]. All over this paper the energy, the temperature, and the length are measured in units of T_{c0} and the coherence length $\xi_0 = v_F/T_{c0} = \xi_{BCS}\pi\Delta_0/T_{c0}$. Here $\xi_{BCS} = v_F/\pi\Delta_0$, where v_F is the Fermi velocity and Δ_0 is temperature dependent uniform gap. The magnetic field $\mathbf{h}$ is given in units of $\phi_0/2\pi\xi_0^2$. The impurity scattering rates are in units of $2\pi T_{c0}$. In calculations the ratio $\kappa = \lambda_{L0}/\xi_0 = 10$ is used. It corresponds to $\kappa_{GL} = 43.3$ [5]. The Riccati equations [Eq. (3 and 4)] are solved by the Fast Fourier Transform (FFT) method [23]. This method is reasonable for dense FLL discussed in this paper. In high field the pinning effects are weak and they are not considered in our paper. After solving the Eilenberger equations the obtained magnetic field distribution $h_E(\mathbf{r})$ is fitted with the London field distribution $h_{EGL}(\mathbf{r})$ (Eq. (1)). To study high field regime we should calculate upper critical field $B_{c2}(T)$ [25].

Our calculations show that in clean superconductors $\xi_h(B)$ dependence has minimum which disappears at low temperatures. The absolute values of ξ_h are smaller than those of the AGL theory predictions, with increasing temperature ξ_h dependences move to higher values.

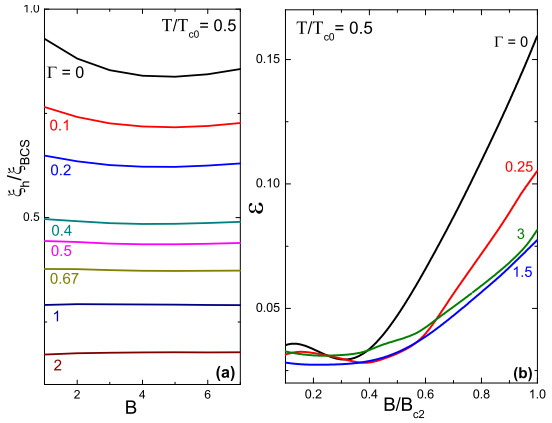

Figure 2. (a) The magnetic field dependence of ξ_h/ξ_{BCS} at $T/T_{c0} = 0.5$ with different impurity scattering Γ. (b) Magnetic field dependence of mean square deviation of the London distribution from the Eilenberger distribution normalized by the variance of the Eilenberger distribution, ε, for $T/T_{c0} = 0.5$ with different impurity scattering Γ.

These effects can be seen in Fig. 1 (a), where $\xi_h(B/B_{c2})$ are presented with $\Gamma = 0$ at $T/T_{c0} = 0.2, 0.4, 0.6, 0.8, 0.95$. The same tendency is also visible in the presence of impurity scattering, but shifting of ξ_h to direction of AGL curve is slower. Fig. 1 (b) presents $\xi_h(B/B_{c2})$ dependence with $\Gamma = 0.5$ at $T/T_{c0} = 0.2, 0.4, 0.6, 0.8, 0.95$. Strong decreasing of ξ_h with decreasing of temperature can be explained by Kramer-Pesch effect [7]. The change of the shape of $\xi_h(B)$ curve in low fields with increasing of scattering rate Γ is shown in details at Fig. 2 (a) at $T/T_{c0} = 0.5$. At high scattering rate, a flat dependence is clearly visible.

We also calculate magnetic field dependence of mean square deviation of h_{EGL} distribution of the magnetic field from the Eilenberger distribution normalized by the variance of the Eilenberger distribution $\varepsilon = \sqrt{\overline{(h_E - h_{EGL})^2}/\overline{(h_E - B)^2}}$, where $\overline{\cdots}$ is average over unit vortex cell. Fig. 2 (b) shows $\varepsilon(B)$ dependence for $T = 0.5$ with different impurity scattering Γ. It can be seen from this picture that accuracy of EGL model is getting better with increasing impurity scattering and saturates at the $\Gamma \approx 1.5$.

We should note that the the similarity of our results to the AGL theory (which is suppose to be quantitavely incorrect [11]) can be considered only as a coincidence. First, in our methods there is only one fitting parameter ξ_h, while in the AGL theory there are two of them, ξ_v and $f_\propto$ ($f_\propto \equiv 1$ in our case). Because of the boundary condition of the field distribution ($h(r) \to B$ at $B \to B_{c2}$) ξ_h is growing function of B at the high fields resulting in the appearance of the minimum. In the AGL theory (and "improved" analytical GL theory [11]) the boundary condition is satisfied by the limit $f_\propto \to 0$ at $B \to B_{c2}$, so the behavior of $\xi_v(B)$ dependence is not predetermined. For example, in the "improved" analytical GL theory there is no minimum in $\xi_v(B)$ [11]. Absence of the minimum in $\xi_h(B)$ results also from local Usadel theory for $\xi_1(B)$ [26] and $\xi_2(B)$ [27] dependences. Second, there is clear impurity dependence of the ξ_h/ξ_{c2} value even at high temperatures (compare Fig. 1 (a) and Fig. 1 (b)), which can not be explained by the local Usadel or "improved" analytical GL theories, where scaling $\xi_h/\xi_{c2} = Const$ (independent on Γ) is expected.

In Fig. 1 the normalization constant ξ_{c2} is dependent on impurity scattering rate Γ. It is well known that at high Γ $\xi_{c2} \sim \sqrt{1/\Gamma} \sim \sqrt{l}$, where l is the mean-free path. Therefore, the

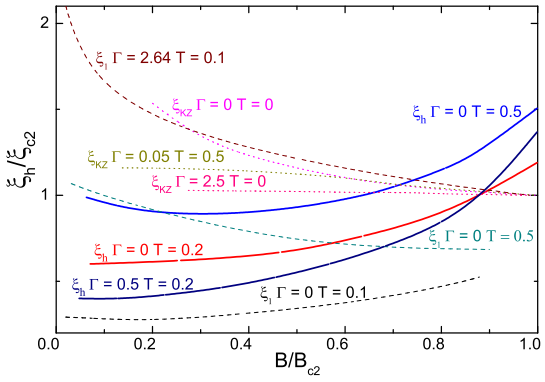

Figure 3. Comparison between field dependences of ξ_h/ξ_{c2} (at $T = 0.2$, $\Gamma = 0; 0.5$ and $T = 0.5$, $\Gamma = 0$, solid lines), ξ_1/ξ_{c2} (at $T = 0.1$, $\Gamma = 0$ and $T = 0.1$, $\Gamma = 2.64$ from Ref. [5] and $T = 0.5$, $\Gamma = 0$ from Ref. [19], dashed lines) and ξ_{KZ}/ξ_{c2} (at $T = 0$, $\Gamma = 0$; $T = 0.5$, $\Gamma = 0.05$ and $T = 0$, $\Gamma = 2.5$ from Ref. [21], dotted lines).

decreasing of the ratio ξ_h/ξ_{c2} with Γ implies the most strong dependence ξ_h on l. It is found that ξ_h in dirty superconductors can be scaled with relaxation time τ

$$\xi_h(B,T,\tau) = \frac{\xi_{pure}(B,T)}{1+\frac{\tau_0(B,T)}{\tau}} \tag{7}$$

where $\xi_{pure}(B,T)$ is the effective coherence length in clean superconductors [22] and τ_0 is a characteristic relaxation time. It results in $\xi_h \sim l$ dependence at high Γ similar to the behavior of nonlocality radius [18] resulting in decreasing of ξ_h/ξ_{c2} at high Γ. Such fast decreasing of ξ_h can be compared with the behavior of the another characteristic length ξ_1. It has been found that at low temperatures impurity scattering suppresses Kramer-Pesch effect in $\xi_1(T)$ dependence resulting in nonmonotonous behavior of $\xi_1(\Gamma)$. On the another hand, it is clearly visible from Fig. 2 (a) that ξ_h monotonously decreases with Γ, where normalization constant ξ_{BCS} is used (ξ_{BCS} is not dependent on Γ).

The data in Figs. 1 and 2 demonstrate nearly universal behavior near T_c and small scattering rates: (i) the nonmonotonous field dependence with a minimum and (ii) the similar slope $d(\xi_h/\xi_{c2})/db$ at $b = 1$ which is weakly dependent on temperature and scattering rate. But the results are very different from the prediction of the KZ theory because of neglection of the Kramer-Pesch effect there. This can be seen from Fig. 3, where predictions of the various theories for clean superconductors and different temperatures are presented. Strong suppression of ξ_h (the ξ_h curves) and ξ_1 (the ξ_1 curves) with temperature lowering is visible in contrast to the increasing of ξ_{KZ} (the KZ curves). But impurity induced behavior is similar for ξ_h/ξ_{c2} and ξ_{KZ}/ξ_{c2}: both decreases with increasing impurity rates.

To conclude, the magnetic coherence length ξ_h (cutoff parameter) in the mixed state of high-κ s-wave superconductors is investigated in framework of quasiclassical Eilenberger theory. Nearly universal field dependence with a minimum is found near critical temperature in clean superconductors. A similar slope $d(\xi_h/\xi_{c2})/d(B/B_{c2})$ at $B/B_{c2} = 1$ weakly dependent on temperature and scattering rate is discovered. Quasiparticle scattering by impurities and lowering of the temperature reduce the value of ξ_h shifting it considerably downward from the the AGL curve and at low temperatures strong influence of the Kramer-Pesch effect is found. It

can explain muon spin rotation experimental results in some low temperature superconductors, where the ratio $\xi_h/\xi_{c2} \ll 1$ [3] is observed in intermediate fields. A comparison with the behavior of the order parameter coherence length ξ_1 and another theories is done. It is found that impurities influence by different way on ξ_h and ξ_1.

This work was supported by the Finnish Cultural Foundation.

References

[1] Sonier J, Brewer J and Kiefl R 1977 *Rev. Mod. Phys.* **72** 769
[2] Sonier J E 2004 *J. Phys.: Condens. Matter* **16** S4499
[3] Sonier J E 2007 *Rep. Prog. Phys.* **70** 1717
[4] Atkinson W A and Sonier J E 2008 *Phys. Rev. B* **77** 024514
[5] Miranović P, Ichioka M and Machida K 2004 *Phys. Rev. B* **70** 104510
[6] Ichioka M, Hasegawa A and Machida K 1999 *Phys. Rev. B* **59** 8902
[7] Nakai N, Miranović P, Ichioka M and Machida K 2006 *Phys. Rev. B* **73** 172501
[8] Usadel K 1970 *Phys. Rev. Lett.* **25** 507
[9] Hao Z, Clem J R, McElfresh M W, Civale L, Malozemoff A P and Holtzberg F 1991 *Phys. Rev. B* **43** 2844
[10] Yaouanc A, de Reotier P D and Brandt E H 1997 *Phys. Rev. B* **55** 11107
[11] Pogosov W V, Kugel K I, Rakhmanov A L and Brandt E H 2001 *Phys. Rev. B* **64** 064517
[12] de Oliveira I G and Thompson A M 1998 *Phys. Rev. B* **57** 7477
[13] Brandt E H 2003 *Phys. Rev. B* **68** 054506
[14] Kogan V G, Prozorov R, Bud'ko S L, Canfield P C, Thompson J R, Karpinski J, Zhigadlo N D and Miranović P 2006 *Phys. Rev. B* **74** 184521
[15] Laiho R, Safonchik M and Traito K B 2007 *Phys. Rev. B* **75** 174524
[16] Lemberger T R, Ginsberg D M and Rickayzen G 1978 *Phys. Rev. B* **18** 6057–6065
[17] de Gennes P 1989 *Superconductivity of Metals and Alloys* Addison–Wesley, New York
[18] Kogan V G, Gurevich A, Cho J H, Johnston D C, Xu M, Thompson J R and Martynovich A 1996 *Phys. Rev. B* **54** 12386
[19] Ichioka M, Hasegawa A and Machida K 1999 *Phys. Rev. B* **59** 184
[20] Kadono R, Higemoto W, Koda A, Larkin M I, Luke G M, Savici A T, Uemura Y J, Kojima K M, Okamoto T, Kakeshita T, Uchida S, Ito T, Oka K, Takigawa M, Ichioka M and Machida K 2004 *Phys. Rev. B* **69** 104523
[21] Kogan V G and Zhelezina N V 2005 *Phys. Rev. B* **71** 134505
[22] Laiho R, Safonchik M and Traito K B 2007 *Phys. Rev. B* **76** 140501(R)
[23] Laiho R, Safonchik M and Traito K B 2008 *Phys. Rev. B* **78** 064521
[24] Lemberger T, Ginsberg D and Rickayzen G 1978 *Phys. Rev. B* **18** 6057
[25] Ovchinnikov Y N and Kresin V Z 1995 *Phys. Rev. B* **52** 3075
[26] Golubov A A and Hartmann U 1994 *Phys. Rev. Lett.* **72** 3602
[27] Sonier J E, Kiefl R F, Brewer J H, Chakhalian J, Dunsiger S R, MacFarlane W A, Miller R I, Wong A, Luke G M and Brill J W 1997 *Phys. Rev. Lett.* **79** 1742

ACTA UNIVERSITATIS LAPPEENRANTAENSIS

448. JABLONSKA, MATYLDA. From fluid dynamics to human psychology. What drives financial markets towards extreme events. 2011. Diss.

449. MYÖHÄNEN, KARI. Modelling of combustion and sorbent reactions in three-dimensional flow environment of a circulating fluidized bed furnace. 2011. Diss.

450. LAATIKAINEN, MARKKU. Modeling of electrolyte sorption – from phase equilibria to dynamic separation systems. 2011. Diss.

451. MIELONEN, JARI. Making Sense of Shared Leadership. A case study of leadership processes and practices without formal leadership structure in the team context. 2011. Diss.

452. PHAM, ANH TUAN. Sewage sludge electro-dewatering. 2011. Diss.

453. HENNALA, LEA. Kuulla vai kuunnella – käyttäjää osallistavan palveluinnovoinnin lähestymistavan haasteet julkisella sektorilla. 2011. Diss.

454. HEINIMÖ, JUSSI. Developing markets of energy biomass – local and global perspectives. 2011. Diss.

455. HUJALA, MAIJA. Structural dynamics in global pulp and paper industry. 2011. Diss.

456. KARVONEN, MATTI. Convergence in industry evolution. 2011. Diss.

457. KINNUNEN, TEEMU .Bag-of-features approach to unsupervised visual object categorisation. 2011. Diss.

458. RUUSKANEN, VESA. Design aspects of megawatt-range direct-driven permanent magnet wind generators. 2011. Diss.

459. WINTER, SUSANNA. Network effects: scale development and implications for new product performance. 2011. Diss.

460. JÄÄSKELÄINEN, ANSSI. Integrating user experience into early phases of software development. 2011. Diss.

461. KÄÄRIÄINEN, TOMMI. Polymer surface modification by atomic layer deposition. 2011. Diss.

462. KOCHURA, ALEKSEY. Growth, magnetic and transport properties of InSb and II-IV-As2 semiconductors doped with manganese. 2011. Diss.

463. PUTKIRANTA, ANTERO. Possibilities and challenges of longitudinal studies in operations management. 2011. Diss.

464. HAPPONEN, ARI. Muuttuvaan kysyntään sopeutuva varastonohjausmalli. 2011. Diss.

465. VASAVA, PARITOSH. Application of computational fluid dynamics in modelling blood flow in human thoracic aorta. 2011. Diss.

466. PURO, LIISA. Identification of extractives and polysaccharides as foulants in membrane filtration of pulp and paper mill effluents. 2011. Diss.

467. LAPPALAINEN, PIA. Socially Competent Leadership – predictors, impacts and skilling in engineering. 2012. Diss.

468. PLAMTHOTTATHIL, ANSHY OONNITTAN. Application of electrokinetic Fenton process for the remediation of soil contaminated with HCB. 2012. Diss.

469. EBRAHIMI, FATEMEH. Synthesis of percarboxylic acids in microreactor. 2012. Diss.

470. JANTUNEN, SAMI. Making sense of software product requirements. 2012. Diss.

471. VILKO, JYRI. Approaches to supply chain risk management: identification, analysis and control. 2012. Diss.

472. TANSKANEN, VESA. CDF modelling of direct contact condensation in suppression pools by applying condensation models of separated flow. 2012. Diss.

473. HUHTANEN MIKKO. Software for design of experiments and response modelling of cake filtration applications. 2012. Diss.

474. PARJANEN, SATU. Creating possibilities for collective creativity
Brokerage functions in practice-based innovation. 2012. Diss.

475. KUKKONEN, SAKU. Generalized differential evolution for global multi-objective optimization with constraints. 2012. Diss.

476. LAAKSONEN, JONNA. Tactile-proprioceptive robotic grasping. 2012. Diss.

477. KALLIO, ANNE. Enhancing absorptive capacity in a non-research and development context
An action research approach to converting individual observations into organizational awareness. 2012. Diss.

478. LÄTTILÄ, LAURI. Improving transportation and warehousing efficiency with simulation based decision support systems. 2012. Diss.

479. OYOMNO, WERE. Usable privacy preservation in mobile electronic personality. 2012. Diss.

480. LINNALA, MIKKO. Simulation and optimization tools in paper machine concept design. 2012. Diss.

481. KORPIJÄRVI, JUHA. Aging based maintenance and reinvestment scheduling of electric distribution network. 2012. Diss.

482. KORHONEN, JUHAMATTI. Active inverter output filtering methods. 2012. Diss.

483. KLODOWSKI, ADAM. Flexible multibody approach in bone strain estimation during physical activity: quantifying osteogenic potential. 2012. Diss.

484. VUORENMAA, MARKKU. Osaamisen johtaminen pk-yrityksen kansainvälisen kasvun elinkaarella. 2012. Diss.

485. RAUTIAINEN, MARITA. Dynamic ownership in family business systems – a portfolio business approach. 2012. Diss.

486. LILIUS, REIJO. THE FINNISH IT INDUSTRIES IN TRANSITION Defining and measuring the Finnish software product and IT services industries by applying theoretical frameworks . 2012. Diss.

487. TUOMINEN, PASI. The purpose of consumer co-operation: implications for the management and governance of co-operatives. 2012. Diss.

488. SAARI, ESA. Suurnopeus-turbokoneroottoreiden termodynaaminen ja mekaaninen mallinnus sekä rakenneanalyysi. 2012. Diss.

489. PAANANEN, MIKKO. On innovative search: the use of internal and external sources of innovation among Finnish innovators. 2012. Diss.